The Pennsylvania State University

The Graduate School

Department of Mechanical and Nuclear Engineering

THERMAL HYDRAULIC ANALYSIS OF TWO-PHASE CLOSED THERMOSYPHON COOLING SYSTEM FOR NEW COLD NEUTRON SOURCE MODERATOR OF BREAZEALE RESEARCH REACTOR AT PENN STATE

A Dissertation in

Mechanical Engineering

by

Melaku Habte

Submitted in Partial Fulfillment
of the Requirements
for the Degree of

Doctor of Philosophy

August 2008

The Dissertation of Melaku Habte was reviewed and approved* by the following:

Savas Yavuzkurt
Professor of Mechanical Engineering
Dissertation Advisor
Co-Chair of Committee

Kenan Ünlü
Professor of Nuclear Engineering
Co-Chair of Committee

Fan Bill Cheung
Professor of Mechanical and Nuclear Engineering

John Mahaffy
Associate Professor of Nuclear Engineering

Li Xiantao
Assistant Professor of Mathematics

Karen A. Thole
Professor of Mechanical Engineering
Head of the Department of Mechanical Engineering

*Signatures are on file in the Graduate School

ABSTRACT

A cold neutron source cooling system is required for the Penn State's next generation cold neutron source facility that can accommodate a variable heat load up to about ~10W with operating temperature of about 28K. An existing cold neutron source cooling system operating at the University of Texas Cold Neutron Source (TCNS) facility failed to accommodate heat loads upwards of 4W with the moderator temperature reaching a maximum of 44K, which is the critical temperature for the operating fluid neon. The cooling system that was used in the TCNS cooling system was a two-phase closed thermosyphon with a reservoir (TPCTR). The reservoir containing neon gas is kept at room temperature.

In this study a detailed thermal analysis of the fundamental operating principles of a TPCTR were carried out. A detailed parametric study of the various geometric and thermo-physical factors that affect the limits of the operational capacity of the TPCTR investigated. A CFD analysis is carried out in order to further refine the heat transfer analysis and understand the flow structure inside the thermosyphon and the two-phase nucleate boiling in the evaporator section of the thermosyphon. In order to help the new design, a variety of ways of increasing the operating range and heat removal capacity of the TPCTR cooling system were analyzed so that it can accommodate the anticipated heat load of 10W or more. It is found, for example, that doubling the pressure of the system will increase the capacity index ζ by 50% for a system with an initial fill ratio FR of 1. A decrease in cryorefrigeration performance angle increases the capacity index. For example taking the current condition of the TCNS system and reducing the angle from

the current value of $\sim 70^0$ by half ($\sim 35^0$) will increase the cooling power 300%. Finally based on detailed analytic and CFD analysis the best operating condition were proposed.

TABLE OF CONTENTS

LIST OF FIGURES

LIST OF TABLES

NOMENCLATURE

A area $[m^2]$

$a_1, a_2 \ldots a_{20}$ constants defined in A.4

$B, C, \cdots H$ relations defined in Eq. 4.2

C_1, C_2 constants in Eq 5.11

C_3 constant in Fig. 5.2 and Eq 5.7

C_{sf} constant used in Eq. 5.6

Cp specific heat $[J \cdot kg^{-1}K^{-1}]$

CHF critical heat flux $\left[W \cdot m^{-2} \cdot K^{-1}\right]$

D outer diameter of thermosyphon $[m]$

d inside diameter of thermosyphon $[m]$

f function of

F dimensionless factor Eq.5.22

FR fill ratio defined by Eq 4.8

FR_O initial fill ratio

g gravitational acceleration $[m \cdot \sec^{-2}]$

h heat transfer coefficient Eq 5.4 $\left[W \cdot m^{-2} \cdot K^{-1}\right]$

h_C heat transfer coefficient at the inside wall of the condenser section of a thermosyphon Eq 5.22 $\left[W \cdot m^{-2} \cdot K^{-1}\right]$

h_E heat transfer coefficient at the inside wall of the evaporator section of a thermosyphon $\left[W \cdot m^{-2} \cdot K^{-1}\right]$

h_{lv} latent heat of vaporization $[J \cdot kg^{-1}]$

h_{lv}' modified latent heat of vaporization Eq 5.19 $[J \cdot kg^{-1}]$

h_{NC} natural convection heat transfer coefficient $\left[W \cdot m^{-2} \cdot K^{-1}\right]$

h_{NB} nucleate boiling heat transfer coefficient Eq 5.12 $\left[W \cdot m^{-2} \cdot K^{-1}\right]$

Ja Jakob number Eq 5.21

k thermal conductivity $\left[W \cdot m^{-1} \cdot K^{-1}\right]$

K_p parameter defined in Eq 5.14

l_L parameter defined in Eq 5.16

l_m bubble length scale defined in Eq 5.14

L length of vertical plate Eq 5.18 $[m]$

L_E length of evaporator section $[m]$

L_C length of condenser section $[m]$

L_{TS} length of thermosyphon $[m]$

L_{Liq_Min} minimum length of liquid level Eq. 4.7 $[m]$

m mass $[kg]$

m_{TS_V} mass of vapor inside thermosyphon $[kg]$

m_{TS} mass of fluid inside the thermosyphon $[kg]$ Eq A.6

M_R mass of fluid inside reservoir $[kg]$

M_T total mass of fluid in the thermosyphon and reservoir $[kg]$

M_L mass of liquid inside the thermosyphon Eq A.14 $[kg]$

M_f mass of liquid film inside the thermosyphon Eq A.14 $[kg]$

$\bar{M}$ molecular weight $\left[gm \cdot mole^{-1}\right]$

$\bar{M}_{Ne}$ molecular weight of neon $\left[gm \cdot mole^{-1}\right]$

n = 4, constant exponent

Nu_D Nusselt number based on diameter Eq 5.20

Nu_x local Nusselt number Eq 5.15

Nu_{NB} Nusselt number for nucleate boiling Eq 5.16

Nu_{CC} combined correlation of Nusselt number for natural convection and nucleate boiling Eq 5.16

Nu_f parameter defined in Eq 5.16

P pressure $[Pa]$

P_{Sat} saturation pressure $[Pa]$

P_{dSat} saturation pressure at dryout condition $[Pa]$

P_{Cr} critical saturation pressure of the fluid $[Pa]$

P_O initial pressure inside thermosyphon and reservoir $[Pa]$

P_L saturation pressure at the liquid temperature $[Pa]$

Pr Prandtl number

Pr_L Prandtl number of liquid

Q heat flow rate $[W]$

Q_d heat load of a thermosyphon at dryout condition $[W]$

Q_{Max} theoretical maximum heat load capacity of a thermosyphon $[W]$

q heat flux Eq. 5.5 $[W \cdot m^{-2}]$

q_C heat flux at the condenser section of a thermosyphon $[W \cdot m^{-2}]$

q_E heat flux at the evaporator section of a thermosyphon $[W \cdot m^{-2}]$

R gas constant $\left[= 8.314\ kJ \cdot kg^{-1} \cdot K^{-1} \right]$

R_u universal gas constant $\left[= 8.314\ kJ \cdot kg^{-1} \cdot K^{-1} \right]$

Ra Rayleigh number Eq 5.21

R_{Ci} convective thermal resistance at the inside wall of condenser section of thermosyphon $[K \cdot W^{-1}]$

R_{Co} conduction thermal resistance of condenser section of thermosyphon $[K \cdot W^{-1}]$

R_{Ei} convective thermal resistance at the inside wall of evaporator section of thermosyphon $[K \cdot W^{-1}]$

R_{Eo} conduction thermal resistance of evaporator section of thermosyphon $[K \cdot W^{-1}]$

R_{ad} axial conduction thermal resistance through the length of adiabatic wall of a thermosyphon $[K \cdot W^{-1}]$

R_{th} thermal resistance $[K \cdot W^{-1}]$

R_{th}' net thermal resistance as given in Eq. 5.25

R_{Eq} Equivalent thermal resistance of thermosyphon Eq. 5.8

Re_x liquid film local Reynolds number Eq 5.14

r constant in Eq. 5.6

s constant in Eq. 5.6

T temperature $[K]$

T_{Sat} saturation temperature $[K]$

T_{dSat} saturation temperature at dryout condition $[K]$

T_{Sat0} saturation temperature evaluated at initial pressure P_O $[K]$

T_O initial temperature $[K]$

T_∞ reservoir temperature or fluid temperature given by Eq 5.4 $[K]$

T_{Min} minimum saturation temperature of the fluid $[K]$

T_{Cr} critical saturation temperature of the fluid $[K]$

T_{Ci} inside wall temperature of condenser section of thermosyphon $[K]$

T_{Co} outside wall temperature of condenser section of thermosyphon $[K]$

T_{Ei} inside wall temperature of evaporator section of thermosyphon $[K]$

T_{Eo} outside wall temperature of evaporator section of thermosyphon $[K]$

T_w wall temperature $[K]$

T_{eff} effective temperature Eq. 4.3 $[K]$

t_{CD} cool down time [sec]

t_{EV} evaporation time [sec]

v specific volume Fig. 4.1 $[m^3 \cdot kg^{-1}]$

V volume $\left[m^3\right]$

V_{Liq} volume of liquid $\left[m^3\right]$

V_{Liq_Min} minimum volume of liquid Eq. 4.7 $\left[m^3\right]$

V_f volume of liquid film $\left[m^3\right]$

V_{fo} volume of liquid film at dryout condition $\left[m^3\right]$

V_{TS} volume of thermosyphon $\left[m^3\right]$

V_R volume of reservoir $\left[m^3\right]$

x distance along evaporator section Eq. 5.14; coordinate direction along which heat flows Eq. 5.3 $[m]$

Z compressibility factor

z_f axial distance of location of film front $[m]$

$\dot{z}_f$ film advance rate $\left[m \cdot \sec^{-1}\right]$

Greek Symbols

α characteristic angle of cryorefrigeration system (heat sink) performance chart $[\text{deg}]$

β volumetric expansion coefficient $\left[K^{-1}\right]$

γ dimensionless parameter Eq. 5.13

Δ change/difference

ζ capacity index defined in Eq. 5.32

η volume ratio Eq. 4.5

θ inclination angle of thermosyphon [deg]

μ dynamic viscosity $[Pa \cdot \text{sec}]$

ν kinematic viscosity $\left[m^2 \cdot \text{sec}^{-1}\right]$

ξ liquid fraction Eq. 4.6

ξ_O liquid fraction at dryout Eq. 4.6

ρ density $[kg \cdot m^{-3}]$

ρ_O density of vapor at P_O and T_O $[kg \cdot m^{-3}]$

ρ_L density of liquid $[kg \cdot m^{-3}]$

σ surface tension $\left[N \cdot m^{-1}\right]$

ϕ angle shown in Fig. 5.7

Subscripts

Al	aluminum
ad	adiabatic
C	condenser
Cr	critical
d	dryout
E	evaporator
f	liquid film
L	liquid
NB	nucleate boiling
NC	natural convection
O	initial
R	reservoir
s	solid wall
Sat	saturated
TS	thermosyphon
v	vapor

ACKNOWLEDGEMENTS

First I would like to thank my advisor Dr. Yavuzkurt for his immeasurable support and guidance. I have high regard for his willingness to share his knowledge and years of experience enthusiastically. I was very lucky to have his support and encouragement for many years.

I would also want to thank Dr. Ünlü for his continuous support in this study. I would like to thank him for sharing his knowledge and valuable suggestions. Without his support it would have been much difficult to accomplish the study.

I want to thank members of my PhD committee, professors John Mahaffy, Fan-Bill Cheung and Xiantao Li for their valuable reviews and suggestions.

I would like to take this opportunity to thank the late Dr. Donald Streit and his family for encouraging me to join Penn State. His sponsoring me and my undergraduate classmate (also now a Penn State Alum) for our graduate entrance exams helped us succeed in our educational endeavor.

I would like to thank my entire family especially my sister Rosa, my mother Tiruwork, and my brother Tekalegn without their continuous support this would have been impossible for me achieve.

Last but not least, I would like to thank god for giving me the patience and the strength, for guiding me make choices in life and helping me in such mysterious way that is impossible for me to explain.

Chapter 1

Introduction

Beams of neutrons produced by nuclear research reactors are used in condensed matter research to study the arrangement and interactions of atoms in materials. Because neutrons are highly penetrating, it is possible to probe deep within materials to characterize micropores, microcracks, small precipitates, polymers, biological macromolecules, etc. Neutrons examine matter at the atomic-scale in a way unmatched by other techniques because of their favorable wavelength to energy ratio. In many applications, the structural information provided by neutrons cannot be obtained in any other way [**Unlu et al 1994**].

All of the above research applications can be enhanced in one way or another by using sub-thermal neutrons or "cold neutrons." Cold neutrons can be defined as neutrons with energies below 5 meV and corresponding velocity and wavelength 980 m/s and 4 Å respectively. Cold neutrons have longer wavelengths and lower kinetic energies on the average than thermal neutrons, the majority of the neutrons normally present in neutron beams from nuclear research reactors [**Unlu et al 1994**].

The "temperature" of a neutron beam can be lowered by passing it through a cold moderator. In order to achieve this, an effective cooling system is needed that can keep the moderator temperature significantly below liquid nitrogen temperature, 77K. This cooling system should be capable of handling variable heat load of up to a maximum of 10W [**Unlu et al 1994**].

1.1 Cold Neutron Source

Cold neutrons are produced by passing thermal neutrons through a cooled moderator as schematically shown in Figure **1-1** . A typical Cold Neutron Source (CNS) consists of: a moderator, moderator fluid and a cooling system for the moderator, in this case a closed two phase thermosyphon. Among the many uses of cold neutrons are: Neutron focusing research, Prompt Gamma Activation Analysis, Neutron Imaging, Neutron Depth Profiling and Neutron Scattering/Diffraction experiments[**Unlu et al 1995**].

Neutrons with sufficiently long wavelengths (cold neutrons) can be reflected from some surfaces and they can be "guided" down cylinders, wave guides, without the normal $\frac{1}{r^2}$ attenuation and can be bent out of the line-of-sight paths followed by other radiation. Only two cold neutron beam facilities were developed at the U.S. university research reactors, namely at Cornell University and the University of Texas at Austin. The Cornell Cold Neutron Beam Facility (CNBF) included a moderator, a cryorefrigerator, copper cold fingers, a neutron guide system, vacuum jackets, shielding, and various connecting and control lines. The mesitylene moderator in the CNBF was cooled by a helium cryorefrigerator via copper cold fingers to maintain the moderator below 30 K at full power reactor operation. Cold neutrons from the mesitylene moderator were transported to an experimental facility using thirteen 1-m long natural Ni coated neutron guide elements. Texas Cold Neutron Source (TCNS) uses mesitylene moderator that is cooled by a cryorefrigerator via a neon thermosyphon. The operation of the TCNS is based on a helium cryorefrigerator, which liquefies neon gas in a 3-m long thermosyphon. The

thermosyphon cools and maintains mesitylene moderator at about 30 K in a chamber. Neutrons streaming through the mesitylene chamber are moderated and thus reduce their energy to produce a cold neutron distribution. The cold neutrons are transported out of the biological shield of the reactor and to a sample chamber location by a 6-m long curved neutron guide and an 80-cm long converging neutron guide [**Unlu et al 1995**].

1.2 Cooling system requirements

Two phase closed thermosyphon (TPCT) is considered as the cooling system that is chosen in this study. The heat load for the cooling system comes from the moderator chamber, as a result of the energy absorbed from the neutron beams that pass through it due to gamma heating. The desired cooling system should be able to accommodate a variable heat load from the moderator chamber in the range of up to 10W with operating temperature in the range of 26K ~ 30K. The cooling system should also be able to carry the heat load from the moderator chamber that is located inside the biological shield through the beam port a total length of 3m to a cryorefrigeration system. The cryorefrigeration system serves as the primary cooling source (heat sink) by cooling the cold end of the thermosyphon. In order to utilize the full cooling power of the primary cooling system (cryorefrigeration) the moderator end of the thermosyphon temperature must be kept as close to the cold end of the thermosyphon as possible. In order to achieve this one needs a highly efficient cooling system capable of operating between a very small mean temperature difference between the evaporator and condenser that are separated over long distance. For the cooling system similar to the TCNS the heat flux at

the evaporator of the thermosyphon can reach up to 10.6 kW/m^2 assuming a 10W heat load and normal operating conditions. However, the heat flux can reach up to 50 kW/m^2 before the coolant fluid dries up inside the thermosyphon.

1.3 Investigation of Two Previous Cooling System Designs

In this section two previous cold neutron source cooling systems for university research reactors are considered. The first one is the Cornell University Cold Neutron Beam Facility (CNBF) and the second one is the Texas Cold Neutron Source (TCNS) cooling systems. The result of the analysis of this study could be used in the development of a third generation cold neutron source at Penn State.

1.3.1 The Cornell Cold Neutron Source Cooling System

The Cornell Cold Neutron Beam Facility (CNBF) is located at one of the radial beam port of the 500 kW TRIGA research reactor and adjacent beam floor area as shown in Figure **1-2** . The CNBF consists of a cooled moderator, a cryorefrigerator, a copper rod (cold finger), and neutron guide elements. The moderator is placed in a neutron beam port close to the reactor core. The moderator fluid used in this system is mesitylene, a 1,3,5-trimethyl benzene. Because mesitylene freezes at 228K and boils at 437K, it is safer and much simpler to use than liquid hydrogen, D_2O ice, or solid methane, the more traditional cold-neutron-source moderators. The moderator is contained in a thin-walled

aluminum right-circular cylinder 7.5 cm diameter by 2.5 cm deep position inside a beam tube at the graphite reflector of the reactor [**Unlu et al 1997**].

In the CNBF the only heat transfer mechanism to cool the moderator is conduction through a 5-9's purity (99.999+%) 1.8 cm diameter, 216 cm long copper rod. The copper rod is connected to the second stage of a cryogenic refrigerator that is located outside the biological shield of the reactor as shown in Figure **1-2** . A Gifford-McMahon cycle Cryomech model GB04 helium cryorefrigerator is used for cooling. Typical measured cooling down and warming up temperatures is shown in Figure **1-3** . The moderator chamber temperature varies from 11K at 0.0 kW reactor power with an evacuated chamber to a 28.5K at 500 kW reactor power with a mesitylene filled chamber [**Unlu et al 1997**].

1.3.2 The Texas Cold Neutron Source Cooling System

The Texas cold neutron source (TCNS) cooling system shown in Figure **1-4** operates in the same way as the CNBF except that the cooling system in the case of TCNS is by using a two-phase thermosyphon, which is cooled by a helium cryorefrigerator, instead of a solid copper rod as in the case of CBNF. The thermosyphon cools and maintains a cold neutron moderating material (mesitylene) at about 30 K in an aluminum chamber located inside the graphite reflector of the UT-Austin 1000-kW research reactor. The heat transfer mechanism inside the thermosyphon involves mainly boiling and condensation of neon gas. The cryorefrigeration system liquefies the neon gas inside the thermosyphon. Once the liquid forms, it flows down due to gravity inside the

thermosyphon pipe and cools the moderator connected at the end of the thermosyphon. The liquid boils by absorbing the moderator heat and the vapor flows back to the cold head (heat sink) of the thermosyphon to be condensed and liquefied completing the evaporation and condensation cycle. The cooling down diagram of the TCNS as shown in Figure **1-5** is similar to the Cornell system. As shown in Figure **1-6** , the performance of the TCNS cooling system breakdowns at heat load of 5W. One of the main objectives of the current study is to address this problem and propose a cooling system that can accommodate a heat load capacity up to 10W as discussed in the next section.

1.4 Problem Statement and Scope of the Investigation

The main goal of this research is to come up with an improved design of closed two phase thermosyphon heat exchanger that alleviates the heat removal limitations exhibited in the TCNS cooling system. In this regard the focus of this work will be directed into the cooling system that was installed at the TCNS. In studying the TCNS cooling system it can be concluded that the heat load from the moderator could not be handled by the thermosyphon cooling system at the given operating condition and equipment size. The heat load from the moderator must be kept below 5W in order for the moderator to remain cooled below 44K. The new design in this study will address this major problem and come up with a cooling system design with an improved thermal performance by studying the effects of various design parameters on the heat exchanger performance. These parameters include thermosyphon volume, cooling gas tank (reservoir) volume, the initial reservoir pressure and operating reservoir temperature, type

of working fluid, the tube wall thickness of the thermosyphon, length of the evaporator and condenser section, and the type and performance characteristics of the cryorefrigeration system (Heat Sink) are the major ones. These parameters directly determine the upper limits of the thermosyphon working temperature, the heat flux ranges and the overall thermal resistance between the evaporator (Moderator) and condenser (Cold head).

1.5 Organization of the Thesis

The introductory and the objective part of this thesis are covered in the current chapter. In chapter 2 a background summary of thermosyphon heat exchangers and a literature review regarding past works on TPCT is discussed. In Chapter 3 the operating principle of closed two phase thermosyphon with reservoir (TPCTR) is discussed. The discussion focuses on the thermosyphon that is used in the TCNS cooling system. In Chapter 4 a thermodynamic analysis of TPCTR is presented. The effects of various thermo-physical and geometric parameters on the performance of such thermosyphons are explored. In Chapter 5 the various heat transfers that occur in the thermosyphon heat exchanger is discussed and the result of the analysis is discussed. In Chapter 6 CFD analysis of natural convection and nucleate boiling heat transfer analysis over a heated plate is carried out using commercial CFD code FLUENT. The result will be used in refining the heat transfer analysis carried out in Chapter 5. In Chapter 7 an overall conclusion and recommendation for a new TPCTR is presented based on the results of all

the preceding analysis. This includes possible future work that extends the current research findings is presented.

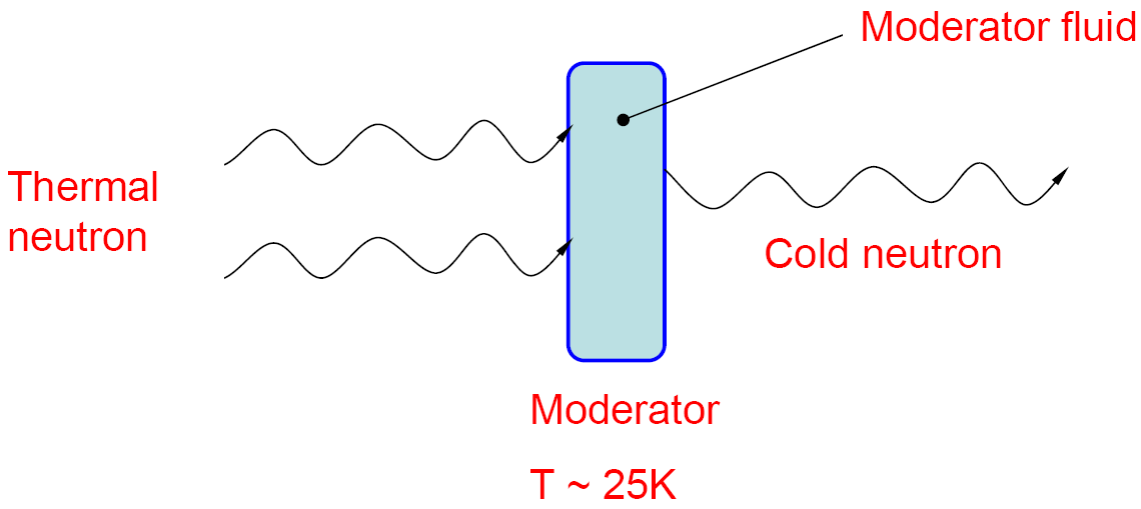

Figure **1-1**: Schematic showing generation of cold neutrons by passing thermal neutrons through cooled moderator

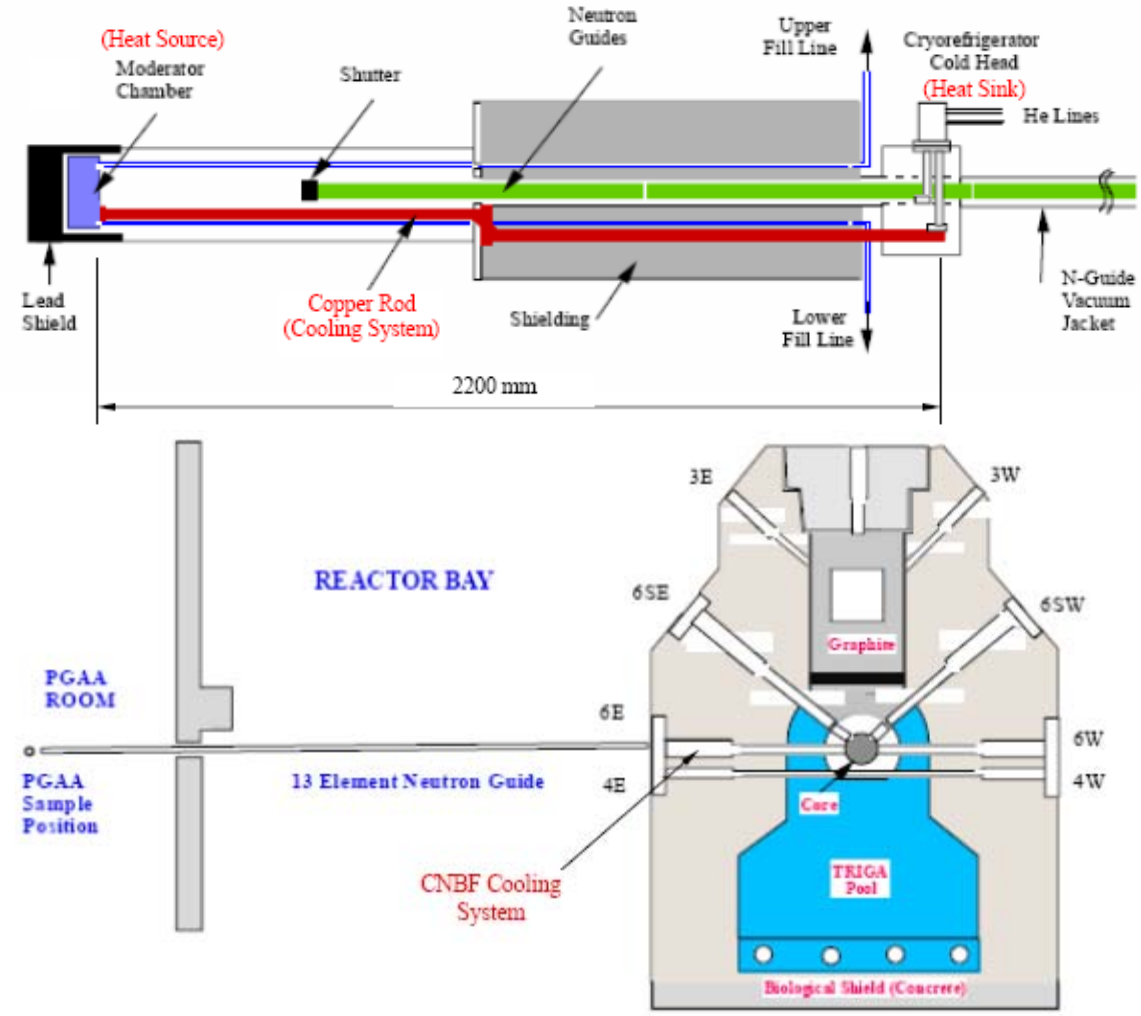

Figure **1-2**: Top: schematic showing the detail of the CNBF cooling system. Bottom: Schematic of CNBF layout [**Unlu et al 1994**]

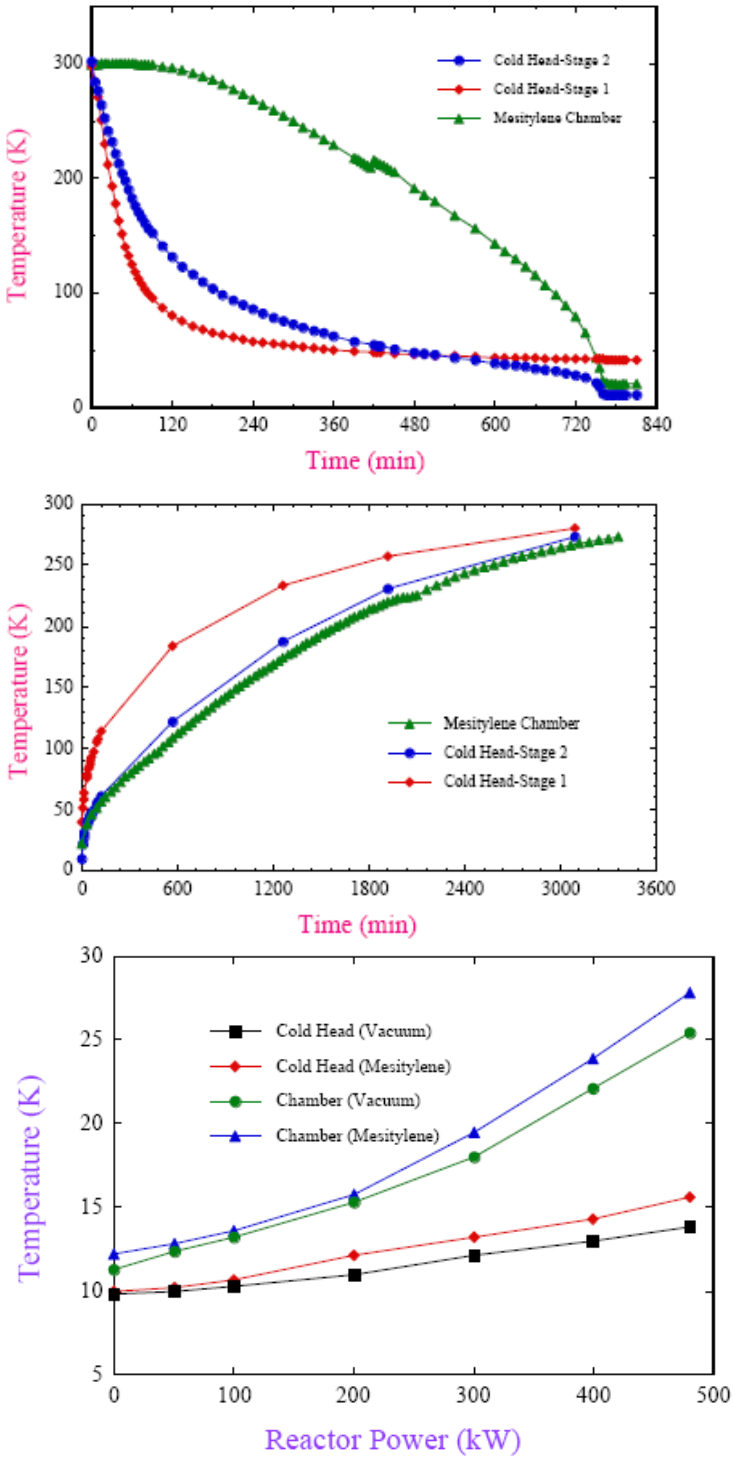

Figure **1-3**: Plots showing measured temperatures of moderator and cold head of the CNBF cooling system[**Unlu et al 1994**]

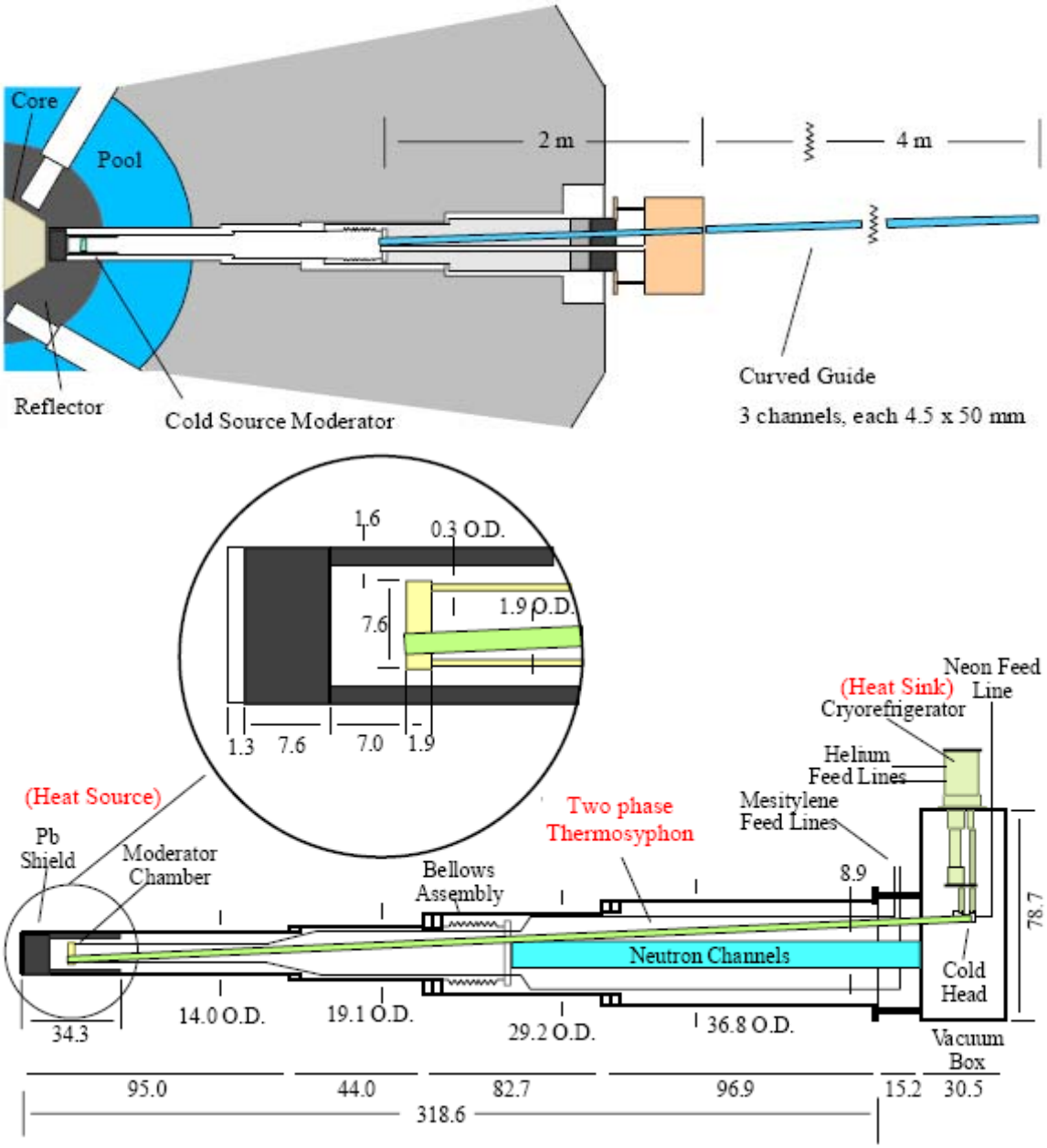

Texas Cold Neutron Source (dimensions are given in cm).

Figure **1-4**: Top: Schematic layout of the TCNS. Bottom: The detail schematic diagram of the TCNS cooling system showing the two-phase thermosyphon and moderator [**Unlu et al 1995**]

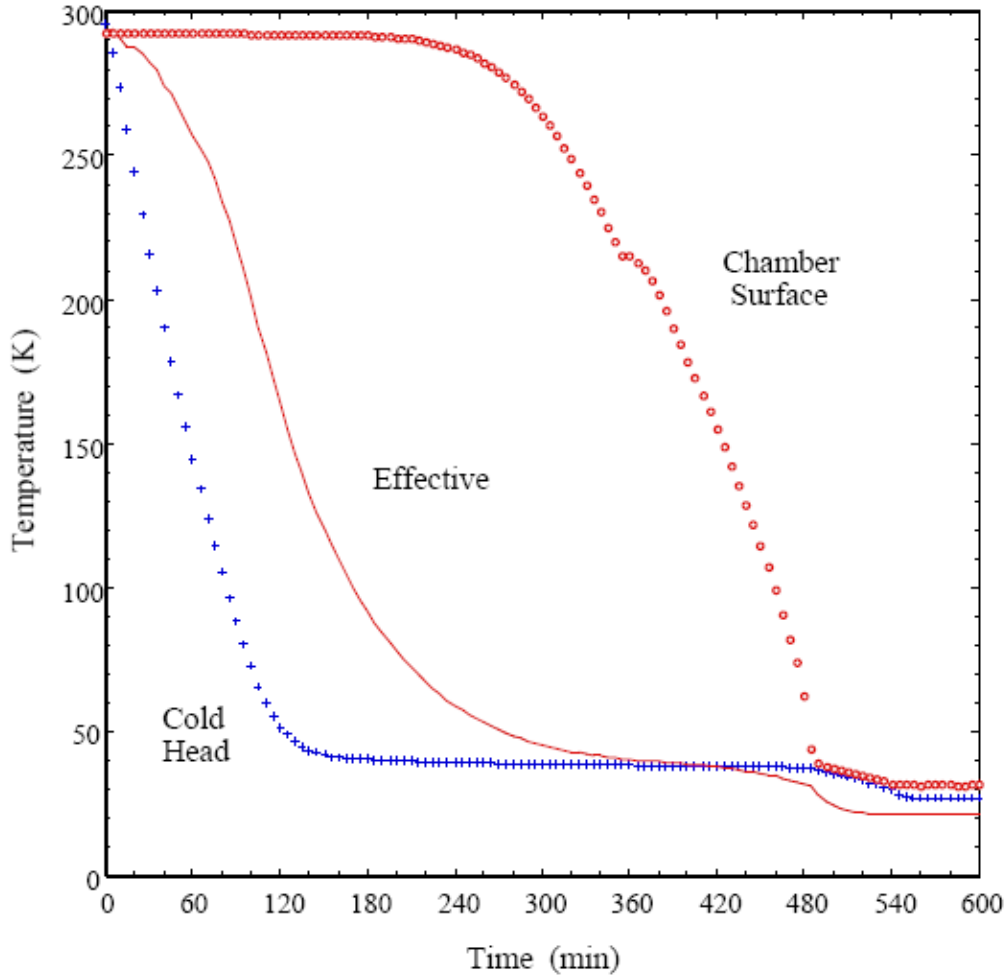

Figure **1-5**: Plot showing temperature history of the TCNS cooling system during cooldown [**Unlu et al 1995**]

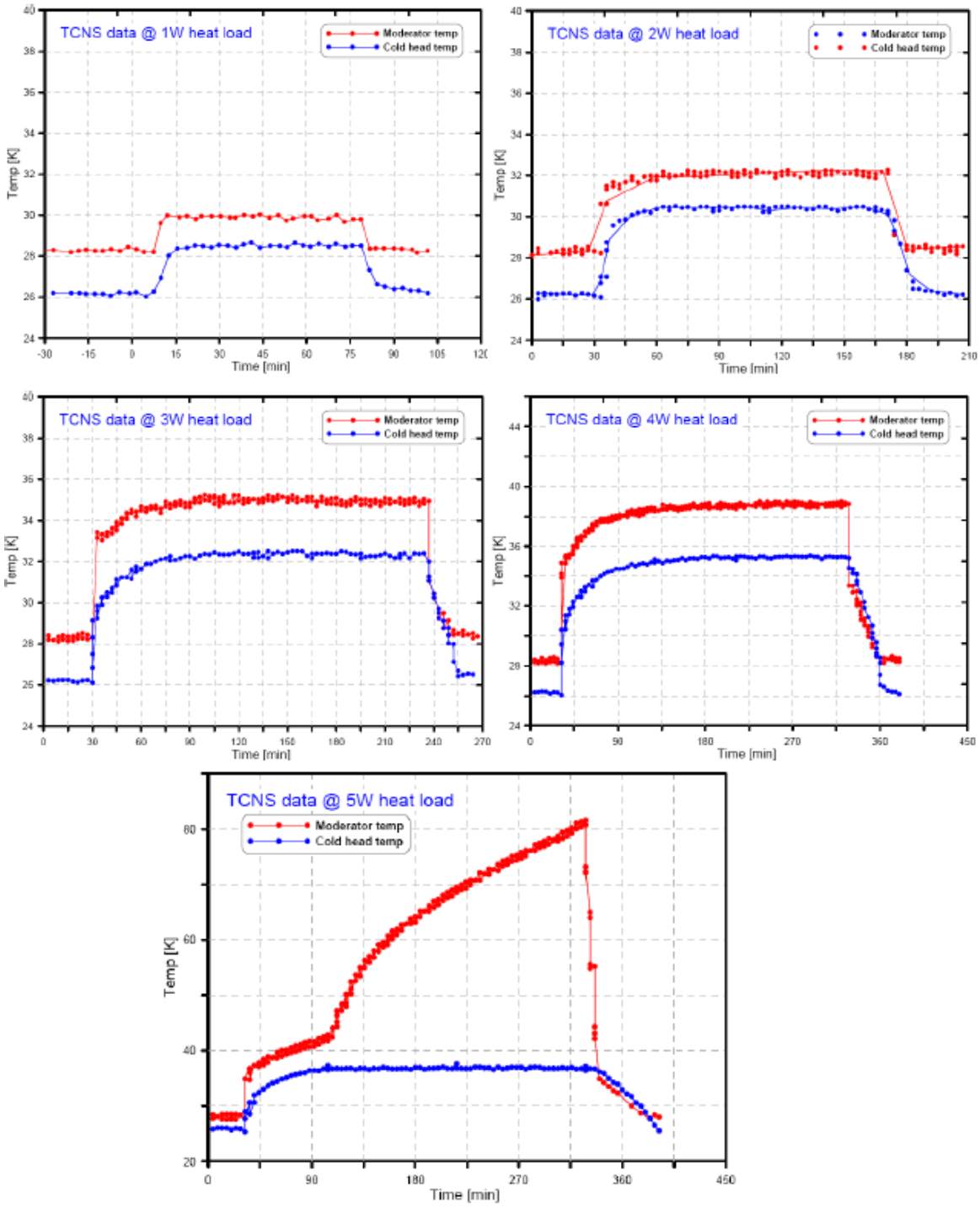

Figure **1-6**: Performance plot of the TCNS showing temperature history of evaporator (Moderator) and condenser (cold head) at 1 – 5W heat loads. At 5W heat load cooling fails[**Unlu et al 1994**]

Chapter 2

Literature Review

In this chapter a background introduction of thermosyphons and heat pipes is presented. Most of the discussions about heat pipes can also be applied to thermosyphons in that heat pipes are in fact thermosyphons with a wick material inside the tube. The two heat exchanger devices are very similar in design and operation. This discussion gives a general perspective about the operation and design aspects of two devices. Next, a review of past studies conducted by others specifically on two phase closed thermosyphons (TPCT) is presented. Finally the scope of this research is described.

2.1 Background and Historical Development

The concept of thermosyphons was first introduced in the mid-1800s by A. M. Perkins and J. Perkins [**Peterson-1994**]. These were patented works focused on devices referred to us Perkins tube as shown in Figure **2-1**, utilized either single phase or two phase processes to transfer heat from a furnace to a boiler. This device laid the ground work for the later development of thermosyphons and heat pipes [**Peterson-1994**].

A heat pipe typically consists of a sealed container lined with a wicking material as shown in Figure **2-2** . Basically, a thermosyphon is a heat pipe without the wick inside the tube. The container is first evacuated and filled with the working fluid. The working

fluid will remain at the saturated condition as long as the operating temperature is between the triple point and the critical state. Thermosyphons and heat pipes consist of three distinct regions: an evaporator or heat addition region, condenser or heat rejection region, and an adiabatic or isothermal region as indicated in Figure **2-2** . In the case of heat pipes, when heat is applied to the evaporator region of the container, the working fluid present in the wicking structure is heated until it vaporizes. The high temperature and corresponding high pressure in this region cause the vapor to the cooler condenser region, where the vapor condenses, giving up its latent heat of vaporization. The capillary forces existing in the wick then pump the liquid back to the evaporator. The most important difference between closed two-phase thermosyphon and a heat pipe is that thermosyphon uses gravity to return condensed liquid back to the evaporator instead of the wick as in heat pipes. The concept of heat pipe as a part of a passive two-phase heat transfer device capable of transferring large quantities of heat with minimal temperature drop was first introduced by Gaugler [**Peterson-1994**].

Thermosyphons or heat pipes can be constructed from glass, ceramics, or metals. In the case of heat pipes the wicking structure can be woven fiberglass, sintered metal powders, screens, wire meshes or grooves. The working fluid varies from nitrogen or helium for low temperatures (cryogenic ~10K – 100 K) to lithium, potassium, or sodium for high temperature applications (~ 1000sK). The container material must be compatible with both the working fluid, the wicking structure (heat pipes), strong enough to withstand the pressures associated with the saturation temperatures encountered during storage and normal operation, ad must have high thermal conductivity. In addition to these characteristics, which are primarily concerned with the internal effects, the

container material must be resistant to corrosion resulting from interaction with the environment and must be malleable enough to be formed into the appropriate size and shape.

2.1.1 Working Fluids

Because of the basis of operation of heat pipes and thermosyphons is the vaporization and condensation of the working fluid, selection of a suitable fluid is an important factor in design and manufacture process. Care must be taken to ensure the operating temperature range is adequate for the application. While most applications involving the use of heat pipes in the thermal control of electronic devices and systems require the use of a working fluid with the boiling temperatures between 250 and 350K, both cryogenic heat pipes (operating in the 5 to 100K temperature range) and liquid metal heat pipes (operating in the 750 to 5000K temperature range) have also been developed and used. Figure **2-3** illustrates the possible temperature ranges for some of the various heat pipe fluids.

2.1.2 Fundamental Operating Principles of Thermosyphons

Both heat pipes and thermosyphons operate on a closed two-phase cycle and utilize the latent heat of vaporization to transfer heat with very small temperature gradients. As mentioned in previous section, the operation of the two devices is significantly different. Heat added at the bottom portion of a thermosyphon (evaporator –

always located below the condenser section) vaporizes the working fluid. During this operation the fluid picks up heat associated with its latent heat of vaporization. Because the vapor in the evaporator section is at a higher temperature and hence at a lower density than the vapor in the condenser, the vapor rises due to buoyancy and flows to the cooler condenser where it gives up the latent heat of vaporization. Gravitational forces then cause the condensate film to flow back down the inside of the thermosyphon wall where it can again be vaporized.

Alternatively, heat pipes utilize capillary force assisted by wick material inside the tube to promote the flow of liquid from the condenser to the evaporator and as a result can be used in horizontal, microgravity, or even applications where the capillary structure must "pump" the liquid against gravity from the evaporator to the condenser. It is this single characteristic – the dependence of local and gravitational field to promote the flow of liquid from the condenser to the evaporator- that differentiates thermosyphons from heat pipes [**Peterson-1994**].

2.1.3 Advantages and Limitations on Heat Transfer Capacity

Several unique characteristics of thermosyphons and heat pipes make them useful over wide variety of applications. First, because of the fact that heat pipes and thermosyphons operate on closed two-phase cycle, the heat transfer capacity may be of several magnitude greater than even the best solid conductors. This results in a small thermal resistance and allows physical separation of the evaporator and condenser without a high penalty of overall temperature drop. Second, increase in the heat flux in

the evaporator may result in an increase in the rate at which the working fluid is vaporized, without a significant increase in the operating temperature. Thus the heat pipe can function as a nearly isothermal device, adjusting the evaporation rate to accommodate a wide range of power inputs while maintaining a relatively constant source temperature. Third, the evaporator and condenser portions function independently needing only a common liquid and vapor stream; for this reason the area over which heat is introduced can differ in size and shape from the area over which it is rejected, provided that the rate at which liquid is vaporized does not exceed the rate at which it can be condensed. Hence, high heat fluxes generated over relatively small areas can be dissipated over large areas with reduced heat fluxes. This is particularly useful in thermal control of electronic components and systems, because it allows the high heat flux generated at the component level to be reduced and allows free or forced convection to be used to dissipate the heat. One additional advantage of heat pipes and thermosyphons is the relative short thermal response time as compared to other types of heat transfer devices, particularly solid conductors and is not a function of length. This is because of the fact that these devices utilize the closed two-phase cycle. Heat pipes unlike thermosyphons are better suited to applications in reduced gravity environments such as space applications since it utilizes capillary action to return liquid from the condenser [**Peterson-1994**].

2.1.4 Effective Thermal Resistance

Because thermosyphons and heat pipes utilize the latent heat of vaporization of the working fluid as opposed to the sensible heat, the required temperature difference is small, and hence effective thermal conductivity may be several orders of magnitude greater than that of even the best solid conductors. For example assume that it is necessary to transfer a 20W thermal energy over a distance of 0.5m in a device 1.75cm in diameter. As shown in Figure **2-4** using a simple Fourier's law, a solid aluminum rod would result in a temperature difference of approximately $460^{O}\mathrm{C}$. A solid copper rod would result in a temperature difference of $206^{O}\mathrm{C}$, while use of a simple copper-water heat pipe with a screen wick could result in a temperature difference between the external evaporator and condenser surfaces of only $6^{O}\mathrm{C}$.

2.2 Previous Studies

One of the early studies on closed two-phase thermosyphons was the experimental studies of [**Shiraishi et al 1981**] that investigated the heat transfer characteristics and effects of parameters such as filling ratio (fraction of liquid volume to that of evaporator), working fluid, working temperature and heat flux. The study was conducted using Freon, water and ethanol as working fluids on a vertical two-phase closed thermosyphon. To model the heat transfer in the condenser, the Nusselt flat plate film condensation theory [**Carey-2008**] was used assuming laminar film to exist inside the tube and justifying that the radius of curvature was large as compared to the film

thickness. They noted that modeling of the evaporator section was complex and they developed an empirical correlation from their experimental data to include the effect of the working pressure inside the thermosyphon. The correlation was developed based on an earlier study by [**Kusuda et al 1973**] on boiling heat transfer coefficient in evaporator of open thermosyphon. The result showed a good correlation in predicting their experimental data of thermal resistance and heat transfer rate of the thermosyphon. The effect of variation of hydrostatic pressure in determining the inside pressure the thermosyphon seems to be significant in their correlation. Their result shows that at a given heat flux the thermal resistance increases as the filling ratio increases. It also shows that thermal resistance of the thermosyphon decreases as the heat flux increases.

The study of [**Dobran et al 1988**] on two phase closed thermosyphon involves both experimental work and analytical modeling. The experimental investigation was carried out on a 5.5 m long and 32mm diameter thermosyphon. The evaporator and condenser sections were 1.4 m and 0.54 m long respectively. The test was conducted using R-11 as a working fluid. Both sections were designed separate to the main thermosyphon tube to accommodate for heat exchange with the applied boundary conditions to the evaporator and condenser ends. The main purpose of the experiment was to study the operational limits of the thermosyphon. The study was conducted by varying the temperature difference between the evaporator and condenser sections. The study showed that an increase of this temperature difference produced at first a maximum heat transfer rate identified with the flooding heat transfer limit. Beyond this point the thermosyphon operation reverted to a different steady state condition producing a lower heat transfer capacity. The study concluded that this condition was attributed to the

simultaneous existence of: 1) a new flooding state near or at the exit of the adiabatic section, and 2) the dryout in the evaporator resulting from the transfer of liquid in the evaporator pool to the condenser during the transient process which leads to thermal blocking condition. The term thermal blocking was defined as a limit in the amount of heat transfer capacity of the thermosyphon beyond which an increase in the temperature difference between the evaporator and condenser sections would result in no change in heat transfer. Analytical model was developed to study the limiting operational modes of the thermosyphon. The model fairly predicted their experimental data prior and post thermal blocking conditions [**Dobran et al 1988**].

Experimental study conducted by [**Luck et al 1989**] shows the effect of geometry on the performance of closed tube thermosyphon. The tests were conducted using air and water as a working fluid. This study was single phase laminar flow with low Rayleigh number. The tests were conducted with an average temperature difference between the evaporator and condenser of 4 K. Three different flow patterns were identified. The effect of geometry was studied in terms of heated-cooled length ratio and heated length-diameter ratio. It was found that the former ratio proved to have a weak monotonic effect. The heated length-diameter ratio was found to have a much stronger effect, exhibited in two ways. Firstly, the location of the transitional Rayleigh number range was lowered as heated length-diameter ratio is increased. Secondly, the Nusselt number decreased as heated length-diameter increased [**Luck et al 1989**]. Although this study is focused on single phase flow, it is important to point out that the flow pattern inside the thermosyphon depends on the temperature difference between evaporator and condenser sections.

The boiling regime in two-phase closed thermosyphon was studied experimentally and analytic correlations were developed by [**Niro et al 1990**]. The study pointed out that closed two-phase thermosyphons can operate in two different ways depending on fluid filling: the falling-film evaporation mode for small fillings (liquid volume less than about 10% of evaporator volume), and pool boiling for medium and large fillings (from 30 to 100% and over of the evaporator volume). For the falling-film evaporation mode all the thermosyphon walls are wetted by continuous liquid film which is stable for only very low heat loads. Whereas in the pool boiling mode the thermosyphon evaporator is flooded and boiling is sustained over wide range of operating fluids and conditions, and allows a higher heat load. The existence of instabilities and unsteady regimes must be avoided to maintain optimal performance of thermosyphons. Unsteady regimes can cause large-amplitude oscillations in evaporator wall temperature that may exceed design values. A detailed discussion of bubble formation and growth during boiling was given. Distinction between fully developed and intermittent boiling frontier was discussed based on bubble waiting time and growth time. The paper also suggested analytical method of determining bubble waiting time and growth time.

The experimental study conducted by [**Lock et al 1992**] investigated the heat transfer in single-phase flow in an inclined thermosyphon. The test was conducted at various inclination angles ranging from 0 to 90 degrees. The result shows that the flow mechanism inside the thermosyphon to be complex. In the vertical position the main flow seems to be axisymmetric counter flow system except in the mid height region where the flow mirrors the lower half. But in the inclined case, the axisymmetry of the flow disappears, producing secondary flows at the bottom and top of the thermosyphon. This

study suggests that the heat transfer rate increases as the inclination angle of the thermosyphon decreases from the vertical: maximum heat transfer rate occurs when the thermosyphon is near horizontal and minimum when it is in the vertical position. This was explained due to the effect of body force due to gravity, for the flow inside the thermosyphon start having two components that equally affect the heat transfer.

Operational envelope for two phase closed vertical thermosyphons was studied by [**ElGenk et al 1998(1)**]. The main focus of their study revolves around prediction of the limits of initial filling ratio. They developed a mathematical model to determine the limits of operation of the thermosyphon in terms of filling ratio and amount of heat throughput. They determined the dryout limit based on the condition when the liquid film from the adiabatic section stretches and flows into the evaporator section reaching a critical thickness where it can no longer reach the liquid pool in the evaporator. This was the criteria used to set the lower boundary of the operational envelop. They set the upper boundary based on the condition that the liquid pool, upon heat addition, expands and reaches the end of the evaporator section thereby reducing the thermal conductance of the thermosyphon. They noted that the film evaporation heat transfer coefficient is an order of magnitude high than that of boiling. The third limit of operation was the critical counter flooding limit that prevents the liquid not to reach the evaporator section independent of initial filling ratio. They carried out some parametric study to see the effect of vapor temperature and working fluid. In order to calculate the liquid pool height they used a semi empirical correlation developed by [**Jialun et al 1992**].

The study conducted by [**Tredtoon et al 2000**] investigated the effect of dimensionless numbers such as Bond number, Froude number, Weber number and

Kutateladze numbers on heat transfer characteristics of closed two-phase thermosyphon. The experimental study was conducted on three copper thermosyphons of 7.5, 11 and 25.4mm inside diameters. They employed working fluids of refrigerants R22, R123, R134a, ethanol and water for the tests. Their tests were conducted on filling ratios of 50, 80 and 100% of the evaporator volume and with aspect ratios (length of evaporator to tube diameter) of 5 – 40. The tests were conducted by varying the inclination angle ranging from horizontal axis to vertical. Their result suggests that the heat transfer was not affected by the filling ratio but the working fluid properties did affect it. They also found that lower latent heat of vaporization seems to increase the heat transfer rate. The result also suggests that the Webber number, Froude number and Bond numbers had no relationship with the heat transfer rate. However there appears to be some correlation between Kutateladze number and heat transfer rate that fit their experimental data. They developed a similar correlation for the maximum thermal resistance. In all the tests the result shows that a maximum heat transfer occurs when the inclination is around 45 degrees from the horizontal.

A more recent work by [**Khandekar et al 2007**] focused on effects of nano-fluids on thermal performance of two-phase closed thermosyphon. Basically nano-fluids are fluids such as water used in ordinary thermal devices with addition of nano particles of high thermal conductivity solids such as copper. The purpose is to increase the thermal performance by altering the thermal conductivity of the fluid. Their result showed that the single phase heat transfer rate has shown a significant improvement while the two-phase heat transfer resulted in having the reverse effect by increasing the overall thermal

resistance of the thermosyphon. This was especially due to the fact that the active nucleation sites in the case of nucleate boiling being blocked by the nano particles.

Another recent mathematical model was developed to predict the effect of filling ratio on the heat transfer performance of closed thermosyphon by [**Jiao et al 2007**]. This study classifies the filling ratios in relation to the flow regimes that would exist in the thermosyphon. They noted five scenarios of the film flow on the inside wall of the tube and the liquid pool at the bottom of the vertical thermosyphon based on the filling ratio. Rohsenow correlation for nucleate boiling at pool in the evaporator is used. In order to calculate the heat transfer at the condenser and film evaporation they assumed a 2D laminar flow and made a Nusselt type of formulation. Their model predicts the experimental heat transfer data well. Although their model doesn't show prediction for operating pressure, the experimental data shows no effect of filling ratio at a given heat input. At this point it is important to point out that the range of filling ratio considered in the experiment is from 13 – 20%. This may not be sufficient to draw conclusion on the operating pressure. The experimental data show an increase in operation pressure with heat input as might be expected, although there was no explicit prediction for pressure in the mathematical model. In their experimental data they found out that the critical fill ratio (the minimum liquid pool that exists just before dryout occurs) is around 9%. However the model predicts an inverse relationship between heat input and critical fill ratio.

2.3 Objectives of Current Study

The main focus of the current research is to carry out fundamental thermodynamic and heat transfer analysis using analytic models, make a parametric study of the major factors affecting the thermal performance and carry out CFD analysis of a two phase closed thermosyphon with reservoir (TPCTR). The thermosyphon considered for this purpose is that of TCNS cooling system described in the previous section. The study investigates the effects of the various thermo-physical and geometrical parameters on the thermal performance limit of the thermosyphon and suggest the optimum design parameters that can enable the TPCTR handle heat loads of up to 10W.

All the previous studies discussed above have taken parameters such as the ratio of volume of liquid to volume of evaporator section of TPCT (fill ratio FR), evaporator length to tube diameter ratio, and inclination angle θ as main parameters of the thermosyphon. The thermosyphons considered in past works are also isolated from their gas reservoirs once they are filled with the working fluid. The presence of the reservoir affects the thermal performance of the thermosyphon. In this study the main parameters that are considered are: ratio of gas reservoir volume to thermosyphon volume (defined as volume ratio η), initial fill ratio FR_O, inclination angle of the thermosyphon θ, initial pressure of the thermosyphon P_O and temperature of the reservoir T_∞. In closed two phase thermosyphon with reservoir (TPCTR), the vapor from the thermosyphon can freely flow back and forth into the reservoir and hence the mass of liquid and vapor in the thermosyphon continuously changes depending on the heat load. This affects the fill ratio, the pressure and temperature inside the thermosyphon. Hence the analysis will

further expand the fundamental understanding of the working principles of TPCTR. The analytic evaluation of the heat transfer in the evaporator is further refined by carrying out CFD analysis. This involves modeling the nucleate boiling two phase heat transfer in the evaporator. The CFD analysis result will be used to validate and optimize the analytic thermal performance result of the thermosyphon.

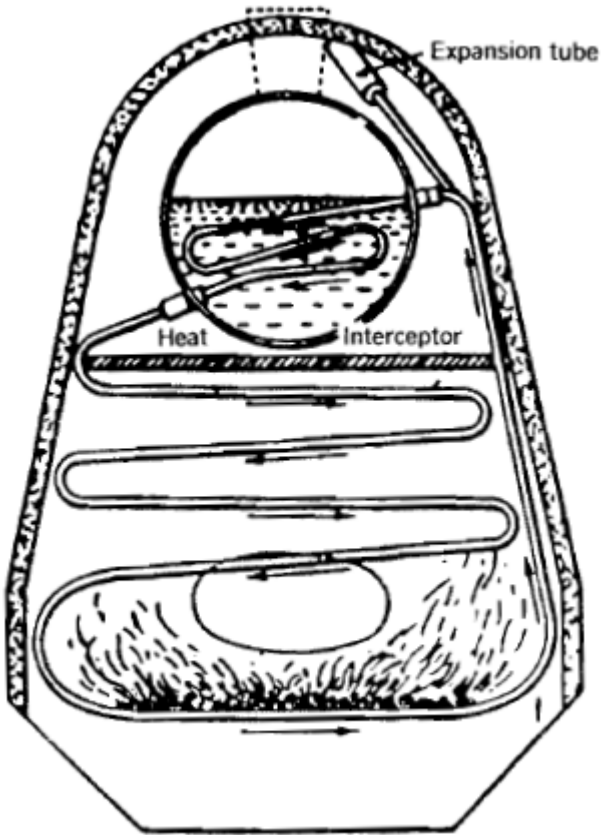

Figure **2-1**: An early example of Perkins tube[**Peterson-1994**]

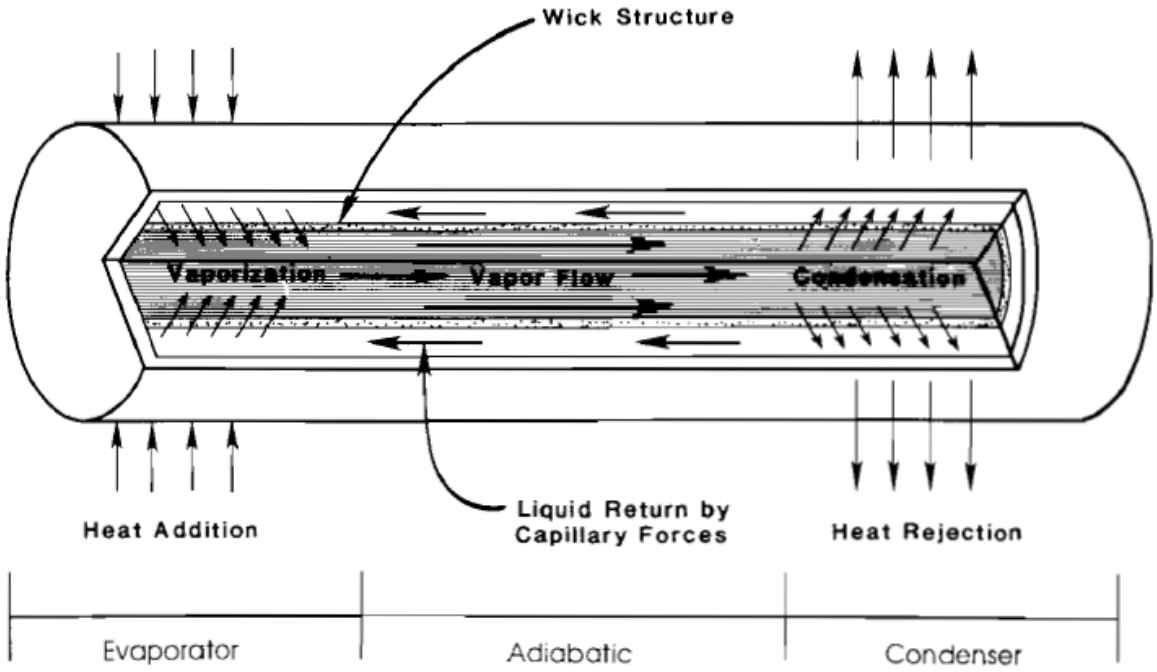

Figure **2-2**: Typical heat pipe structure and operation[**Peterson-1994**]

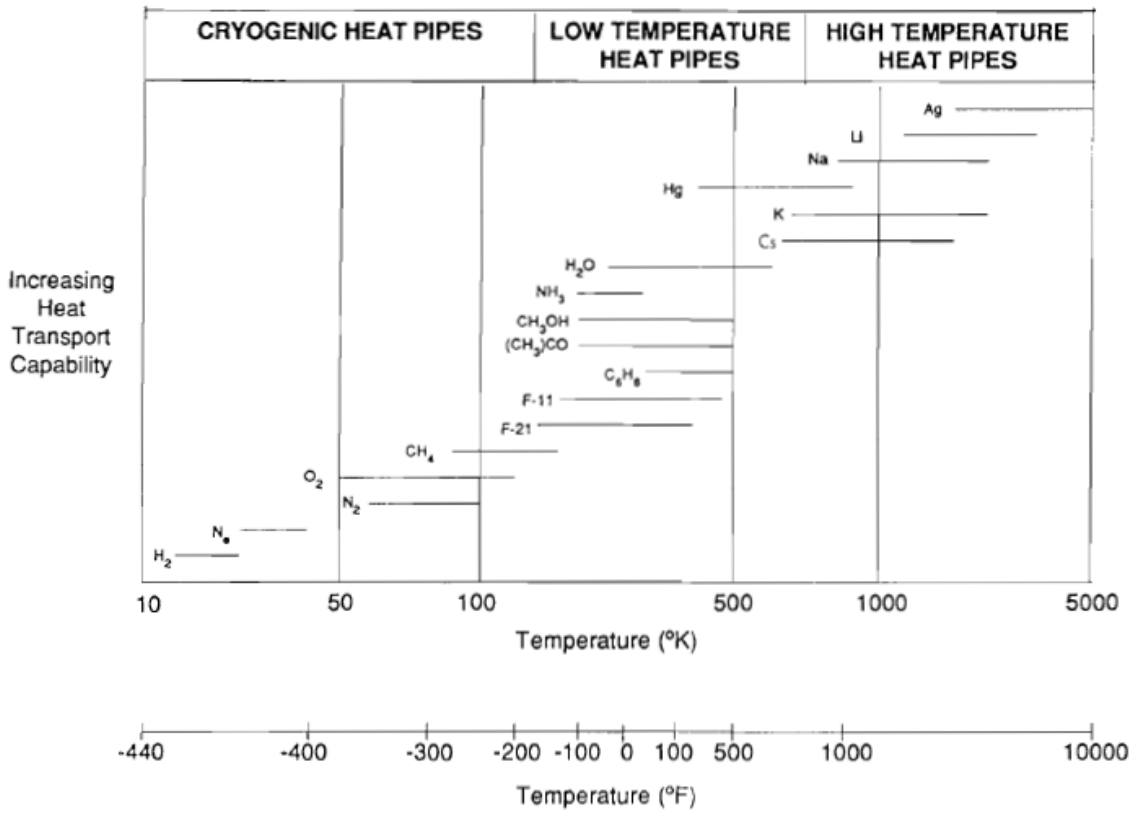

Figure **2-3**: Possible temperature ranges for some of the various working fluids for thermosyphon [**Peterson-1994**]

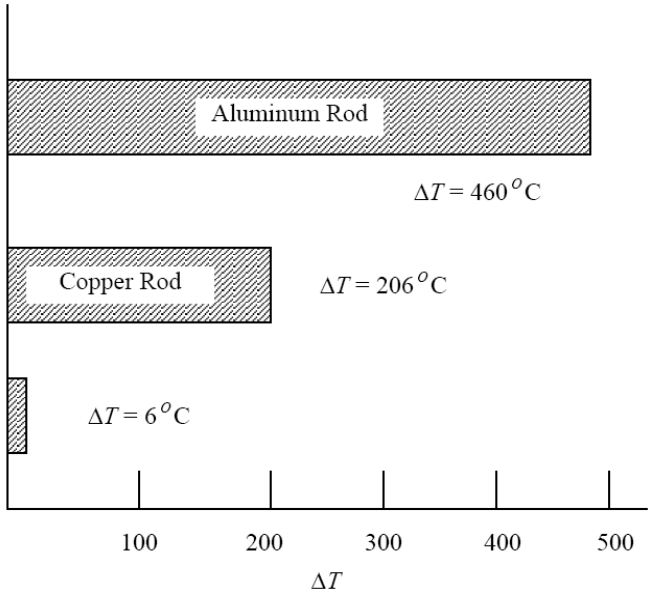

Figure **2-4**: Comparison of heat pipes and solid conductors [**Peterson-1994**]

Chapter 3

Operating Principles of the TCNS Closed Two Phase Thermosyphon Cooling System

In this section the various operating parts of the TCNS closed two phase thermosyphon heat exchanger is discussed. As it is discussed in the previous chapter the focus of this study is mainly directed towards the TCNS cooling system. Unlike an isolated thermosyphon, the discussion focuses on the operation of closed two phase thermosyphon with reservoir (TPCTR) containing the working fluid connected to it. This system is chosen since it was implemented in the TCNS cooling system. The operating conditions and the various modes of heat transfer of each of the sections are explained.

3.1 Major Parts of Closed Two Phase Thermosyphon with Reservoir (TPCTR)

Closed two phase thermosyphon is a heat exchanger device similar to heat pipes but without a wick material inside the tube. The most important difference between closed two phase thermosyphones (TPCT) and heat pipes is that in the case of thermosyphon the condensate is returned back to the evaporator due to gravity while that on the heat pipes is due to capillary action through the wick material. Figure **3-1** shows the essential parts of closed two phase thermosyphon with reservoir (TPCTR). In the case of TCNS thermosyphon, neon gas is used as a working fluid. The thermosyphon is made of aluminum of 3.37m long and 19mm outside diameter with 1.6mm wall thickness. The

reservoir, which has a volume of 6.5 liter, is connected to the thermosyphon by a 3.2 mm diameter steel pipe providing the necessary gas to be condensed in the condenser section depending on the heat load. The cryorefrigerator provides the primary cooling by attaching it to the cold end of the thermosyphon. The moderator that is to be cooled is attached at the evaporator end of the thermosyphon as shown Figure **3-1** . The moderator end is section of the TPCTR where the heat removal by evaporation and boiling process takes place. The detailed description of each of the various heat transfer sections are discussed in the following sections.

3.1.1 Evaporator Section of the Thermosyphon

This is the section of the thermosyphon where the heat load from the moderator end is applied through the moderator chamber to the thermosyphon. The moderator itself contains fluid through which the neutron beam passes. This section is the lower tip of the thermosyphon and is 19mm in length. The moderator fluid in the case of TCNS cooling system was mesitylene. The mesitylene in the moderator flows through the moderator chamber and is separately cooled by a different cooling system. As the neutron beam passes through the moderator it looses its thermal energy to the moderator fluid and becomes cold neutron beam. The moderator fluid in turn transfers this heat to the evaporator section of the thermosyphon. The detailed parts of the evaporator end are shown in Figure **3-2**. The condensed liquid from the condenser section flows down along the length of the inner wall of thermosyphon. Once it reaches the evaporator end, where it boils or evaporates depending on the heat load, and return to the condenser section as a

vapor where it condenses and returns back to the moderator end again. The evaporation and/or boiling process removes the heat load that comes from the moderator chamber and moderator fluid by conduction radially through the thermosyphon wall into the condensed liquid pool in the evaporator end. The heat then passes from the inside wall of the evaporator section to the liquid pool causing evaporation or boiling depending the on the amount of heat flux. As it is discussed in the introduction section the evaporation/boiling phase change process is capable of removing large amount of heat. This gives the most important advantage to the thermosyphon heat exchangers. As the heat load from the moderator increases, the heat transfer mechanism in the evaporator changes from natural convection at very small heat loads to nucleate boiling at higher heat flux. As the heat flux increased further and passes the critical heat flux, the heat transfer rate from the moderator deteriorates because of either of the following two reasons. One is that the liquid level inside the thermosyphon drops and eventually dryout occurs. At higher heat loads the primary refrigeration system (heat sink - cryorefrigerator) operation characteristics is such that the condenser temperature increases proportionally as the heat load is increased as shown in Figure **3-4** . As a result of this the saturation temperature inside the thermosyphon will increase. This results in a corresponding increase of evaporator wall temperature. When the evaporator wall temperature reaches the critical saturation temperature for the given initial pressure and temperature of the system, the rate of evaporation and/or boiling exceeds that of condensation and eventually there will be no liquid present at the evaporator section. The second reason could be that instead of nucleate boiling there could be film boiling due to increased heat flux while still having liquid pool. Either of the two cases leads to a lower

convective heat transfer coefficient there by increasing the overall thermal resistance of the thermosyphon. When the liquid dryout occurs the heat transfer process relies on only pure conduction instead of due to phase change. This will cause the evaporator temperature to continuously rise until the temperature difference between the evaporator and condenser sections reach a new steady value sufficient to carry the heat load axially by conduction through the solid wall with a much larger thermal resistance. This was the fundamental problem that was observed in the TCNS cooling system when the heat load was increased above 4W [**Unlu et al 1994**].

3.1.2 Adiabatic Section

This section is the longest part of the thermosyphon between the evaporator and the condenser ends. In this section is the insulated part of TPCTs and the only heat transfer from the outside of the thermosyphon is due to radiation (if no proper insulation is provided). If properly insulated, it can be considered as an adiabatic system. The condensed vapor from the condenser flows due to gravity along this section to reach the evaporator end. A fraction of the heat load from the evaporator end and radiation from the surrounding of the thermosyphon flows through the wall of this section to the condenser end. This section allows the thermosyphon to operate efficiently between the condenser and evaporator sections separated by a very long distance, 3.35m long in the case of TCNS.

3.1.3 Condenser Section

This is the section of the thermosyphon where heat that is applied at the evaporator end is transfer to the cryorefrigerator, called “cold head” in this study, by the process of condensation. It is located at the upper tip of the thermosyphon and is of 50mm in length. The vapor that is formed at the evaporator flows up the thermosyphon tube through the adiabatic section and condenses on the inside wall of the condenser section. The condensate then flows back to the evaporator removing the heat load and hence completes the cycle. The cryorefrigerator acts as a heat sink. In the TCNS cooling system a Cryomech GP40 cryocooler was used [**Unlu et al 1994**]. Figure **3-3** shows schematic diagram of the condenser section of the thermosyphon. The heat sink (cryorefrigerator) is attached to the outside surface of the condenser section. The heat released from the thermosyphon during condensation and any heat leak that comes from radiation through the adiabatic wall by conduction is transferred through the condenser wall to the heat sink cryorefrigerator by conduction. The end of the condenser is attached to a small tube that connects the thermosyphon to the gas reservoir that is kept at room temperature, as in the case of TCNS system. The temperature of the cold head is proportional to the heat load as described earlier and shown in Figure **3-4** .

3.2 Operating Principles of Closed Two Phase Thermosyphon with Reservoir (TPCTR)

The steady state operation of TPCTR depends mainly on the amount of heat load. At normal operation, the cryorefrigeration unit removes a given amount of heat load at a

proportional cold head temperature. This is usually determined by the manufacturer of the cryocooler or any primary cooling system (heat sink) as a specification for the particular system. In general as the operating heat load increases the cold head temperature also increases which in turn determines the operating condenser and evaporator temperatures. Figure **3-4** shows the performance curve of the TCNS cryocooler. As can be seen from Figure **3-4** the cold head temperature increases linearly with the cooling power. As an example the cryocooler delivers a cooling power of 13W at a cold head temperature of 24K. If the heat load is further increased, the cold head temperature increases accordingly. The performance curve shown in Figure **3-4** is extrapolated from the data obtained in the performance curve manual of the Cryomech cryocooler [**Cryomech-Inc 2008**]. The characteristic angle α is an important parameter as it is explained in the next chapters as an important parameter determining the maximum capacity of the TPCTR.

3.2.1 Cool down process

The cool down process is a transient heat transfer process in which the entire thermosyphon is brought from room temperature to a steady state operating condition at a given heat load. The process can be categorized into three major stages. In stage-I the process starts with the cold head (condenser section) temperature decreasing as heat starts to be removed from the condenser end by the cryocooler as shown in Figure **3-5** . In the case of the TCNS cooling system the cold head takes about 150 minutes, starting from room temperature and pressure of 10 atm, to reach below the saturation temperature

37.3K of the working fluid (Neon) at the prevailing pressure of about 1 MPa. Up to this time there will be no liquid accumulation at the evaporator end. When the inside wall temperature of the condenser drops just below the saturation temperature of 37.3K for the given initial pressure, condensation starts and liquid neon forms on the inside wall. This marks the beginning of stage-II of the cooldown process as shown in Figure **3-5** . Further heat removal results in a small temperature drop in the condenser but more and more liquid forms and eventually starts to flow down along the inside wall of the thermosyphon due to gravity. The thermosyphon of the TCNS cooling system has an inclination angle of 2.5^{o}. Upon further condensation, the liquid film starts to flow downwards along the inside walls of the thermosyphon tube and accumulates at the bottom of the condenser section. The condensate then flows along the bottom wall down to the evaporator section. As the liquid film flows along the inside wall of the tube, the wall temperature of the thermosyphon is brought to the cold head temperature due to the fact that the wall undergoes a transient cooling process as a result of the evaporation of the cold liquid film front. This stage is characterized by simultaneous condensation at the cold head and evaporation as the liquid film front moves down the pipe. The cold liquid film front is continuously being supplied by the condensate that forms at the cold head. This continuous evaporation of liquid film front and condensation of vapor from the evaporator at the cold head nearly balance each other until the entire thermosyphon wall is brought to near the cold head temperature. This process takes the first 450 minutes for the TCNS cooling system. This marks the beginning of stage-III of the cooldown process as shown in Figure **3-5** . At this time the evaporation of the film front will be negligible if there is no heat load in the evaporator section. The condensation process still continues

and the net effect will produce more and more liquid to accumulate at bottom of the evaporator section. This stage is characterized by a very sharp drop in the system overall pressure. This is due to the fact that the evaporation rate of the liquid film is negligible and the vapor inside the thermosyphon is continuously condensing thereby reducing the total mass of the gas and temperature. It is also important to note that throughout the cooling down process vapor from the reservoir continuously flows through the connecting pipe into the thermosyphon as a result of density gradient. This accounts for the relatively small initial overall system absolute pressure decline. The rate of pressure drop becomes very fast at the end of the 450 minutes owing to the fact that the rate of condensate accumulation becomes high. The cooldown process ends when the cold head temperature stabilizes at a final value as shown in Figure **3-5** . The entire process took about 550 minutes for the TCNS system [**Unlu et al 1994**].

3.2.2 Steady State and Transient State of Operation of the TCNS Thermosyphon

At the steady state operating condition of the thermosyphon, both the moderator and cold head temperatures stabilize. A typical steady state condition for the TCNS cooling system is shown in Figure **3-6** . Initially the thermosyphon exists at a steady temperature of 26.3K and 28.3K at the cold head and moderator end respectively. Up on addition of heat load of 1W the cold head shifts to a new steady state temperature of 28.5K which is determined by the cryocooler performance curve shown in Figure **3-4** . Accordingly the moderator temperature rises to a new steady state value of 30K. The system took about 15 minutes to stabilize and reach to steady state values.

As the heat load increases, the length of time to reach to steady state also increases. This can be observed from the figures Figure **3-6** through Figure **3-9** . The heat load is increased from 1W to 4W. The evaporator temperature rose from a steady state value of 28.5K at 1W to 38.8K at 4W. When the heat load is increased to 5W the system fails as shown in Figure **3-10** where the evaporator temperature continuously increases until the heat load is removed and the system comes back to its steady state value.

The loss of cooling discussed above is the main problem existing in the TCNS cooling system. In this study, a detailed thermo-fluid analysis is carried out. Main factors that affect the loss of cooling are investigated and a new system that can handle a heat load up to 10W is proposed.

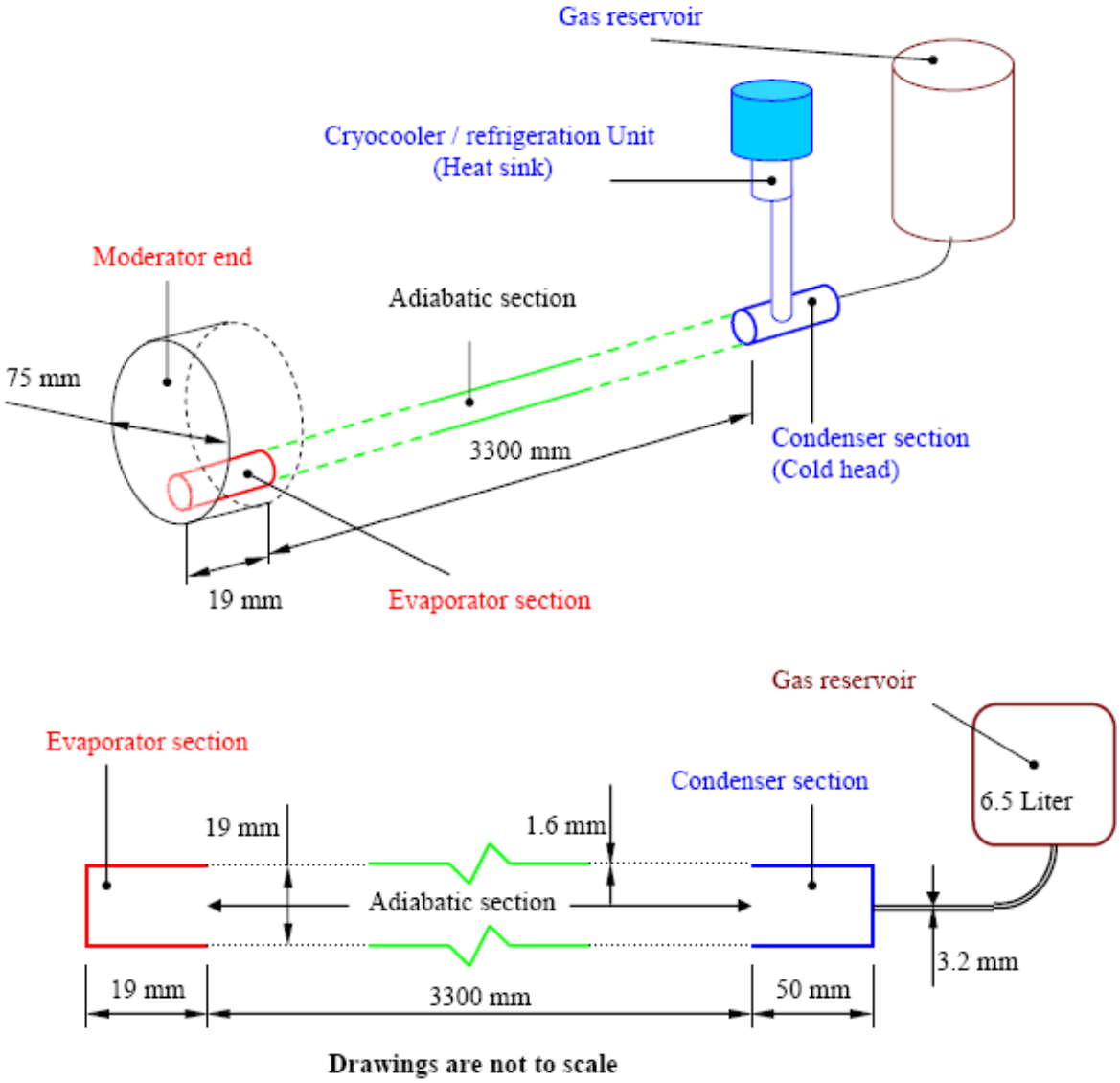

Figure **3-1**: Schematic showing the major parts (top) and relative dimensions of the closed two phase thermosyphon cooling system used in TCNS cooling system (bottom).

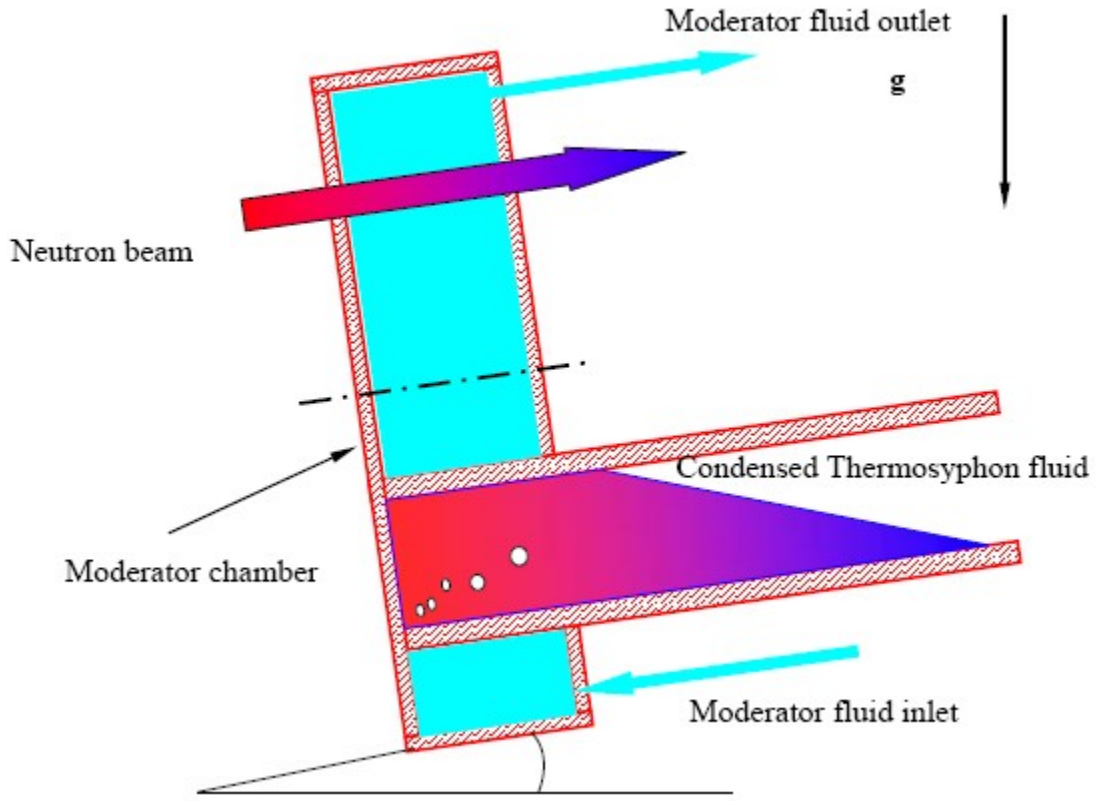

Figure **3-2**: Evaporator section attached to the moderator of the TCNS cooling system thermosyphon

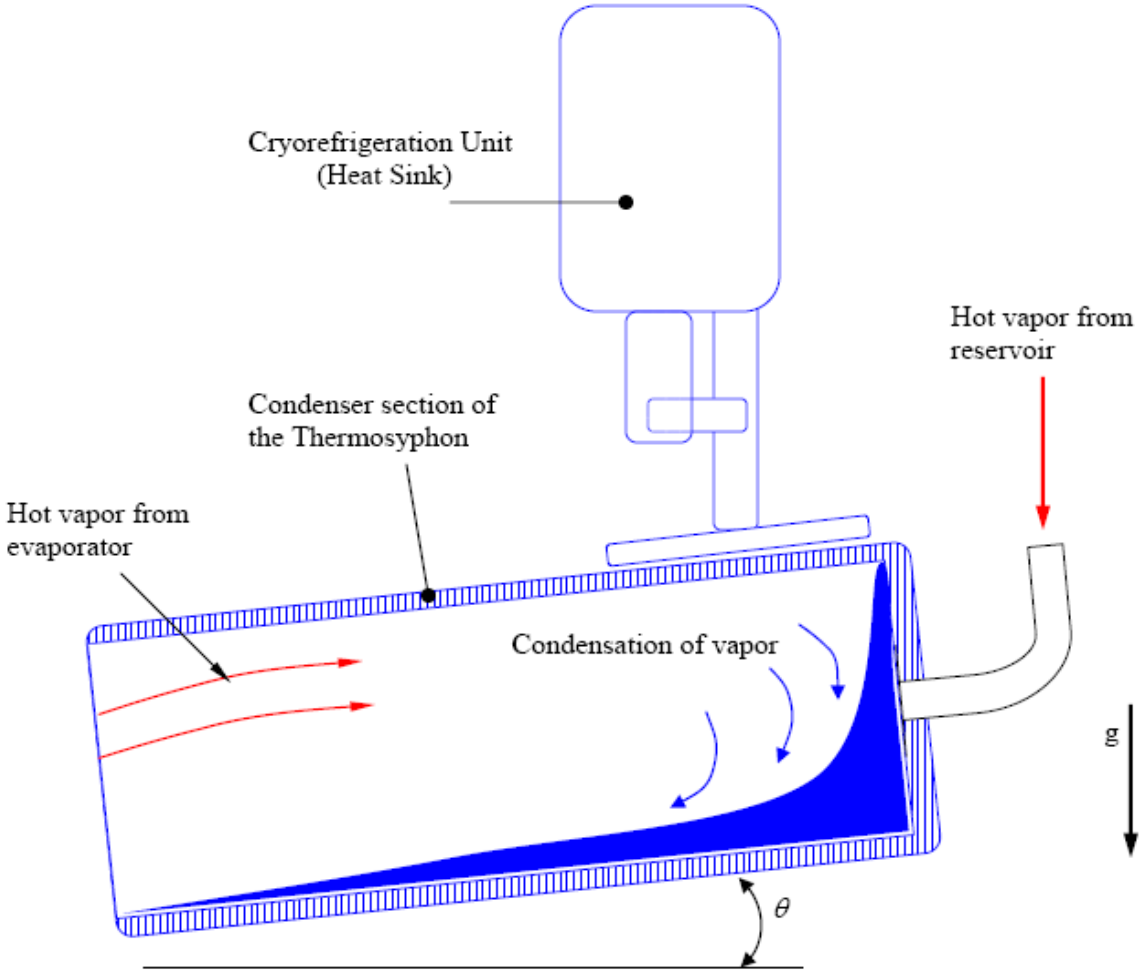

Figure **3-3**: Schematic showing the various parts of the condenser section of the thermosyphon with the attached cryocooler (heat sink)

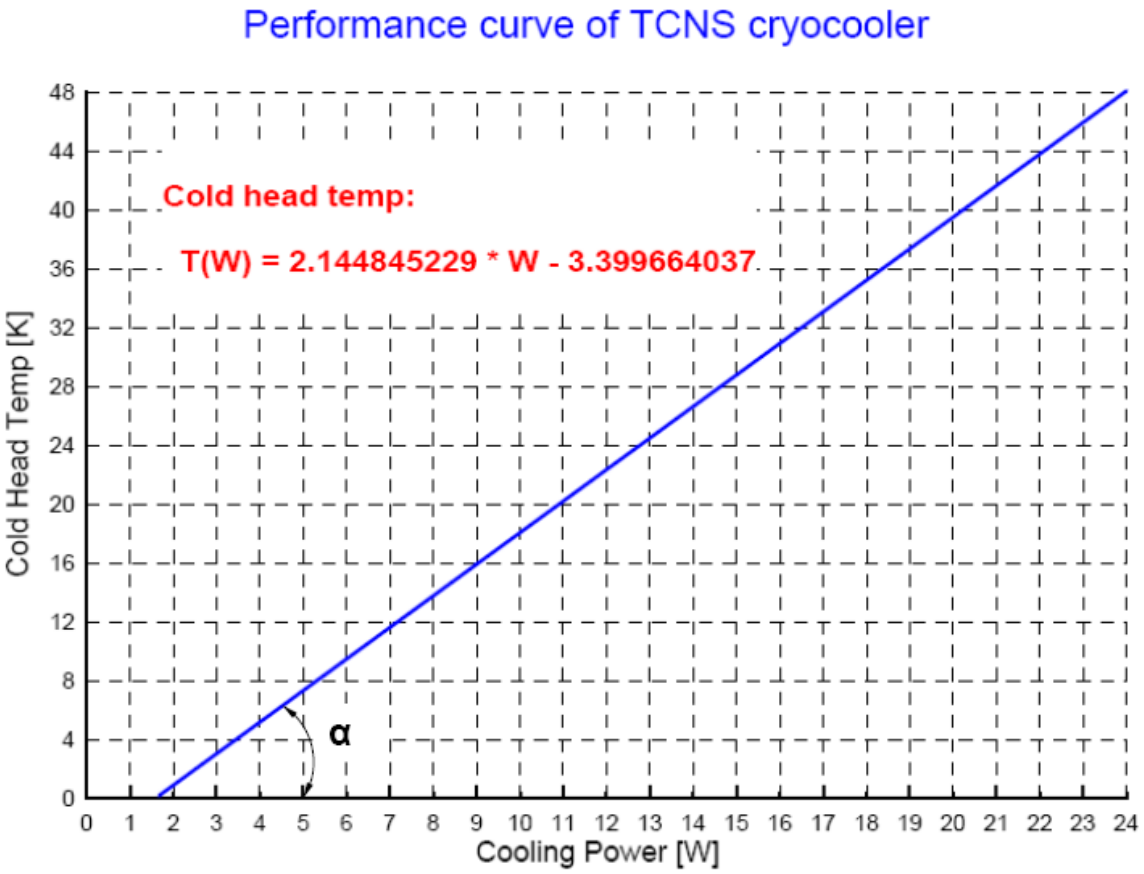

Figure **3-4**: A reproduced performance curve of the cryocooler used in TCNS cooling system. Data from[**Cryomech-Inc 2008**]

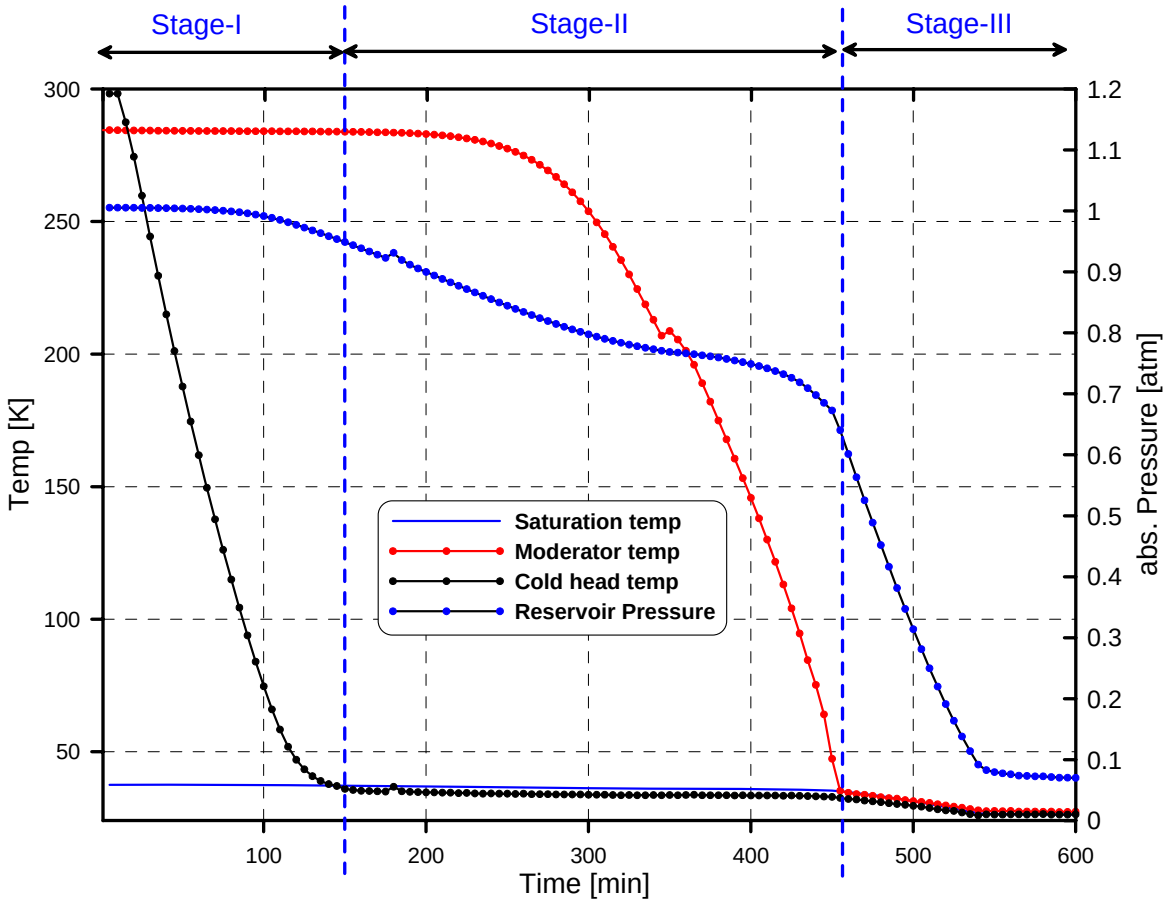

Figure **3-5**: The various cooldown stages showing moderator and cold head temperatures and reservoir pressure vs. time of the TCNS cooling system [**Unlu et al 1995**].

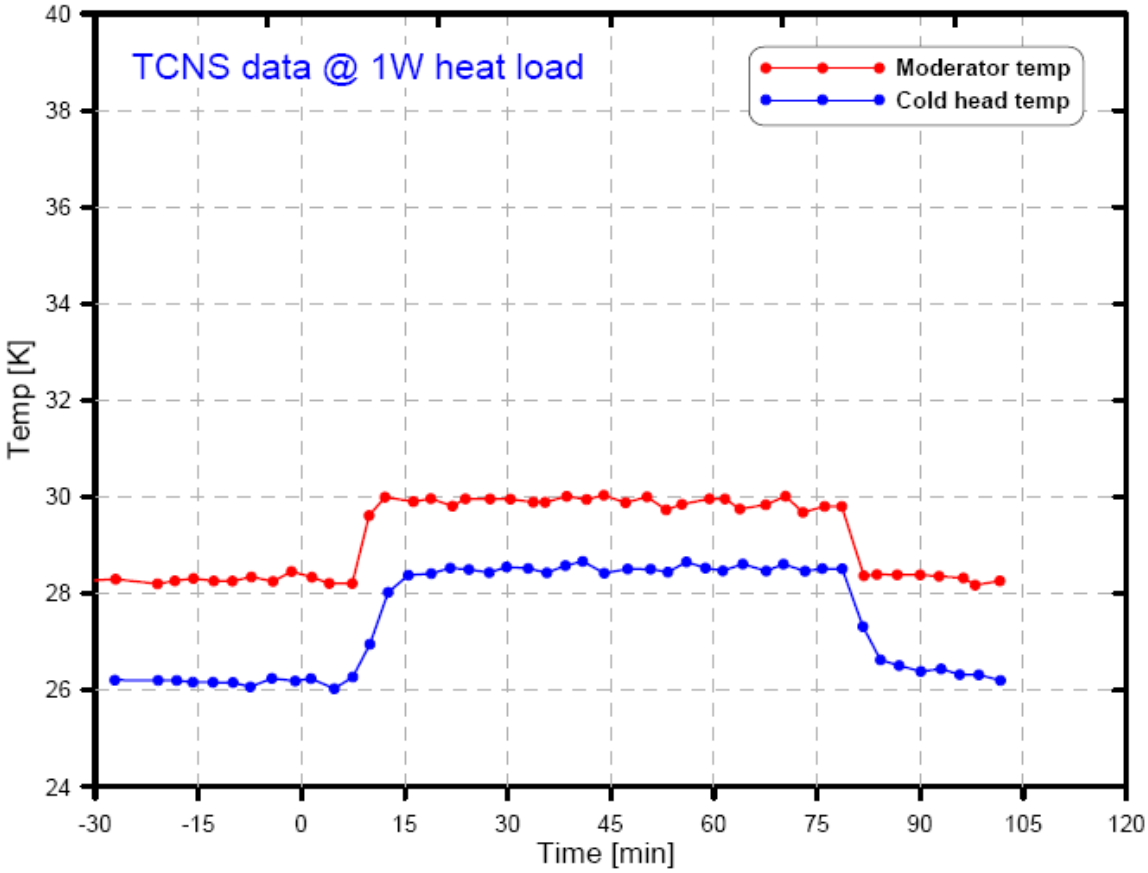

Figure **3-6**: Temperature history of Evaporator and Condenser sections of the TCNS thermosyphon approaching steady state steady temperature at 1W heat load [**Unlu et al 1994**]

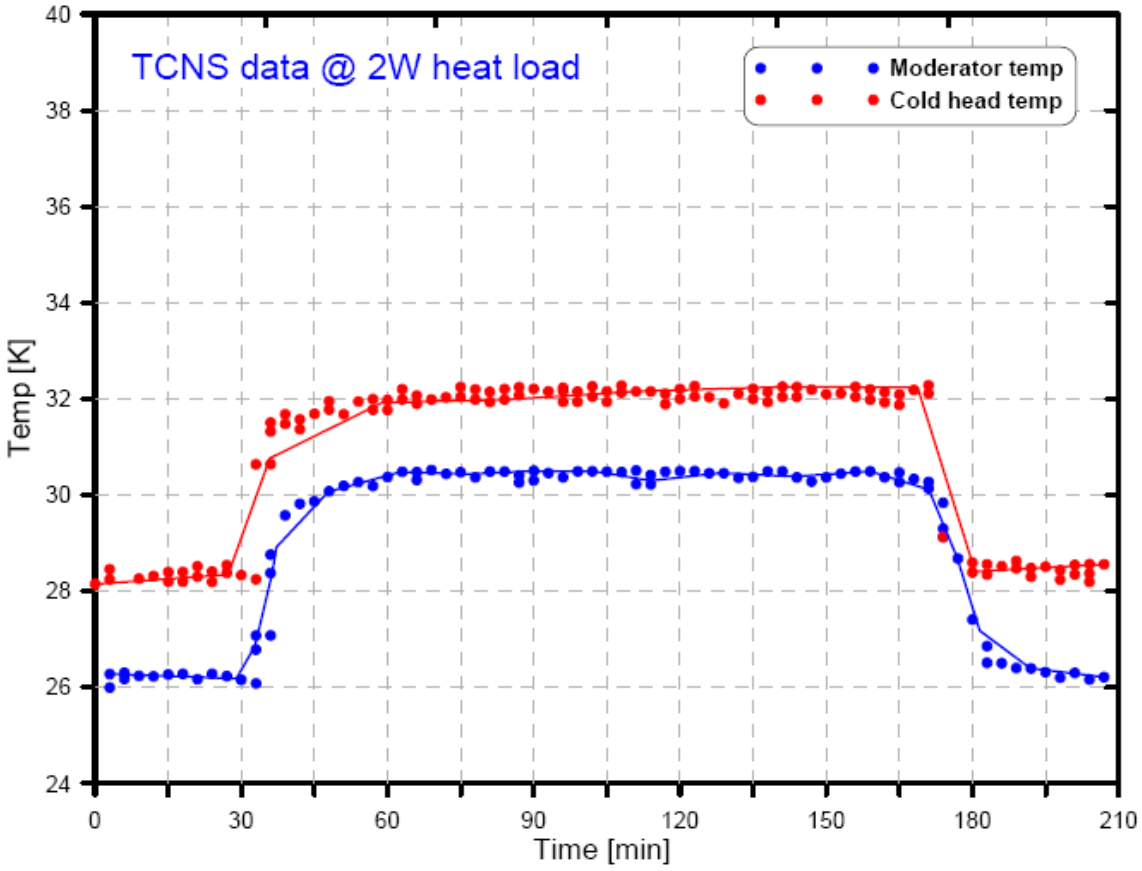

Figure **3-7**: Temperature history of Evaporator and Condenser sections of the TCNS thermosyphon approaching steady state steady temperature at 2W heat load [**Unlu et al 1994**]

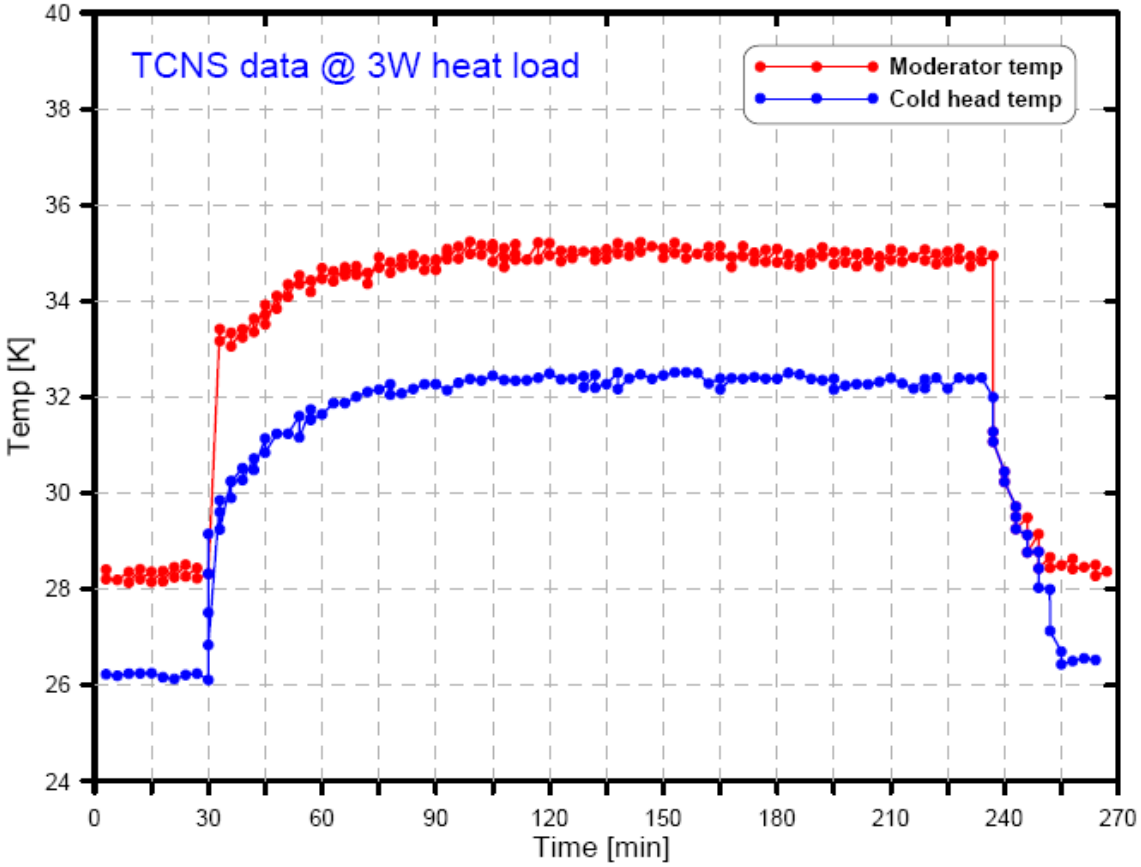

Figure **3-8**: Temperature history of Evaporator and Condenser sections of the TCNS thermosyphon approaching steady state steady temperature at 3W heat load [**Unlu et al 1994**]

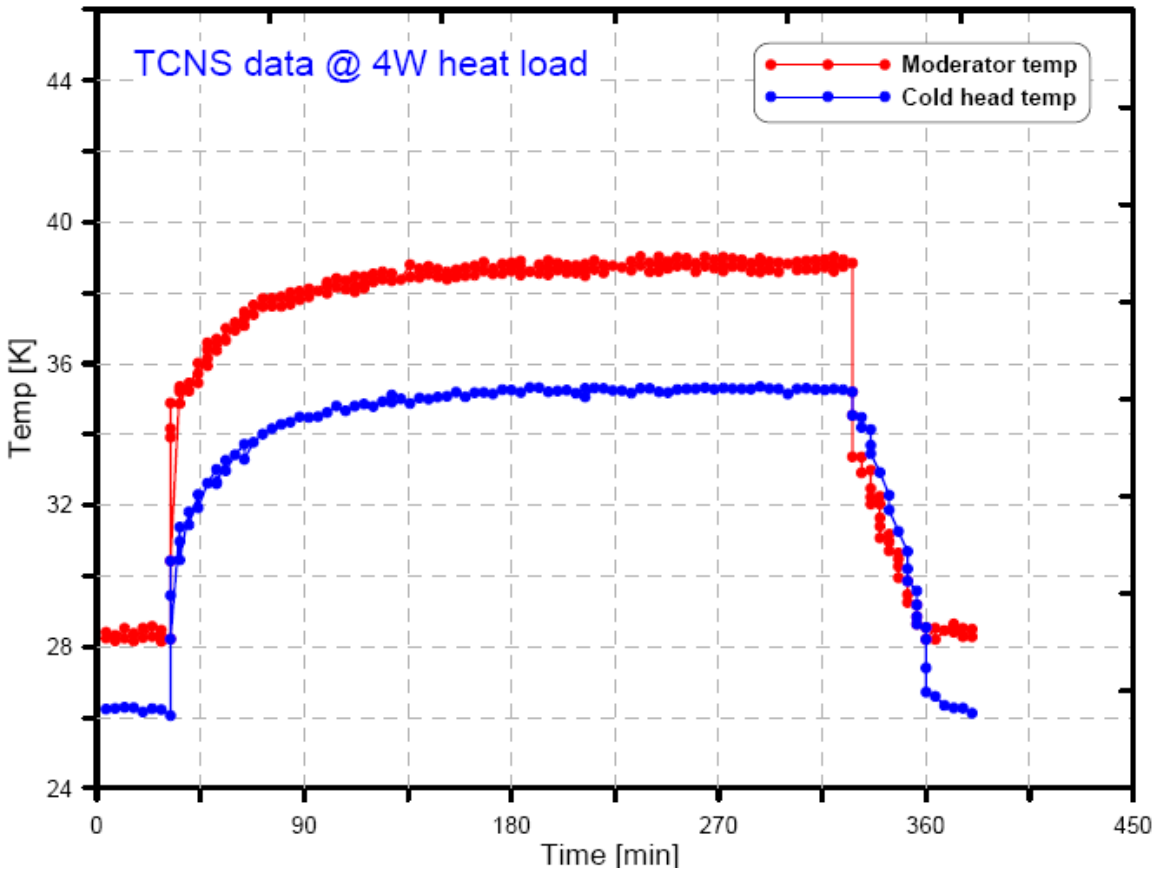

Figure **3-9**: Temperature history of Evaporator and Condenser sections of the TCNS thermosyphon approaching steady state steady temperature at 4W heat load [**Unlu et al 1994**]

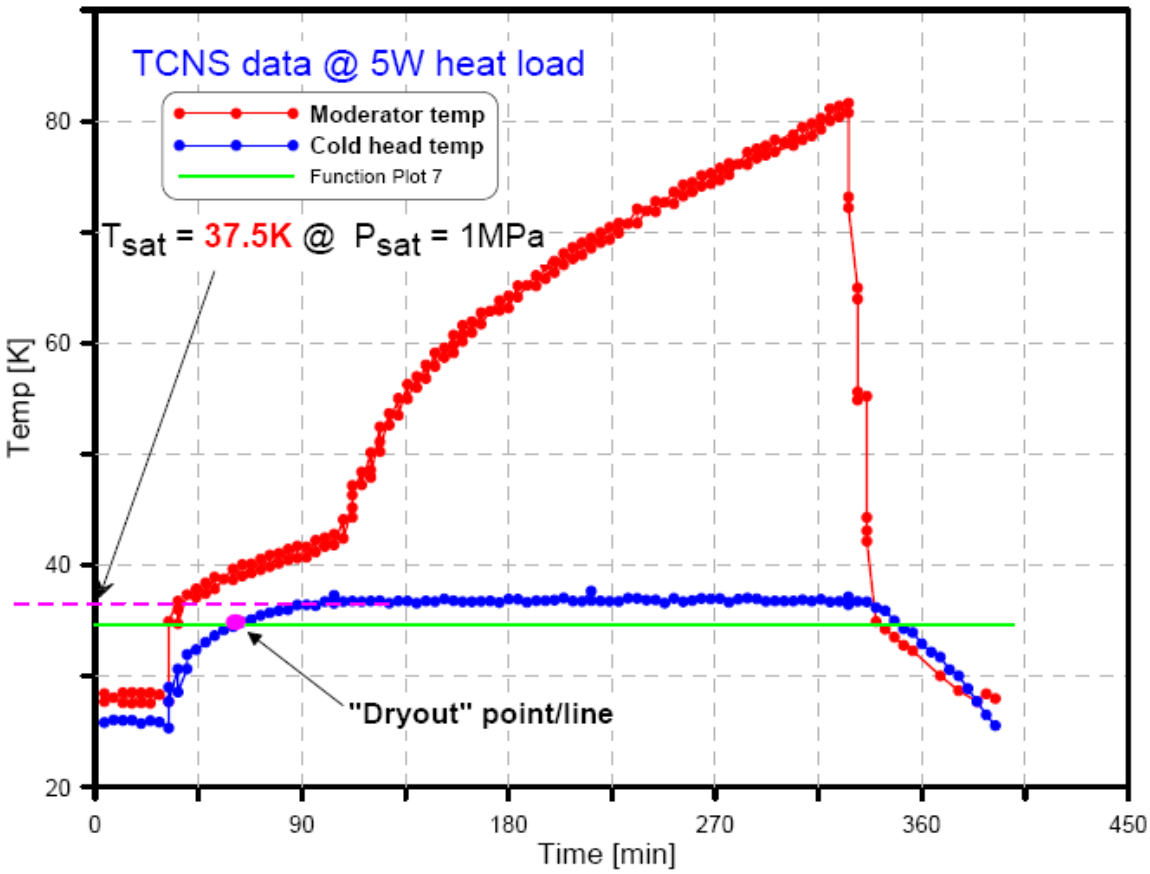

Figure **3-10**: Temperature history of Evaporator and Condenser sections of the TCNS thermosyphon at 5W heat load when the liquid in the evaporator dries out indicating that a maximum heat load is reached [**Unlu et al 1994**]

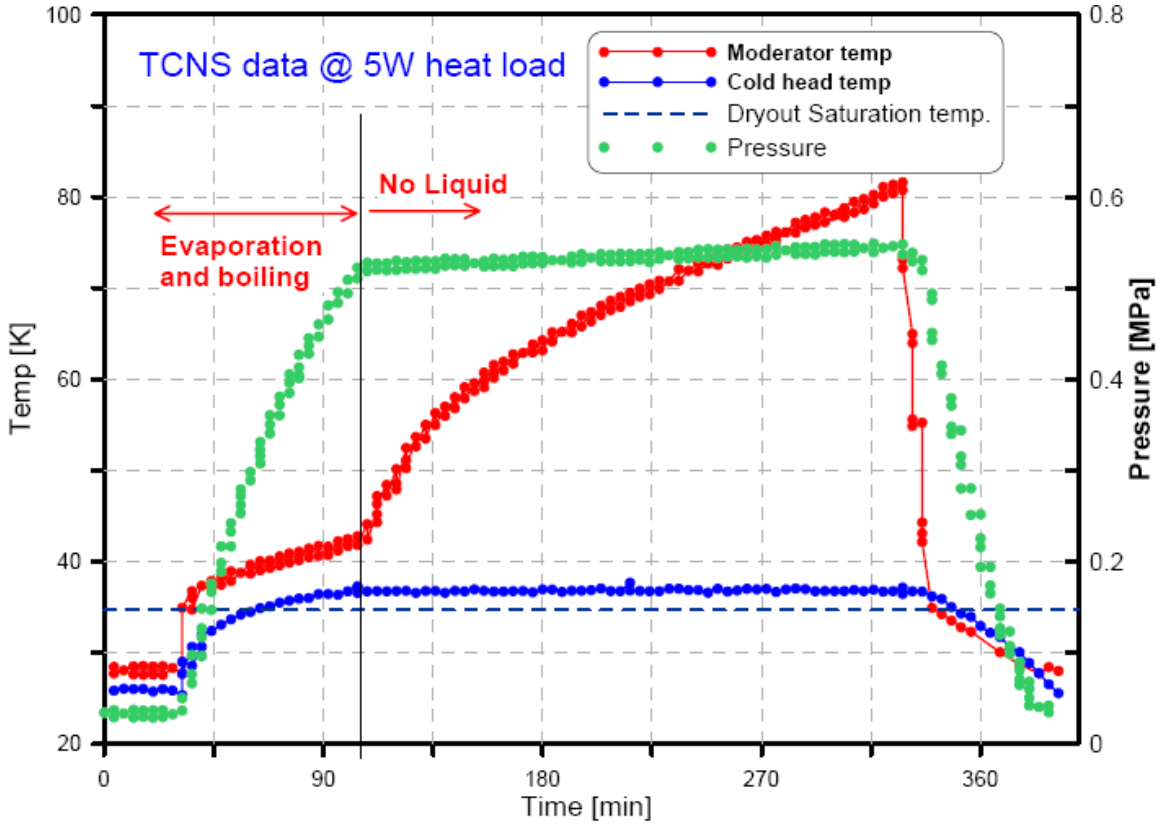

Figure **3-11**: Temperature history of Evaporator and Condenser sections and pressure of the TCNS thermosyphon at 5W heat load when the liquid in the evaporator dries out indicating that a maximum heat load is reached [**Unlu et al 1994**]

Chapter 4

Thermodynamic Analysis of Closed two phase Thermosyphon with Reservoir (TPCTR)

In this section a detailed thermodynamic analysis of the two-phase closed thermosyphon cooling system is described. In the first section the fundamental thermodynamic processes occurring in each section of the thermosyphon is presented. The various assumptions that lead to simplifications of the analysis are given. Attempts were made to accurately capture the physics and account for the most important thermo-physical factors that determine the heat exchange process. To help the analysis keep consistency, the working fluid is considered to be neon and all geometric and thermal parameters are that of the TCNS system unless specified so

Before proceeding it is important to introduce the various terminologies used in this section. The dryout saturation temperature T_{dSat} and dryout saturation pressure P_{dSat} are the temperature and pressure at the state point that exists in the closed two phase thermosyphon when the condensate liquid film that flows down along the tube first starts to accumulate at the evaporator section. This state point is given by the end of stage-II in the cooling down process of the TCNS cooling system diagram as shown in Figure 3-5 in the previous chapter. The temperature T_{dSat0} represents the saturation temperature at initial pressure P_O .The film advance rate $\dot{z}_f$ is the rate at which the liquid film from the condenser flows down the thermosyphon during the second cooldown period denoted by

stage-II in Figure 3-5 . Cooldown time t_{CD} is the time required for the entire thermosyphon to reach the steady state from an initial room temperature condition. Evaporation time t_{EV} is amount of time required by the thermosyphon to reach the dryout saturation condition from some initial state. This is the time required for the liquid film to reach the evaporator section in other words it is the time duration of stage-II in the cooldown process shown in Figure 3-5 . From this definition it is clear that $t_{EV} < t_{CD}$ The evaporation time is obviously strongly depends on the geometry and thermal properties of the solid material of thermosyphon.

4.1 The Steady State Thermodynamic Analysis

In this section the steady state thermodynamic analysis of the closed two phase thermosyphon is described. The main purpose of this analysis is to determine the dryout saturation temperature and pressure of the thermosyphon. In addition the analysis predicts the limits of the various operating conditions and the influence of geometric parameters such as the volumes of the reservoir and thermosyphon and thermo-physical parameters such as initial operating pressure and temperature of the working fluid

4.1.1 Equation of State

The fluid in the thermosyphon undergoes a series of thermodynamic states during the cooling down and normal working condition. In carrying out the thermodynamic analysis of the cooldown process, as the one outlined in Appendix A.1, it important first

to consider the cooling process of the gas phase in both the reservoir and thermosyphon. In this analysis the following important assumptions were made:

1. The gas inside the reservoir is assumed to be at room temperature T_∞ . This assumption can be justified due to the fact that the reservoir tank that is connected to the thermosyphon with a small diameter tube is outside the vacuum chamber where it is exposed to the surrounding ambient temperature as shown in Figure **A-1** . Hence it is reasonable to assume that the temperature in the reservoir is essentially equal to the ambient temperature at all time unless external cooling is provided.
2. The pressure in both the thermosyphon and the reservoir is approximately uniform. This is also justified for two reasons. The first reason is obviously due to the fact that the reservoir and thermosyphon are connected by a small pipe. This allows vapor to flow freely back and forth and attain an equilibrium value. The second reason is the fact that the flow inside the thermosyphon is driven by the density gradient that is created as a result of the cooling process. As the cooling process progresses the mean temperature inside the thermosyphon decreases gradually and this momentarily creates to a small pressure difference between the reservoir and thermosyphon just enough for more vapor to flow into the thermosyphon from the reservoir and attain equilibrium.
3. The mean temperature inside the thermosyphon at any time is assumed to be uniform. This is merely an approximation but an important one in estimating the total mass of the vapor at any given time. Clearly there is

temperature gradient along the length of the thermosyphon due to the fact that the cold head is connected to the cryorefrigeration system where condensation occurs. During cooldown period the temperature in the vicinity of the cold head is approximately equal to that of the cold head temperature. Similarly the temperature at the evaporator end of the thermosyphon is close to the evaporator temperature. This temperature gradient drives a natural convection flow inside the thermosyphon. This flow creates sufficient mixing that justifies the assumption that the *mean* temperature of the vapor in the thermosyphon is uniform in the entire thermosyphon tube at any given time

The temperature of the vapor inside the thermosyphon continuously decreases during the cooldown periods of stage-I and stage-II. The temperature range that the vapor undergoes starting from room temperature up to the normal operating temperature that is around 28K demands that the ideal gas model can not be used. Therefore it is important to consider an equation of state that can cover the temperature range with a reasonable accuracy. In this study the Bender equation of state is used. The 19 parameters used to evaluate the equation of state were obtained from the results of the work of Ghazouani et. al.[**Ghazouani et al 2005**]. The Bender equation is generally written in terms of compressibility factor Z as a function of temperature T and density ρ .as:

$$Z = \frac{P\bar{M}}{R_u T \rho} = 1 + \frac{B\rho}{R_u} + \frac{C\rho^2}{R_u} + \frac{D\rho^3}{R_u} + \frac{E\rho^4}{R_u} + \frac{F\rho^5}{R_u} + \frac{\left(G + H\rho^2\right)\rho^2}{R_u} e^{-\frac{\rho^2}{a_{20}}} \qquad \textbf{4.1}$$

Where: $\bar{M}$ is molecular weight of the fluid, R_u is the universal gas constant and the values of B through H are functions of temperature and are given by:

$$B = a_1 + \frac{a_2}{T} + \frac{a_2}{T^2} + \frac{a_2}{T^3} + \frac{a_2}{T^4}$$
$$C = a_6 + \frac{a_7}{T} + \frac{a_8}{T^2}, \quad D = a_9 + \frac{a_{10}}{T} \qquad \textbf{4.2}$$
$$E = a_{11} + \frac{a_{12}}{T}, \quad F = \frac{a_{13}}{T},$$
$$G = \frac{a_{14}}{T^3} + \frac{a_{15}}{T^4} + \frac{a_{16}}{T^5}, \quad H = \frac{a_{17}}{T^3} + \frac{a_{18}}{T^4} + \frac{a_{19}}{T^5}$$

The values of the parameters from a_1 through a_{20} for neon are listed in Appendix **A.4**

4.1.2 Description of the Equilibrium Thermodynamic States

The thermosyphon cooldown process is a non equilibrium one. However the initial and the final steady states of the various components of the thermosyphon can be described in a temperature volume diagram as the one shown in Figure **4-1** . State point 1 indicates the initial state of neon gas in both the thermosyphon and the reservoir at room temperature before cooldown process starts. The temperature and pressure at this state are T_O and P_O respectively, where in this case $T_O = T_\infty$. State point 2 and 4 show the final states of neon gas in the reservoir and the thermosyphon respectively. The isobar (constant pressure line), given by $P = 0.07MPa$ represents the minimum temperature T_{Min} for neon beyond which neon exists as a solid. The maximum temperature, also known as critical temperature T_{Cr} , shown in Figure **4-1** is the temperature beyond which

neon exists only as in gaseous form. Hence liquid neon exists between the critical and the minimum temperatures. The cooling process in the reservoir is indicated by the path 1-2. This is essentially an isothermal process since the surrounding temperature of the vapor reservoir is room temperature T_∞. Path 1-3-4 indicates an approximate state of cooling path followed by the neon gas in thermosyphon from an initial room temperature to the final steady state condition at state point 4. This path is approximate since the temperature in the thermosyphon is not exactly uniform. However, as it is explained in the next section that it is assumed to be uniform for the purpose of analysis. State point 3 indicates the dryout saturation condition. At this state the thermosyphon will start to have liquid accumulation at the bottom of the evaporator section. It is so called dryout point since for an already cooled system that exist below this temperature with some liquid accumulation, any increase in temperature will result in evaporation and hence the dryout point signifies the temperature and pressure when no liquid is left in the evaporator.

4.1.3 Dryout Saturation State

It is important to determine the saturation temperature at which liquid starts to accumulate in the thermosyphon during cooldown process or in other words the saturation condition that exists when no liquid is left during warming up of the thermosyphon. This section describes the methodology used in determining the critical saturation condition and the parameters that affect it.

After the thermosyphon is charged with the working fluid, in this case neon gas, to an initial temperature and pressure of T_O and P_O respectively, cooldown process starts

by starting the cryorefrigeration unit which is shown schematically in Figure **3-1** . The cryorefrigeration unit serves as a heat sink in this cooling system. Initially the vapor inside the thermosyphon starts to cooldown that result in a natural convection flow. There will be no condensation occurring in any part of the thermosyphon during stage-I of the cooldown process. This is because the wall temperature of the coldest surface in the system, which is the condenser section, is higher than the saturation temperature of the neon vapor at the given pressure. Immediately after the condenser inside wall temperature T_{Ci} reaches below that of the saturation temperature T_{Sat} at the given pressure P condensation starts which marks the beginning of stage-II of the cooldown process. The condensate film flows from the top of the tube wall and accumulates at the bottom and then flows due to gravity and reaches a point down along the bottom wall of tube where it evaporates thereby removing sensible heat from the solid wall of the thermosyphon. As a result the wall temperature of the thermosyphon approaches that of the condensed liquid film temperature. In this study the distance from the condenser end along the thermosyphon wall to a point where the condensate evaporates is defined as film front z_f . The rate at which this film front advances down along the thermosyphon inside wall is defined as film advance rate $\dot{z}_f$ as indicated in the beginning of this chapter. By the time when the film front reaches the evaporator section of the thermosyphon the evaporation rate of the film drops far below that of condensation. As a result the film starts to accumulate as liquid at the bottom of the evaporator section provided that there is no heat load in the evaporator. At this condition the saturation temperature and saturation pressure of the vapor inside the thermosyphon are defined as

dryout saturation temperature and pressure T_{dSat} and P_{dSat} respectively. It is very important to determine these critical values since it directly determines the maximum temperature that the evaporator section can reach without loss of liquid as discussed in the last chapter and shown in Figure **3-10** . If the evaporator reaches the dryout temperature, then the heat transfer mechanism changes dramatically from phase-change type such as boiling to conduction through the wall of the thermosyphon. Before this transition though there is a very narrow temperature range just immediately above the dryout point where the heat transfer mechanism will be due to evaporation of liquid film. These mechanisms are discussed in detail in the next chapter. The result of increase in temperature beyond dryout would be a very high thermal resistance that will lead to further increase in temperature of the evaporator. Hence the evaporator must always operate below this dryout temperature.

In this study, two procedures are developed for determining the dryout saturation conditions. The first method is an iterative procedure that utilizes the Equation of state outlined in the previous section **4.1.1** . The details of the procedure are discussed in Appendix **A.1** .The second method is analytical equation derived using conservation of mass and equation of state that can be applied to any system that involves a thermosyphon and reservoir similar to the one used in TCNS cooling system. This analysis is more general and much easier to use and help analyze the effect of various parameters. The derivation of this equation is outlined in Appendix **A.2** .

In order to determine the dryout conditions using the iterative procedure, the following assumptions are made:

1. The rate of condensation equals that of evaporation during stage-II of the cooldown period.
2. The total mass of liquid film that remains during stage-II of the cooldown period is assumed to be linearly proportional to the temperature of the vapor inside the thermosyphon during that stage.
3. The effective temperature of the thermosyphon T_{eff} equals that of the saturation temperature during stage-III of the cooldown period.

To help the analysis, the thermodynamic conditions at initial and the dryout saturation condition anticipated at the end of stage-II of the cooldown process are outlined in the schematic shown in Figure **4-2** . To facilitate the analysis, the saturation curve of the working fluid must be known as a function of saturation pressure and temperature. For this study the saturation curve of neon was obtained from [**NIST**] and curve fitted to obtain a polynomial function that can easily be evaluated at any give saturation pressure or saturation temperature. This is shown in Figure **4-3** .

The effective temperature of the thermosyphon T_{eff} is defined as the temperature that would give the same mass if the thermosyphon were filled with neon gas of uniform temperature T_{eff} . Let the mass of neon gas (vapor) inside the thermosyphon be m_{TS_V} at a given pressure P . In general the temperature inside the thermosyphon varies. The effective temperature at this condition would be given by

$$T_{eff}(P) = \frac{P\bar{M}}{R_u \dfrac{m_{TS\_V}}{V_{TS}}}; \qquad \textbf{4.3}$$

where $m_{TS\_V} = m_{TS\_V}(P)$

Here $\bar{M}$ is molecular weight of the gas. From the saturation curve fit we have

$$T_{Sat} = f\left(P_{Sat}\right),\ and\ P_{Sat} = f\left(T_{Sat}\right) \tag{4.4}$$

Solving Eq. **4.3** and Eq. **4.4** simultaneously gives the dryout saturation temperature and pressure T_{dSat} and P_{dSat}. A more detailed procedure of determining the dryout state is available in Appendix **A.1** . This point marks the end of stage-II of the cooldown process. The effective temperature in stage-III is approximated to be the saturation temperature at the given pressure. This is due to the fact that the vapor and liquid are now coexisting inside the thermosyphon. This concludes the first procedure of determining the dryout conditions.

The analysis using the second procedure is just applying the equations derived in Appendix **A.2** . Here only the final equation is presented. The dryout saturation temperature and pressures are calculated using Eq. **4.5**

$$P_O\left(\frac{1+\eta}{\frac{T_\infty}{T_{dSat}}+\eta}\right) - f(T_{dSat}) = 0 \tag{4.5}$$

$$\text{where}\quad f(T_{dSat}) = P_{dSat}$$

$$\eta = \frac{V_R}{V_{TS}}$$

Here the volume ratio parameter η is an important dimensionless quantity that is used to study the effect of reservoir and thermosyphon volumes.

Both of the above procedures were applied in the TCNS cooling system in order to validate the various assumptions and approximation. The two procedures gave the same results when compared to the experimental data. The result is shown in Figure **4-4** .

From the figure it is clear that the analysis accurately predicts the critical saturation condition namely T_{dSat} of 34.48K and P_{dSat} of 0.6MPa. The result of the analytic procedure is shown in Figure **4-5** . It is clear from the figure that the pressure in the thermosyphon is accurately predicted suggesting that the assumptions that were made in deriving Eq. **4.5** were reasonable. This analysis can now be applied to a similar system with various parameters such as: volumes of the reservoir and thermosyphon, initial system temperature and pressure, type of working fluid etc.

The dryout saturation state is a very important parameter in that it determines the upper limit of the temperature of the evaporator. If the evaporator is loaded in such a way that the vapor temperature inside the thermosyphon exceeds the dryout saturation temperature then there will be no liquid present at the evaporator section. This is due to the fact that the evaporation rate at the evaporator section exceeds the rate of condensation in the condenser. This results in lack of liquid in the evaporator and hence the heat transfer process becomes due to conduction only rather than boiling and evaporation. This leads to an increase in thermal resistance in the evaporator which deteriorates the efficiency of the heat exchanger. The experimental data of the TCNS cooling system is plotted in Figure **4-6** . It is clear from the figure that the pressure rise is exponential during the evaporation region. This is due to the fact that more and more liquid enters the vapor phase due to evaporation. Evidently the rate of pressure increase abruptly slows when the evaporator temperature shows a sudden jump. This also shows that there is no more liquid left and the mass of vapor is now nearly constant and hence the pressure stabilizes, increasing only due to vapor heating. It is also clear that the evaporator temperature shows an abrupt jump at 5W heat load. This is the point when the

thermosyphon is out of liquid neon. Hence the TCNS cooling system could not operate above 4W heat load as a result of this. All the liquid at this stage evaporated and the heat transfer mechanism changed from boiling and evaporation into conduction, which has up to three orders of magnitude higher thermal resistance than that of boiling and evaporation. In order for the system to be able to handle more heat loads the limiting dryout saturation temperature must be increased. The next sections discuss about the ways how to improve the dryout saturation conditions.

4.2 Study of Effects of Geometric and Thermal Parameters on Dryout Condition at Steady State

In order to achieve an enhanced thermal performance of the system that is applicable over a wide range of operating heat loads, one has to maximize the dryout saturation conditions of the given thermosyphon cooling system. This condition is affected by various geometric and thermo-physical parameters. The following sections discuss the effects of these parameters.

4.2.1 Effect of Volume

4.2.1.1 Effect of Reservoir Volume

The volume of the gas reservoir is an important parameter in that it directly determines the total mass of the neon in thermosyphon cooling system. Figure **4-7** shows plot of the dryout temperature normalized by the critical temperature T_{Cr} of neon vs

reservoir volume normalized by the current reservoir volume. For comparison purposes, the plot was made at three thermosyphon volumes V_{TS} operating at the same initial pressure P_O. From the figure it is clear that the dryout temperature can be increased by increasing the reservoir volume. For example doubling the gas reservoir volume improves the current dryout temperature by about 5%. This translates to a temperature improvement of about 2K. This is, as it will be discussed later, an important improvement considering the range of temperature that liquid neon exists, only 25K to 44K which is a difference of 20K. This extends the operating temperature range by 10%. Figure **4-8** shows the same plots as Figure **4-7** but at a higher initial pressure of $1.6P_O$ to show the effect of initial fill pressure. In this case a 60% increase in initial fill pressure resulted in a 10% increase in dryout temperature from the current condition, which is about 4K, This expands the operating temperature range by 20%. Hence a higher initial pressure increases the dryout temperature more than a similar increase in reservoir volume.

4.2.1.2 Effect of Thermosyphon Volume

The volume of the thermosyphon is also a parameter in determining the dryout temperature. Similar to the previous section Figure **4-9** shows plot of the dryout temperature normalized by the critical temperature of neon vs thermosyphon volume normalized by the current thermosyphon volume. For comparison purposes, Figure **4-9** and Figure **4-10** were plotted at three reservoir volumes operating at the initial pressures of P_O and $1.6P_O$ respectively. In this case the effect of thermosyphon volume is minimal as

compared to that of the reservoir volume. For example a 100% increase in thermosyphon volume results in less than an increase that could have been obtained by increasing the reservoir volume by 60%.

4.2.1.3 Effect of Volume Ratio η

In the last section the effect of each of the volumes on the dryout saturation temperature is analyzed. However it is more efficient to analyze the volume effect in terms of the volume ratio η since it incorporates both the reservoir and thermosyphon volumes at once. Figure **4-11** shows the plot of normalized dryout saturation temperature predicted using the method outlined in section **4.1.3** versus volume ratio. The plot is made at a reservoir temperature of 300K normalized by the critical temperature of neon and for four initial pressures normalized by the critical pressure of neon. In this case the critical temperature and pressure of neon are $T_{Cr} = 44.49K$ and $P_{Cr} = 2.679MPa$ respectively. The minimum saturation temperature (melting point) for neon is $T_{\min} = 24.5K$. Hence the range of the dryout saturation temperature between the critical (maximum) and minimum is 20K. The normalization is made to make comparison with subsequent results more convenient. The dashed line in Figure **4-11** indicates the dryout temperature when the initial pressure is 10atm, which is the case in the TCNS cooling system. In that case the volume ratio is $\eta = 10$. For the current system of TCNS cooling system the normalized dryout saturation temperature is 0.5, which is half way through the entire range of 20K. Any improvement in increasing the dryout temperature will have to

result in a normalized saturation temperature of above 0.5. Figure **4-12** shows a similar plot but this time at four reservoir (room) temperatures and at an initial pressure of 10atm, a value corresponding to the current TCNS cooling system. Considering only the effect of volume ratio it is clear from the two figures that as the volume ratio η increases the dryout temperature also increases. However it can be observed from Figure **4-12** that there will not be a huge improvement just only by increasing the volume ratio. In order to have a better improvement the initial pressure in the system has to also be increased. The effect of the thermo-physical parameters is discussed next.

The most important result one may note in these results is the fact that there was no particular restriction in developing the analysis that restricts the shape of the reservoir or the thermosyphon, except the ratio of the two volumes and the way they are connected.

4.2.2 Effect of Initial Pressure and Reservoir Temperature

As discussed in the preceding sections the reservoir of the TCNS cooling system was kept at room temperature. The initial fill pressure of the system was at 10atm. In this section the results of the analysis on the effect of initial pressure and reservoir temperature on dryout saturation temperature is presented. The results are obtained using similar analytic procedures used in the analysis discussed in the last section. In Figure **4-13** a plot of analytic result of dryout saturation temperatures vs normalized reservoir temperatures (room temperatures) is shown at initial pressures and at a volume ratio of $\eta = 10$ corresponding to the current value. Clearly as the reservoir becomes warmer, the dryout saturation temperature decreases. This suggests that the operating temperature

limit reduces as the reservoir is kept in a warmer room than a colder one. In other words cooling the reservoir would improve the dryout limit. A similar plot is shown in Figure **4-14** where this time the dryout saturation temperature is plotted versus the normalized reservoir temperature at four volume ratios and an initial pressure of 10atm. Again in this case the same conclusion can be made in addition that to the fact that the effect of volume ratio decreases as the reservoir temperature decreases. In other words for example it is possible to have the same dryout limit as the current condition under a scenario where the reservoir size is 20 times smaller as long as the reservoir temperature is kept at about 1/3 of the current temperature.

The effect of initial fill pressure is shown in Figure **4-15** and Figure **4-16** . From both figures it is clear that as the initial fill pressure is increased the dryout limit also increases. It is interesting to note from the two figures that at any pressure the percentage improvement in dryout limit of a system that can be achieved either by increasing volume ratio or reduction of reservoir temperature is the same for any other system that exists at a different initial fill pressure.

4.3 Fill Ratio

The fill ratio FR of closed two phase thermosyphons is an important parameter that determines the cooling performance. In this section an appropriate definition is given that is relevant to an inclined thermosyphon. The effect of volume ratio, initial temperature and pressure, inclination angle and length of evaporator section will be discussed.

4.3.1 Definition of Fill Ratio

The Fill Ratio FR is defined as the ratio of volume of liquid to the volume of evaporator of the thermosyphon. This parameter is particularly used in literatures as an important factor in determining the operational characteristics of thermosyphons. It indicates the extent of liquid in the evaporator. Figure **4-17** shows the various states of fluid inside thermosyphon as cooling progresses. When condensation first starts, a thin liquid film appears at the bottom of the condenser section. After the end of stage-II of cooling process there will be a finite volume of liquid film formed over the bottom surface of the thermosyphon as shown. In this study the volume of liquid film in this stage is denoted as V_f and the volume at the end of stage-II when dryout point is reached is denoted by V_{f0}. The ratio of liquid volume to that of the thermosyphon, liquid fraction, is denoted by ξ. The liquid fraction at any temperature during stage-II and stage-III is given by:

$$\xi = \left(\frac{T - T_{Sat0}}{T_{dSat} - T_{Sat0}} \right)^n ; n = 4 \text{ and } T_{dSat} < T < T_{Sat0}$$

$$\xi = \frac{\frac{\rho_O}{\rho_L}(1+\eta) - \frac{\rho}{\rho_L}\left(\eta \frac{T}{T_O} + 1\right) + \xi_O}{\left(1 - \frac{\rho}{\rho_L}\right)}; \quad T_{sat\_min} < T < T_{dSat} \qquad \textbf{4.6}$$

$$\text{where } \rho = \frac{f(T_{Sat})}{R_u T_{Sat}}; \; \xi_O = \frac{V_{f0}}{V_{TS}}$$

The details of the derivation of Eq. **4.6** are given in section **A.3** . The volume of liquid inside the thermosyphon can now be computed once the inside temperature of the thermosyphon is known. In the current study the definition remains the same with slight

modification. Figure **4-18** shows a schematic with the minimum liquid level that just covers the entire evaporator section of closed two phase thermosyphon. In this study the minimum liquid volume $V_{Liq\_\min}$ is defined as the minimum liquid volume that just covers all the inside surface of the evaporator section and is given by

$$V_{Liq,\min} = \frac{\pi}{4} d^2 \left(L_E + 0.5 L_{Liq,\min} \right) \qquad \textbf{4.7}$$

$$where \quad L_{Liq,\min} = \frac{d}{\tan\theta}$$

Where d is the inside diameter of the thermosyphon, θ the inclination angle of the thermosyphon with the horizontal and L_E is length of evaporator section as shown in Figure **4-18** . And the fill ratio is can now be defined as

$$FR = \frac{V_{Liq}}{V_{Liq,\min}} = \xi \frac{V_{TS}}{V_{Liq,\min}} \qquad \textbf{4.8}$$

Typical values indicated in past works rang from 0.15 to 0.25 or 15% to 25%. These values are normally reported as the percentage of evaporator volume for vertical thermosyphons. In the current study instead of the evaporator volume, the minimum liquid volume is taken as defined above.

The past research works such as [**Shiraishi et al 1981**] on two closed phase show the importance of fill ratio. According to the experimental and theoretical study carried out by [**Niro et al 1990**] shoed that closed two phase thermosyphons operate in one of two ways depending on fill ratio. These are: the falling-film evaporation mode for small fillings (liquid volume less than about 10% of evaporator volume), and pool boiling for medium and large fillings (from 30 to 100% and over of the evaporator volume). It

further suggests that in the pool boiling regime the range of operational heat load is larger and stable.

It is therefore important to have the optimum fill ratio in the thermosyphon that guarantee a liquid pool inside the evaporator at a given heat load. Figure **4-19** shows comparison of experimental fill ratio of TCNS thermosyphon and predicted using the above analytic equations. The experimental results are obtained by converting the pressure and temperature measurements done on the TCNS thermosyphon. The saturation temperature was taken as the average between the evaporator and condenser temperatures. Both the temperature obtained this way and the measured pressures were used in the analytic equation to obtain the corresponding experimental fill ratio. The predicted value is similarly obtained but only using the saturation curve of neon. From the figure it is clear that the predicted fill ratio is within a maximum of 15% error with the experimental result. In the same figure the liquid fraction is plotted that obviously shows the same trend. The dryout point is indicated in this case at around $T_{dSat} = 34.5K$. It is also important to note the maximum possible and the current operational range of the current TCNS thermosyphon. It is clear that current the operational regime is near the pool boiling range for very low temperatures of around 28-32K where the fill ratio is still above 50%. At a fill ratio of around 0.1 or 10%, dryout occurs. The steady state fill ratio at a condition where the thermosyphon has no heat load is a little over 100% which occurs at around 27K.

In the next section the effect of thermo-physical and geometric parameters on fill ratio and operational range of closed two phase thermosyphon is discussed

4.3.2 Effect of geometrical Parameters on Fill Ratio

In this section the geometric parameters such as volume of thermosyphon and reservoir and inclination angle of the thermosyphon is discussed.

4.3.2.1 Effect of Volume Ratio η on Fill Ratio

The effect of volume ratio on dryout saturation conditions is discussed in the previous sections. In this section the effect of η on another equally important parameter, fill ratio FR is discussed. Figure **4-20** shows parametric plot of fill ratio vs saturation temperature at five volume ratio η as a parameter. As the volume ratio increases, the initial fill ratio also increases proportionally. In particular as the volume ratio doubles the initial fill ratio also doubles but it is also important to note that the dryout saturation temperature increases from 34.4K to 35.8K. In other words if we keep the same TCNS cooling system but just double the reservoir volume, there will be liquid present in the evaporator with a corresponding fill ratio of 0.5 – that is 50% of the evaporator will have liquid rather than dryout condition. Another interesting observation besides an increase in dryout temperature is that the range of temperatures where liquid pool exists increases with volume ratio. This increases the temperature range where pool boiling occurs and hence an increased capacity to handle larger heat loads over wider temperature ranges. The limiting factor in volume ratio is the size of the reservoir volume – in order to have a volume ratio of 100 for the TCNS thermosyphon it requires a 650Liter reservoir. The current reservoir has a capacity of 6.5Liters.

4.3.2.2 Effect of Inclination Angle θ of Thermosyphon

The inclination angle of the thermosyphon is another important parameter. The condensate flow in thermosyphons is entirely due to gravity. The amount of liquid the accumulated at the bottom of the evaporator section depends on the inclination angle θ of the thermosyphon. Past works of [**Tredtoon et al 2000**] has shown that the heat transfer is best when the thermosyphon inclination was near horizontal and minimum when vertical as discussed in chapter 2. However, the current parametric study as shown in Figure **4-21** suggests that the fill ratio is highest when the inclination angle is near vertical. It is true that there will be more liquid in the evaporator at higher inclination angles but the reason that may reduce the heat transfer rate under high inclination angles could be due to changes in the flow characteristic. At near horizontal inclination the liquid and vapor are stratified in that there will be less blockage effect and minimal entrainment.

4.3.3 Effect of Initial Pressure and reservoir Temperature on Fill Ratio

The effect of thermo-physical parameters such as reservoir temperature and initial pressure on fill ratio is the most important one. Both parameters determine the amount of fluid inside the thermosyphon and the dryout temperature. Figure **4-22** shows the effect of reservoir temperature on fill ratio. As the reservoir temperature increases the fill ratio at steady state and at dryout generally decreases. This suggests that the fill ratio can be improved by placing the reservoir in a cooler environment before charging the fluid into the system. Comparing Figure **4-22** and Figure **4-20** it is interesting to see that doubling

the size of the reservoir has nearly the same effect as reducing the temperature of the reservoir by half.

At last the effect of initial pressure on fill ratio is shown in Figure **4-23** . The result suggests that an increase in initial pressure increases the fill ratio. The important effect of initial pressure that differentiates it from other parameters is that the initial fill ratio remains substantially higher for a much larger temperature ranges. A 60% decrease in initial temperature improves the operating temperature range by 1.3K that is a 6.5% of the maximum possible temperature range for neon, which is 20K. On the other hand a 60% increase in initial pressure improves the temperature range by 3K that is a 15% of the maximum range. This suggests that the initial pressure is the most important parameter that determines the operation range of the closed two phase thermosyphon.

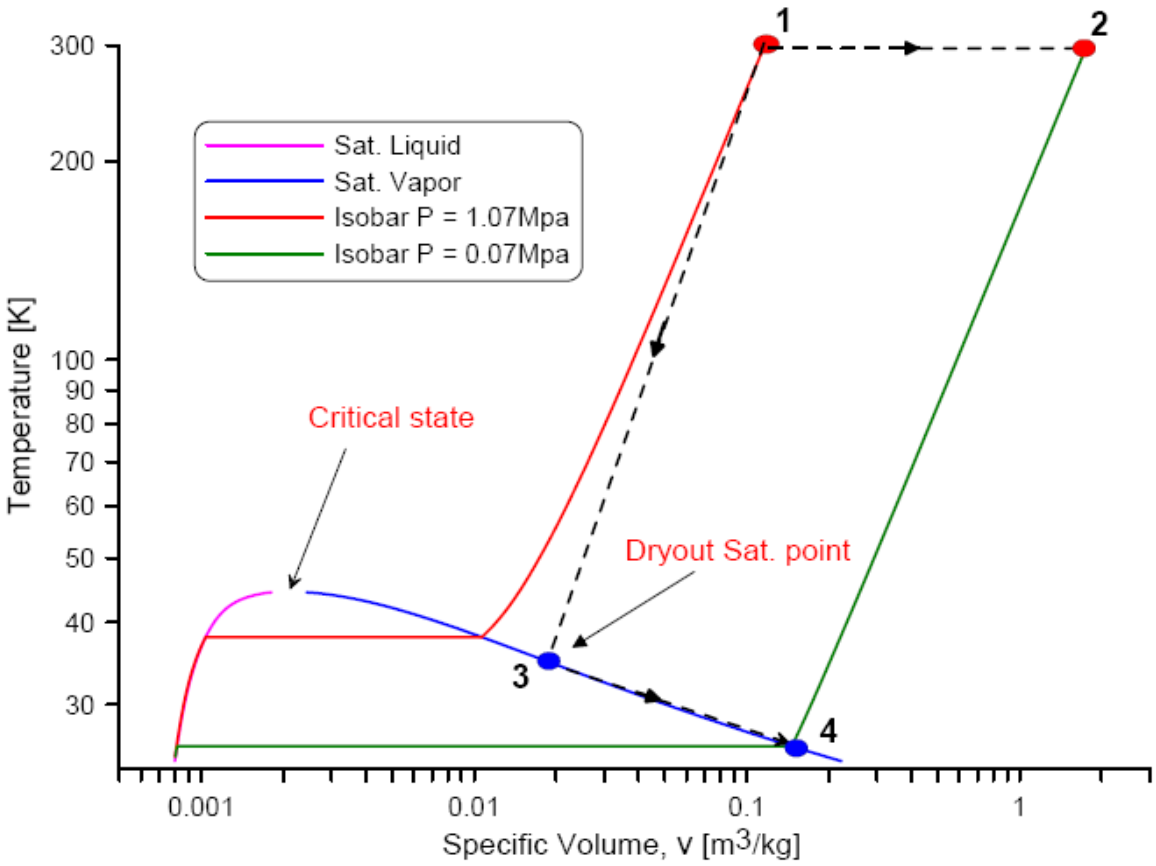

Figure **4-1**: Various thermodynamic states of the thermosyphon cooling system during cooldown

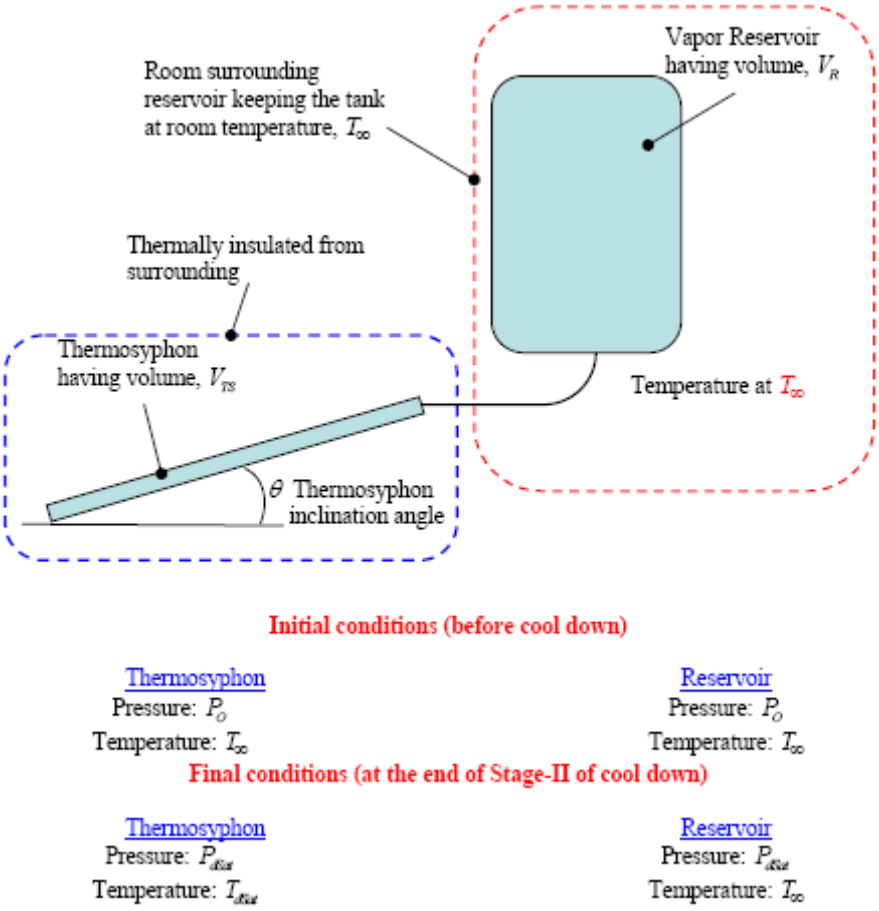

Figure **4-2**: Schematic diagram of the thermosyphon showing thermodynamic parameters

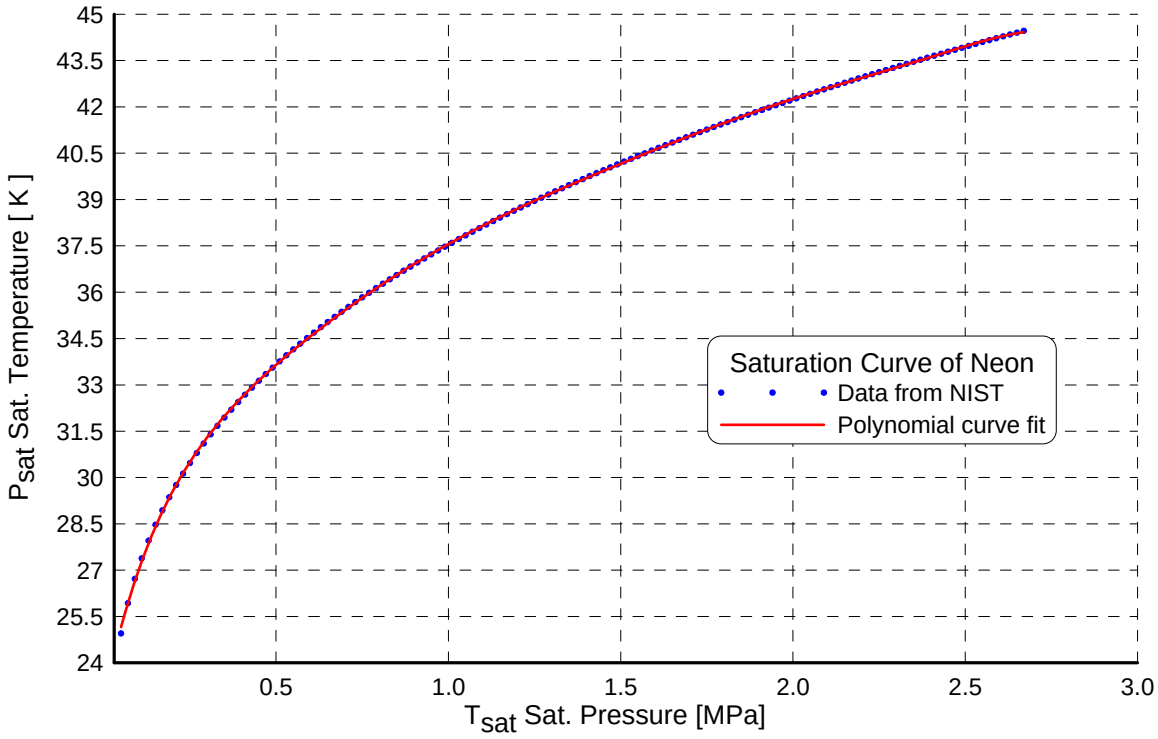

Figure **4-3**: Saturation data of neon obtained from NIST plotted with a polynomial curve fit

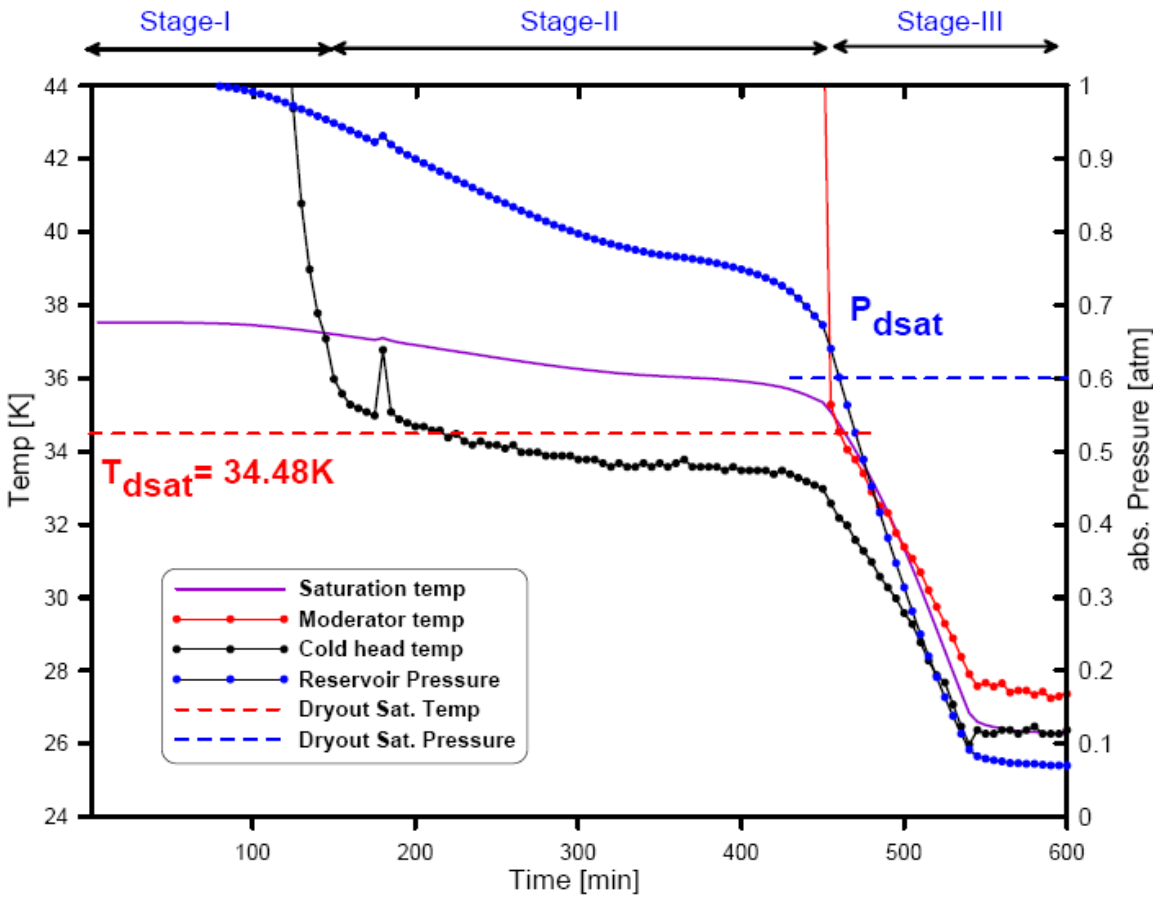

Figure **4-4**: Calculated dryout saturation temperature and saturation pressure shown on TCNS cooling system cooldown temperature and pressure diagrams

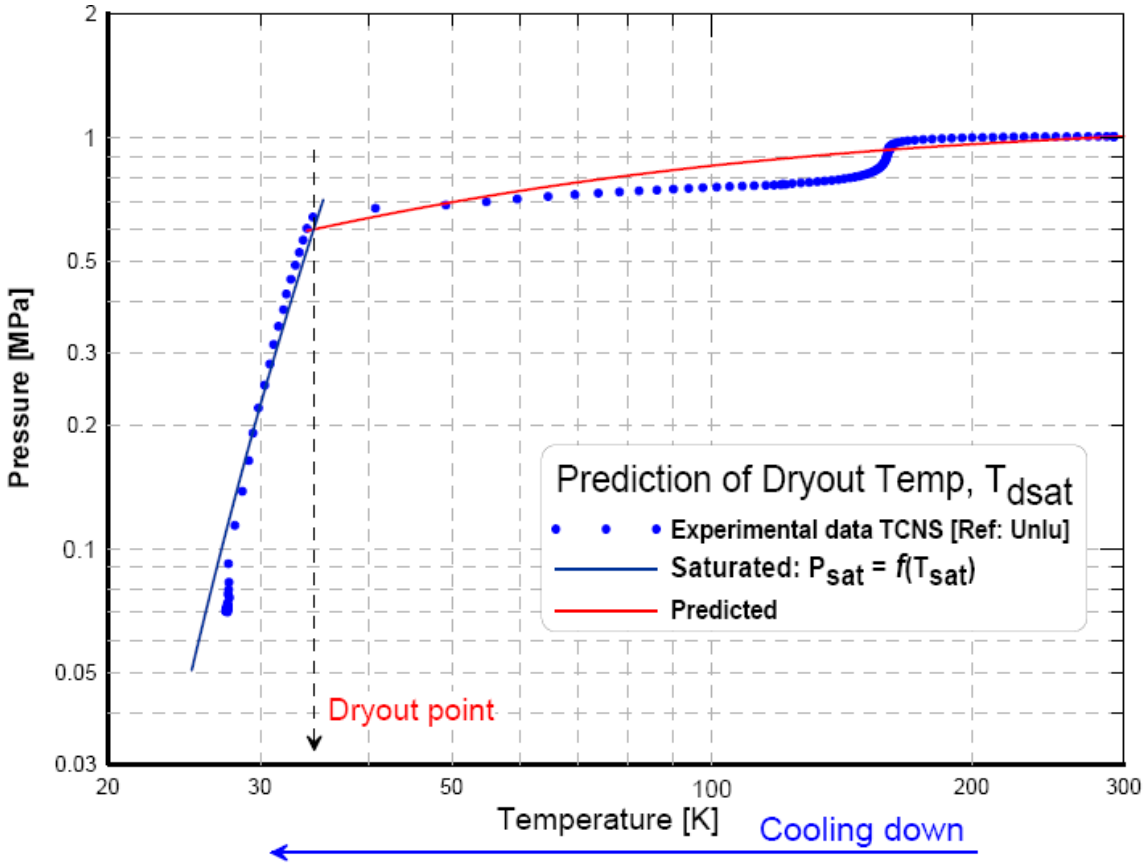

Figure **4-5**: Calculated dryout saturation temperature and saturation pressure for the TCNS cooling system cooldown diagram. The vapor temperature was taken to be the average of evaporator and condenser temperatures during stage-II

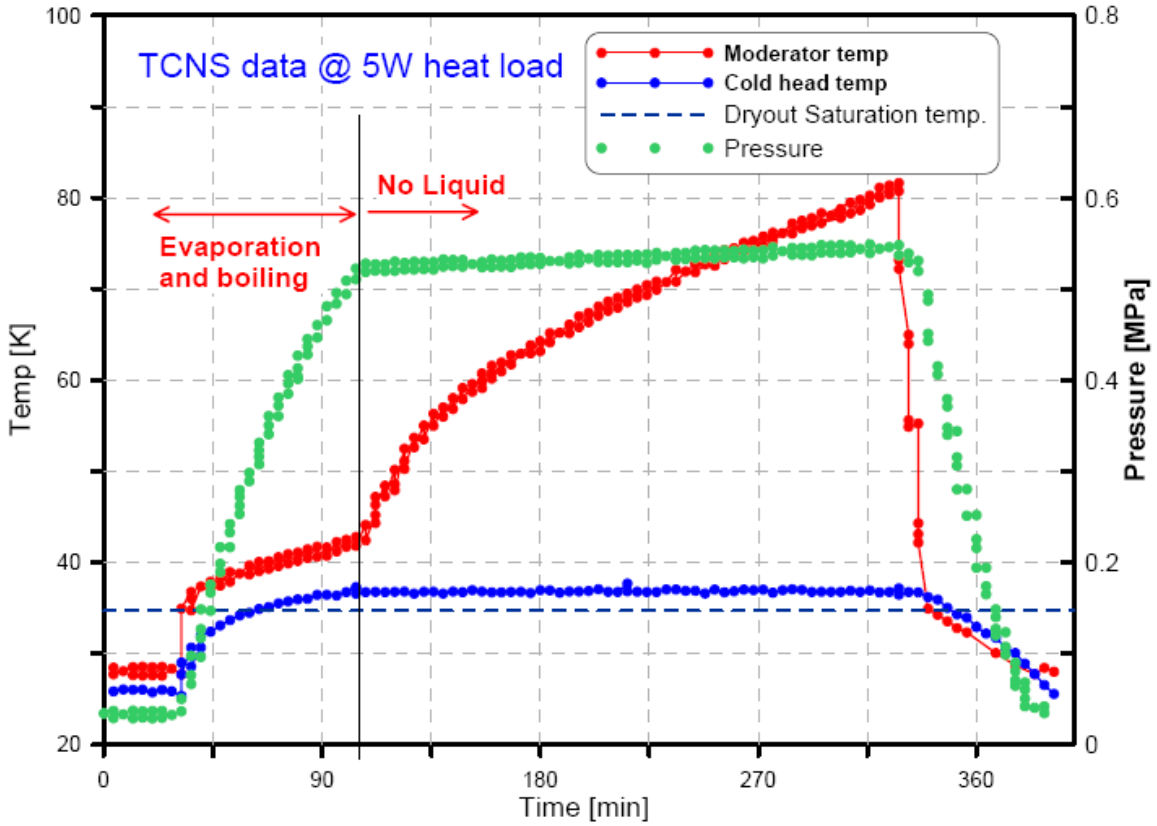

Figure **4-6**: Experimental plot of thermosyphon pressure, evaporator and condenser temperature showing the transient response of the TCNS cooling system at applied heat load of 5W.

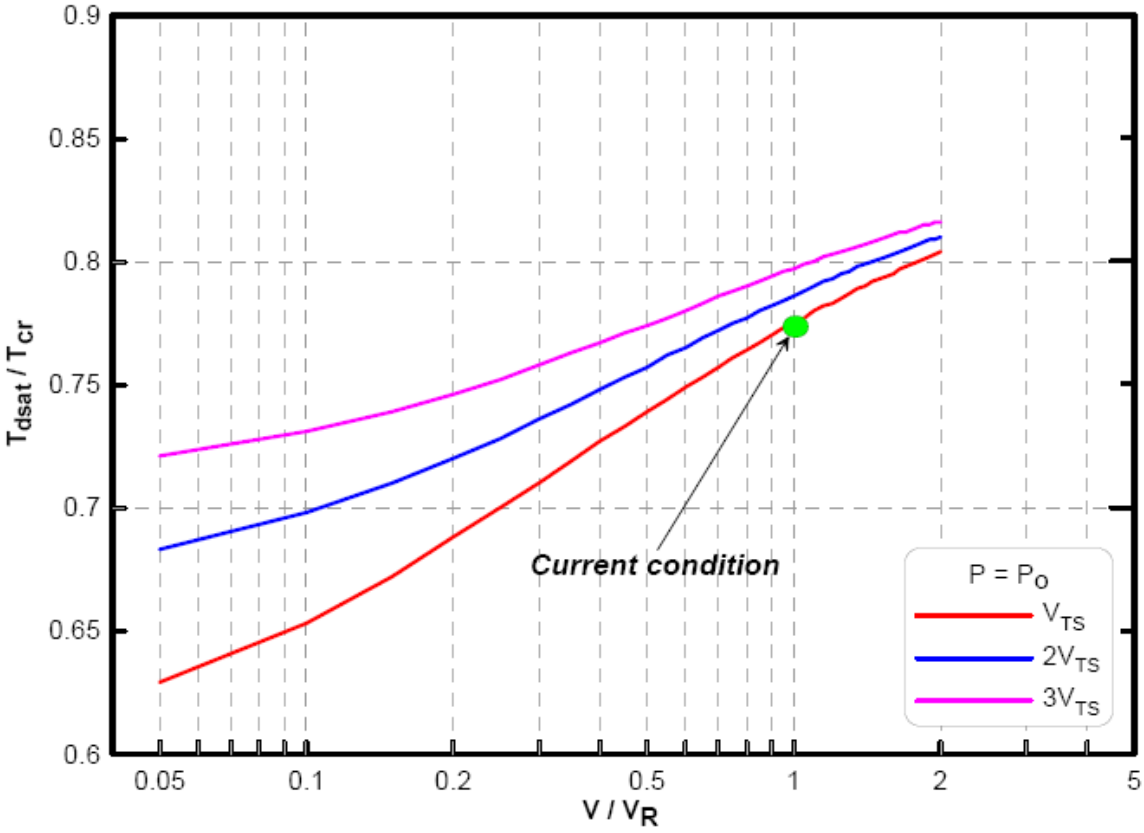

Figure **4-7**: Plot showing calculated normalized dryout temperature vs normalized reservoir volume at three thermosyphon volumes and with the same initial pressure used in TCNS cooling system

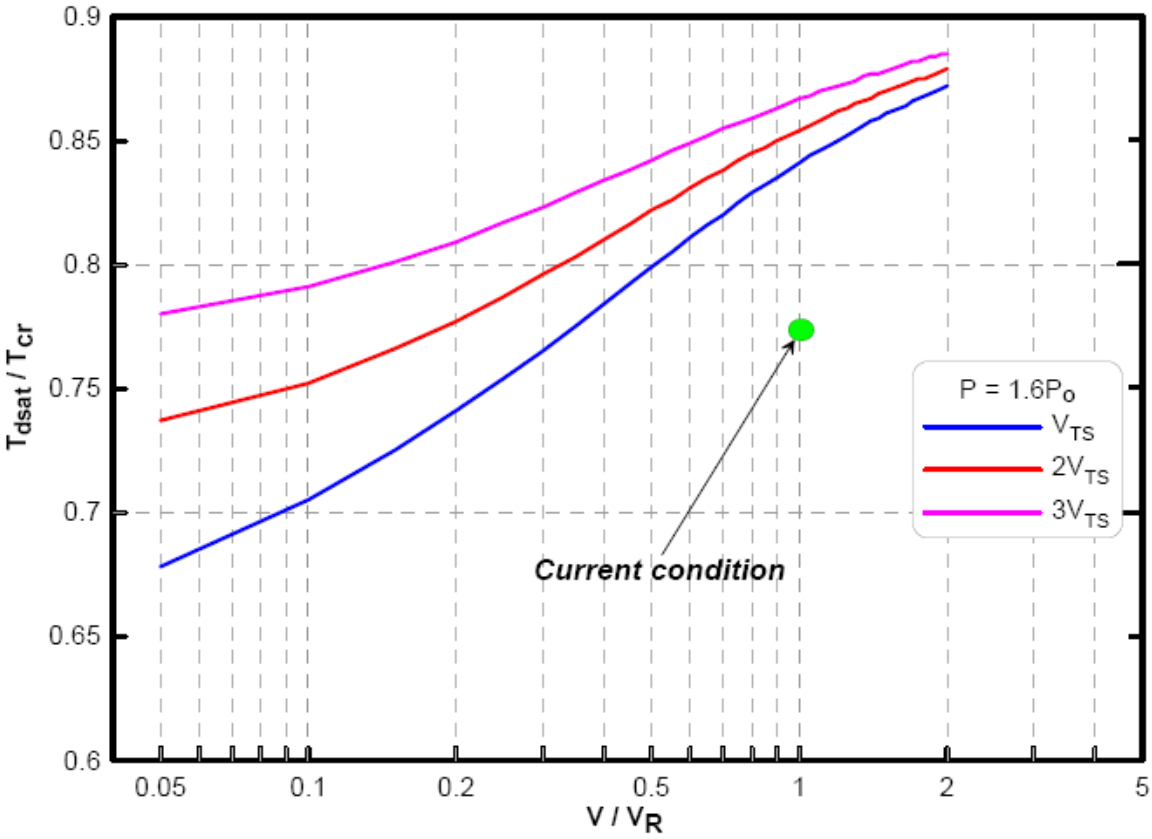

Figure **4-8**: Plot showing calculated normalized dryout temperature vs normalized reservoir volume at three thermosyphon volumes and with 1 1.6 times the initial pressure used in TCNS cooling system

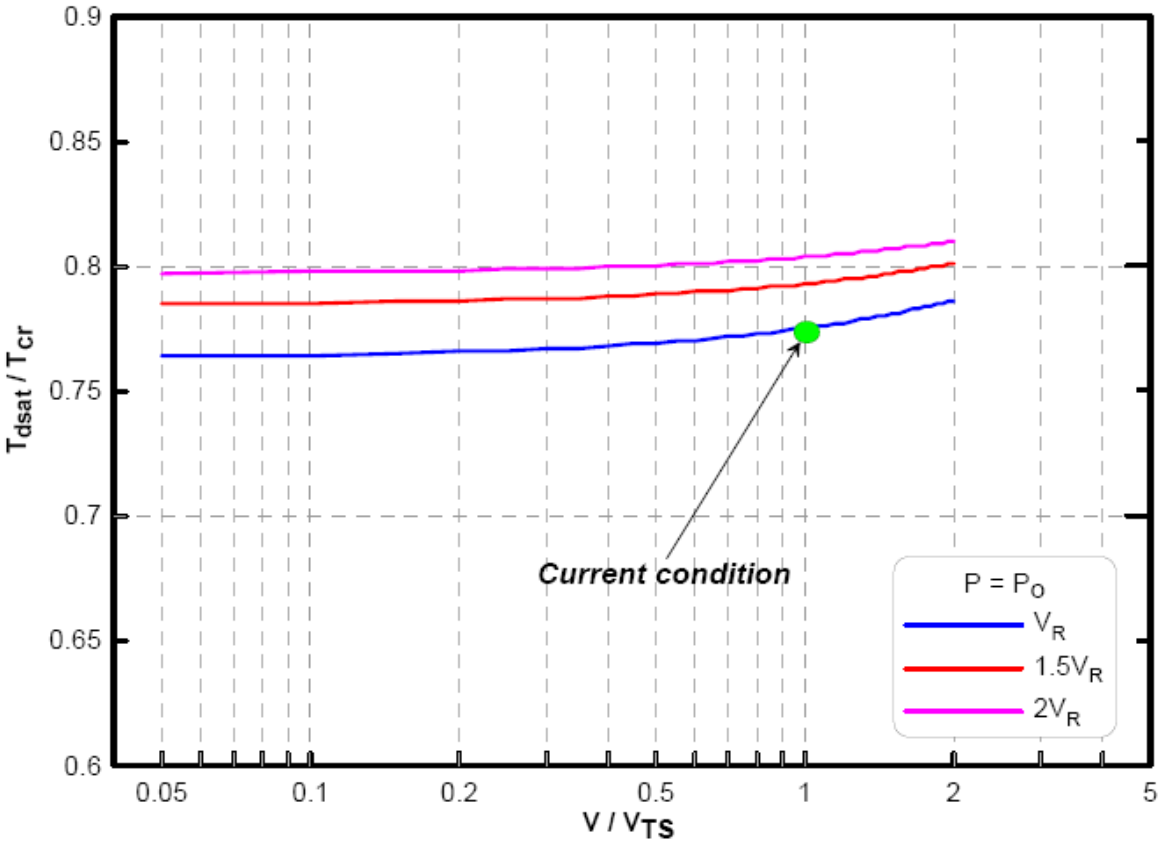

Figure **4-9**: Plot showing calculated normalized dryout temperature vs normalized thermosyphon volume at three reservoir volumes and with the same initial pressure used in TCNS cooling system

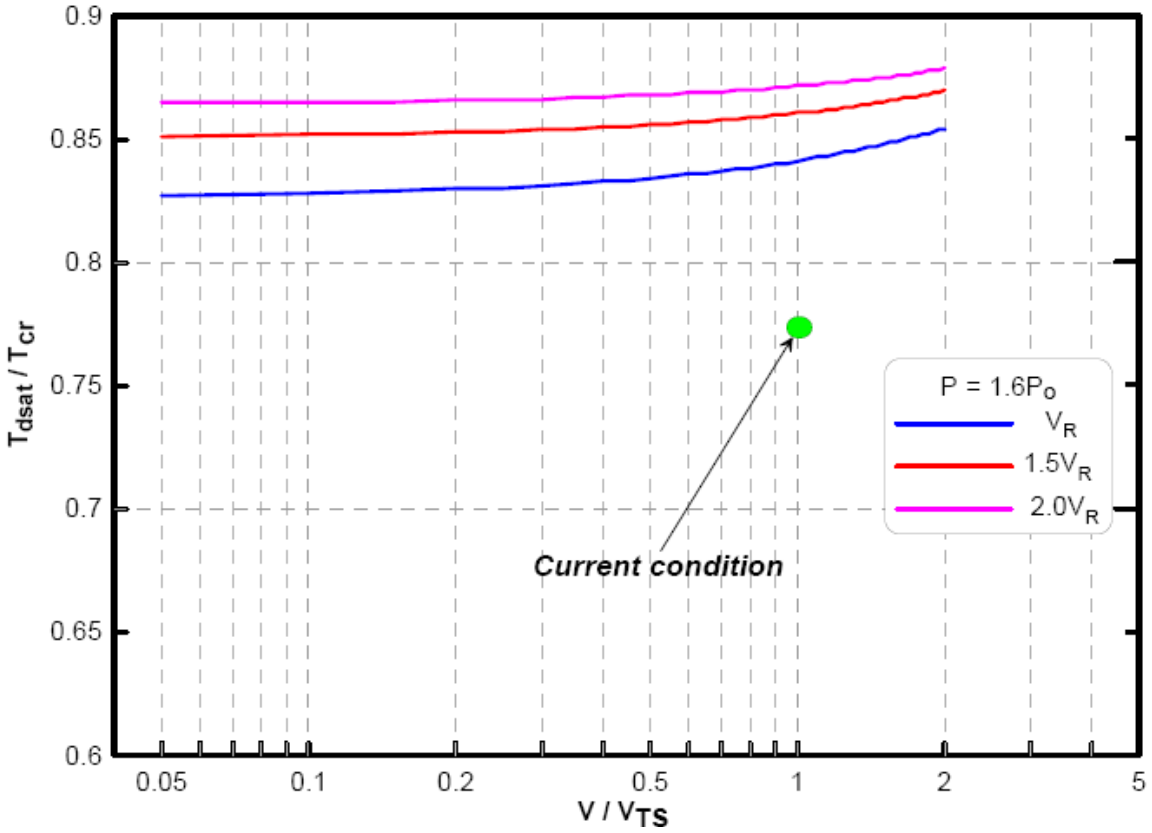

Figure **4-10**: Plot showing calculated normalized dryout temperature vs normalized thermosyphon volume at three reservoir volumes and with the same initial pressure used in TCNS cooling system

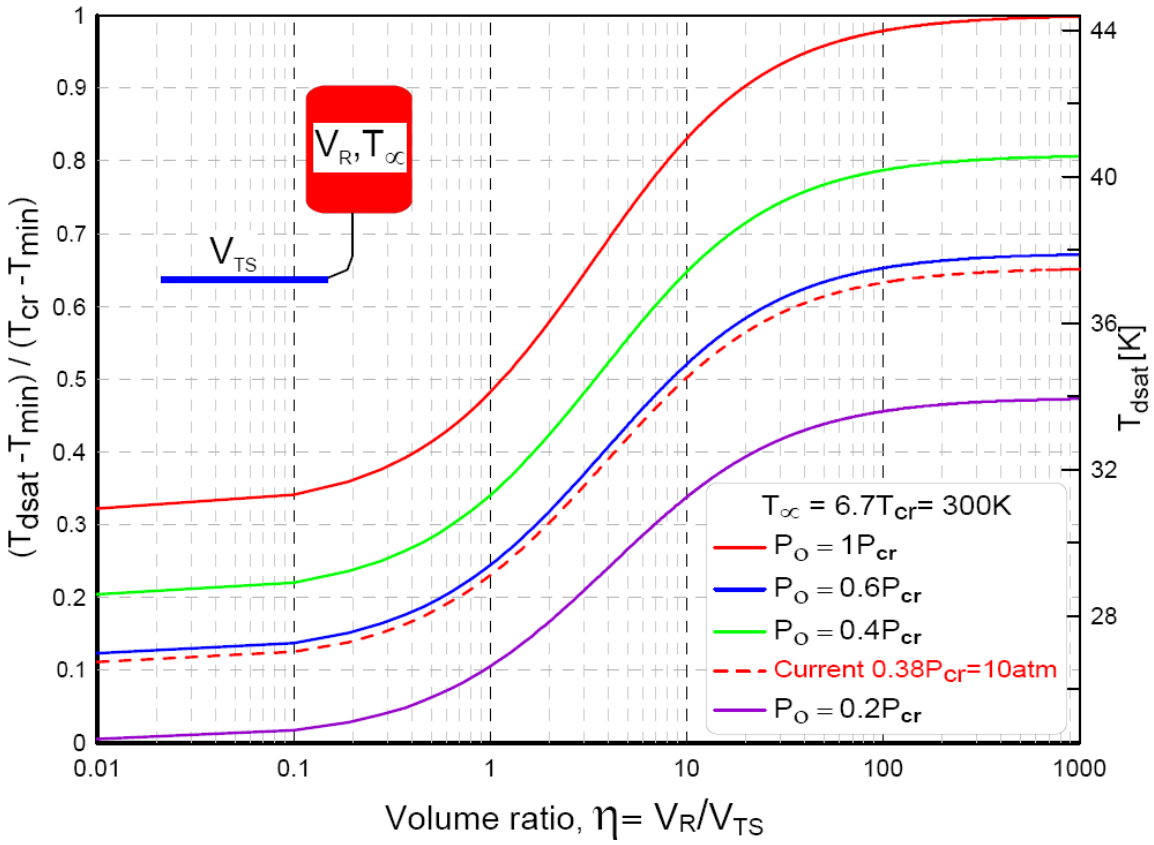

Figure **4-11**: Parametric plot showing the variation of normalized dryout saturation temperature vs volume ratio at various initial pressure and at reservoir temperature of 300K

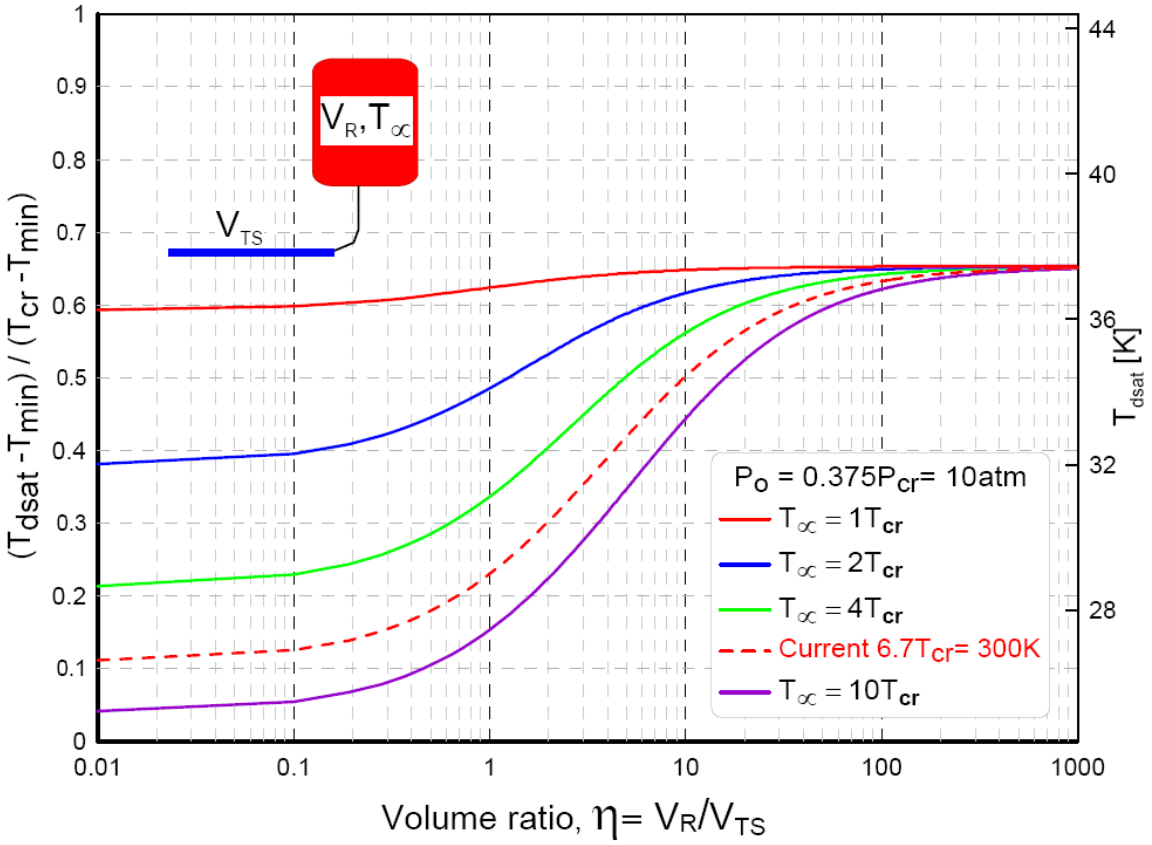

Figure **4-12**: Parametric plot showing the variation of normalized dryout saturation temperature vs volume ratio at various reservoir temperature and an initial pressure of 10atm

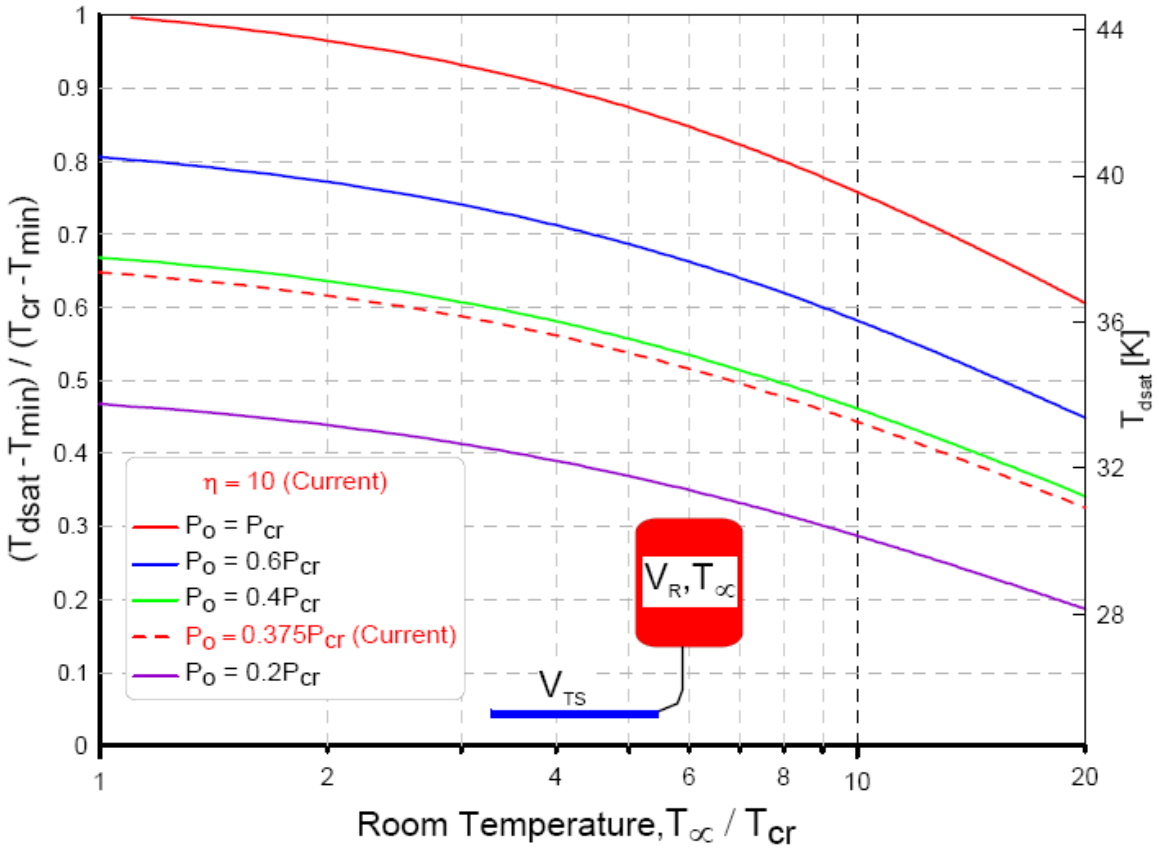

Figure **4-13**: Parametric plot showing the variation of normalized dryout saturation temperature vs normalized reservoir temperature at various initial pressure and a volume ratio of 10

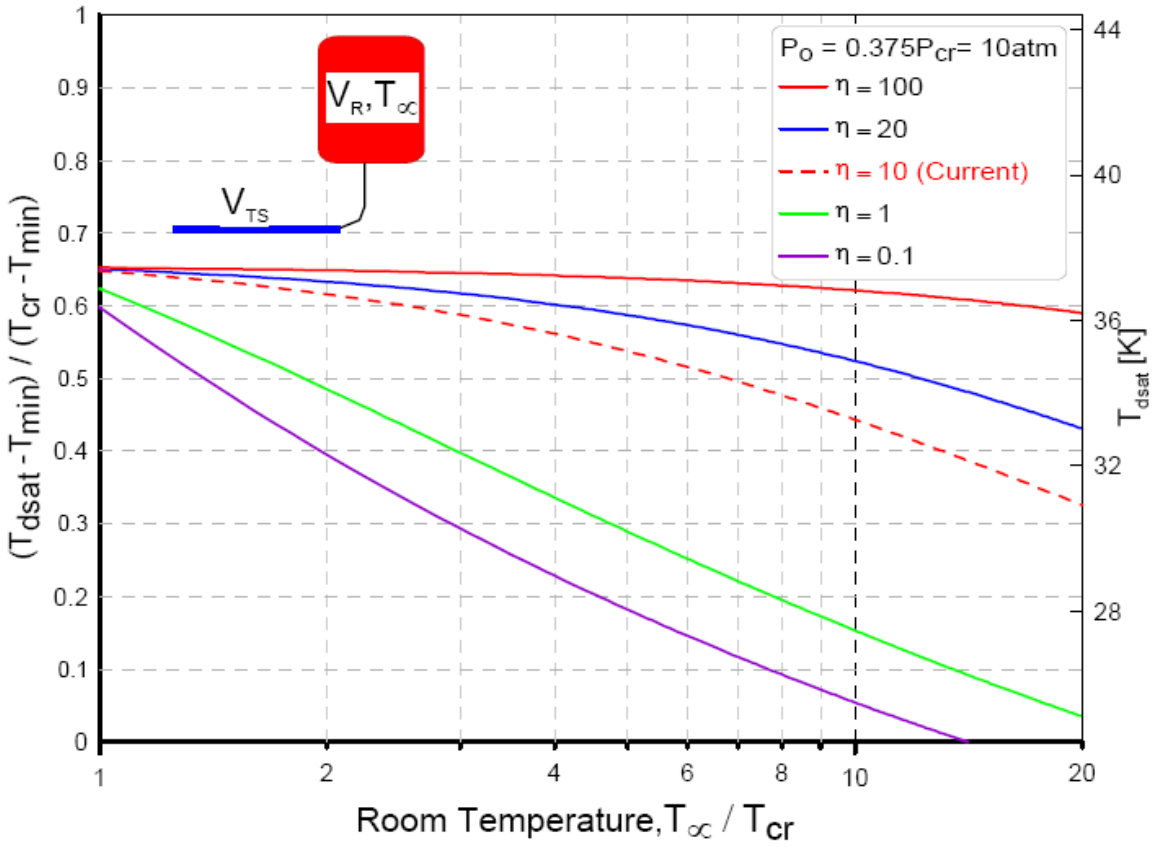

Figure **4-14**: Parametric plot showing the variation of normalized dryout saturation temperature vs normalized reservoir temperature at various volume ratio and initial pressure of 10atm

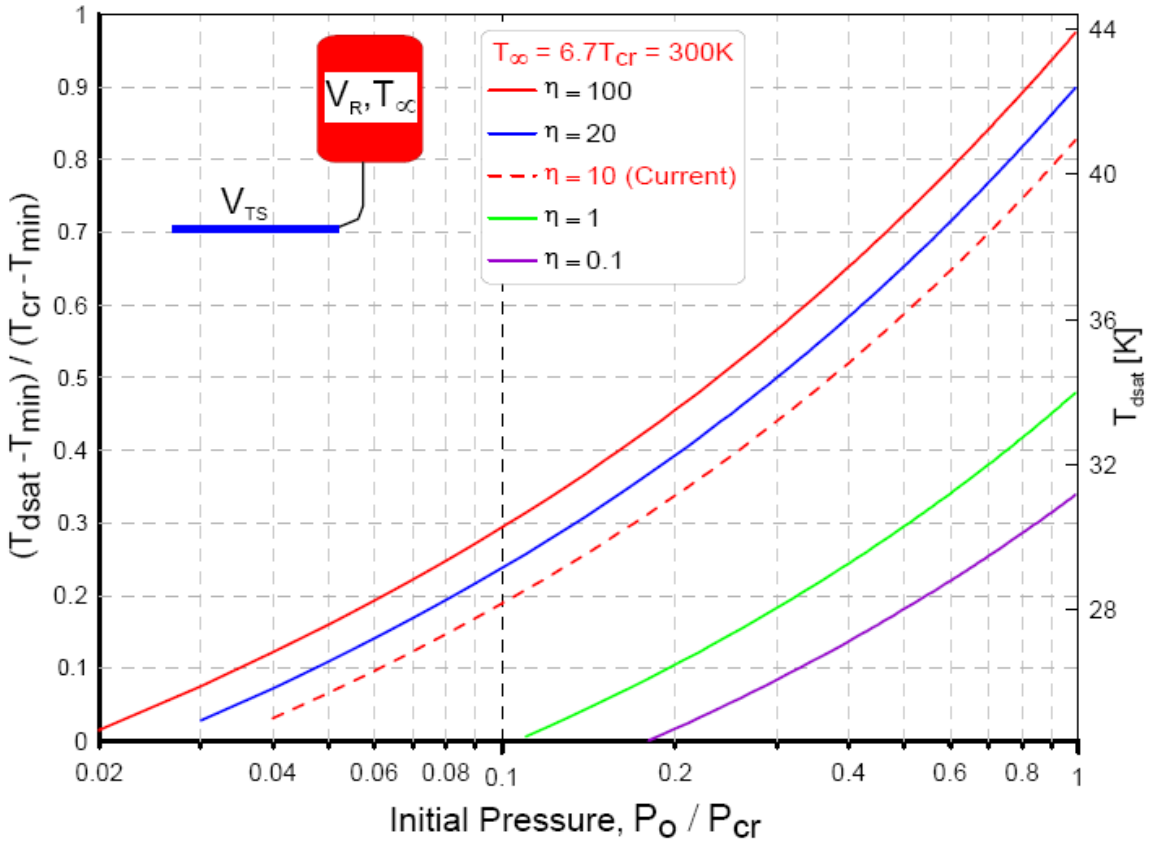

Figure **4-15**: Parametric plot showing the variation of normalized dryout saturation temperature vs normalized initial pressure at various volume ratio and reservoir temperature of 300K

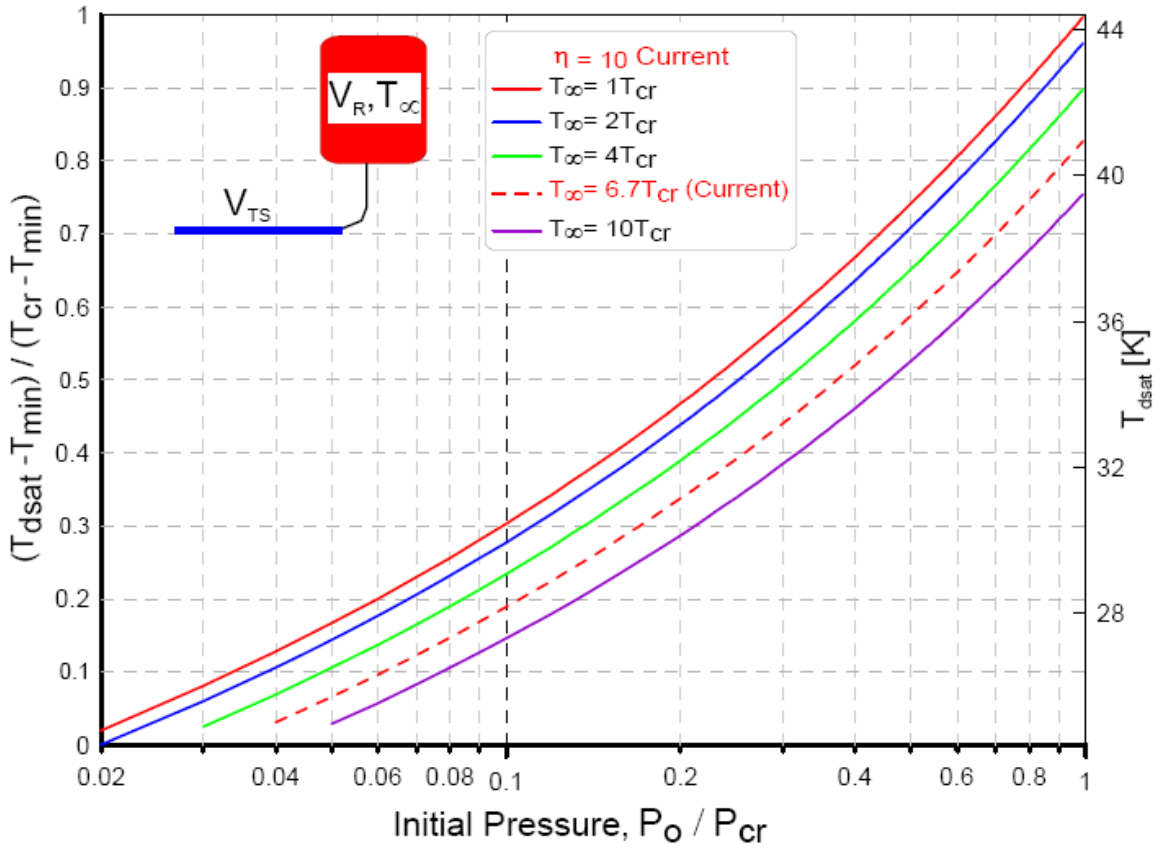

Figure **4-16**: Parametric plot showing the variation of normalized dryout saturation temperature vs normalized initial pressure at various reservoir temperature and a volume ratio of 10

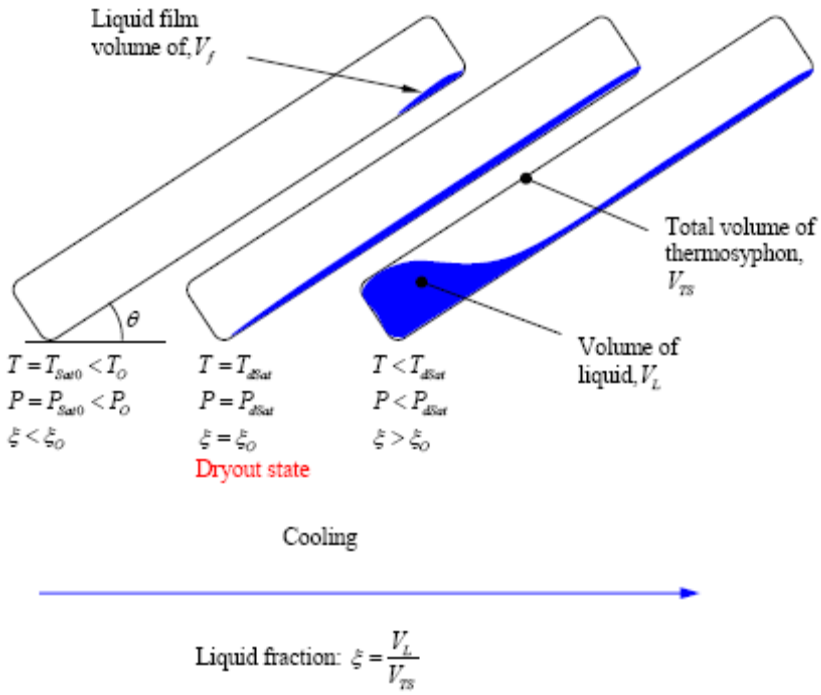

Figure **4-17**: Various thermodynamic states of fluid inside the thermosyphon during stage-II of cooldown process

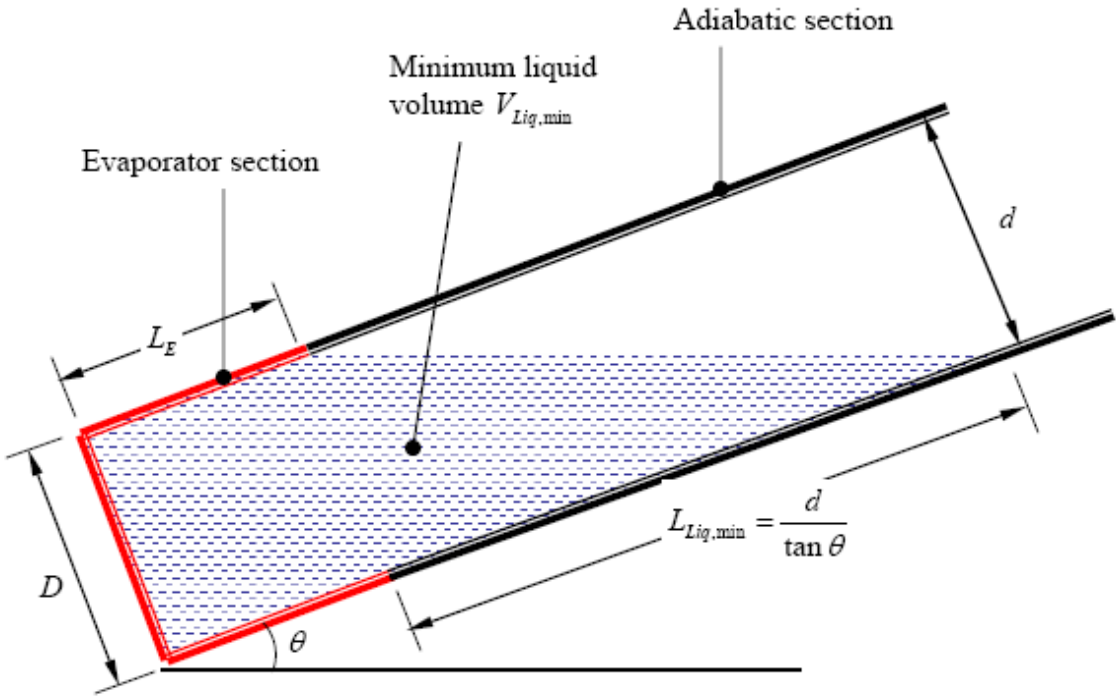

Figure **4-18**: Schematic showing the minimum liquid amount in an inclined two phase thermosyphon that will just cover the entire evaporator section

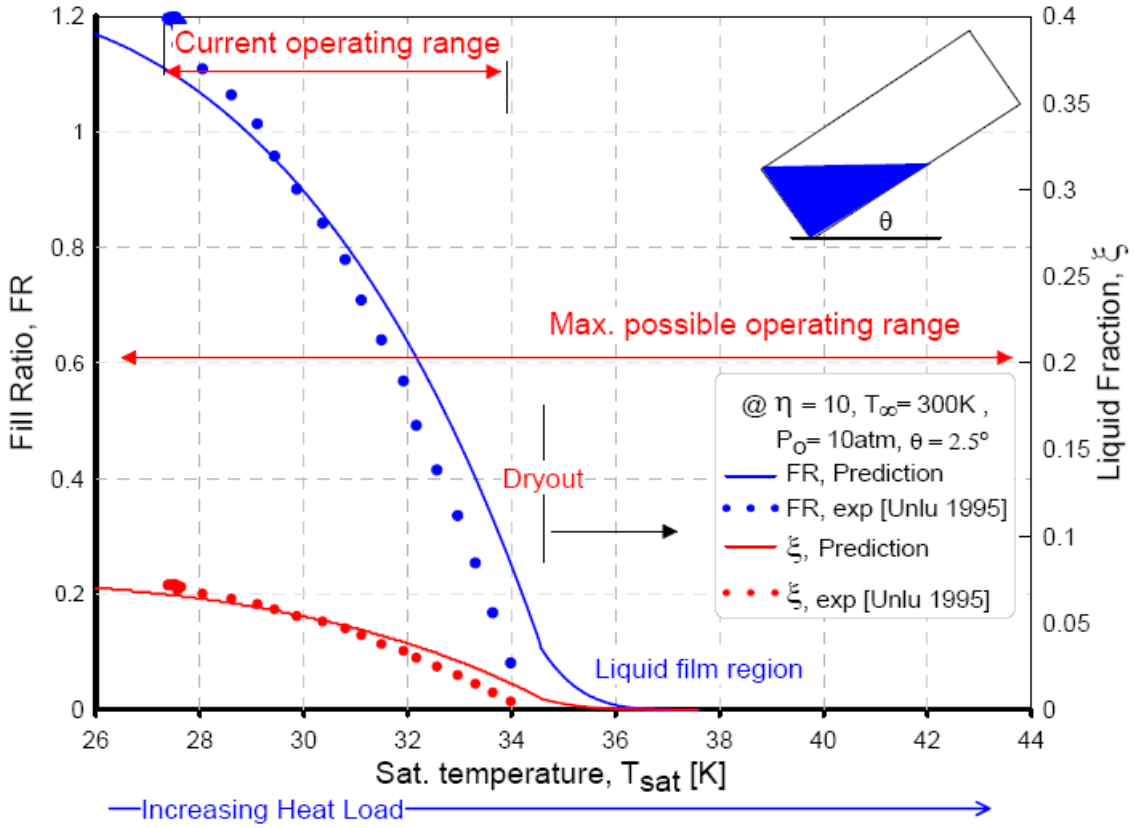

Figure **4-19**: Plot showing the fill ratio and liquid fraction vs saturation temperature of closed two phase thermosyphon. It also shows the experimental result calculated from data of pressure and temperature of the TCNS cooling system

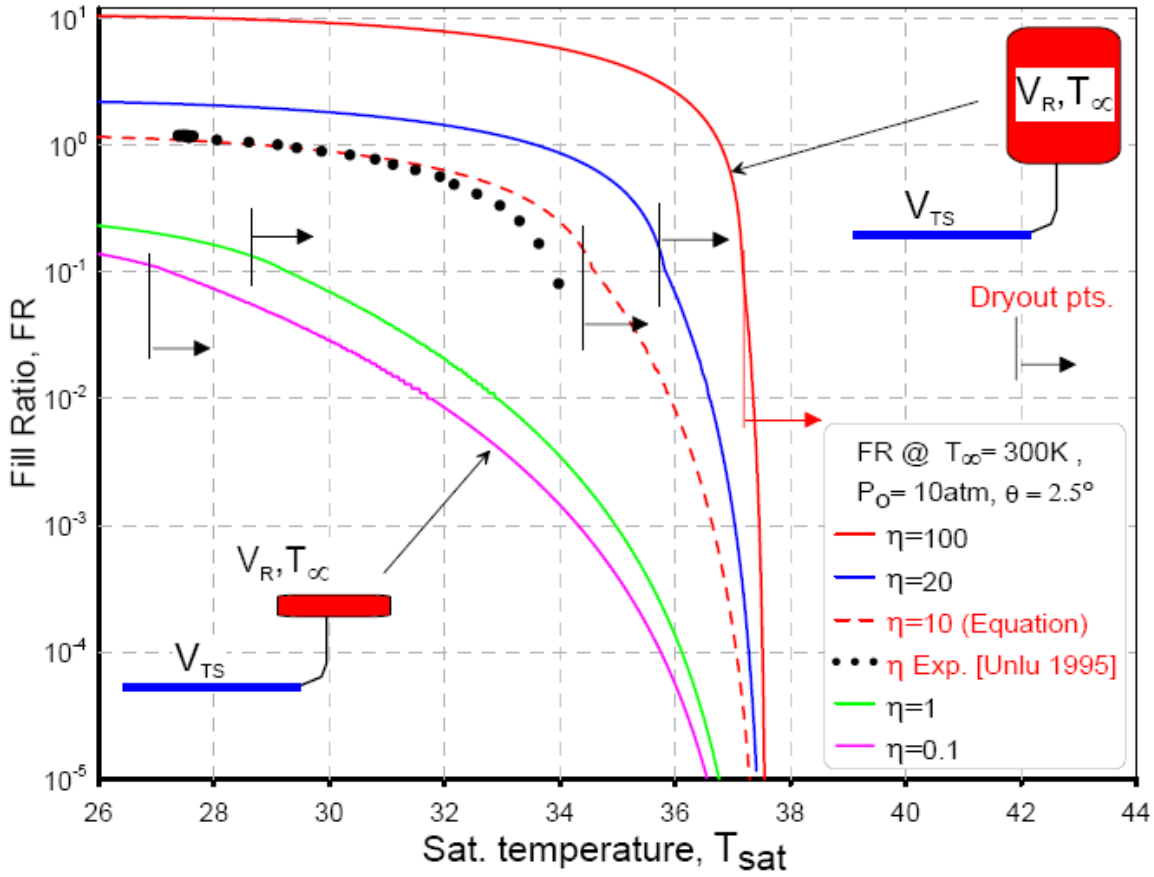

Figure **4-20**: Parametric plot showing of the effect of volume ratio η on fill ratio FR of closed two phase thermosyphon. The constant parameters correspond to the TCNS thermosyphon

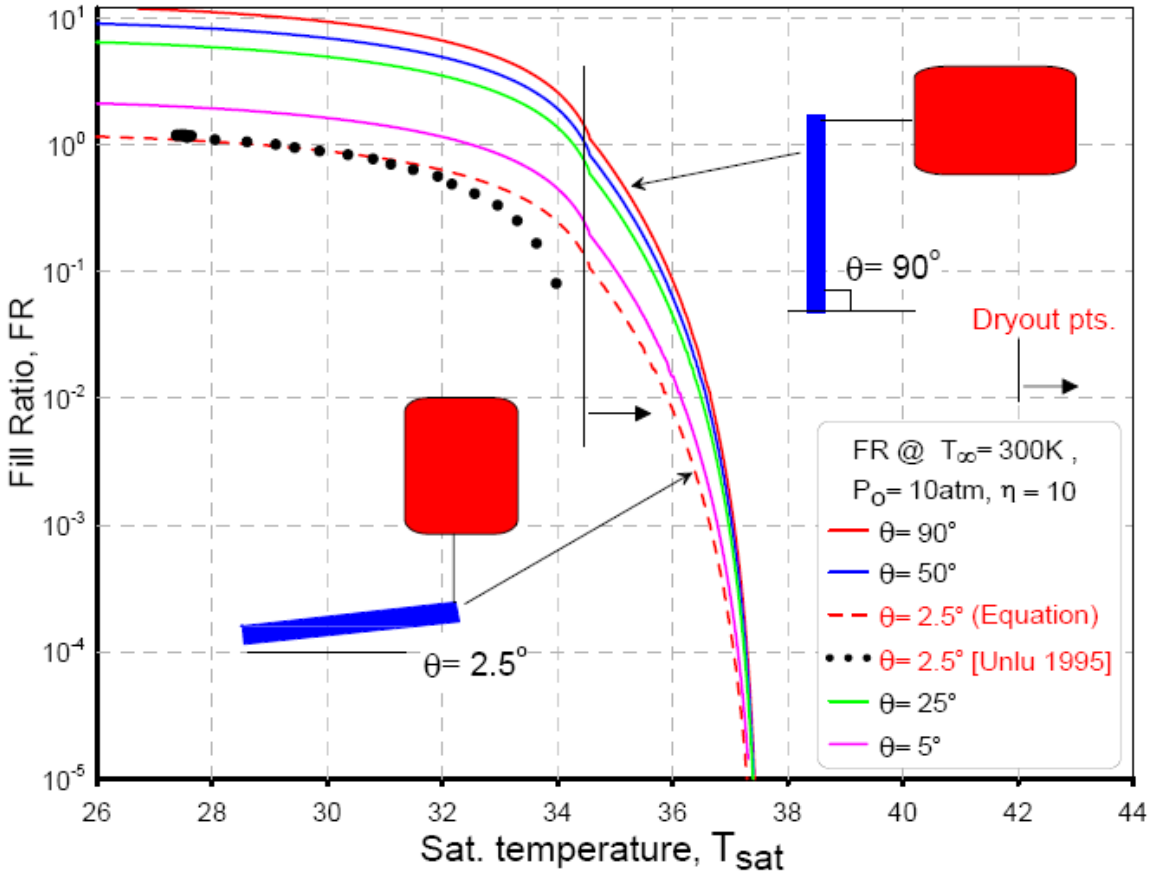

Figure **4-21**: Parametric plot showing of the effect of inclination angle θ on fill ratio FR of closed two phase thermosyphon. The constant parameters correspond to the TCNS thermosyphon

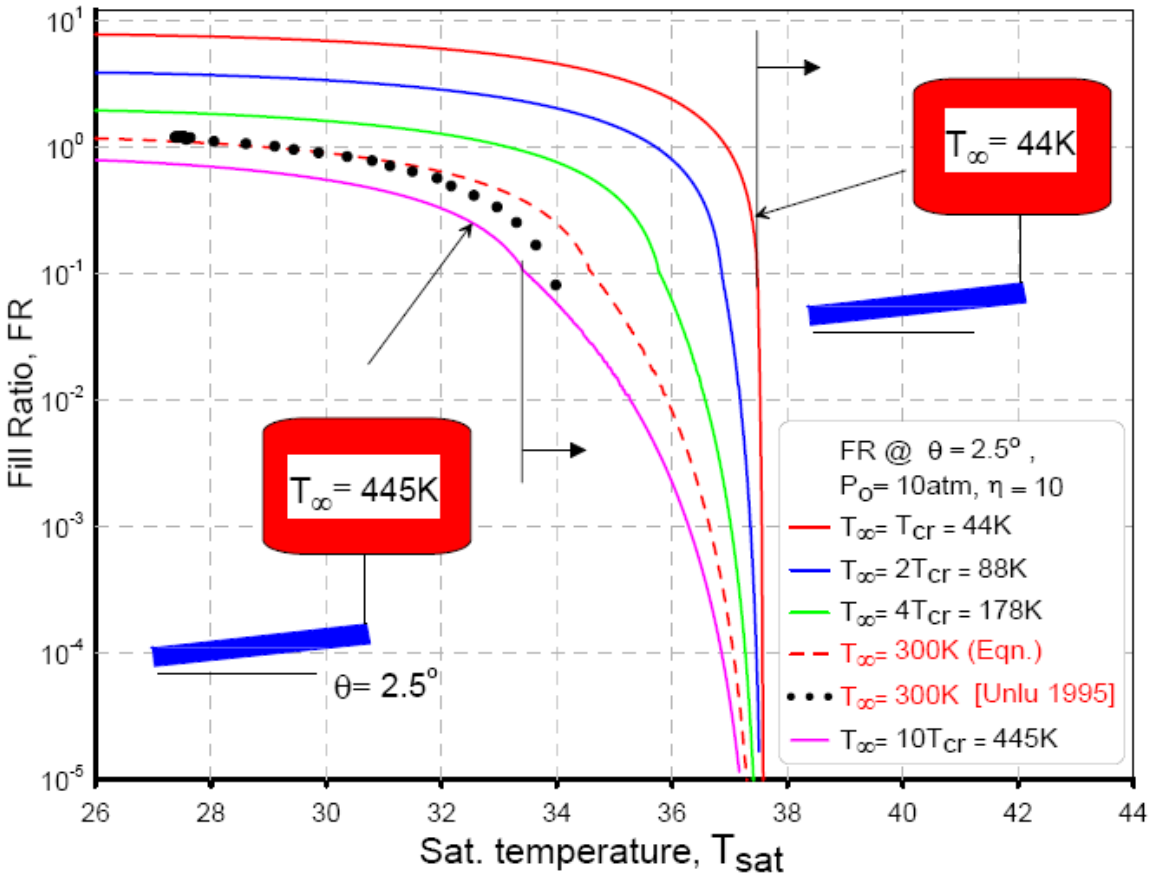

Figure **4-22**: Parametric plot showing of the effect of reservoir temperature T_∞ on fill ratio *FR* of closed two phase thermosyphon. The constant parameters correspond to the TCNS thermosyphon

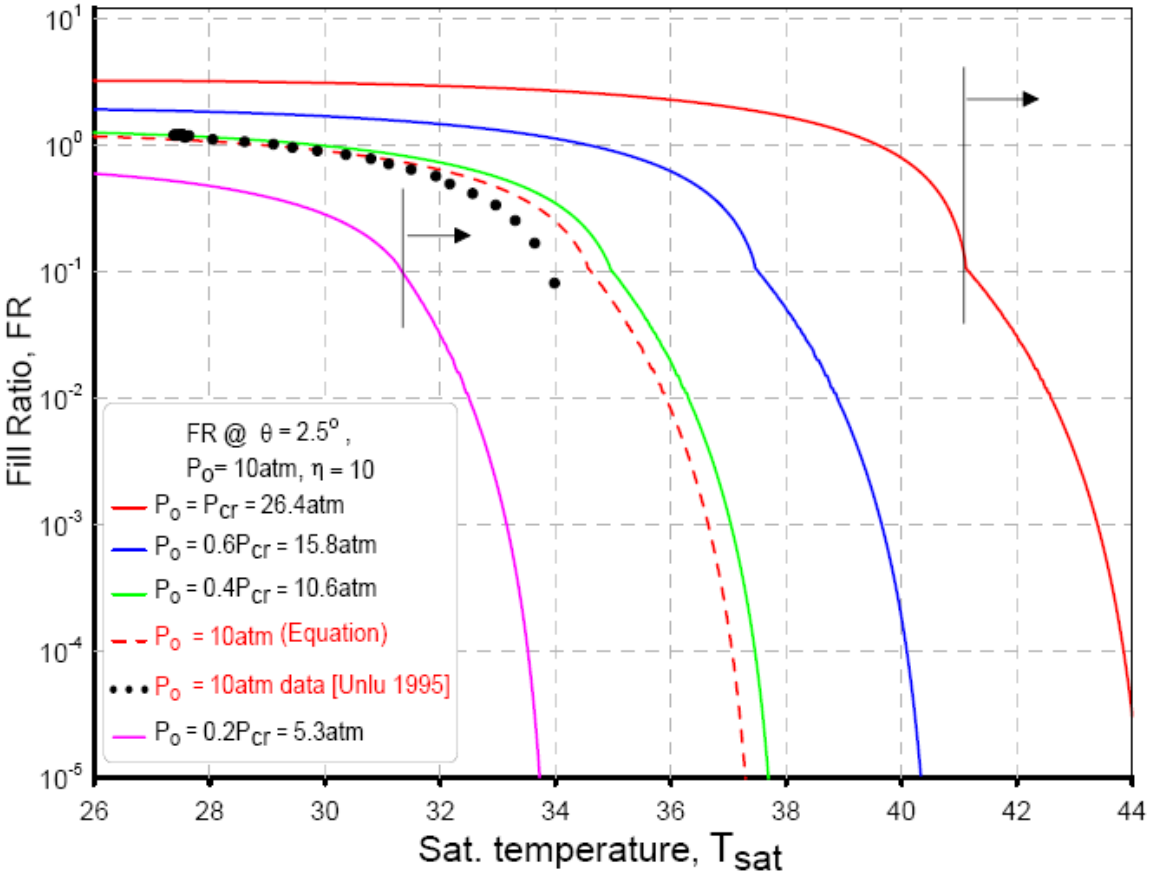

Figure **4-23**: Parametric plot showing of the effect of inclination angle P_O on fill ratio FR of closed two phase thermosyphon. The constant parameters correspond to the TCNS thermosyphon

Chapter 5

Heat Transfer Analysis for a Two Phase Closed Thermosyphon with Reservoir

In this chapter the various heat transfer mechanisms that exist in a closed two phase thermosyphon is discussed. The thermal performance is carried out analytically and comparison is made with experimental results obtained from the TCNS system.

5.1 Steady State Heat Transfer Analysis of a Closed Two Phase Thermosyphon with Reservoir (TPCTR)

5.1.1 Modes of Heat Transfer

The three basic modes of heat transfer are conduction, convection and radiation. In the thermal analysis of closed two phase thermosyphon the first two modes are relevant. The heat flow across a boundary is defined as

$$Q = \frac{\Delta T}{R_{th}} \tag{5.1}$$

Where: Q is the heat flow rate; R_{th} is the thermal resistance across the boundary and ΔT is the temperature difference. When the heat transfer occurs across several boundaries a more general form of Eq. **5.1** can be given as:

$$Q = \frac{\Delta T_{overall}}{\sum R_{th}} \tag{5.2}$$

Where: $\sum R_{th}$ is the net thermal resistance across all the boundaries; $\Delta T_{overall}$ is the overall temperature difference across the boundaries. In conduction heat transfer, the heat flow is proportional to the temperature gradient normal to the boundary and is given by:

$$Q = -kA\frac{\partial T}{\partial x} \quad \textbf{5.3}$$

Where k is the thermal conductivity; A is the normal cross sectional area of the boundary across which heat flows. This is the heat transfer mode that involves the solid walls of the thermosyphon tube. On the other hand, convection heat transfer occurs when heat flows through a fluid-solid interface. This type of heat transfer occurs between the inside walls of the thermosyphon and the fluid contained inside. The heat transfer rate is related to the temperature difference between the solid wall and the surrounding fluid as

$$Q = hA\left(T_w - T_\infty\right) \quad \textbf{5.4}$$

Where: h is the convective heat transfer coefficient; T_w and T_∞ are the wall and the surrounding fluid temperatures respectively. As shown in Table **5-1** boiling heat transfer gives a very large heat transfer coefficient as compared to other modes of heat transfer. The term heat flux q is often used in heat transfer analysis and is defined as the heat flow per unit area:

$$q = \frac{Q}{A} \quad \textbf{5.5}$$

Boiling heat transfer is the most important heat transfer mechanism in thermosyphons. It offers a very high heat transfer coefficient and hence very low thermal resistance as compared to the other forms of heat transfer. Boiling occurs when a surface

is exposed to a liquid and is maintained at a temperature above the saturation temperature of the liquid. When the heated surface is submerged below the free surface of the liquid the process is called pool boiling. If the temperature of the liquid is below the saturation temperature, the process is called subcooled boiling. If the liquid is maintained at the saturation temperature, the process is called saturated boiling [**Holman-1997**]. The various regimes of boiling are shown in the boiling curve reproduced from [**Holman-1997**] as shown in Figure **5-1** .The heat flux data from platinum wire is plotted against the wall superheat (temperature excess) $T_w - T_{Sat}$. In region-I the free convection current are responsible for the motion of fluid near the surface. In this region the liquid near the surface is slightly superheated, and it subsequently evaporates as it rises to the surface. The heat transfer in this region is calculated using free-convection relations. In region-II the bubbles begin to form on the surface and dissipated in the fluid after breaking away from the surface. This region indicated the beginning of nucleate boiling. As the temperature excess increases more and more bubbles are released from the surface faster and rise to the surface of the liquid this is indicated by region-III. Eventually bubbles are released so rapidly that they blanket the entire heating surface and prevent inflow of fresh liquid to the surface. At this point the bubbles coalesce and form a vapor films which covers the surface. The heat must be conducted through this film before it can reach the liquid and effect boiling process. The thermal resistance in this film causes a reduction in heat flux, and this phenomenon is illustrated in region-IV, the film boiling region this region represents a transition from nucleate to film boiling and is unstable. Stable film boiling is encountered in region-V [**Holman-1997**].

In analysis of two phase heat transfer such as boiling, it is important to determine the heat transfer coefficient that is often given in the form of empirical correlation. The earliest and most widely used correlation for nucleate boiling is Rohsenow's correlation [**Carey-2008**] given by

$$\frac{q}{\mu_L h_{lv}}\left[\frac{\sigma}{g\left(\rho_l-\rho_v\right)}\right]^{\frac{1}{2}}=\left(\frac{1}{C_{sf}}\right)^{\frac{1}{r}}\mathrm{Pr}_L^{-\frac{s}{r}}\left[\frac{Cp_L\left(T_w-T_{Sat}\left(P_L\right)\right)}{h_{lv}}\right]^{\frac{1}{r}} \qquad \textbf{5.6}$$

Where: h_{lv} is latent heat of the fluid, σ surface tension, ρ_l and ρ_v are densities of liquid and vapor phase of the fluid, μ_L viscosity of the liquid, $\mathrm{Pr}_L=\left(\mu Cp/k\right)_L$ Prandtl number of the liquid, Cp_L specific heat of the liquid, $T_{Sat}\left(P_L\right)$ saturation temperature at the liquid pressure. The constant values of $r=0.33$ and $s=1.7$ were recommended for the correlation. Subsequently Rohsenow recommended that for water only, s be changed to 1.0. The values of the constant C_{sf} are often tabulated depending on the surface-liquid combination and typical the values of as 0.0058 to 0.01 are common [**Carey-2008**].

A more recent result from Stephan and Abdelsalam [**Carey-2008**] that is based on dimensional analysis and fits to optimal experimental data gives a more compact form. For cryogenic fluids they proposed the following equation:

$$q=\left\{C_3\left(\rho\cdot Cp\cdot k\right)_S^{0.117}\left[T_w-T_{Sat}\left(P_L\right)\right]\right\}^{\frac{1}{0.376}} \qquad \textbf{5.7}$$

The constant C_3 for cryogenic fluids can be obtained from Figure **5-2** . For neon this value is 20 at a pressure of 10 bar. In Eq. **5.7** the units to be used are

kg/m^3 for ρ, $kJ/kg\,^oC$ for Cp, W/m^oC for k, ^oC for $T_w - T_{Sat}(P_L)$ and W/m^2 for q. The term $(\rho \cdot Cp \cdot k)_S$ represents the indicated properties of the heated surface [**Carey-2008**].

5.1.2 Heat Transfer in the Evaporator Section

The evaporator section as shown in Figure **5-3** is where the heat load from the moderator of the cooling system applied on the thermosyphon. The head absorbed by the moderator fluid, flowing inside the moderator chamber, passes radially through the evaporator wall by conduction. The heat passing through the thin wall evaporates and/or boils the condensed liquid returning from the condenser, depending on the heat flux. In Figure **5-3** an equivalent thermal resistance diagram for the evaporator is shown. The various thermal resistances in the evaporator section are: the radial conduction resistance across the evaporator wall $R_{E,o}$, the boiling and evaporation resistance inside the evaporator wall $R_{E,i}$ and the axial conduction resistance through the long thermosyphon adiabatic wall R_{ad}. Using Fourier's law, the radial conduction resistance is given by:

$$R_{E,o} = \frac{\ln\left(\frac{D}{d}\right)}{2\pi L_E \cdot k_{Al}} \qquad \textbf{5.8}$$

Where L_E is length of the evaporator section, k_{Al} the thermal conductivity of the aluminum wall and D and d are the outside and inside diameter of the thermosyphon respectively. Similarly the axial thermal resistance of the adiabatic wall is given by

$$R_{ad} = \frac{4\left(L_{TS} - \left(L_E + L_C\right)\right)}{\pi\left(D^2 - d^2\right)k_{Al}} \qquad \textbf{5.9}$$

Where L_{TS} is total length of the thermosyphon; L_C is the length of the condenser section. The thermal resistance in the inside wall due to evaporation and boiling is given by

$$R_{E,i} = \frac{1}{\pi d \cdot L_E \cdot h_E} \quad \textbf{5.10}$$

Where h_E is the inside wall heat transfer coefficient of the evaporator. This heat transfer coefficient depends on the nature of the heat flux. The main forms of heat transfer mechanism that exist in the liquid-solid wall interface are natural convection that exists at low heat flux, nucleate boiling at a higher heat flux and evaporative liquid film at low filling ratio conditions. It is possible that film boiling could occur if the heat flux is increased above the critical value as shown in Figure **5-1** but this operation must be avoided since film boiling is very inefficient form of heat transfer.

For natural convection, the heat transfer coefficient is given by

$$h_{NC} = C_1 \frac{k_L}{L_E} \left(\frac{g \beta \rho_L Cp_L q_E L_E}{k_L^2 \nu_L} \right)^{C_2} \quad \textbf{5.11}$$

Where the constants C_1 and C_2 depend on the flow pattern, laminar or turbulent; β is the volumetric expansion coefficient of the liquid; q_E is the heat load at the evaporator section [**Jiao et al 2007**].

For higher heat flux the mode of heat transfer will be nucleate boiling. The nucleate boiling heat transfer coefficient can be obtained by rearranging Eq. **5.7** as:

$$h_{NB} = \left\{ C_3 \left(\rho \cdot Cp \cdot k \right)_S^{0.117} \left[T_w - T_{Sat}\left(P_L \right) \right]^{0.624} \right\}^{\frac{1}{0.376}} \quad \textbf{5.12}$$

Figure 5-4 summarizes the various heat transfer regimes that are anticipated to exist at various levels of heat load inside the evaporator. At lower heat flux, where natural convection is the major heat transfer mechanism, the fill ratio is close to 1 or 100%. The liquid pool covers the entire inside wall of the evaporator. As the heat flux increases the flow regime is expected to change from natural convection type to nucleate boiling. The fill ratio will decrease and less and less amount of liquid will touch the evaporator surface. This by itself increases the heat flux. A further increase in heat load will bring the saturation temperature to the dryout point where only liquid film exists. The liquid film in this last stage, although having a relatively higher heat transfer coefficient than nucleate boiling, will eventually disappear due to excessive rate of evaporation.

5.1.2.1 Heat Transfer in Liquid Film of Evaporator

In the post-dryout condition where the saturation temperature reaches above the dryout temperature $T_{Sat} > T_{dsat}$ the boiling/evaporative heat transfer area becomes very small due to less and less liquid touching the inside of the evaporator walls. This reduction in area together with increasing heat load will increases the heat flux q to the evaporator. The mechanism of heat transfer in this liquid film is investigated in the past and appropriate correlations for the various flow regimes were suggested based on previous experimental works [**El-Genk et al(2) 1998**]. As shown in Figure 5-5 the heat transfer coefficient for film liquid is classified in three regions depending on the dimensionless parameter η which is defined as

$$\gamma = \left(\frac{q_E l_m}{\rho_v h_{lv} \upsilon_L} \right)^2 K_P^2 \frac{\mathrm{Re}_x}{\mathrm{Pr}_L} \qquad \textbf{5.13}$$

Where: l_m is the bubble length scale, υ_L kinematic viscosity of the liquid, K_P a dimensionless number, Re_x liquid film local Reynolds number and Pr Prandtl number of the liquid respectively are given by [**El-Genk et al(2) 1998**]

$$l_m = \left(\frac{\sigma}{g(\rho_L - \rho_v)} \right)^{0.5}$$
$$K_P = \frac{P l_m}{\sigma}; \quad \mathrm{Re}_x = \frac{4 q_E (L_E - x)}{\mu_L h_{lv}}; \quad \mathrm{Pr}_L = \frac{\mu_L C p_L}{k_L} \qquad \textbf{5.14}$$

Where: σ is surface tension, P is pressure and x is distance measured from the beginning of the evaporator section along the wall of the evaporator [**El-Genk et al(2) 1998**]. The heat transfer coefficient in the natural convection region ($\gamma \le 10^9$) is given by

$$Nu_x = \left(\frac{4}{3} \right)^{\frac{1}{3}} (\mathrm{Re}_x)^{-\frac{1}{3}} \text{ ; valid for } \gamma \le 10^9 \qquad \textbf{5.15}$$

The heat transfer coefficient in the nucleate boiling region ($\gamma \ge 2.7 \cdot 10^{10}$) is given by [**El-Genk et al(2) 1998**]

$$Nu_{NB} = 1.155 \cdot 10^{-3} N_{\mu f}^{0.33} \mathrm{Pr}_L^{0.35} K_P^{0.7} \left(\frac{q_E l_m}{\rho_v h_{lv} \upsilon_L} \right)^{0.7} \text{ ; for } \gamma \ge 2.7 \cdot 10^{10}$$
$$\text{where } N_{\mu f} = \left(\frac{l_L}{l_m} \right)^{1.5} \text{ ; and } l_L = \left(\frac{\mu_L^2}{g \rho_L (\rho_L - \rho_v)} \right)^{\frac{1}{3}} \qquad \textbf{5.16}$$

When the flow regime is in between the nucleate boiling and natural convection a combined heat transfer correlation Nu_{CC} is suggested as shown in Figure **5-5** and is given by [**El-Genk et al(2) 1998**]

$$Nu_{CC} = \left[Nu_x^3 - Nu_{NB}^3 \right]^{\frac{1}{3}}; \quad \text{for } 10^9 < \gamma < 2.7 \cdot 10^{10} \tag{5.17}$$

All the heat transfer correlations discussed in this section are applicable in the liquid film boiling and evaporation after the dryout point is reached.

5.1.3 Heat Transfer in the Condenser Section

The condenser section is shown in Figure **5-6** . In this section the vapor that is returning from the evaporator, flowing through the adiabatic section, condenses on the inside wall of the condenser section thereby releasing the heat that was absorbed at the evaporator section into the cryorefrigeration heat sink. The wall temperatures of the condenser, and hence that of the evaporator, are determined by the cryorefrigeration performance characteristic shown in Figure **3-4** of Chapter 3. It shows that for a given steady state heat load the cryorefrigeration system maintains a proportional constant temperature at the condenser wall. Therefore as the heat load increases the heat sink temperature increases proportionally. This will have a very important parameter that determines the operational range of the thermosyphon.

As the vapor reaches the inside wall of the condenser heat is released. The amount of heat release at this section q_C is equal to that of the evaporator q_E . Almost all the heat flow through the outside wall of the condenser, as shown in Figure **5-6** comes from the

condensation of vapor on the inside wall. A negligibly small fraction of the heat, due to very high thermal resistance, may come though the adiabatic wall. This will be discussed in the next section

There are many ways of formation film condensation. Figure **5-7** shows a few of those. Analysis of the laminar film condensation on a vertical plate is one of the most commonly encountered and relatively easier to tackle. The average heat transfer coefficient for a vertical plate of length L laminar film condensation was developed by Nusselt in 1916 [**Whalley-1987**] and is given by:

$$h_C = \frac{\sqrt{8}}{3}\left[\frac{\rho_L\left(\rho_L-\rho_v\right)g h_{lv} {k_L}^3}{\mu_L\left(T_{Sat}-T_w\right)L}\right]^{\frac{1}{4}} \qquad \textbf{5.18}$$

Accounting for the subcooling of the liquid film can easily be made when a linear temperature profile is assumed in the thin film. As a result the latent heat h_{lv} in Eq. **5.18** should be modified as h_{lv}' and given by:

$$h_{lv}' = h_{lv} + \frac{3}{8} Cp_L\left(T_{Sat}-T_w\right) \qquad \textbf{5.19}$$

Rohsenow later suggested factor $\frac{3}{8}$ should be modified to be 0.68 since the film never has the chance to assume a linear temperature profile [**Whalley-1987**].

For the flow over a horizontal cylinder the mean heat transfer coefficient for film wise condensation as shown in Figure **5-7** is given by:

$$Nu_D = \frac{h_C D}{k_L} = 0.728\left(\frac{Ra}{Ja}\right)^{\frac{1}{4}} \qquad \textbf{5.20}$$

In Eq. **5.20** the dimensionless numbers Rayleigh denoted by Ra and Jackob denoted by Ja are given by:

$$Ra = \frac{g\left(\rho_L - \rho_v\right)\mathrm{Pr}_L\, D^3}{\rho_L{}^2 \nu_L{}^2}$$
$$Ja = \frac{Cp_L\left(T_{Sat} - T_w\right)}{h_{lv}} \qquad \textbf{5.21}$$

The film condensation inside the condenser section of the thermosyphon is closely related to the stratified film wise condensation shown in Figure **5-7** . In all the film condensation relations discussed above the basic equation are in the same form as the classic Nusselt relation for the vertical laminar film condensation. In stratified flow film wise condensation, such as the one in thermosyphons, a general equation can be written as:

$$h_C = F\left[\frac{\rho_L\left(\rho_L - \rho_v\right)g h_{lv} k_L^3}{\mu_L\left(T_{Sat} - T_w\right)d}\right]^{\frac{1}{4}} \qquad \textbf{5.22}$$

Where the factor F is 0.73 for flow outside a horizontal tube; However for flow inside horizontal tube it is commonly assumed that there will be no condensation in the stratified layer and all the condensation occurs in the top part of the tube. The value of factor F changes with the angle ϕ for two reasons. First, less of the tube wall will be available for condensation. Taking the area effect crudely would suggest that F declines linearly as ϕ increases. Second, at the top of the tube the film is thin. This means that the top part of the tube is more efficient in condensation terms than the bottom. This suggests that the fall-off in the value of the factor F is not linear as illustrated in Figure **5-8** .

Sometimes in the absence of other information the value of $F = 0.58$ is taken that corresponds to the angle $\phi = 60^o$ [**Whalley-1987**].

After determining film condensation the heat transfer coefficient h_C as shown in the above correlations the inside thermal resistance $R_{E,i}$ in the condenser section of the thermosyphon can now be calculated as:

$$R_{C,i} = \frac{1}{\pi d \cdot L_C \cdot h_C} \qquad \textbf{5.23}$$

The radial conduction resistance, similar to the evaporator section, can be calculated as:

$$R_{C,o} = \frac{\ln\left(\frac{D}{d}\right)}{2\pi L_C \cdot k_{Al}} \qquad \textbf{5.24}$$

5.1.4 Overall Thermal Resistance and Heat Transfer Coefficient of the Thermosyphon

A simplified equivalent thermal resistance diagram is shown in Figure **5-9** for the entire thermosyphon. These are sequentially, the radial conduction resistance of the evaporator wall $R_{E,o}$, the boiling/evaporative resistance in the inner wall of the evaporator $R_{E,i}$, the axial resistance through the adiabatic wall R_{ad}, the condensation resistance in the inner wall of the condenser $R_{C,i}$ and the radial conduction resistance of

the condenser wall $R_{C,o}$. The net thermal resistance between the inner wall of evaporator and condenser can be calculated as:

$$R_{th}' = \frac{R_{E,i} + R_{C,i}}{\frac{R_{E,i} + R_{C,i}}{R_{ad}} + 1} \qquad \textbf{5.25}$$

From Figure **5-10** that shows relative magnitudes of the conduction resistances given in Eq. **5.25** the axial thermal resistance is much larger than either of the condenser or evaporator conduction resistances. For example at a typical working temperature of 32K the axial thermal resistance is more than $6.3 \cdot 10^4$ times larger than the corresponding condenser thermal resistance. To put this in perspective Figure **5-11** shows the effect of wall thickness of the thermosyphon. In the figure the outer and inner diameters of the current thermosyphon are denoted by D and d respectively. If we allow the outer diameter to vary, as denoted by d' in the figure, it is clear that the conduction resistance of the evaporator and condenser are much smaller than that of the adiabatic wall. This is due to the fact that the cross sectional area for axial conduction through the adiabatic wall is very small at smaller outer diameters. As the outer diameter increases i.e. for thicker walls, the thermal resistance of the adiabatic wall decreases. In order to reach at a level of comparable thermal resistance to that of evaporator and condenser, the outer diameter of the thermosyphon has to be at least 18 times bigger. But for the current condition the adiabatic wall (axial) thermal resistance is extremely large as compared to the evaporator and condenser sections as noted above Therefore in the limit as $R_{ad} \to \infty$ the value of R_{th}' can be calculated as

$$\lim_{R_{ad}\to\infty}\left(R_{th}'\right)=\lim_{R_{ad}\to\infty}\left(\frac{R_{E,i}+R_{C,i}}{\frac{R_{E,i}+R_{C,i}}{R_{ad}}+1}\right)=R_{E,i}+R_{C,i} \qquad \textbf{5.26}$$

The overall thermal resistance of the closed two phase thermosyphon can then be calculated as

$$R_{Eq}=R_{E,o}+R_{E,i}+R_{C,o}+R_{C,i} \qquad \textbf{5.27}$$

In order to maximize the efficiency of the thermosyphon the overall thermal resistance must be minimized. One of the goals of this research is to find a way to reduce this. Substituting the proper values for each term in Eq. **5.27** and arranging the overall thermal resistance can be calculated as:

$$R_{Eq}=\frac{1}{2\pi k_{Al}}\ln\left(\frac{D}{d}\right)\left(\frac{1}{L_E}+\frac{1}{L_C}\right)+\frac{1}{\pi d}\left(\frac{1}{L_E h_E}+\frac{1}{L_C h_C}\right) \qquad \textbf{5.28}$$

Examining the terms in Eq. **5.28** , the first term in the right hand side represents the radial conduction resistances and it is mainly affected by the geometry of the evaporator and condenser sections besides the thermal conductivity of the tube. The effect of diameter has already been discussed and shown in Figure **5-11** . As the length of the evaporator increases the thermal resistance decreases exponentially. A 100% increase of the current evaporator length would decrease the combined conduction thermal resistance of the evaporator and condenser by about 100% as shown in Figure **5-12** . The second term in the RHS of Eq. **5.28** represents the inside wall resistances of the evaporator and condenser due to boiling/evaporation and condensation respectively.

These terms are affected by both the geometry and also by the thermo-physical parameters and the flow regimes.

5.2 Results and Discussions of Heat Transfer Analysis

The above heat transfer analysis is used in determining the thermal performance of the TCNS two-phase closed thermosyphon. Figure **5-13** shows experimental result of evaporator (Moderator) and condenser (Cold head) temperatures of the TCNS thermosyphon [**Unlu et al 1994**] vs. that of results of analytic prediction of the evaporator temperature. It is clear that the analytic result accurately predicts the data with less than 5% maximum error. The result shows that as soon as the saturation temperature reaches the dryout region, the evaporator temperature increases rapidly where it eventually jumps when the liquid film completely evaporates from the thermosyphon. From the plot it is clear that the maximum heat load that can be safely accommodated by the thermosyphon is about 4W.

The result of the above thermal analysis shows various important factors that determine the maximum limit of the heat exchanger capacity of the thermosyphon. These factors include initial pressure, reservoir temperature, volume ratio η, performance characteristic of the heat sink (cryorefrigeration system) represented by α and the critical temperature of the fluid T_{Cr}. In addition, the heat transfer coefficient at the evaporator determines the critical heat flux (CHF). Figure **5-14** shows a representative sketch of performance characteristics of two phase closed thermosyphon operating under two hypothetical cryorefrigeration systems(heat sinks) having characteristic angle of α_1 and

α_2. The saturation temperature is assumed to be linearly proportional to the heat load as it is the case in that of TCNS system. In this case the minimum and maximum possible saturation temperature for the fluid is denoted by T_{Min} and T_{Cr} respectively. Hence the heat loads at any saturation temperature can be estimated by

$$Q = \frac{T_{Sat} - T_{Min}}{\tan(\alpha)} \qquad \textbf{5.29}$$

And the heat load at the dryout condition is given by

$$Q_d = \frac{T_{dSat} - T_{Min}}{\tan(\alpha)} \qquad \textbf{5.30}$$

The maximum possible heat load is given by

$$Q_{Max} = \frac{T_{Cr} - T_{Min}}{\tan(\alpha)} \qquad \textbf{5.31}$$

At this point it is convenient to introduce the definition of Capacity Index ζ used in this study as the ratio of the heat load at dryout condition Q_d to the maximum heat load Q_{Max} and is given by

$$\zeta = \frac{T_{dSat} - T_{Min}}{T_{Cr} - T_{Min}} \qquad \textbf{5.32}$$

This index shows the measure of the heat load carrying capacity of the thermosyphon. From Eq. **5.32** it is clear that the Capacity Index ζ is independent of the characteristics of the cryorefrigeration unit α. From Figure **5-14** is clear that as the dryout temperature increases from point "a" towards the maximum "b" the heat load increases proportionally from Q_{d1} to Q_{Max}. This can be achieved by altering various parameters discussed above. The factors initial temperature, initial pressure and volume ratio η can

all be observed by plotting the Capacity Index ζ versus initial fill ratio FR_O (the fill ratio at T_{Min}) as shown in Figure **5-15** . From the figure it can be observed that the Capacity Index ζ is independent of the initial fill ratio for large values of volume ratio ($\eta \gg 1$). At such high values of η the Capacity Index ζ appears to be only a function of initial pressure P_O. On the other hand for very small values of volume ratio ($\eta \ll 1$) the Capacity index ζ is linearly proportional to the initial fill ratio. At intermediate values of volume ratio, ζ is dependent on all the three parameters: initial pressure T_O, initial pressure P_O and volume ratio η. By properly selecting the above parameters one can achieve a maximum Capacity Index for a given two phase thermosyphon and hence attain maximum heat load by moving the dryout point from point "a" to point "b" in Figure **5-14** . This is of course not the only way to achieve the maximum heat load. The other important parameter is the characteristic angle α of the cryorefrigeration (Heat sink) performance curve as defined above. As performance curve characteristic angle α decreases the dryout heat load Q_d increases indicated by line "c - d" as shown in Figure **5-14** . The smaller the characteristic angle α, the more powerful the cryorefrigeration systems in handling higher heat loads. As shown in Figure **5-16** , the maximum heat flux at dryout point of a two phase closed thermosyphon is determined by the Capacity Index ζ and the cryorefrigeration system (Heat sink) characteristic angle α. From Figure **5-16** it can be observed that the TCNS system has a Capacity Index of about 0.5. Using the heat sink which has a characteristic angle of 68 degrees the maximum improvement that can be achieved is nearly twice the current maximum heat load. This

can be achieved by altering the various thermo physical and geometric parameters in order to achieve the Capacity Index of 1. However one can obtain nearly a 400% increase in maximum capacity by using the same thermosyphon but having a cryorefrigeration system with characteristic angle of half the current system. This type of heat sink is commercially available [**Cryomech-Inc**] as the one shown in Figure **5-17** . In this case the characteristic angle $\alpha = 40^{\circ}$.

Although one can theoretically approach excessively large (infinite) heat flux ($Q_d \to \infty$) as the characteristic angle decreases ($\alpha \to 0$), there is obviously a practical limit to the amount of heat flux that one can handle at a given surface. This limit is known as the critical heat flux (CHF). This limit is reached when the nucleate boiling heat transfer rate reaches the maximum limit just before film boiling starts as indicated by point "a" in the boiling curve of Figure **5-1** . The boiling curves of some cryogenic fluids that used in extremely low temperature applications, such as the one in TCNS cooling system is shown in Figure **5-18** . From the figure it can be observed that the critical heat flux for the case of neon is about $CHF = 6\frac{W}{cm^2}$. In order to have a two phase closed thermosyphon that can handle large heat loads, one has to make sure that it operates below the critical heat flux. This requires a detailed heat transfer analysis of the evaporator. This is one of the focuses of the next chapter.

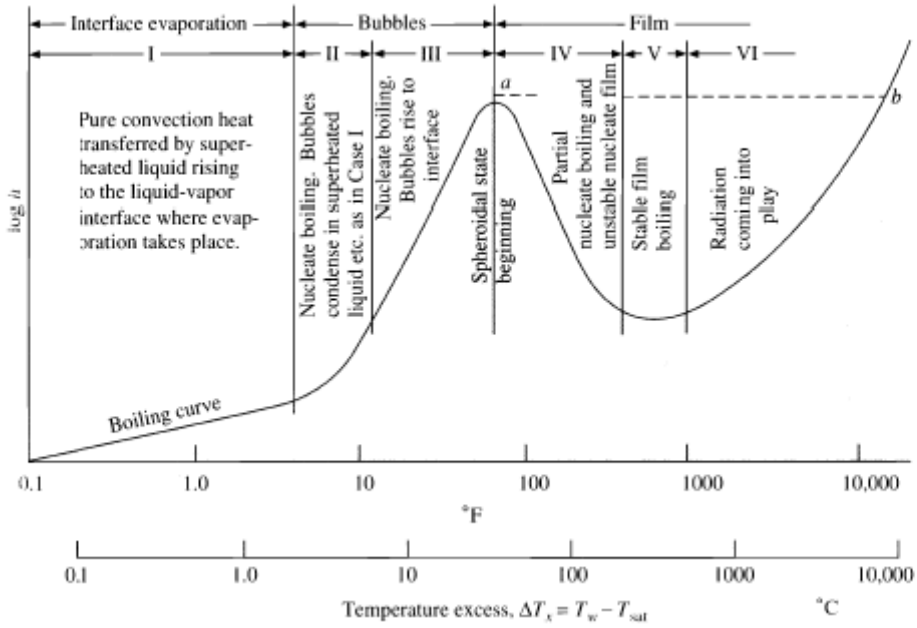

Figure **5-1**: Boiling curve showing heat flux data from an electrically heated platinum wire [**Holman-1997**]

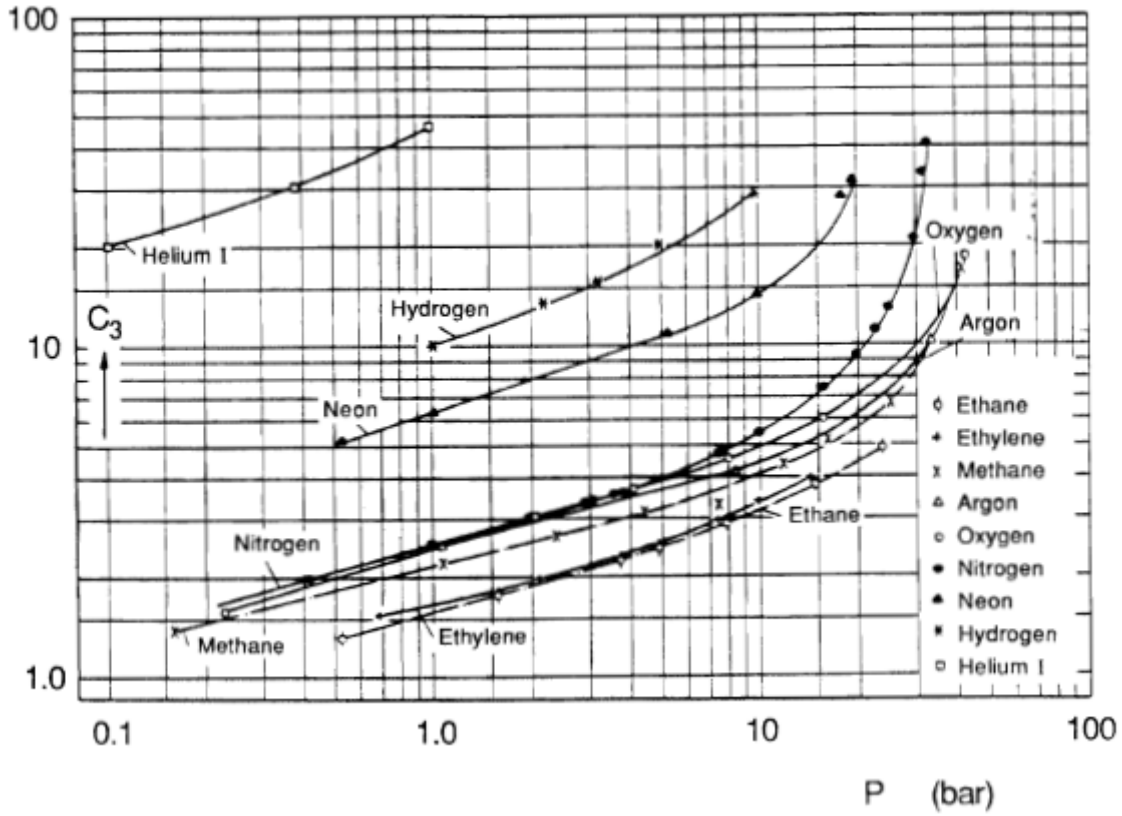

Figure **5-2**: Variation of parameter C_3 in Eq. **5.7** with pressure[**Carey-2008**]

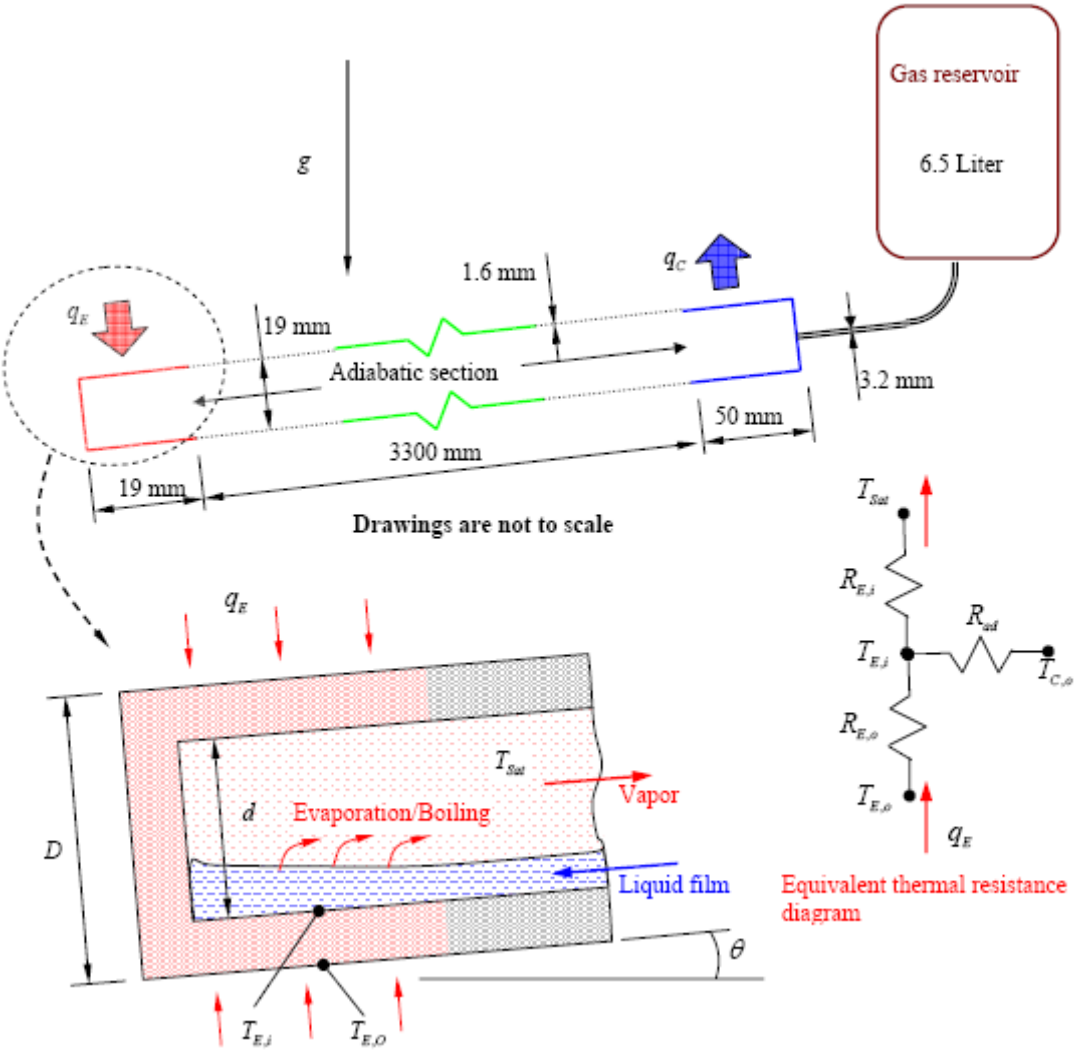

Figure **5-3**: Schematic showing the heat transfer in the evaporator section of closed two phase thermosyphon. The equivalent thermal resistance diagram shown on the right

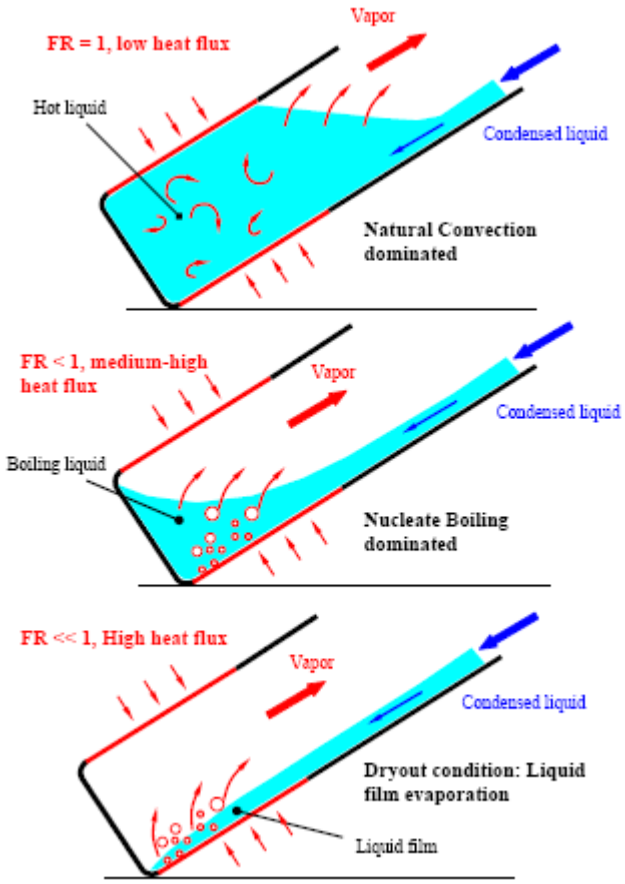

Figure **5-4**: Schematic showing the various expected heat transfer regimes inside the evaporator section of two phase closed thermosyphon, depending on the heat flux

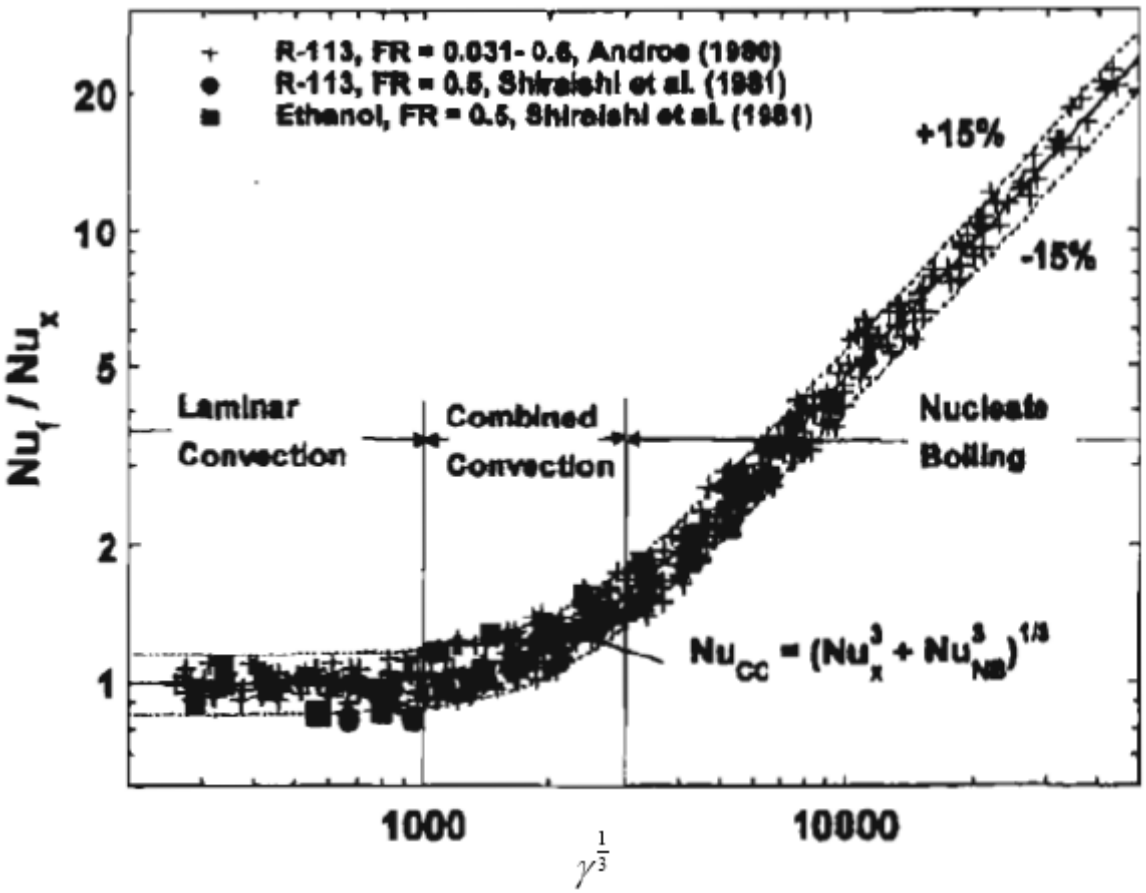

Figure 5-5: Heat transfer correlation for film liquid in evaporator section of closed two phase thermosyphon [**El-Genk et al(2) 1998**]

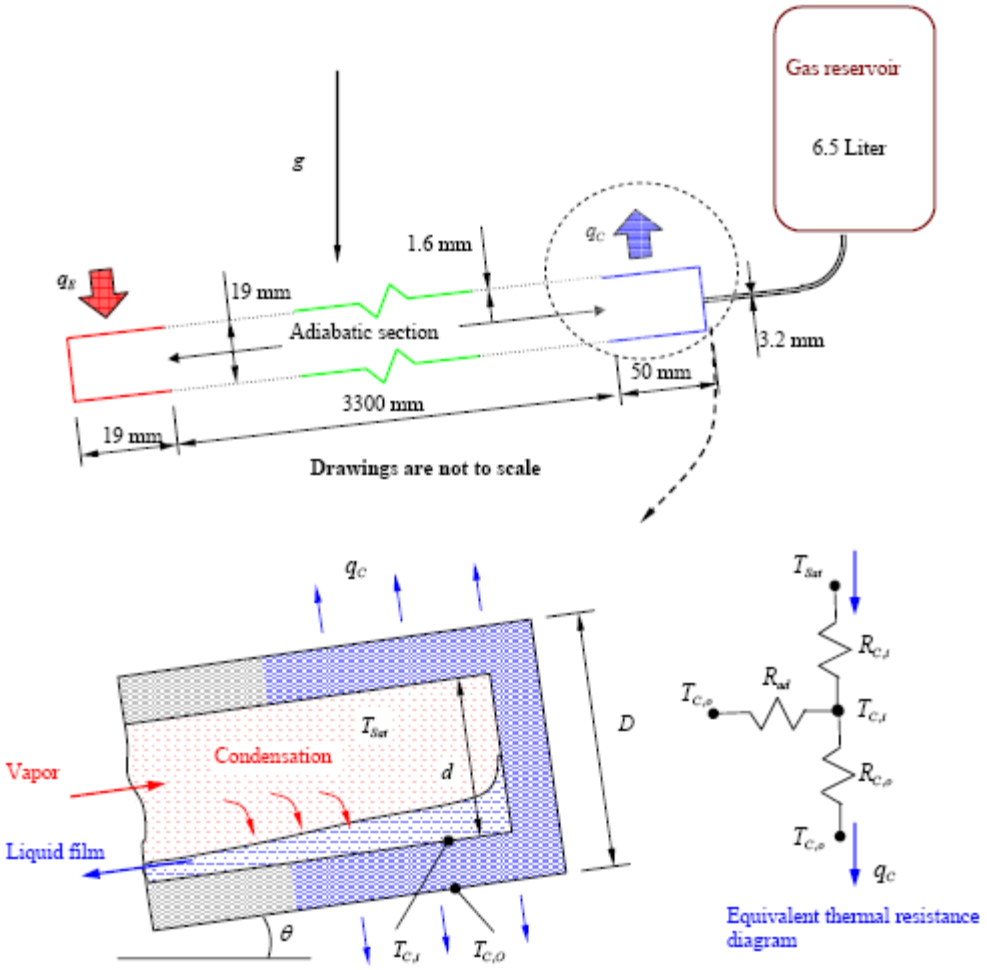

Figure **5-6**: Schematic showing the heat transfer in the condenser section of closed two phase thermosyphon. The equivalent thermal resistance diagram shown on the right

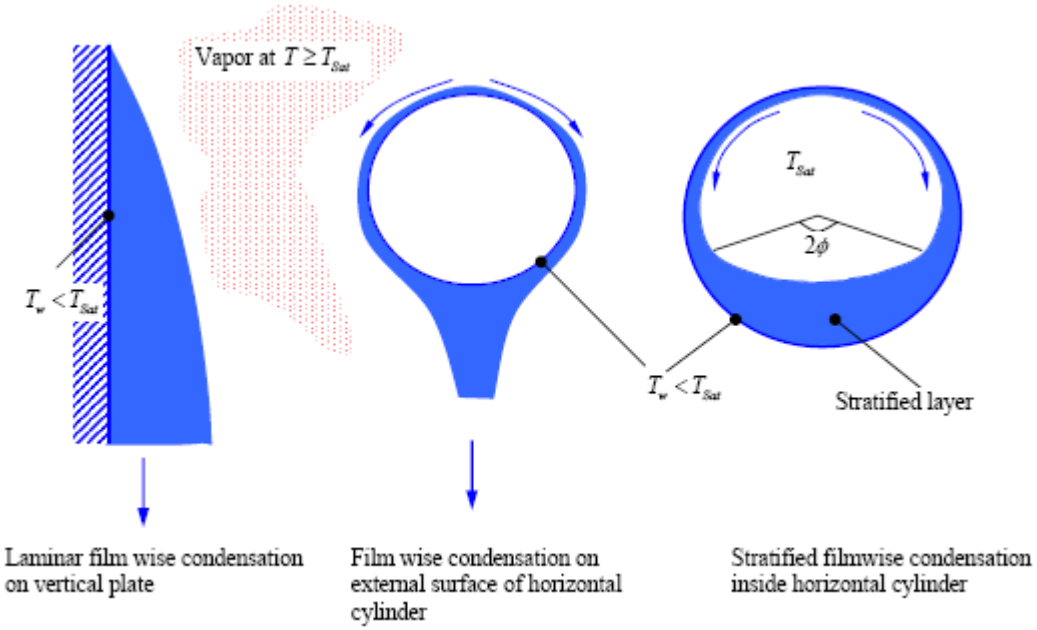

Figure **5-7**: Schematic showing formation of film wise condensation on surfaces

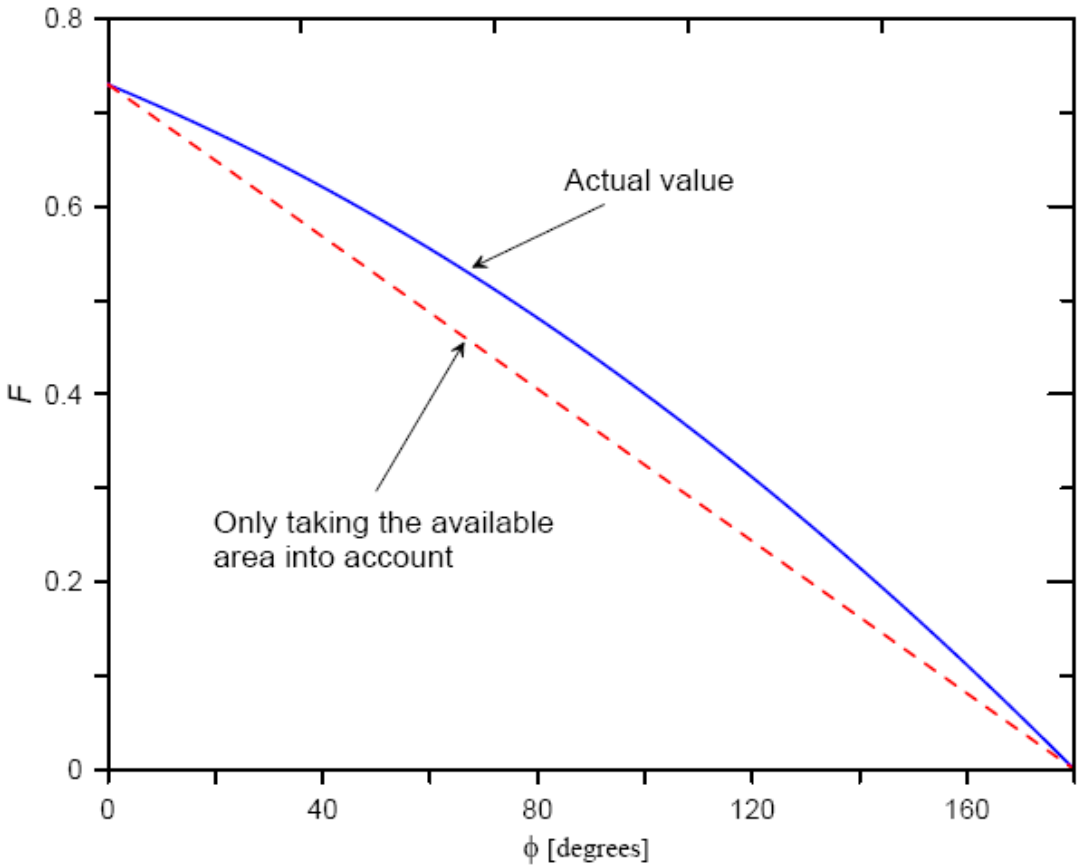

Figure **5-8**: Nusselt equation correlation factor for stratified flow reproduced from [**Whalley-1987**]

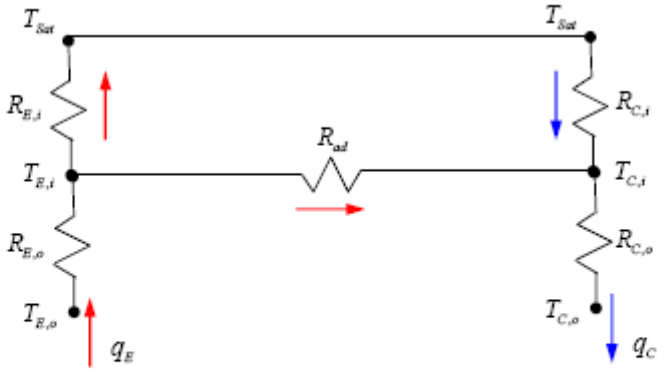

Figure **5-9**: Schematic of equivalent thermal resistance diagram for the closed two phase thermosyphon

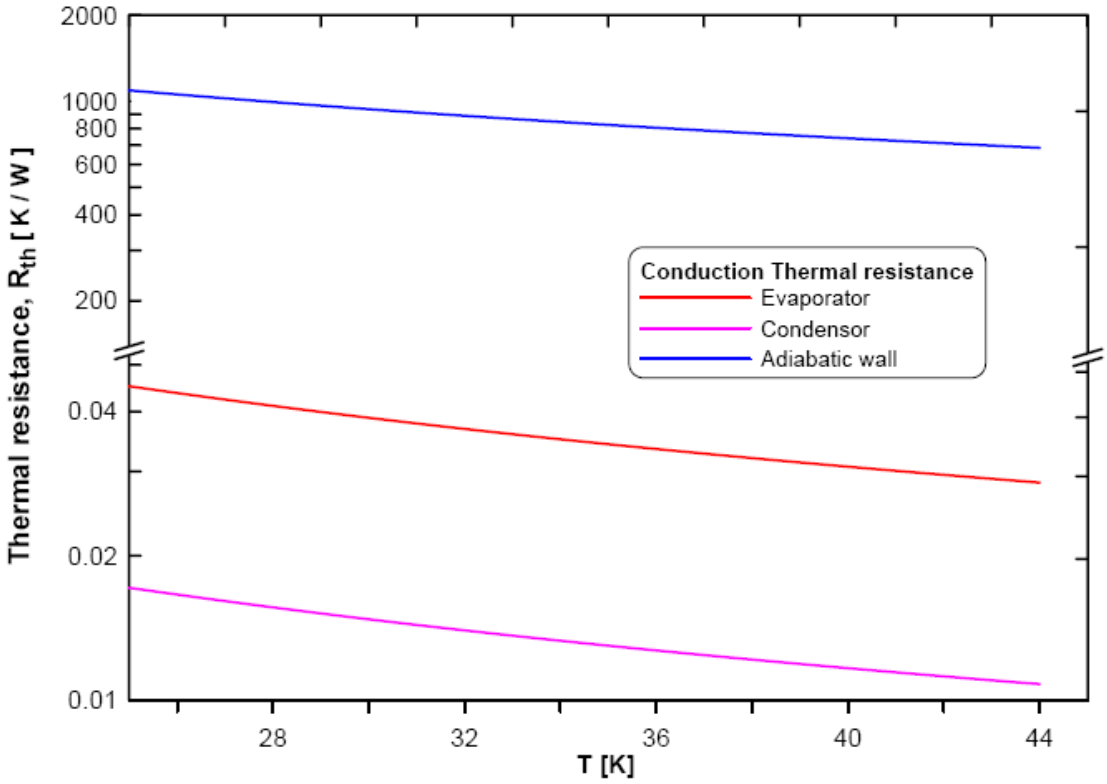

Figure **5-10**: Plot showing comparison of thermal resistance of evaporator, condenser and adiabatic section of the thermosyphon. Clearly the adiabatic section thermal resistance is extremely large

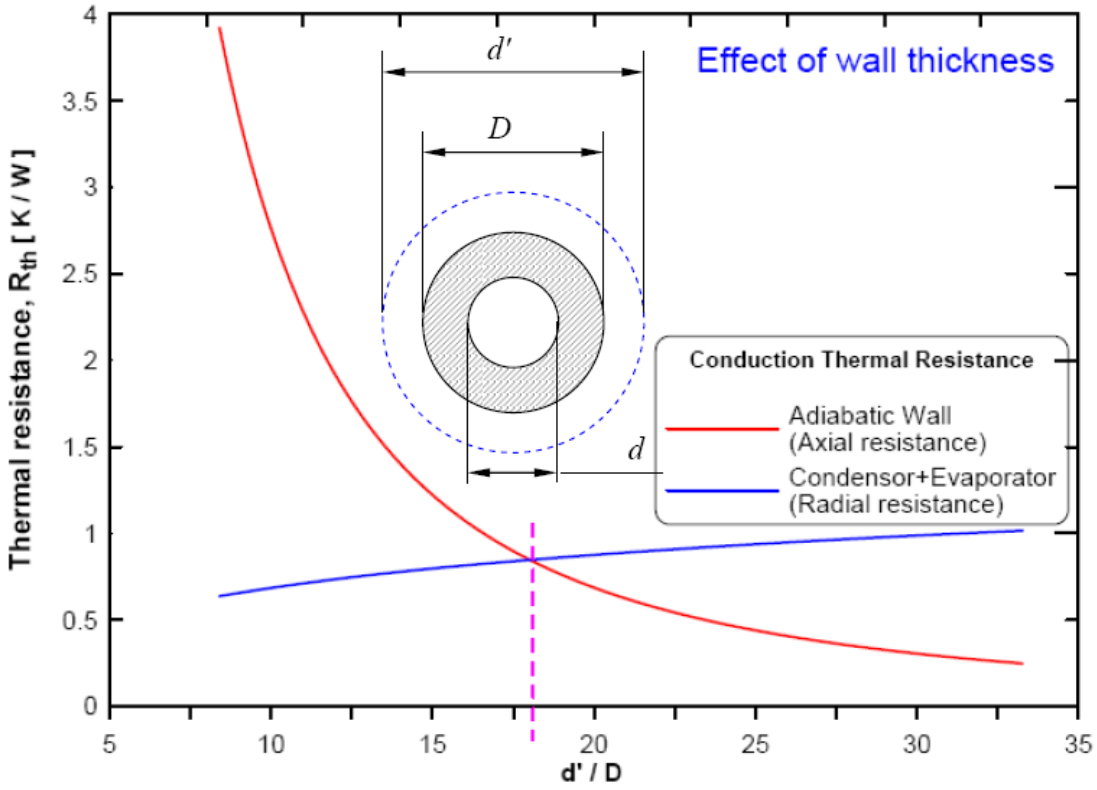

Figure **5-11**: Plot showing effect of thermosyphon tube wall thickness on conduction thermal resistances of evaporator, condenser and adiabatic sections. D is the outer diameter of the TCNS thermosyphon

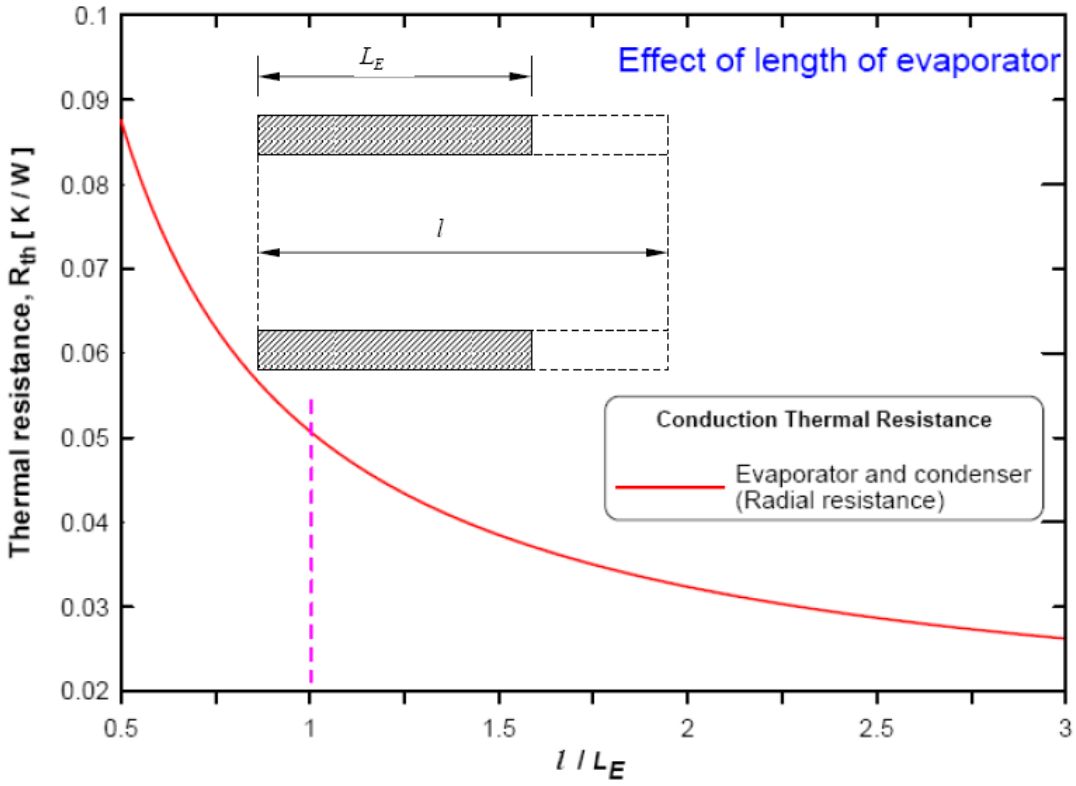

Figure **5-12**: Plot showing effect of thermosyphon evaporator length on combined conduction thermal resistances of evaporator and condenser

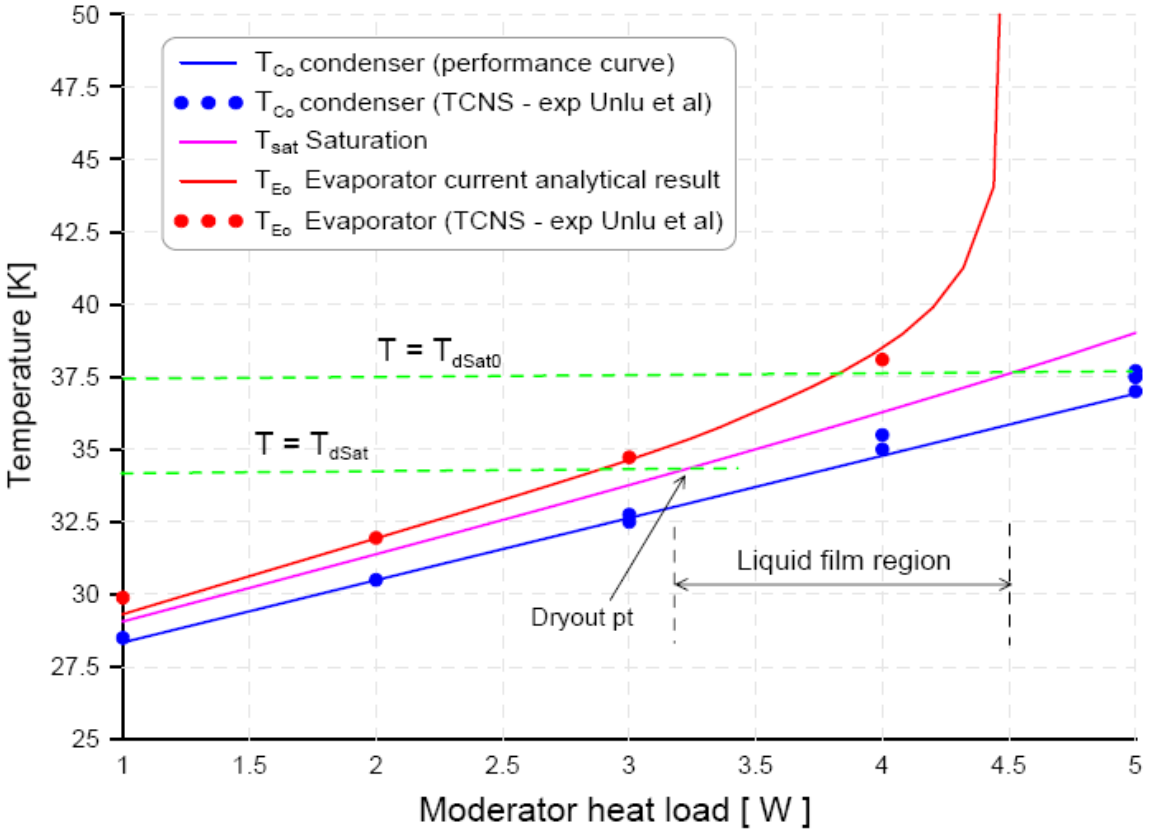

Figure **5-13**: Plot showing comparison of experimental results of the TCNS closed two phase thermosyphon and current analytic prediction of evaporator (Moderator) temperature at various heat loads

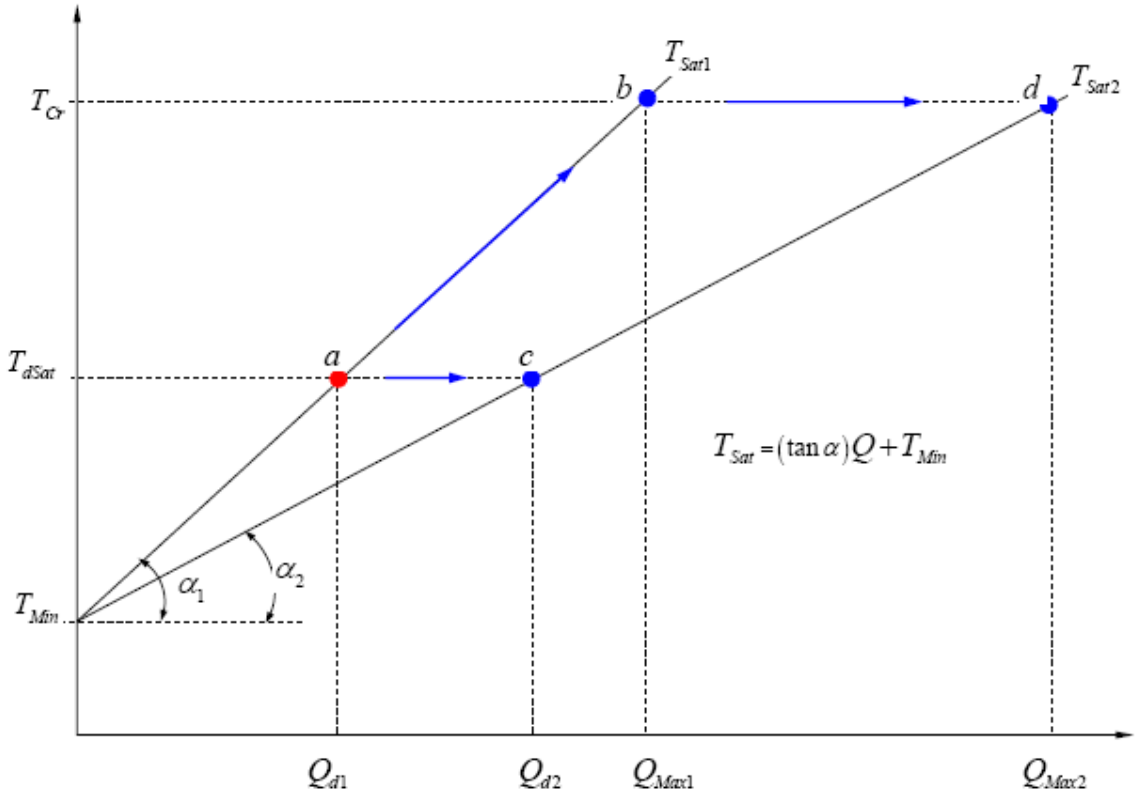

Figure **5-14**: Schematic plot showing saturation temperature vs. heat load.

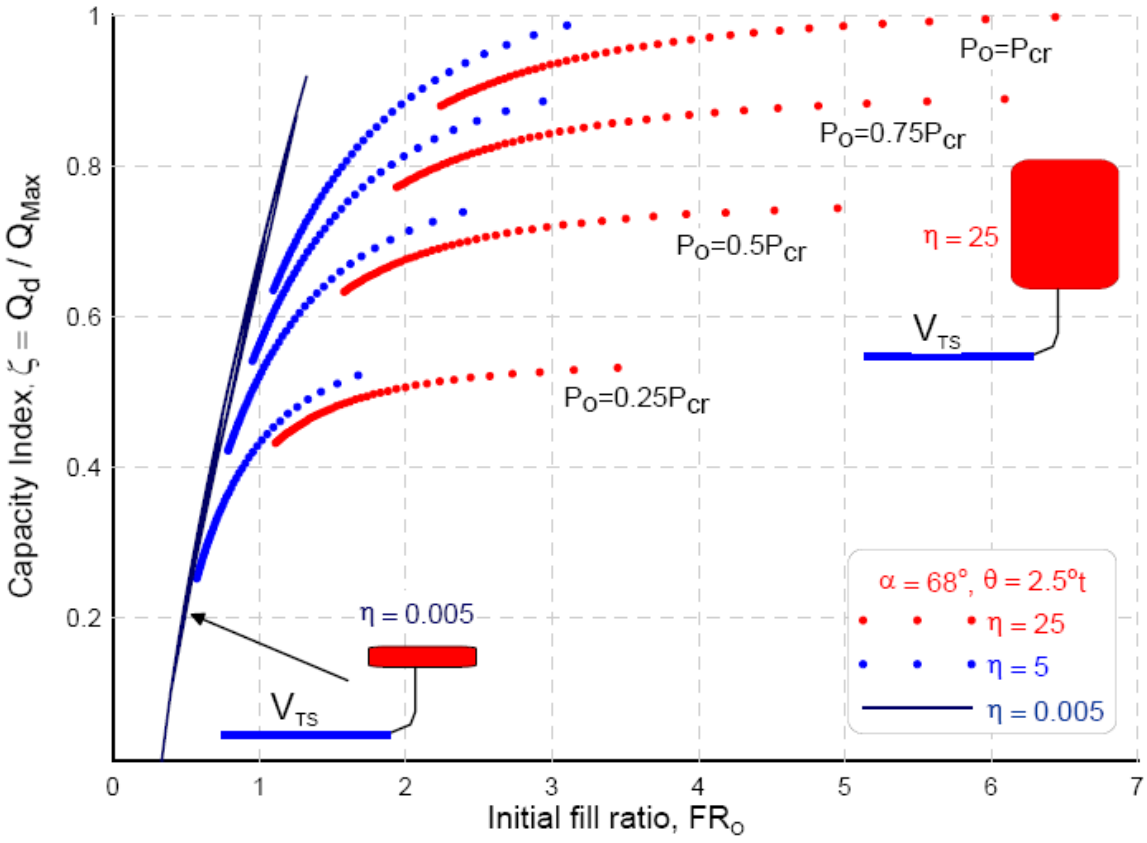

Figure **5-15**: Parametric plot showing Capacity Index versus Initial fill ratio for a two phase closed thermosyphon.

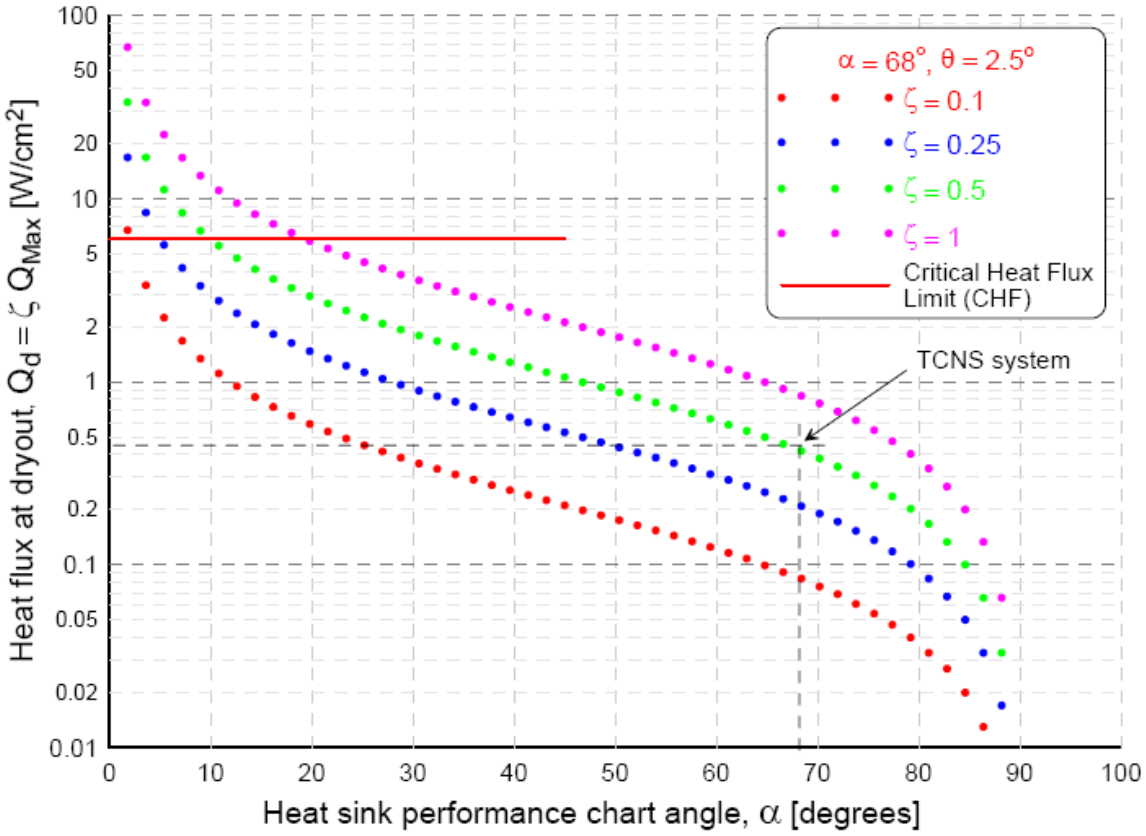

Figure **5-16**: Parametric plot of the heat flux at dryout versus the performance characteristic angle α of the cryorefrigeration system (heat sink) at various Capacity Index of two phase closed thermosyphon

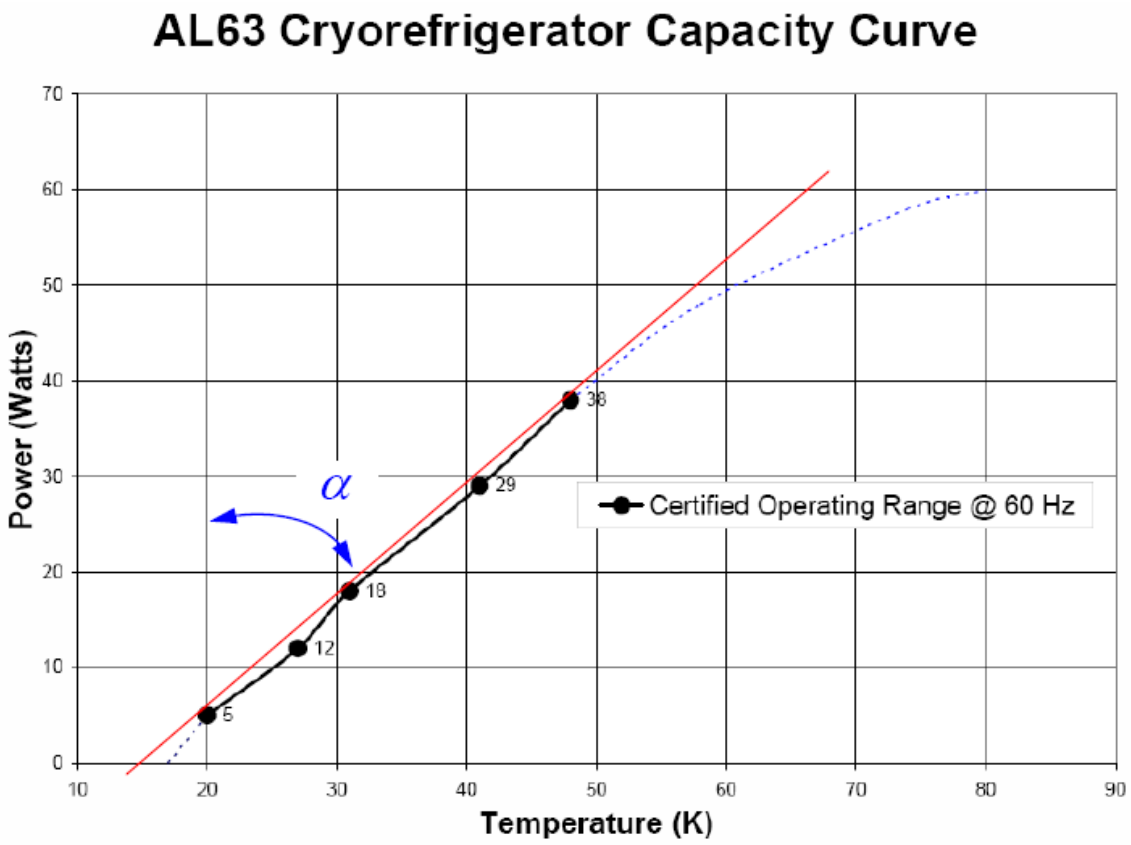

Figure **5-17**: Cryorefrigeration system performance chart showing characteristic angle (emphasis added) [**Cryomech-Inc 2008**]

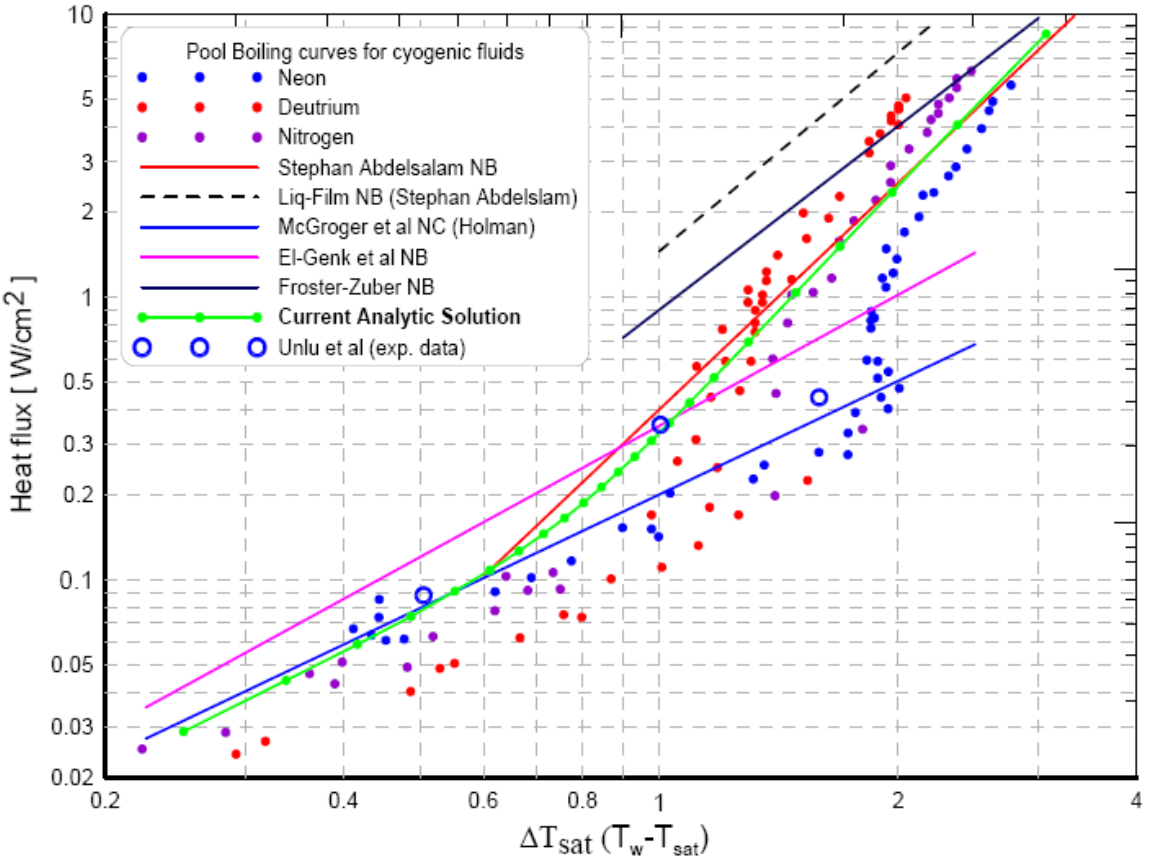

Figure **5-18**: Plot of experimental data and correlations for Heat flux versus wall super heat of common cryogenic fluids

Table **5-1**: Approximate values of convection heat transfer coefficients [**Holman-1997**]

Mode of heat transfer	Heat transfer coefficient $h\,[\frac{W}{m^2K}]$
Free convection: Vertical plate 0.3m high in air with temp. difference of 30K	4.5
Free convection :Horizontal cylinder, 5 cm in diameter, in air	6.5
Forced convection: Air flow at 2 m/s over a 0.2m square plate:	12
Forced convection: Air flow at 35 m/s over a 0.75m square plate:	75
Forced convection: water flow at 0.5 kg/s in a 2.5 cm diameter tube	3500
Boiling water: In a pool or container	**2500 – 35,000**
Boiling water: In a tube	**5000 – 100,000**

Chapter 6

CFD Analysis of the Heat Transfer Mechanism inside the Evaporator Section of the Closed two Phase Thermosyphon

In this chapter a two phase flow CFD analysis using commercial code [**FLUENT6.3**] is presented. In the first section, the various attempts that were made in conducting the transient cool down process is presented. Next, the result of a CFD analysis of the steady state two phase flow profile inside a thermosyphon is presented. Finally a detailed analysis of nucleate boiling inside the thermosyphon evaporator section is simulated using a heated flat plate. This will provide a separate validation to the correlations used in the heat transfer analysis in the previous chapter.

6.1 Basic Conservation Equations

In simulating the fluid flow and heat transfer one needs to solve the governing conservation equations of Mass, Momentum and Energy along with any constitutive equations to model a particular physical phenomenon. The commercial CFD code [**FLUENT6.3**] which is being used in this study has various multi-phase flow analysis tools. The particular model called volume of fluid (VOF) model is used in this study. The model basically used to track interface between one or more phases in a multiphase flow where the fluids in the mixture are considered to be immiscible. The governing equations used in this analysis are:

Conservation of mass:

$$\frac{\partial}{\partial t}\left(\alpha_q \rho_q\right) + \nabla \bullet \left(\alpha_q \rho_q \vec{v}_q\right) = \sum_{i=1}^{n}\left(\dot{m}_{pq} - \dot{m}_{qp}\right) \qquad \textbf{6.1}$$

where $n = 2$

Volume fraction Equation:

$$\sum_{q=1}^{n} \alpha_q \;;\; n = 2 \qquad \textbf{6.2}$$

Conservation of Momentum

$$\frac{\partial}{\partial t}\left(\rho \vec{v}\right) + \nabla \bullet \left(\rho \vec{v}\vec{v}\right) = -\nabla p + \nabla \bullet \left[\mu\left(\nabla \vec{v} + \nabla \vec{v}^{T}\right)\right] + \rho \vec{g} \qquad \textbf{6.3}$$

The Conservation of Energy:

$$\frac{\partial}{\partial}\left(\rho E\right) + \nabla \bullet \left(\vec{v}\left(\rho E + p\right)\right) = \nabla \bullet \left(k_{eff} \nabla T\right)$$

$$\textit{where } E = \frac{\sum_{q=1}^{n} \alpha_q \rho_q E_q}{\sum_{q=1}^{n} \alpha_q \rho_q} \qquad \textbf{6.4}$$

Here both E and T are mass weighted averages. The density used in the conservation equation is evaluated as

$$\rho = \alpha_2 \rho_2 + \left(1 - \alpha_2\right)\rho_1 \qquad \textbf{6.5}$$

In all the conservation equations, the physical properties such as thermal conductivity k_{eff} are defined this way.

The mass transfer due to evaporation and condensation has to be separately modeled and incorporated into the solver using User Defined Function (UDF) feature of FLUENT.

6.2 Transient Simulation of Cool-down Process

As the name implies the cool-down process is the cooling of the TPCTR from room temperature of about 300K to the operating temperature below 34K as shown in Figure **3-5** and repeated here in Figure **6-1** . Several attempts were made to simulate this process using CFD code FLUENT. The following sections describe the various challenges in simulation of transient cooldown process.

6.2.1 Thermal Boundary Conditions at the Condenser Wall

The first major initial challenge in the simulation process is to identify the type of boundary condition that can be used at the condenser end. The condenser section of the TPCTR is attached to the cryorefrigeration system. As it is described in the previous chapters the amount of heat load that the cryorefrigeration system removes depends on the wall temperature at the condenser section. The wall temperature in turn depends on the amount of heat load. In addition to this interdependence the heat load continuously varies with time during the cooldown process.

The first attempt was to simulate single phase flow inside the TPCTR with a constant wall temperature boundary condition (Dirichlet boundary condition.) As shown in Figure **6-2** the simulation was started by assuming that the temperature at the condenser end reached a steady state value and using it as a boundary condition. The result shows a good agreement with the data up to about 200 minutes into the cooldown process. The simulation starts to diverge after that. There are two main reasons for this. The first being that the flow is in fact not entirely single phase and second that the

temperature of the at the evaporator end started to come down signaling that the transient cooling of the TPCTR material (Aluminum) is approaching the steady state temperature of the condenser.

Second attempt was using constant heat flux boundary condition (Neumann B.C.) at the condenser wall. An average heat load of 10W was assumed at the condenser wall and the simulation result shown in Figure **6-3** . From the result it is clear that the simulation couldn't predict the wall temperature of the condenser but the pressure result was closer to the data. Again the simulation breaks once it is in stage-II of the cooling down process.

Lastly, a somewhat mixed boundary condition was considered based on the experimental data at the wall. This result is shown in Figure **6-4** . From the plot it is clear the simulation result fails to predict the experimental pressure data in stage-II of the cooldown process.

6.2.2 Operating Pressure

The other major challenge in the above and subsequent simulations of the TPCTR is the fact that the pressure inside the thermosyphon continuously changes. The absolute pressure varies from 10atm initially to about 100 kPa (0.1 atm) at around normal operating conditions. The simulation results of the pressure and evaporator (moderator) temperatures are shown in Figure **6-5** and Figure **6-6** respectively. In this simulation single phase flow of neon vapor inside the TPCTR is considered. From the plots is clear that the simulations could not predict the experimental data accurately beyond stage-I of

the cool down process. The main reason for this is the fact that once the temperature inside the condenser reach the saturation condition, condensate forms and the condensate in turn flows and cools the inside wall of the thermosyphon thereby lowering the temperature of the thermosyphon. Single phase simulation cannot predict this simulate condensation and evaporation.

6.2.3 Cooldown Simulation with Two-Phase

From the last section it is clear that both condensation and evaporation have to be included during the cooldown process in order to accurately predict the flow and heat transfer inside the TPCTR. In this section a simple two phase flow model is included in FLUENT general purpose two phase flow model called VOF (Volume of Fluid) model using UDF (User Defined Function) feature. The evaporation and condensation model was simple mass exchange UDF based on saturation temperature of the mixture of the two phases as suggested in FLUENT user manual. The simulation result of pressure and evaporator temperature is shown in Figure **6-7** and Figure **6-8** respectively. Clearly there is an improvement in the predicting the data especially in stage-I and stage-II of the cooling down process. The main problem in this simulation is the inability to capture the sharp decrease in pressure at the end of stage-II. This is of course the stage where dryout occurs. After analyzing this result it was clear that it was necessary to reevaluate the effect of thermo-physical properties of the working fluid and the solid material of the TPCTR. This is the topic of the next section.

6.2.4 Thermo-Physical Properties of Working Fluid and Material of TPCTR

The cooldown process spans a temperature range from 300K to about 28K. The effect of this temperature range on the properties of the fluid and material of the TPCTR is assumed minimal in the preceding analysis. In this section the effect of this temperature change is included in the cool down simulation.

First, the variation in specific heat and thermal conductivity of Aluminum alloy-6061, from which the TPCTR is made, is shown in Figure **6-9** and Figure **6-10** respectively. It is clear from the plots that both the properties change over the entire range of the cooldown process from 300K to the operating condition of about 28K. this suggests that the variation in properties will undoubtedly affect the rate of cooling.

Second, the variation in the physical and thermal properties of the working fluid (Neon) is investigated. The specific heat and thermal conductivities of Neon vapor and liquid phases are shown in Figure **6-11** and Figure **6-12** respectively. It is interesting to see that the specific heat of neon liquid increases while thermal conductivity decreases as the temperature decreases. The reverse is true for the vapor phase.

All the above variation in properties are included in the two phase simulations discussed in the previous sections. The result is shown in Figure **6-13** . The result of this simulation predicts the experimental pressure data closely up to the dryout point. The pressure continuously drops beyond the dryout point which suggested that further modification to the simulation is needed to capture the steady state phenomena after dryout point. All the above simulations were carried out using FLUENT as the main CFD code and GAMBIT as a preprocessor to construct the computational mesh. Various

mesh sizes were considered until an optimum size is reached that gives the best compromise between accuracy and simulation time. Due to the nature of the flow, the variables involved and the geometry of the flow, the analysis required a very small time step (~10E-5sec).

6.3 Simulation of Natural Convection and Nucleate Boiling

The goal of this section is to simulate natural convection and nucleate boiling on a flat plate and compare the result with the previous experimental boiling curve data of neon and the correlations used in the evaporator section of the TPCTR heat transfer analysis explained in the preceding chapter. This simulation will help as a separate estimation of the heat transfer in the evaporator section.

6.3.1 Computational Domain and boundary Condition

The flow domain for the simulation is shown in Figure **6-14** . It consists of the heated plate placed at the bottom center of the domain. The heated plate has an area of $10mm^2$ with a small hole placed at the center with an area of $0.02mm^2$ representing the active nucleation site on the heated plate. The heated plate is part of a larger plate of area $36mm^2$.Figure **6-15** shows the computational mesh of the entire flow domain. The computational domain has a total of 32k hexahedral cells with zero skewness. Details of the mesh construction on the heated plate and the active nucleation site are given in Figure **6-16** and Figure **6-17** respectively.

The top of the flow domain is set to PRESSURE OUTLET boundary condition. The four side walls and the unheated bottom plate are set to WALL boundary condition with adiabatic thermal boundary condition. The heated plate is set HEAT FLUX boundary condition. The nucleation site is set to MASS FLOW INLET boundary condition. The fluid inside the flow domain is set to an initial temperature while the heat flux at the heated wall is maintained constant.

6.3.2 CFD Modeling of Nucleate Boiling

The CFD simulation that is employed in this case is similar to the one carried out by [**Geisler-2007**]. The difference in this case is the fact that here the simulation is carried out in 3D rather than 2D and different correlation is used in calculating the bubble parameters as explained below.

The modeling starts with determining the cavity radius for the active nucleation site. This depends on the material property and surface of the heated surface. In this case a cavity radius of $r_c = 50\mu m$ is assumed. As given in [**Carey-2008**], the waiting time for the bubble is calculated using

$$t_w = \frac{1}{4\alpha_l}\left\{\frac{r_c}{erfc^{-1}\left(\frac{T_{Sat}-T_\infty}{T_w-T_\infty}+\frac{2\sigma T_{Sat}\left(v_v-v_l\right)}{\left(T_w-T_\infty\right)h_{lv}r_c}\right)}\right\}^2 \qquad \textbf{6.6}$$

Where $T_w, \nu_v, \nu_l, \alpha_l$ and σ are wall temperature, specific volume of vapor, specific volume of liquid, thermal diffusivity of the liquid and surface tension of the liquid respectively.

In determining the bubble departure diameter and frequency, there are numerous correlations as listed in [**Kim-2006**]. In this simulation the correlation developed by [**Kim-2006**] is used to calculate bubble diameter at departure and the bubble growth time given by

$$d_b = 2\left(25\frac{\sqrt{27}}{2}Ja\cdot\alpha\sqrt{\frac{\rho_l}{\sigma}}\right)^2$$
$$t_d = 60\frac{9}{4}Ja\cdot\alpha\frac{\rho_l d_b}{2\sigma} \qquad \textbf{6.7}$$

Where the Jakob number is given by

$$Ja = \frac{\rho_l Cp_l\left(T_w - T_{Sat}\right)}{\rho_v h_{lv}} \qquad \textbf{6.8}$$

The total time for the bubble cycle is the sum of the waiting time t_w and the growth time t_b. The bubble frequency is then given by

$$f = \frac{1}{t_w + t_b} \qquad \textbf{6.9}$$

The nucleation density is calculated from correlation given in [**Narumanchi-2008**] as

$$n = \left(200\left(T_w - T_{Sat}\right)\right)^{1.8} \qquad \textbf{6.10}$$

Based on the above parameters for a given wall super heat and properties of liquid and vapor, one calculate the mass flux of vapor through the nucleation site as a function of time. Details of this procedure outlined in Appendix.

6.4 Result of Simulation

As described in the previous sections, the main purpose of this simulation is to obtain a separate CFD validation for the boiling heat transfer correlation used in the heat transfer analysis of the evaporator section. Figure **6-18** shows a cycle of the formation of bubble on the heated plate at the active nucleation site. It is also clear that the liquid pool temperature rises as near the plate. The heat flux through the heated wall which is maintained at a constant temperature is shown in Figure **6-19** . The heat flux peaks during the bubble formation and departure while it drops to the minimum value during the waiting period of the bubble formation. The increase in heat flux shows how the formation and departure of bubbles help increase the heat transfer rate on the heated surface. At last the result of this simulation was compared with the experimental data of [**Astruc et al 1969**] as shown in Figure **6-20** . The CFD prediction closely predicts the natural convection regime of neon boiling curve. The prediction for the nucleate boiling regime follows the experimental trend. With an improved modeling it could be possible to get a more accurate prediction.

6.5 Flow Field Inside the Thermosyphon

The flow field inside the thermosyphon is complex and unsteady. Understanding the flow field and temperature profile could help in the thermal hydraulic analysis and design the thermosyphon. In this section the steady state CFD simulation result of flow and heat transfer is presented. In the analysis the VOF multiphase flow module of the CFD code FLUENT is utilized. Figure **6-21** shows the volume fraction of vapor inside the TCNS thermosyphon at a typical operating condition. The accumulation of the liquid at the evaporator section is due to the inclination of the thermosyphon. It is clear from the figure that the liquid level at the top wall of the evaporator is much smaller than that at the bottom. Figure **6-22** shows the temperature and velocity profiles inside the condenser section of the thermosyphon. It is clear that the condensed vapor flows to the bottom of the condenser leaving the hot vapor returning from the evaporator at the top. This complex flow structure can be seen from the velocity profile with the velocity vectors showing the flow direction. This complex flow is generated due to buoyancy. The flow in the evaporator and condenser sections is in fact three dimensional and should not be modeled with 2D assumptions. The velocity profile in the condenser section is also shown in Figure **6-23** . It is clear that the two velocity profiles tend to be mirror images of one another.

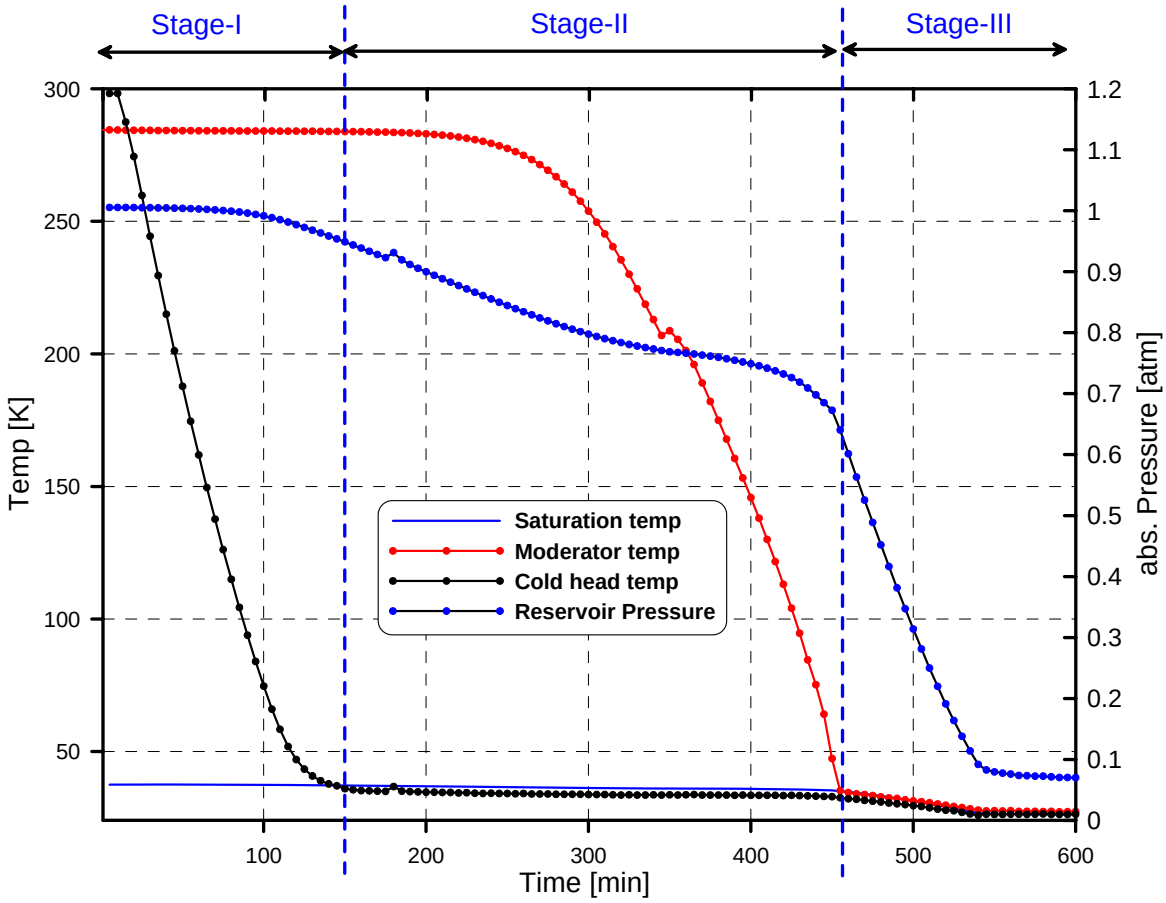

Figure **6-1**: The various cooldown stages showing moderator and cold head temperatures and reservoir pressure vs. time of the TCNS cooling system [**Unlu et al 1994**].

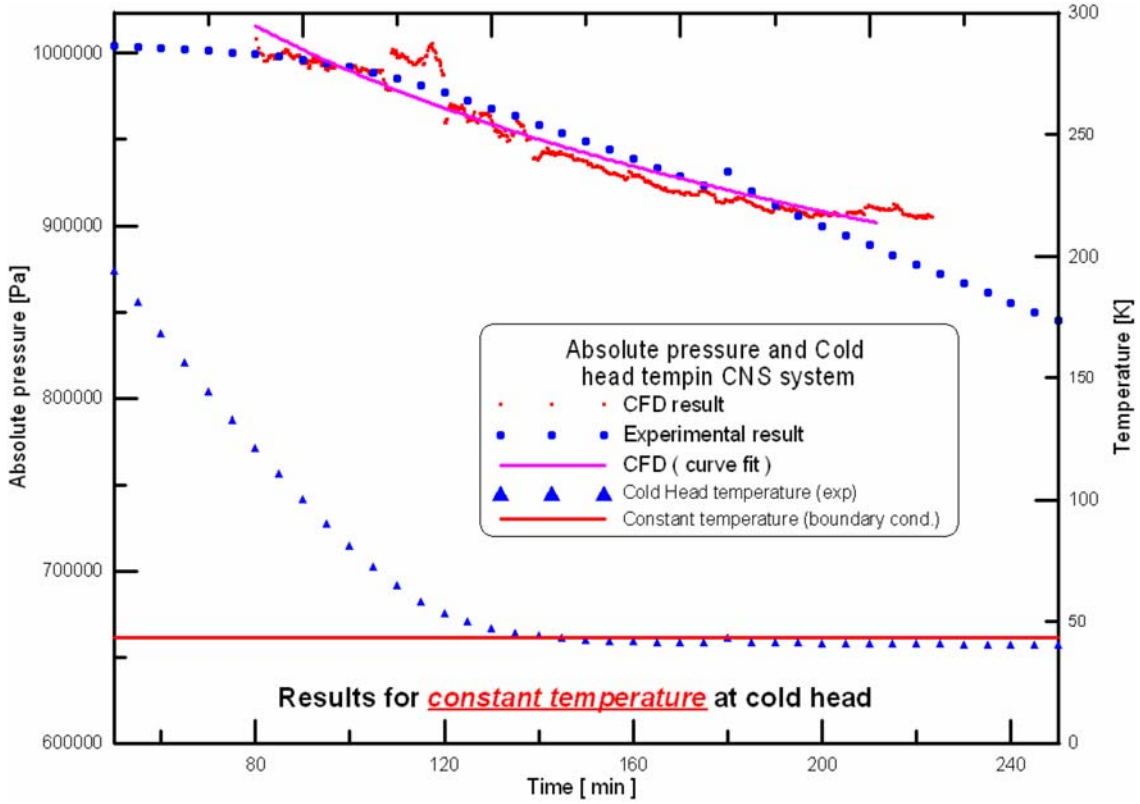

Figure **6-2**: Transient cooldown simulation for single phase flow with constant temperature boundary condition

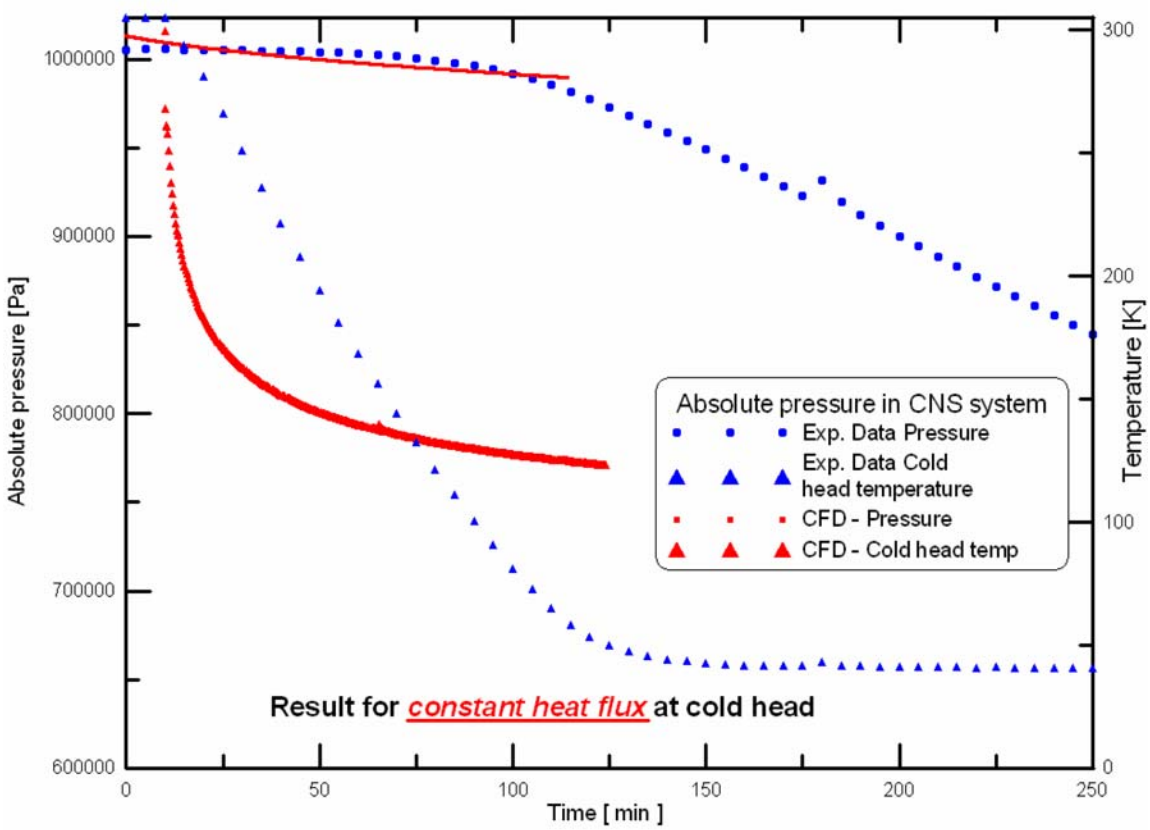

Figure **6-3**: Transient cooldown simulation for single phase flow with constant heat flux boundary condition

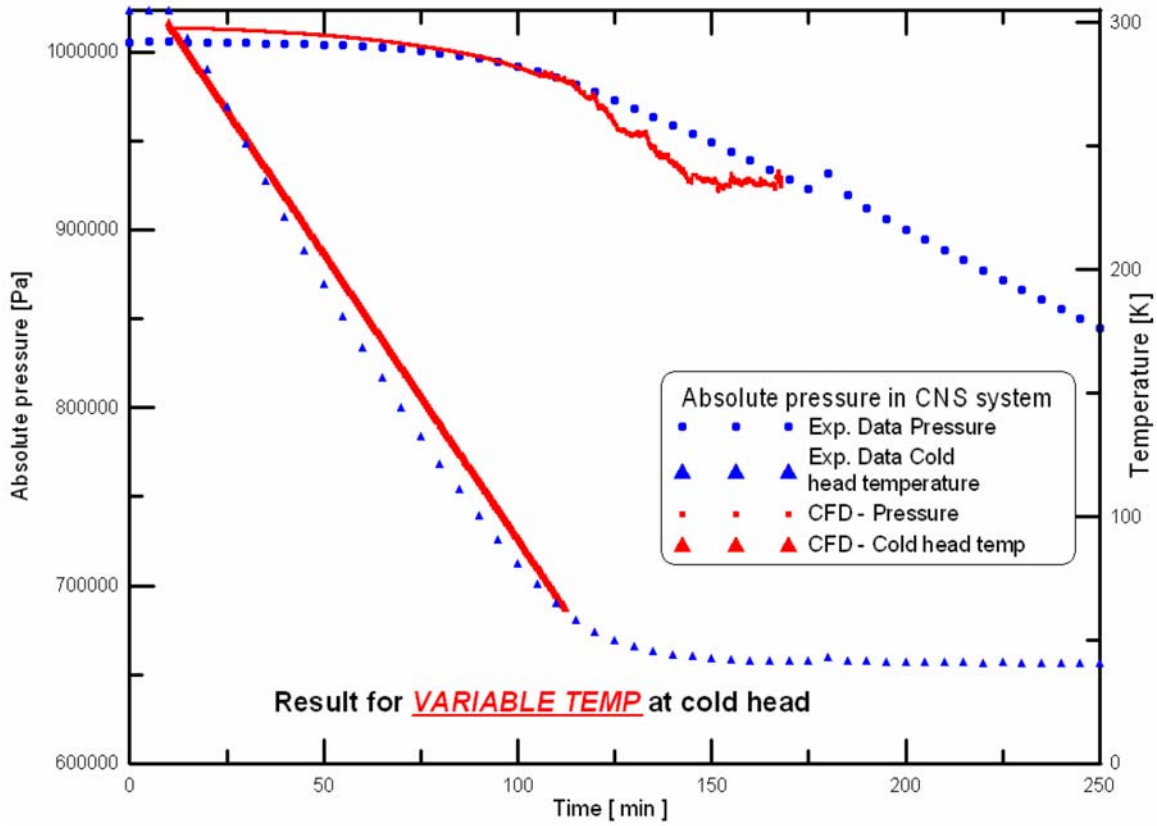

Figure **6-4**: Transient cooldown simulation for single phase flow with variable temperature boundary condition (mixed boundary condition)

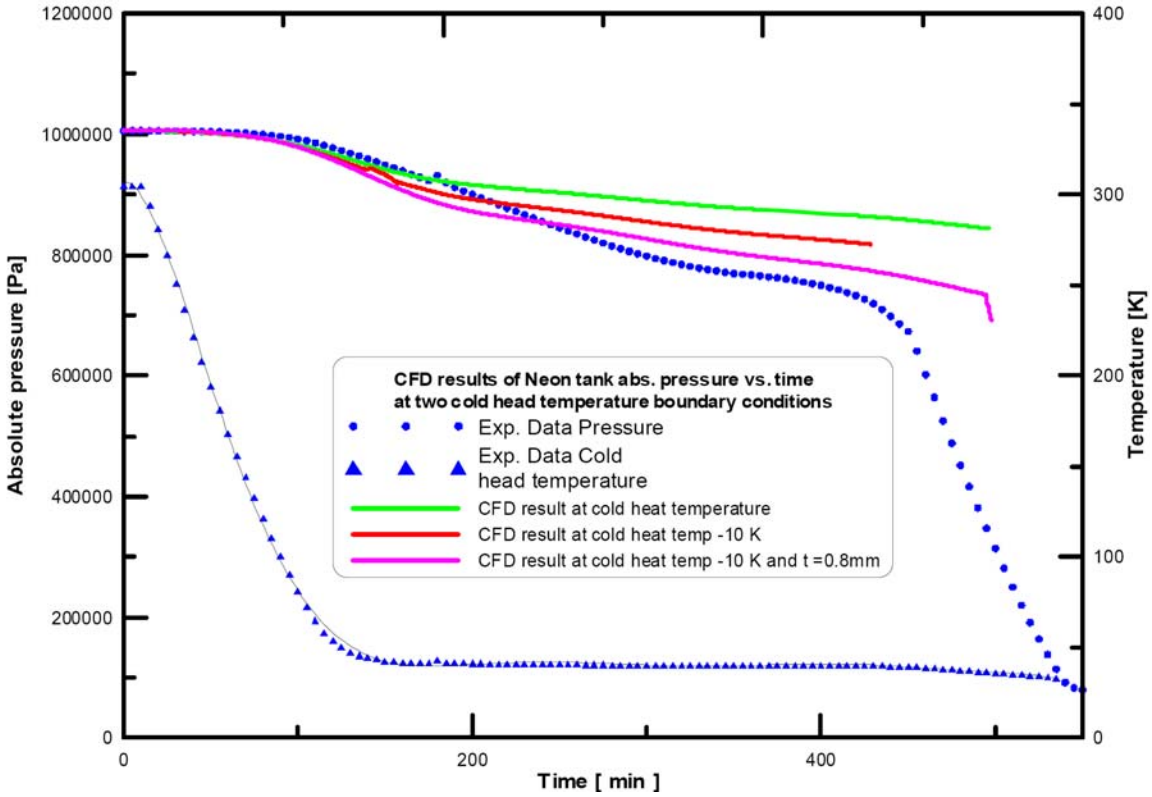

Figure **6-5**: Transient cooldown simulation showing pressure inside the TPCTR for single phase flow with variable temperature boundary condition (using polynomial curve fit of exp. data)

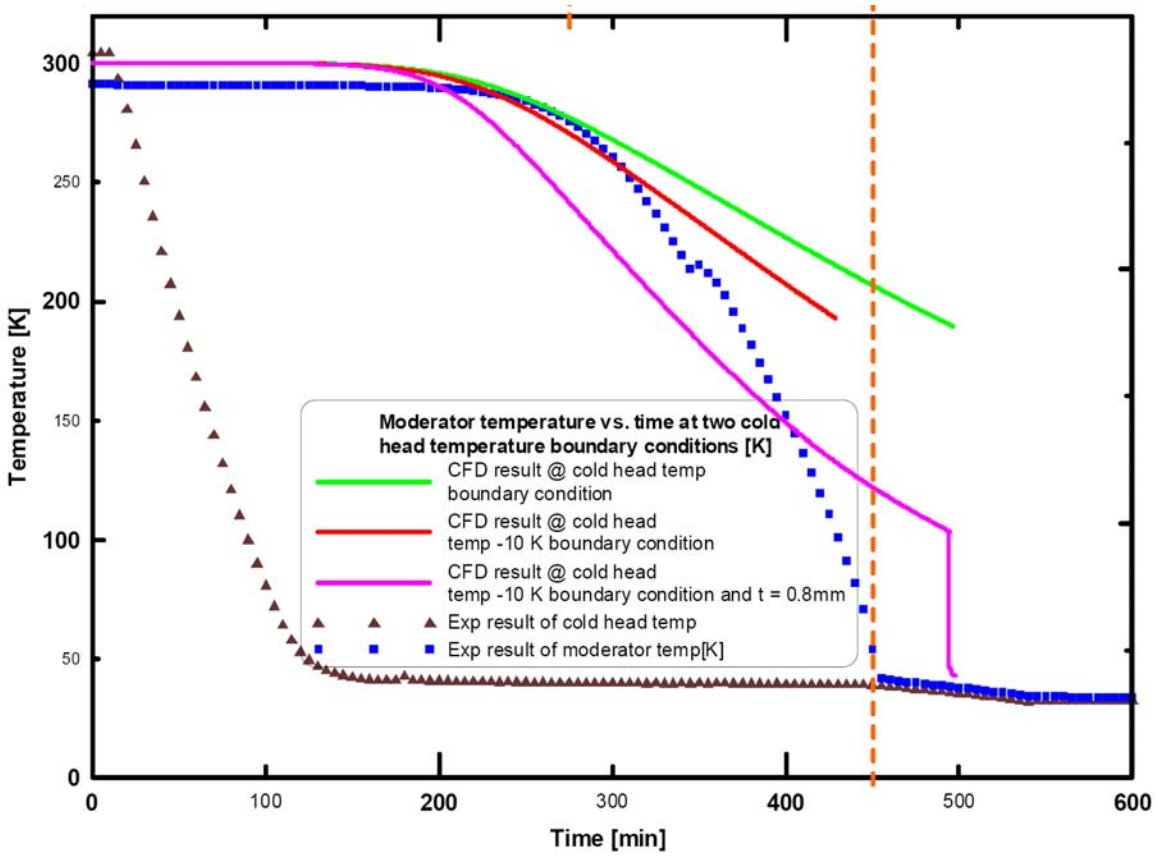

Figure **6-6**: Transient cooldown simulation showing moderator(evaporator) temperature of the TPCTR for single phase flow with variable temperature boundary condition (using polynomial curve fit of exp. data)

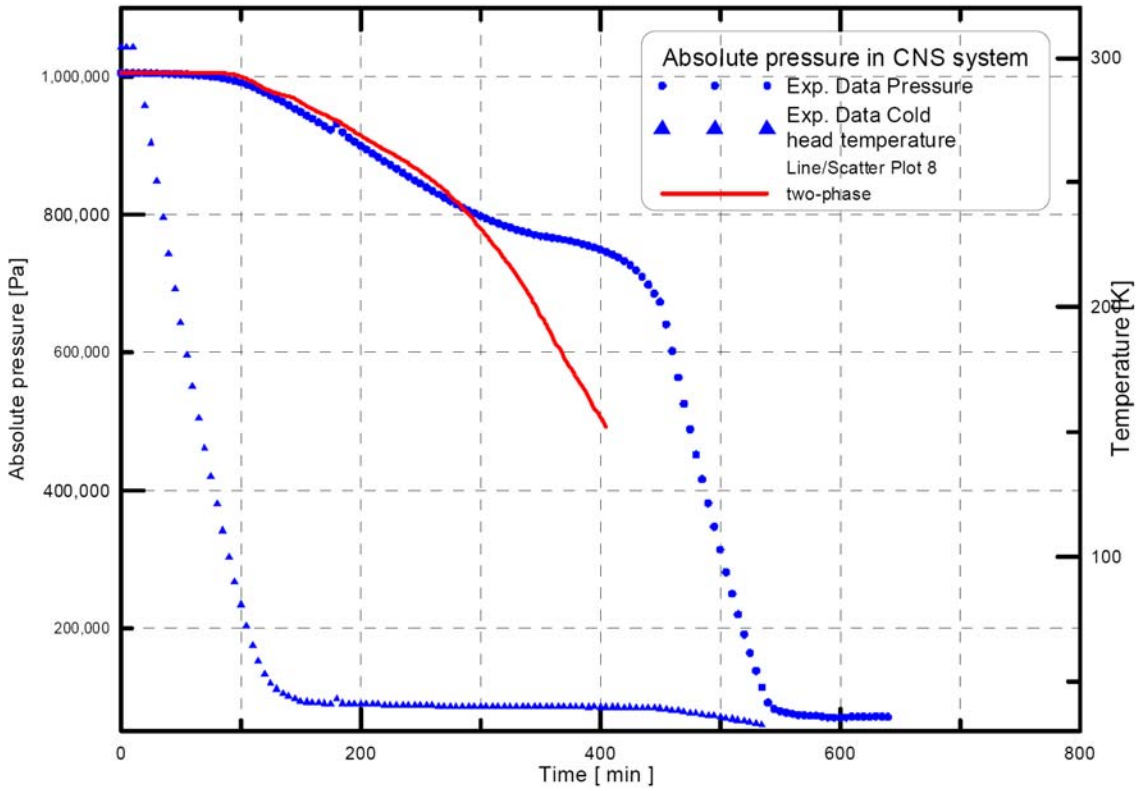

Figure **6-7**: Transient cooldown simulation showing pressure inside the TPCTR for two phase flow with variable temperature boundary condition (using polynomial curve fit of exp. data)

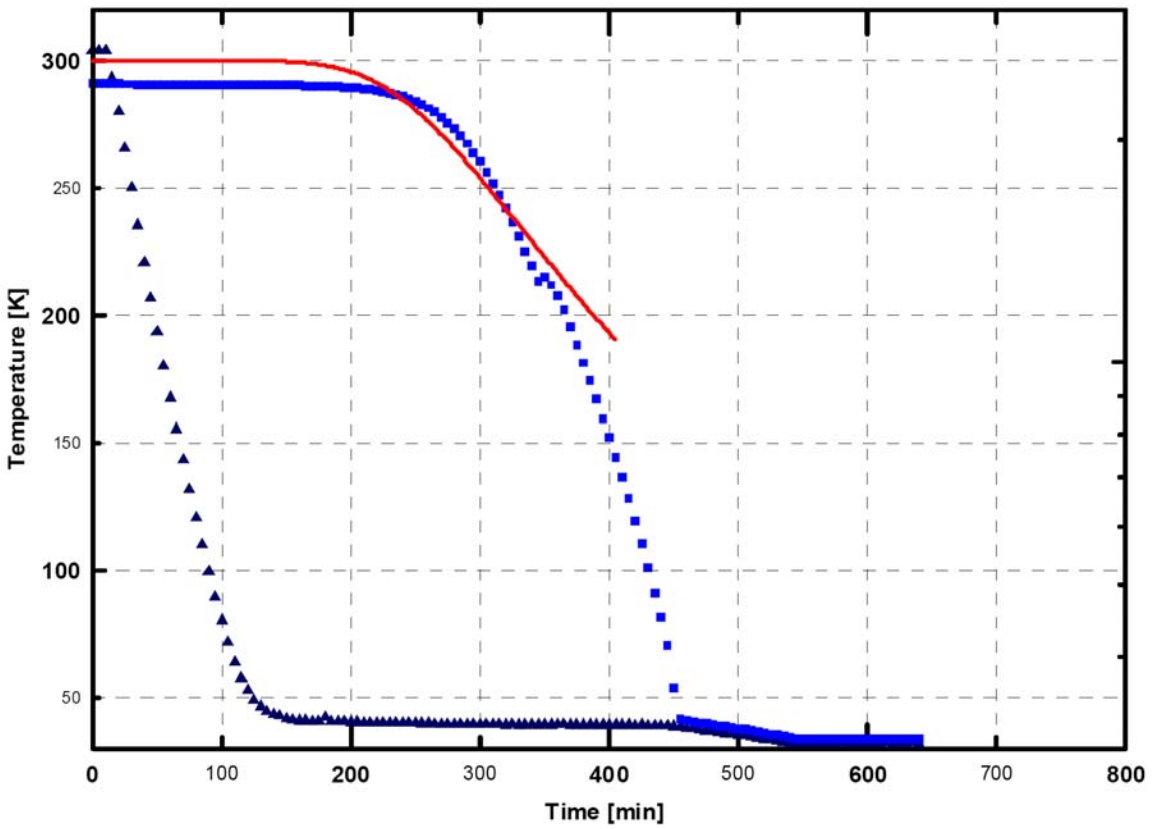

Figure **6-8**: Transient cooldown simulation showing moderator(evaporator) temperature of the TPCTR for two phase flow with variable temperature boundary condition (using polynomial curve fit of exp. data)

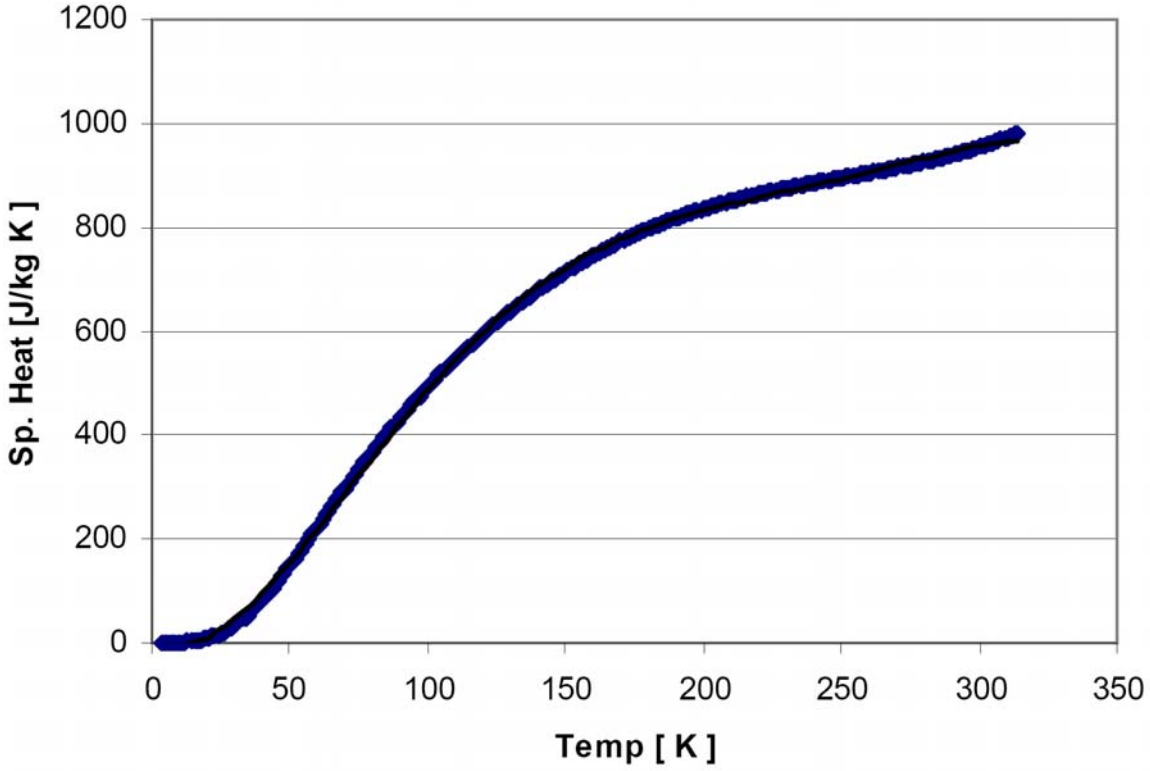

Figure **6-9**: Specific heat of Aluminum alloy 6061 as a function of temperature

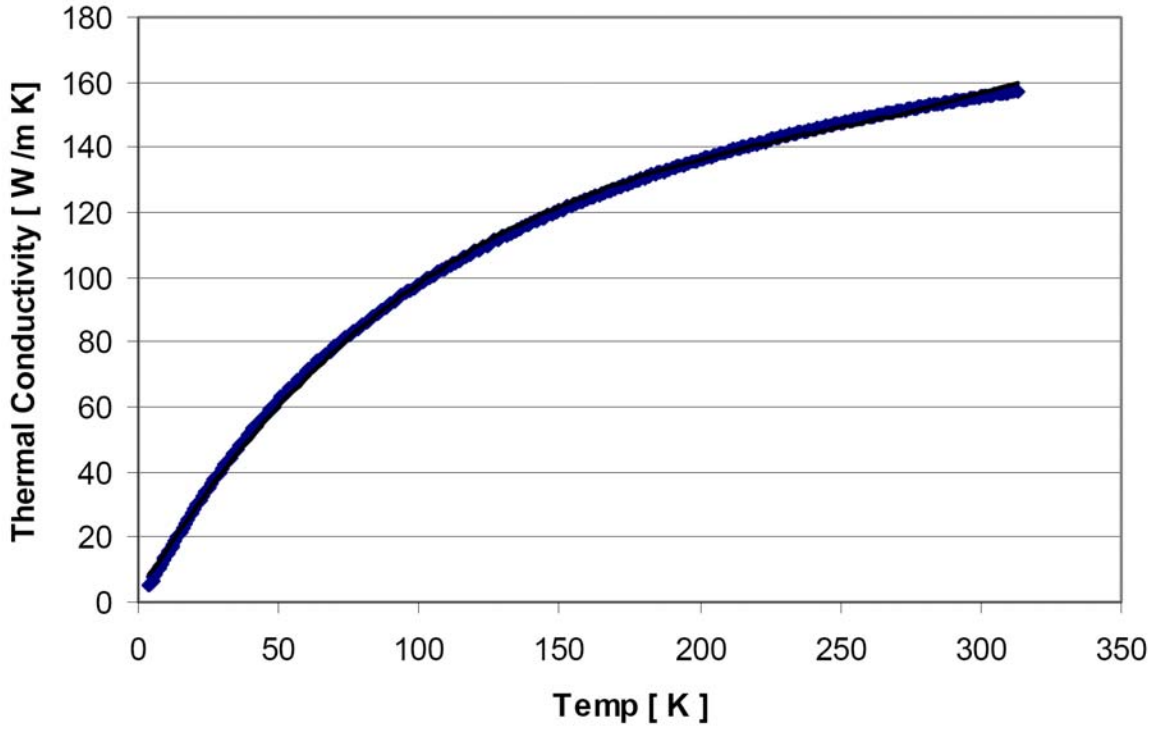

Figure **6-10**: Thermal Conductivity of Aluminum alloy 6061 as a function of temperature

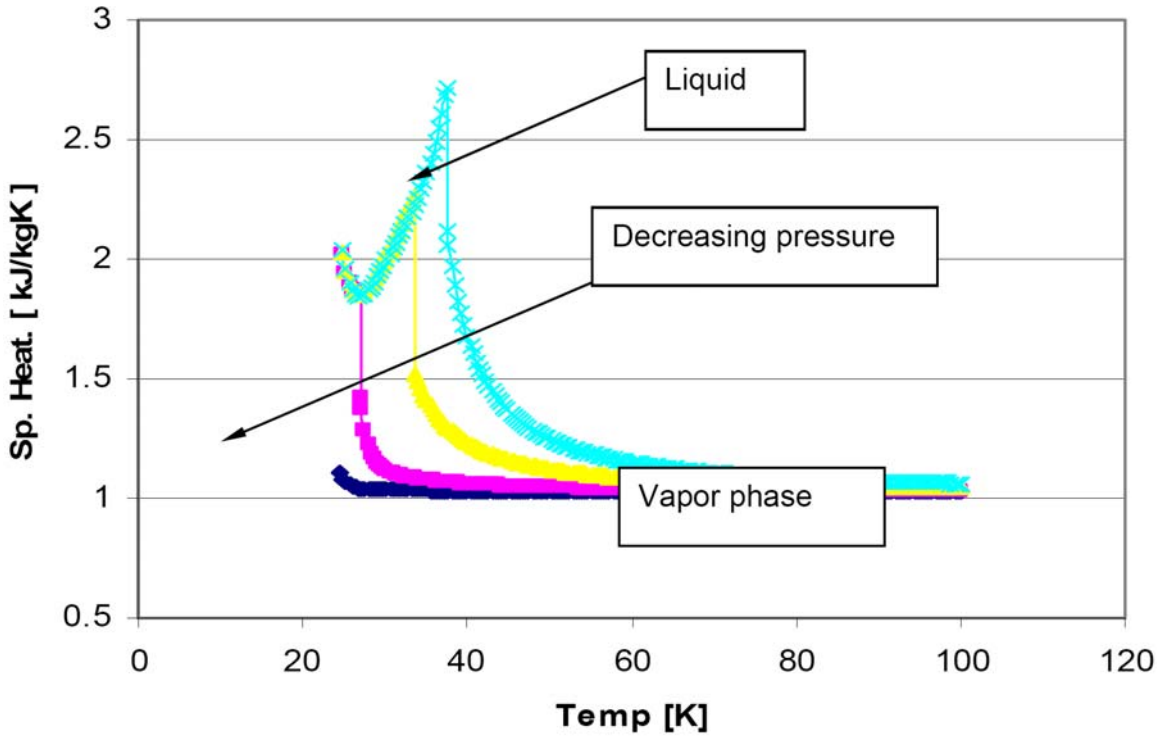

Figure **6-11**: Specific heat of neon liquid and vapor as a function of temperature

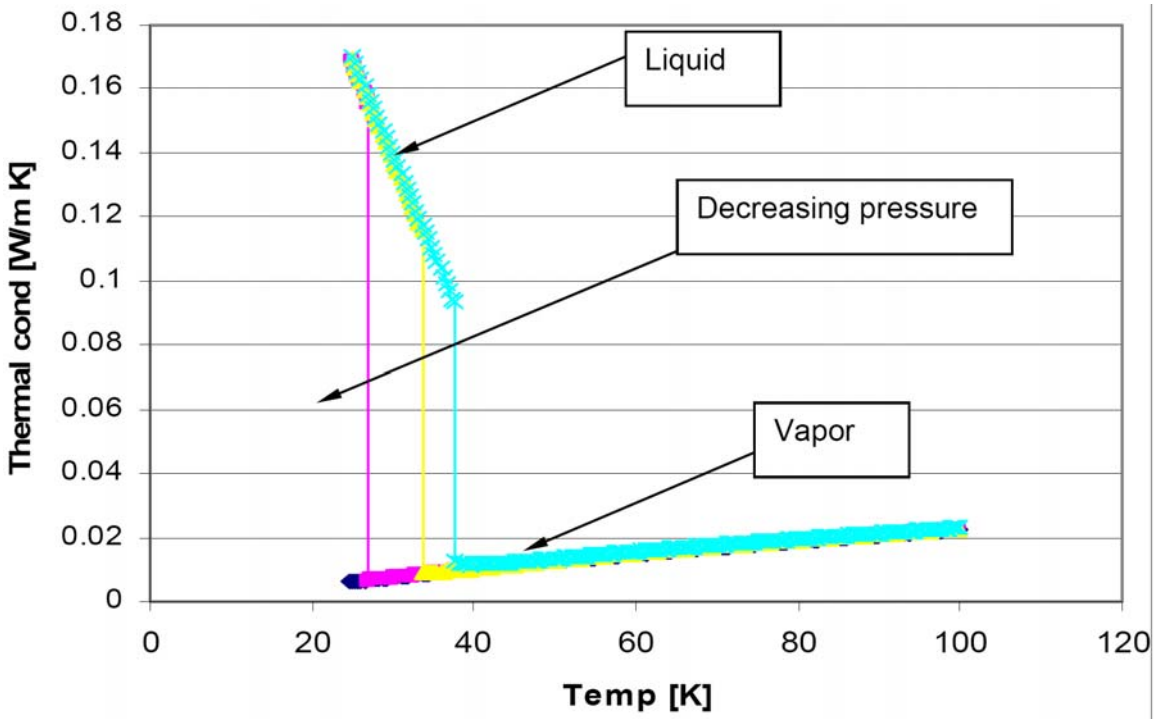

Figure **6-12**: Thermal conductivity of neon liquid and vapor as a function of temperature

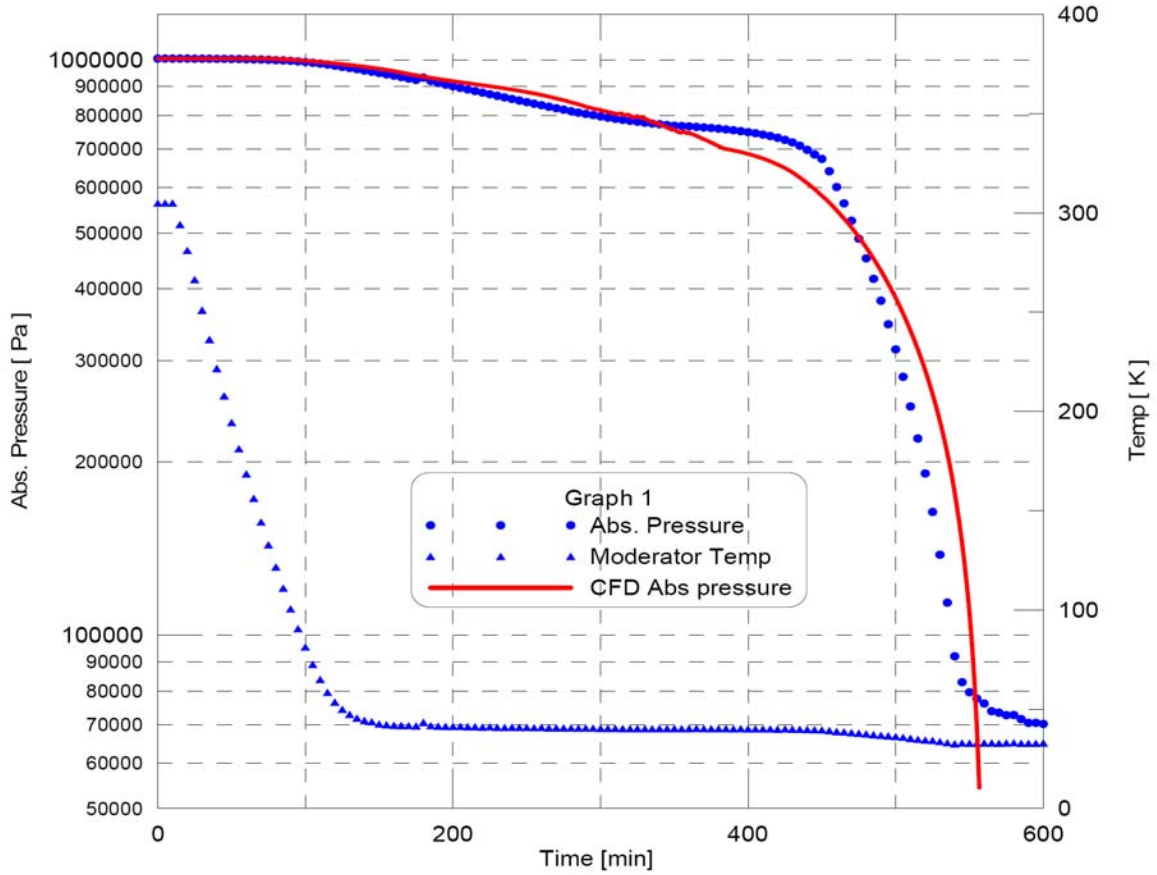

Figure **6-13**: Transient cooldown simulation showing moderator(evaporator) temperature of the TPCTR for two phase flow with variable temperature boundary condition (using polynomial curve fit of exp. data) with variable material and fluid properties

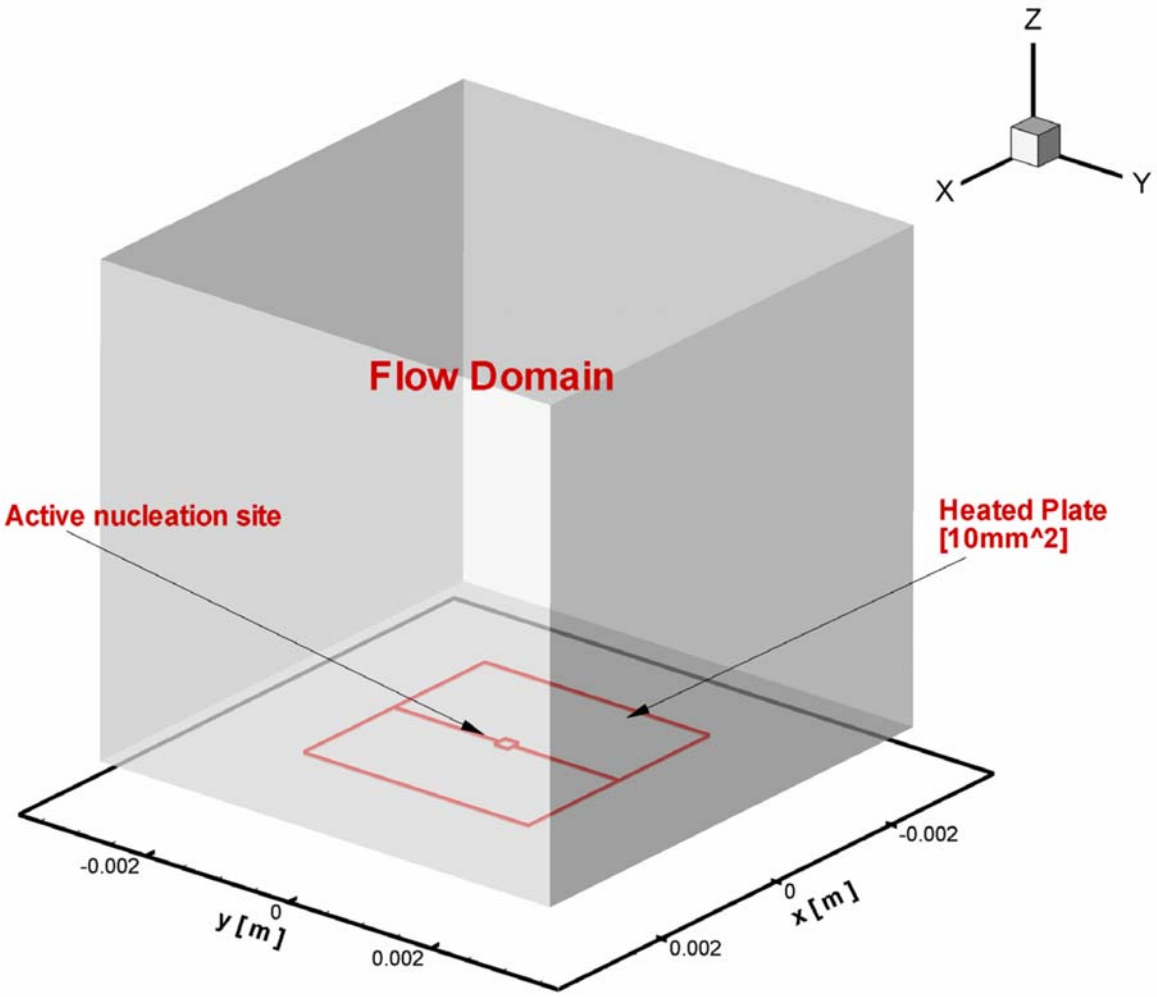

Figure **6-14**: Schematic showing the computational flow domain used in simulation of nucleate boiling over a heated plate of $10mm^2$ with one active nucleation site

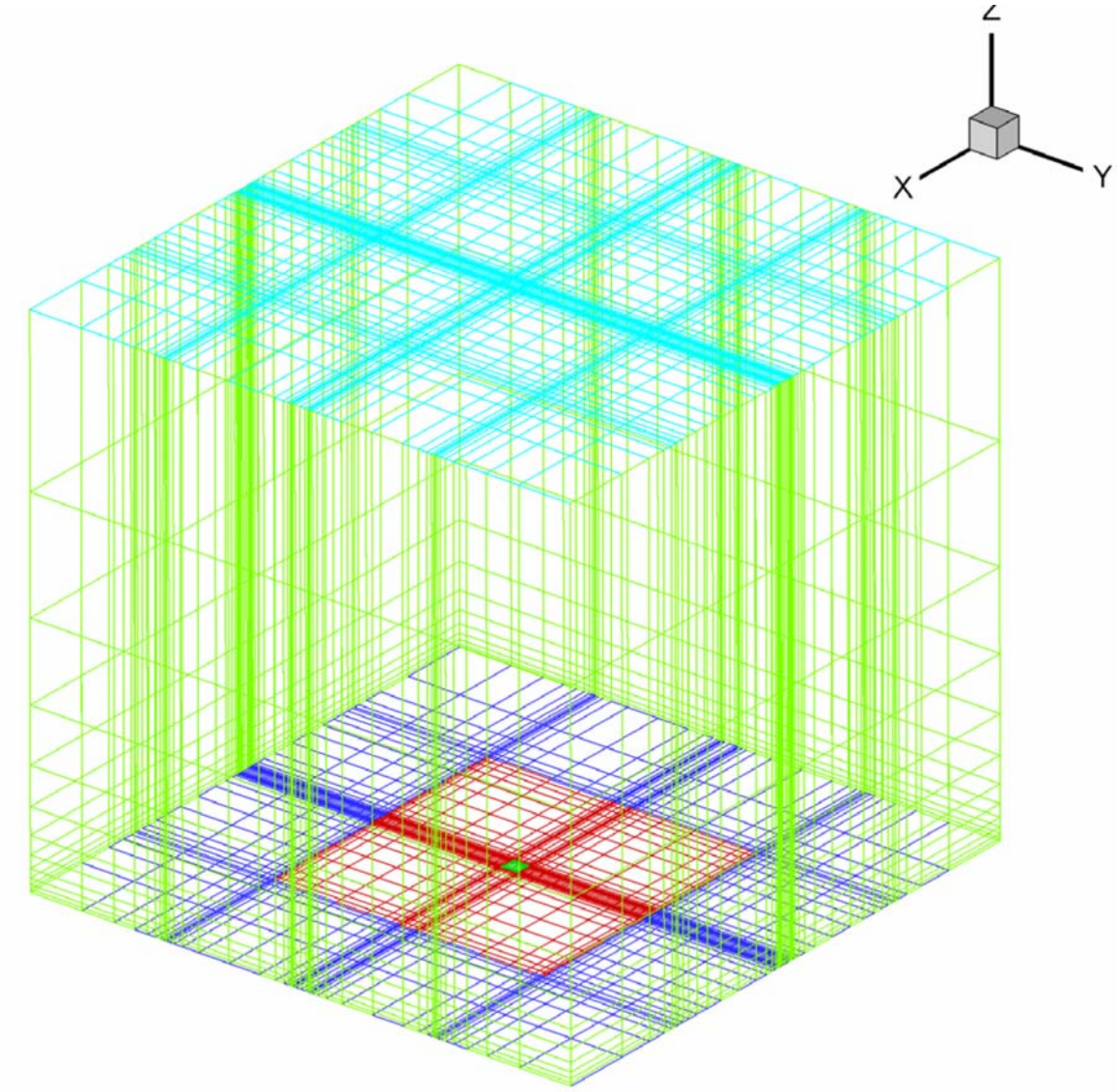

Figure **6-15**: Schematic showing the computational mesh of flow domain used in simulation of nucleate boiling over a heated plate of $10mm^2$ with one active nucleation site

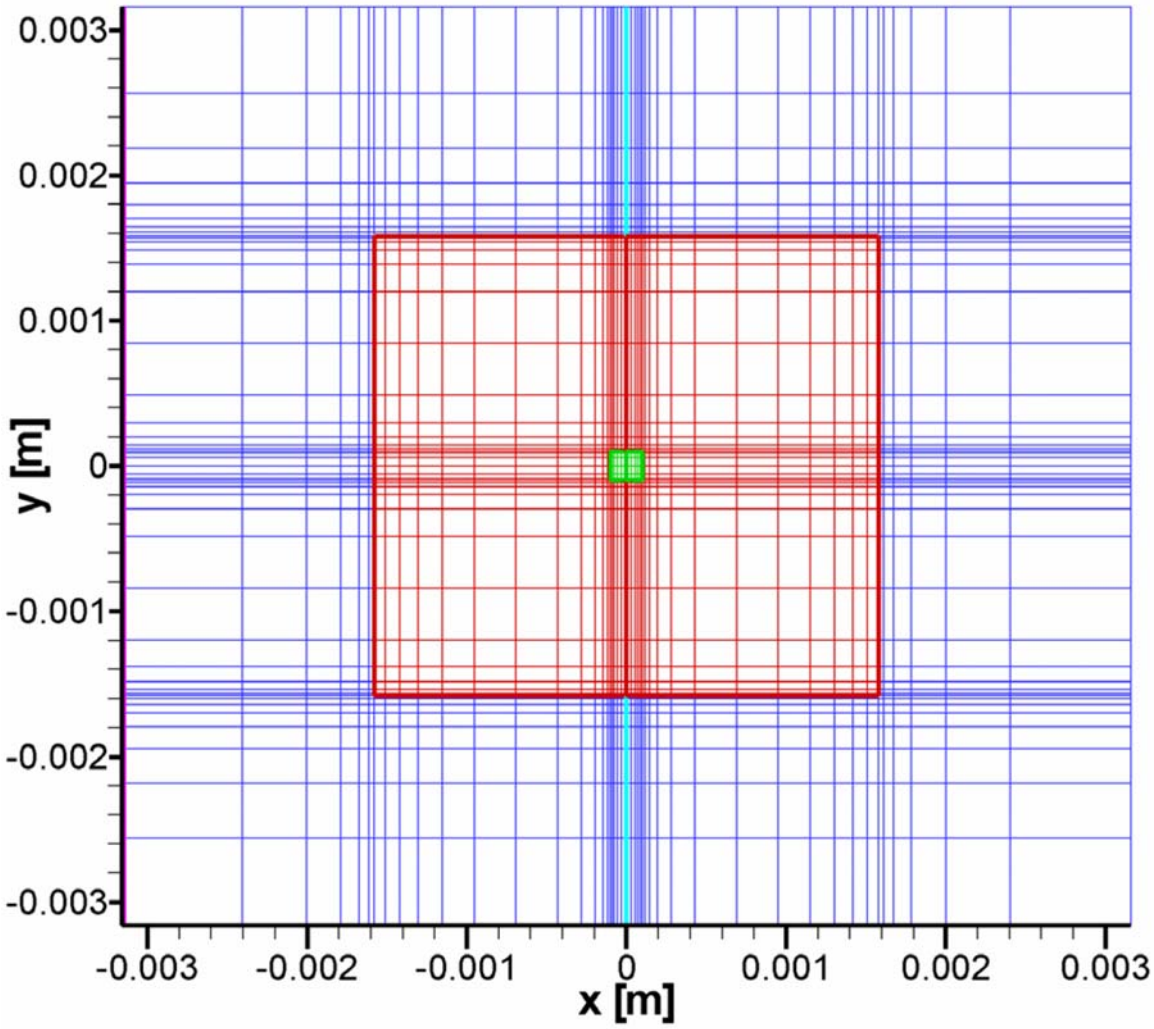

Figure **6-16**: Schematic showing the computational mesh of the bottom plate of flow domain used in simulation of nucleate boiling over a heated plate of $10mm^2$ with one active nucleation site

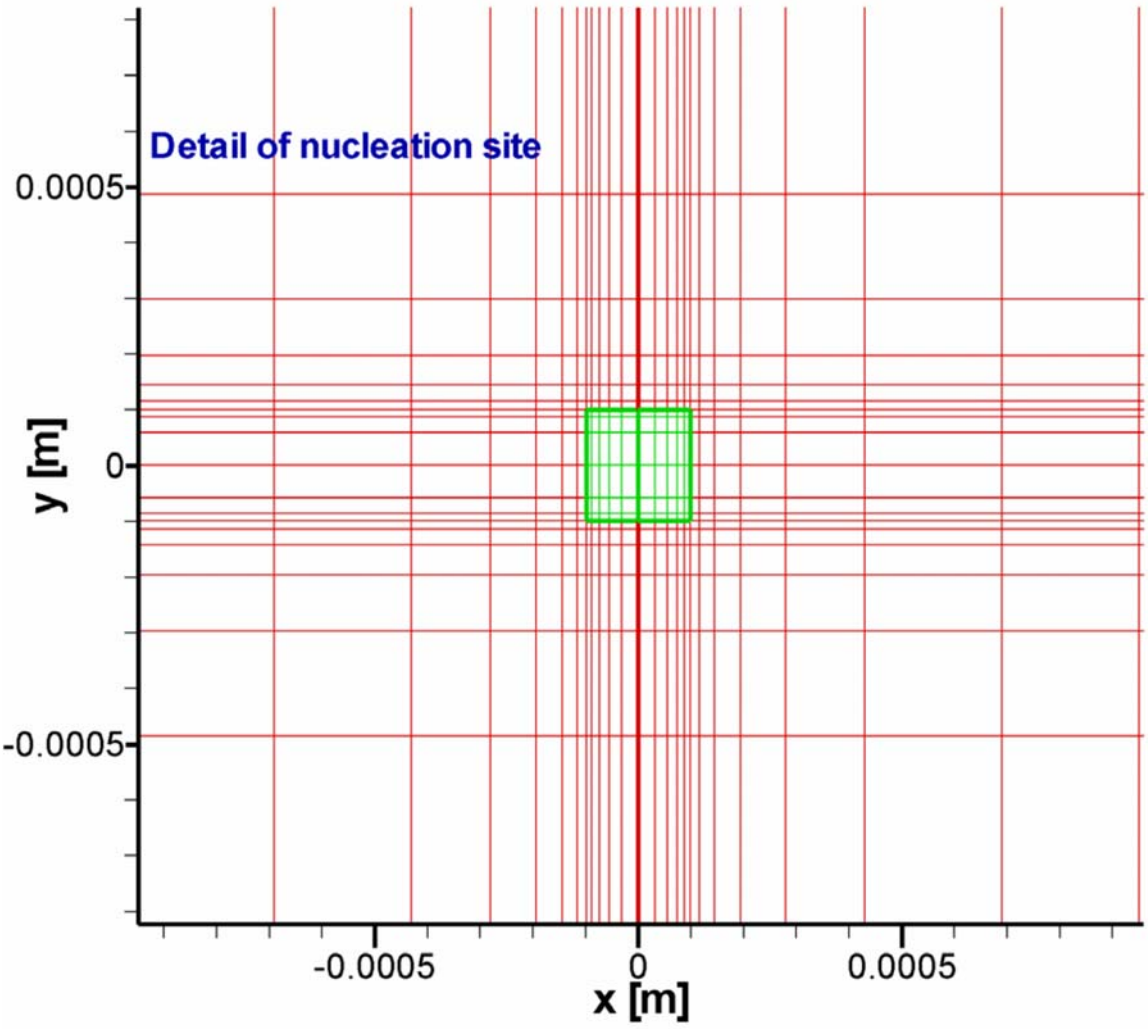

Figure **6-17**: Schematic showing detail of the computational mesh of the nucleation site of the flow domain used in simulation of nucleate boiling over a heated plate of 10mm^2 with one active nucleation site

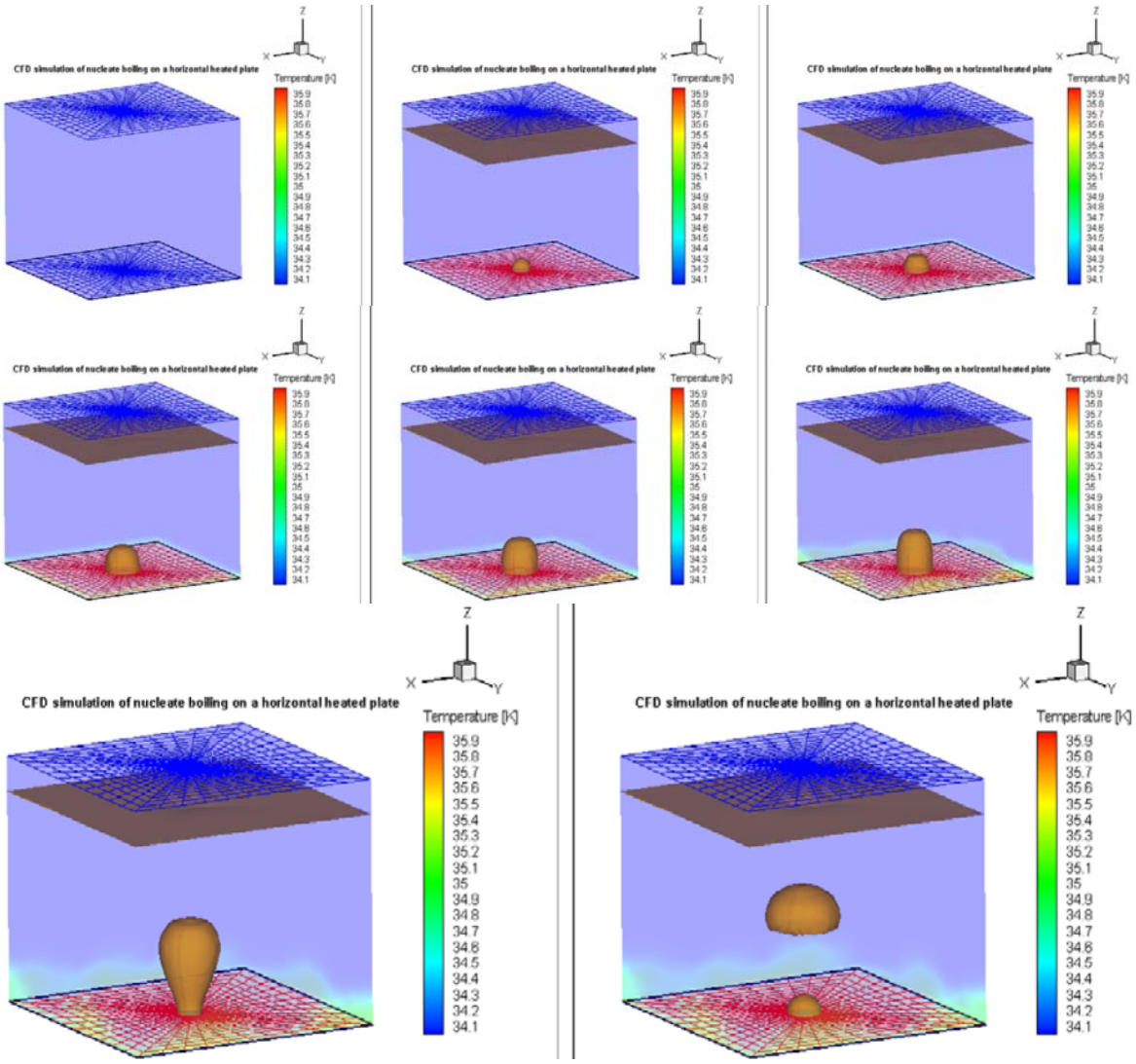

Figure **6-18**: CFD simulation showing a cycle of formation of bubble at an active nucleation site on a heated plate

Figure 6-19

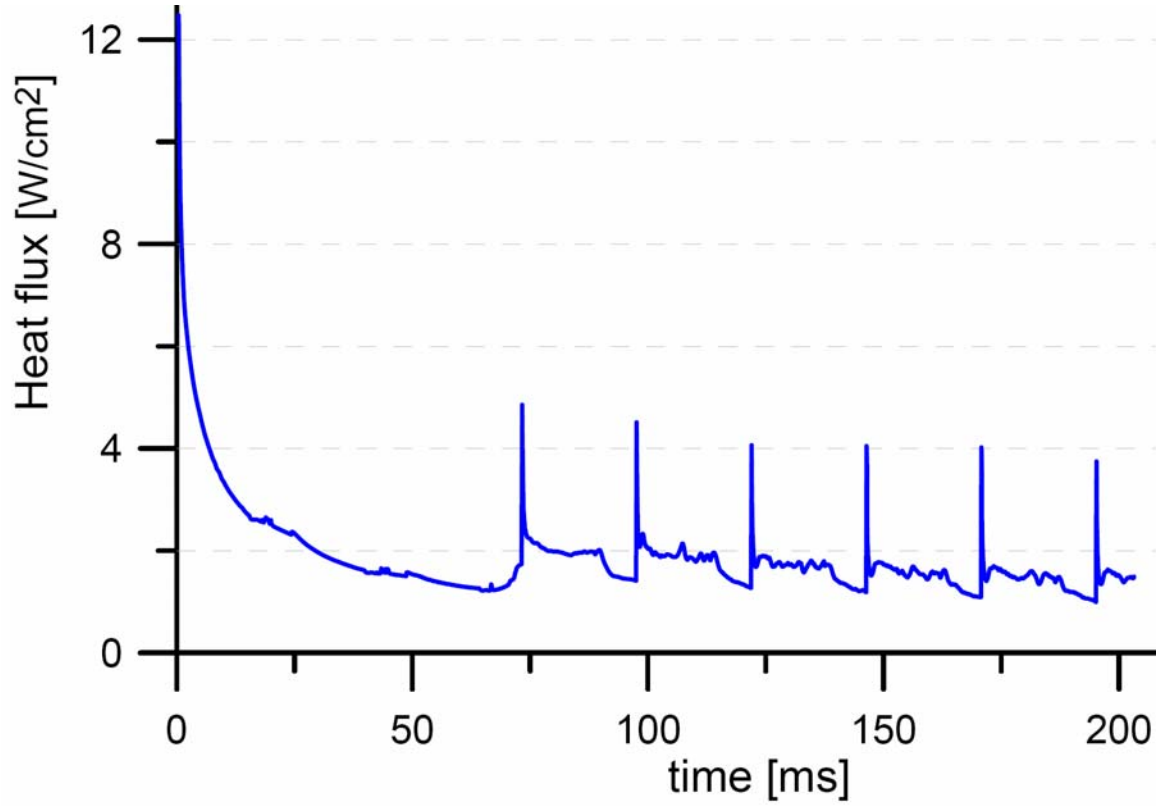

Figure **6-19**: Plot showing CFD result of typical heat flux on the heated plate during bubble formation cycles

Figure 6-20

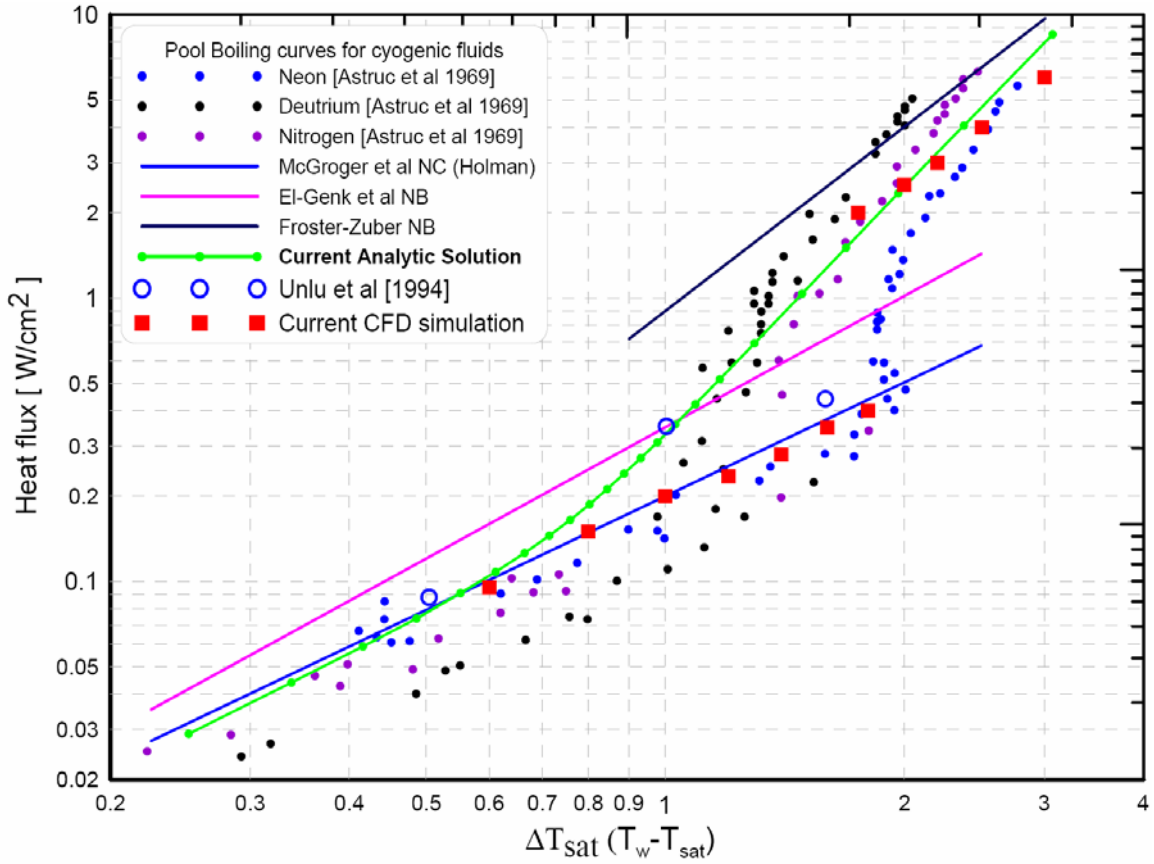

Figure **6-20**: Comparison of CFD prediction and experimental and correlations of boiling heat transfer of liquid neon

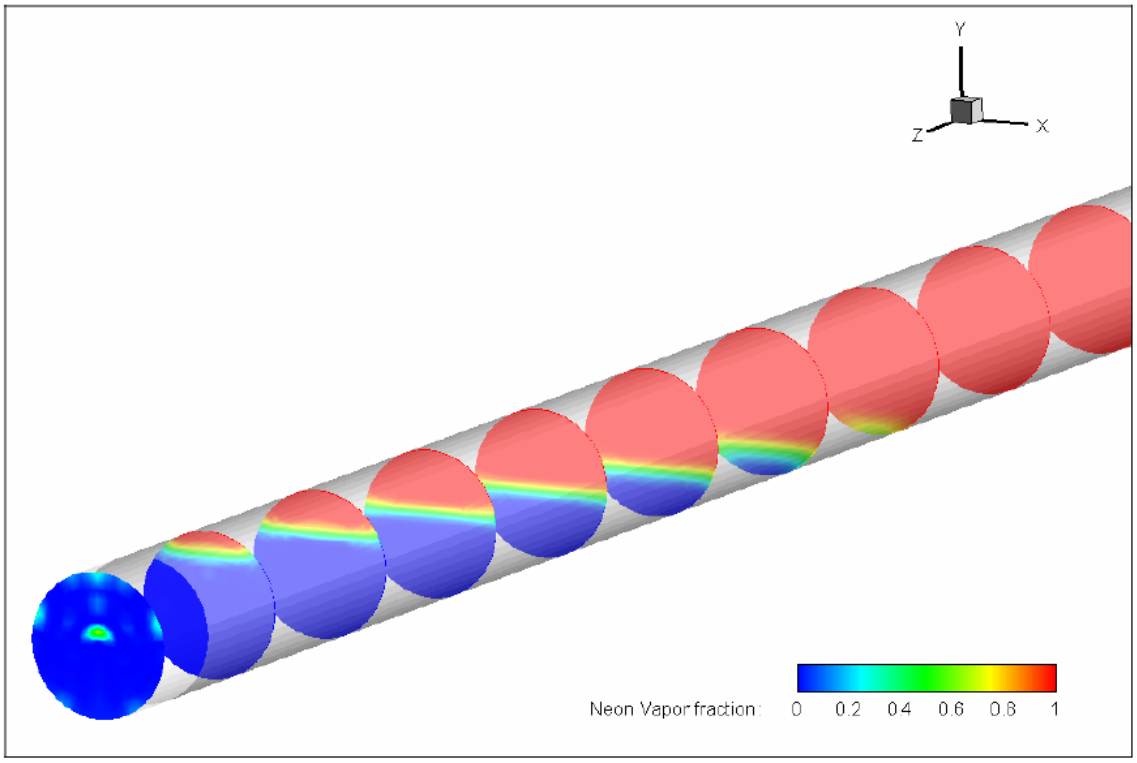

Figure **6-21**: Steady state CFD simulation result showing volume fraction of vapor inside CTPT

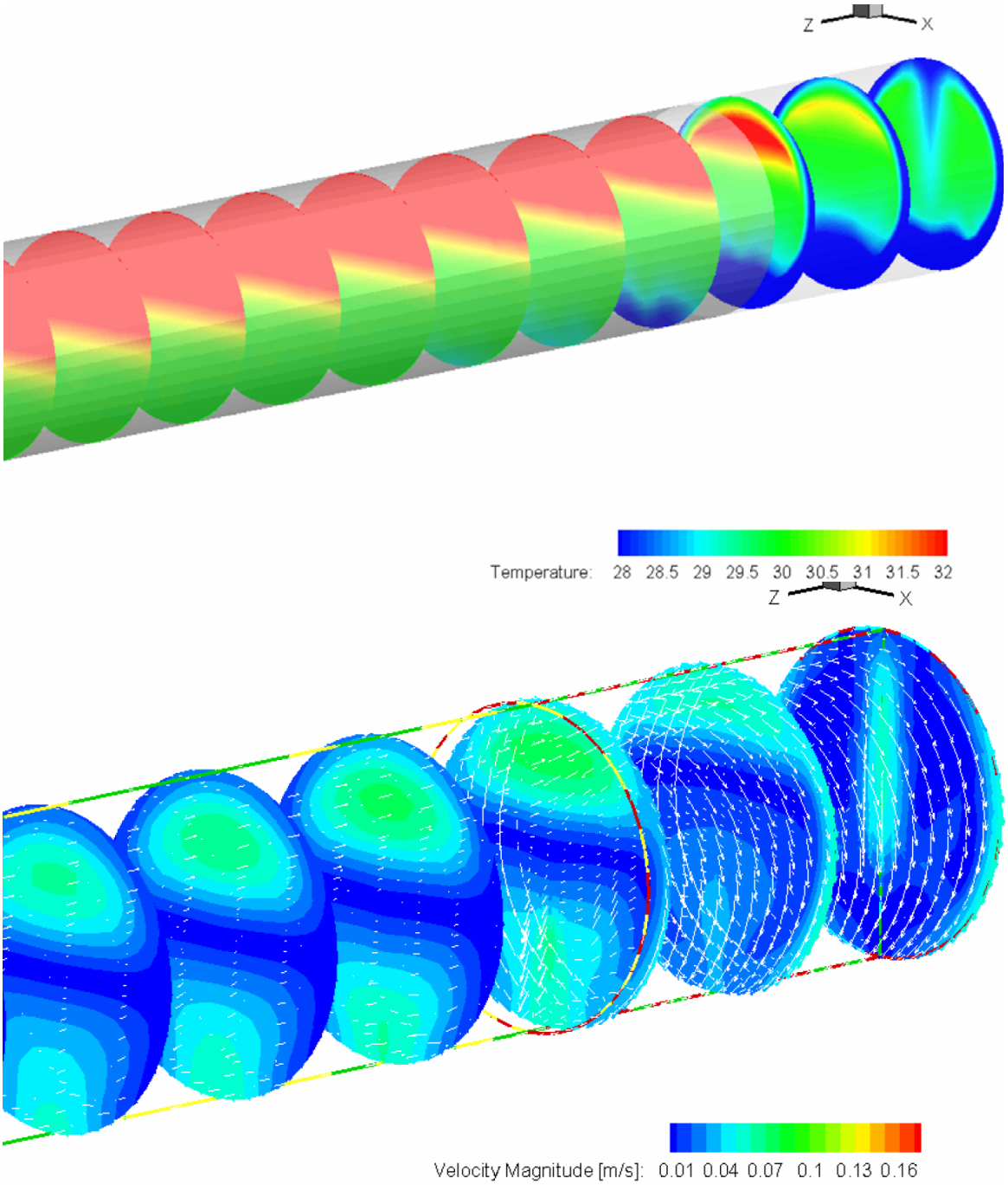

Figure **6-22**: Steady state CFD simulation result showing temperature and velocity profiles of the flow inside the evaporator section of the CTPT

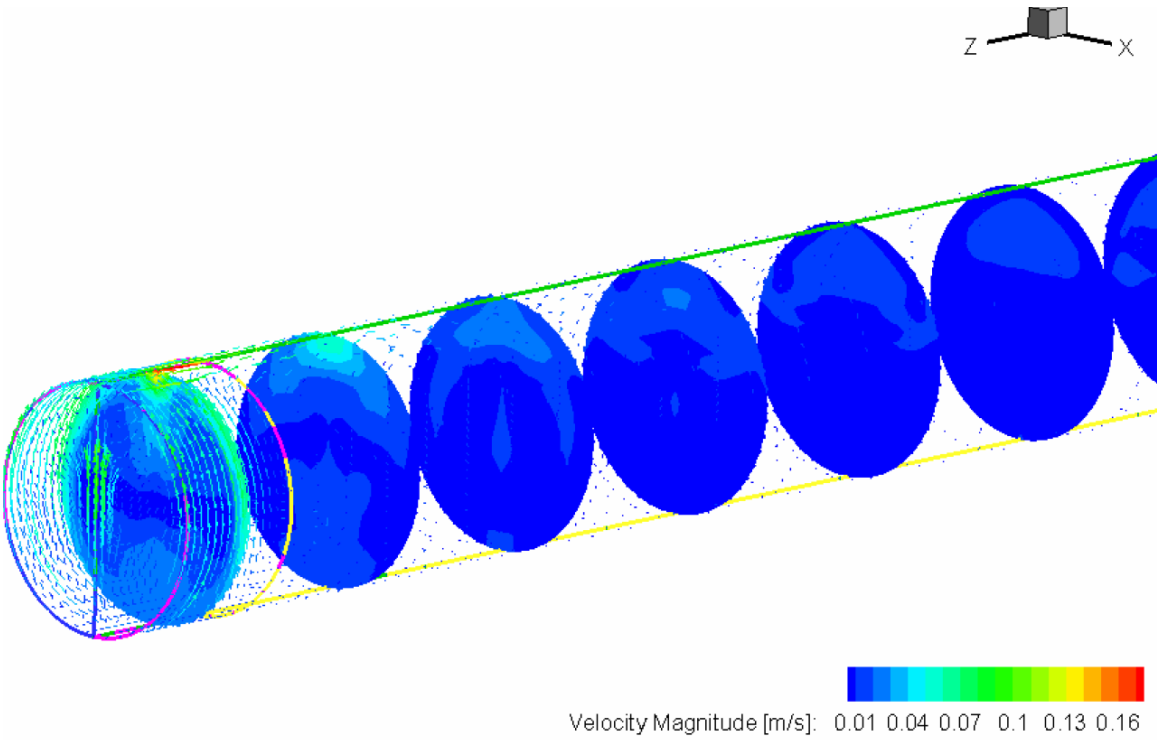

Figure **6-23**: Steady state CFD simulation result showing velocity profiles of the flow inside the condenser section of the CTPT

Chapter 7

Summary and Conclusions: Design Recommendation and Future Work

In this chapter a summary and conclusion of the study is presented. A general recommendation and specific suggestion of design parameters for future ideal design of a cold neutron source cooling system using TPCTR as a heat exchanger is given. Finally a summary of possible future work is outlined.

7.1 Design Recommendations for an Ideal Cooling System for Cold Neutron Source

In this section a design recommendation for a new TPCTR cooling system is presented based on the following hypothetical parameters and/or requirements. This cooling system can safely handle a heat load of 10W without any dryout problem. A factor of safety of about 1.2 of the anticipated maximum heat load is considered. A cryorefrigeration system with characteristic angle of $\alpha = 40^0$ is considered. The various design parts are discussed below.

7.1.1 Material Selection for Thermosyphon

In order to efficiently transfer heat from the moderator (heat source) to the cold head (cryorefrigerator heat sink) the material out of which the thermosyphon is made of should be a material that has as low thermal conductivity as possible. It is also desirable

to have a low heat capacity material for quick cooldown and warm up. In this regard two materials are chosen as possible candidates. Figure 7-1 and Figure 7-2 the thermal conductivities of aluminum and copper alloys near cryogenic temperatures. copper alloy Cu RRR=500 shows the best thermal conductivity of the two alloys near the operation temperature range of 24K to 44K of Neon. Among the four alloys of aluminum shown in the figure the alloy AL 1100 shows the best thermal conductivity. The material used for the construction of the TCNS thermosyphon was AL 6061. It is clear that this alloy shows the least thermal conductivity at the operation temperature range. Based on this analysis it is recommended that Cu RRR=500 be the material used to construct the thermosyphon. If for radiation reasons copper is not to be used, then the next best material should be aluminum alloy AL 1100.

7.1.2 Operating Pressure and Size of Evaporator Section of the TPCTR

The selection of the primary cooling system is critical in the design of this cooling system since it determines the capacity index defined in the previous chapters. It is recommended that a cryocooler that has the smallest performance angle α should be selected. As it is defined in the previous chapters this angle is obtained from the manufacture's performance chart of the cryocooler. Based on survey of manufacturer's it is recommended that cryocooler AL63 with performance angle of 40^0 as shown in Figure 7-3 is chosen. The maximum heat load under these conditions can be selected from the parametric chart shown in Figure 7-4 . For the given performance angle the maximum heat load will be 12 W for thermosyphon system using the same dimensions

and material as that of the TCNS. Any improvement to the TCNS will potentially increase the performance of such system up to a capacity close to 30 W.

For the current design and factor of safety, the dryout heat load is given by:

$$\begin{aligned} Q_d &= f_S \cdot Q \\ &= 1.2(10W) = 12W \end{aligned} \qquad \textbf{7.1}$$

Using the above result and in Figure 7-4 the capacity index can be obtained. For this case the capacity index is $\zeta = 0.5$. Using this value of capacity index and the given initial fill ratio, the initial pressure can be obtained from Figure 7-5 . In this case the pressure is $P_O = 0.5P_{Cr} = 1.4MPa$. From these results the maximum allowable evaporator surface area can be calculated as:

$$\begin{aligned} A_{Evap\_\min} &\le \frac{Q_d}{q_d} \\ &= \frac{12W}{1.2\dfrac{W}{cm^2}} = 10cm^2 \end{aligned} \qquad \textbf{7.2}$$

This estimates the size of the evaporator section of the thermosyphon.

7.1.3 Size of Gas Reservoir and Thermosyphon

The relative sizes of the thermosyphon and reservoir is given by the volume ratio as discussed in the previous chapters. The actual volume of the thermosyphon is also constrained by the length of the thermosyphon. In this case a total length of 3.5m is taken as the length of the thermosyphon. For an initial fill ratio of 1 and the calculated liquid fraction of $\xi = 0.054$ at the end of cool down period, the evaporator length will

be $L_{Evap} = 1.89cm$ .Using the evaporator area calculated above one can estimate the diameter of the thermosyphon which in this case will be $d = 1.689cm$. This will set the diameter and length of the evaporator section of the thermosyphon, which in turn determines the length of the moderator. From the calculated volume ratio one can estimate the volume of the reservoir which in this case will be $V_R = 3.87Liter$. Such analysis can be made with various combinations until optimum size is obtained.

7.1.4 Working Fluid

The operating temperature required for cold neutron source cooling system requires that the available fluids that exist as a liquid at ultra-low temperatures. Some of the fluids that exist as liquid at such low cryogenic temperatures are Hydrogen, Neon and Nitrogen. Among these fluids Neon should be selected as a working fluid. Although Hydrogen exists at lower temperature, its combustibility is not suitable for such applications. Nitrogen does not meet the temperature range that is needed for the cooling system of cold neutron source. Neon was the fluid used in the TCNS and pose no risk in using it as the cooling medium.

7.2 Summary and Conclusions

Thermodynamic, heat transfer and CFD analysis for cooling system for cold neutron source of research reactor has been carried out. Two previous research reactor cold neutron source cooling systems were investigated. The investigation of the Texas

Cold Neutron Source cooling system, that uses liquefied neon inside a closed thermosyphon showed that the dryout temperature of the two-phase closed thermosyphon with reservoir (TPCTR) to be the crucial parameter in determining the overall operational capacity of the cooling system for cold neutron source cooled with neon thermosyphon. Dryout in the thermosyphon occurs due to lack of liquid returning to the evaporator section of the TPCTR as the heat load increased. The increase in heat load results in increase in the saturation temperature and pressure of the cooling fluid (neon). When the saturation temperature reaches above the dryout temperature, the liquefied neon will be completely evaporates and the system losses its cooling power. The mechanism of heat transfer inside the evaporator section of the TPCTR then changes from the highly efficient boiling and evaporation to conduction through the solid wall and the vapor phase. This results in extremely high thermal resistance between the moderator and the cryorefrigeration system, as a result the temperature of the moderator increases with further increase in heat load.

The first finding of this investigation developing a model that is able to determine the dryout temperature of any TPCTR that has a known cooling fluid property (in this case neon). The model accurately predicts the experimental data of the TCNS given in [**Unlu et al 1994**]. The higher the dryout temperature, the better the system will be capable in handling higher heat loads.

This investigation identified the various parameters that determine the dryout temperature. Among the many factors: initial pressure, reservoir temperature, volume ratio η and the primary cooling system (cryorefrigeration) performance angle α are the most important ones. It is found, for example, that doubling the pressure of the system

will increase the capacity index ζ by 50% for a system with an initial fill ratio FR of 1. A decrease in cryorefrigeration performance angle increases the capacity index. For example taking the current condition of the TCNS system and reducing the angle from the current value of $\sim 70^0$ by half ($\sim 35^0$) will increase the cooling power 300%.

The CFD analysis that is carried out using commercial code FLUENT 6.3 showed that the flow structure inside the evaporator and the condenser section of the TPCTR is three dimensional and complex. In order to compare the nucleate boiling correlations that are used in the heat transfer analysis, a CFD modeling of natural convection and nucleate boiling was carried out. The result confirmed that bubble formation during nucleate boiling enhance the heat transfer coefficient. The prediction was well within 5% of experimental data from literature

7.3 Future Work

In this study most of the analysis was carried out using analytic tools and assumptions. Although some experimental data from previous tests were used to validate the assumptions and analysis, it is important to carry out a thorough experimental work to validate the conclusions that were drawn from the analytic work. The major experimental work that could be carried out would be to study the effect of the various parameters on the dryout condition of the TPCTR cooling system. The result of such experimental work will be valuable in future design and manufacturing work of the cooling system.

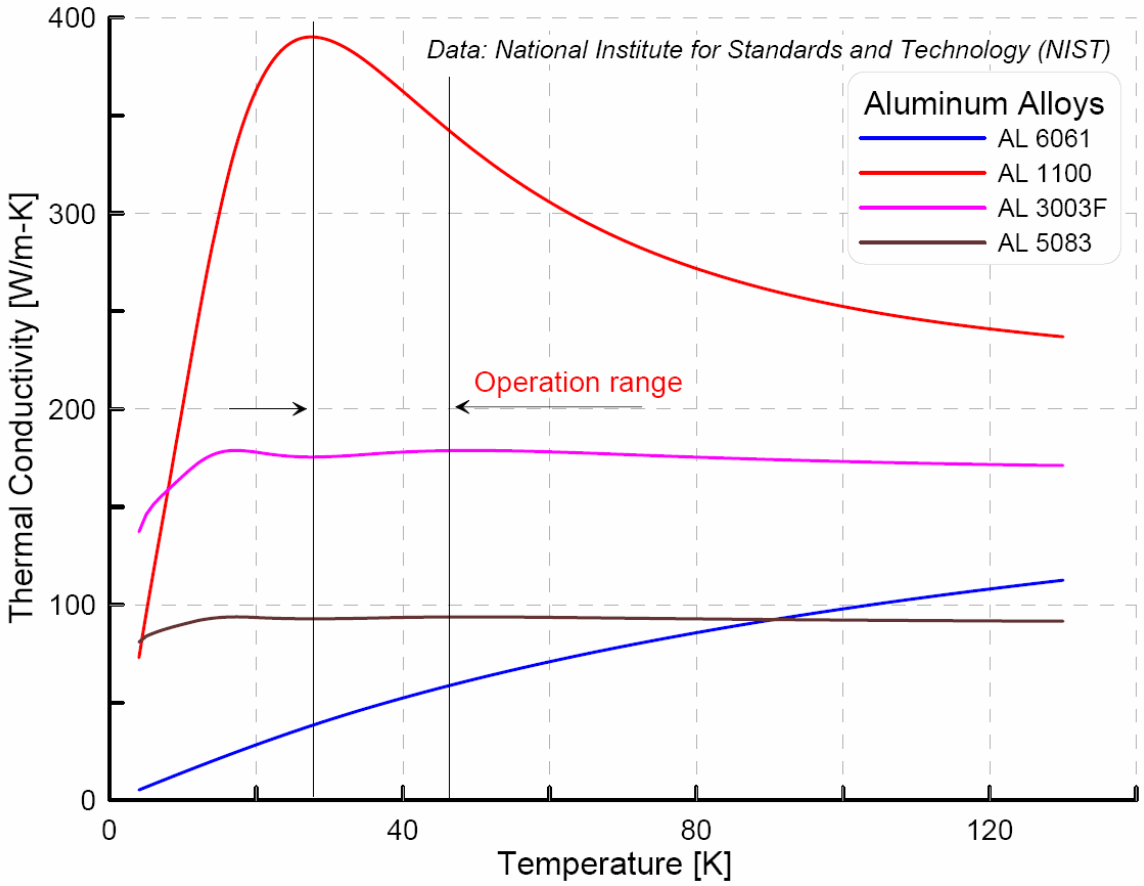

Figure **7-1**: Variation of Thermal conductivity of Aluminum alloys near cryogenic temperatures

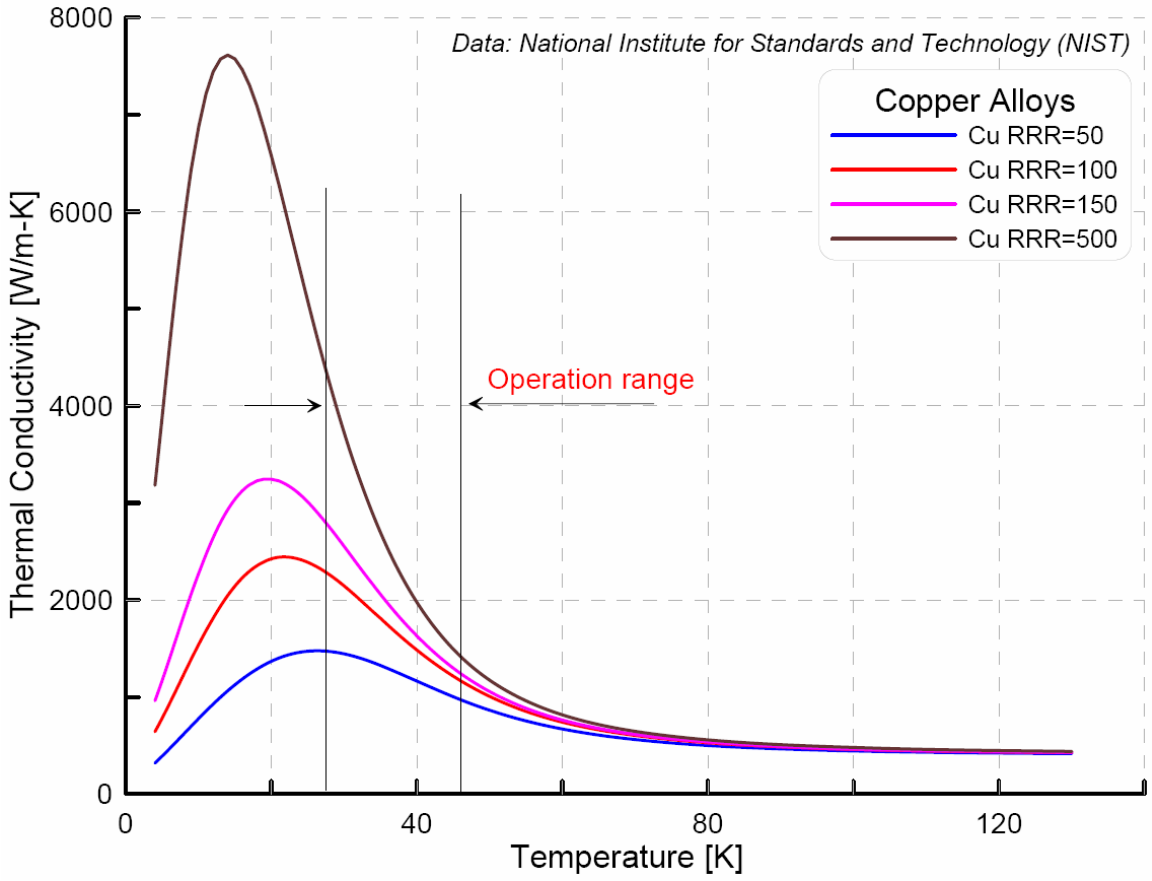

Figure **7-2**: Variation of Thermal conductivity of Copper alloys near cryogenic temperatures

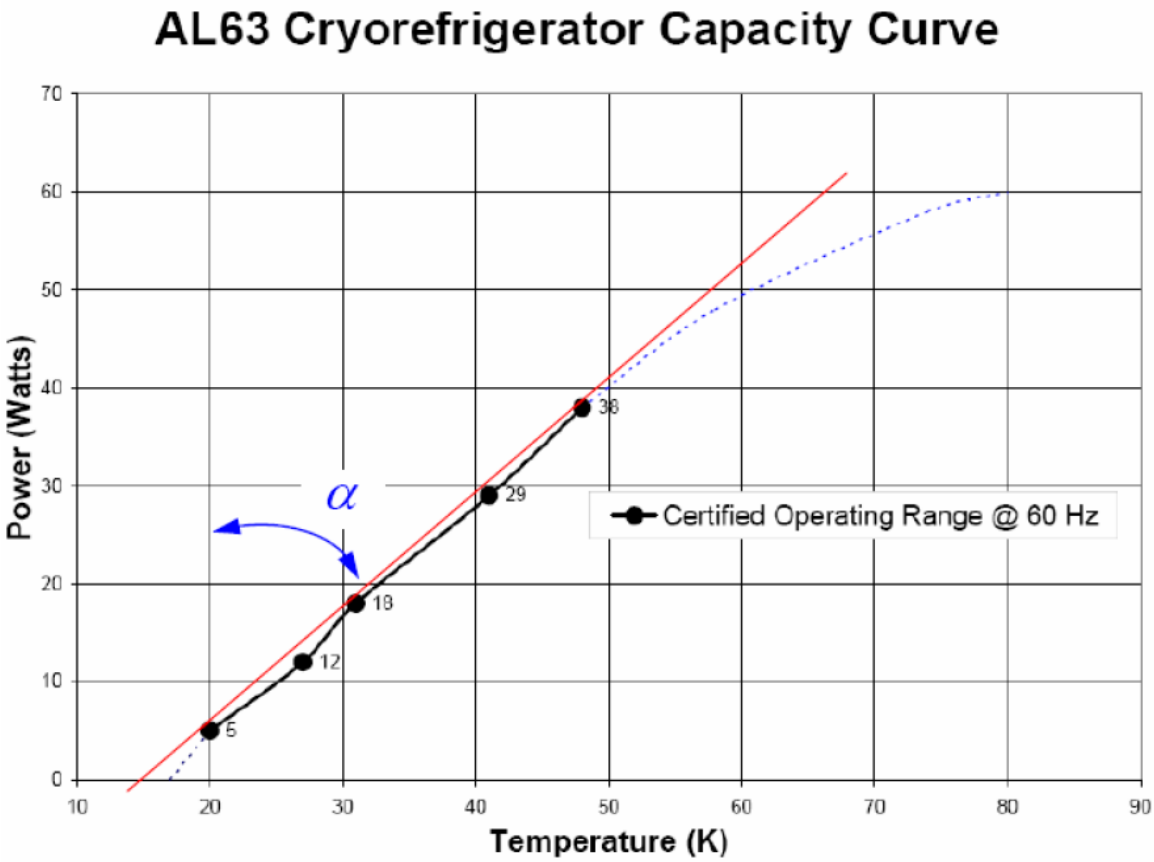

Figure **7-3**: Performance chart of cryocooler showing characteristic angle [**Cryomech-Inc 2008**]

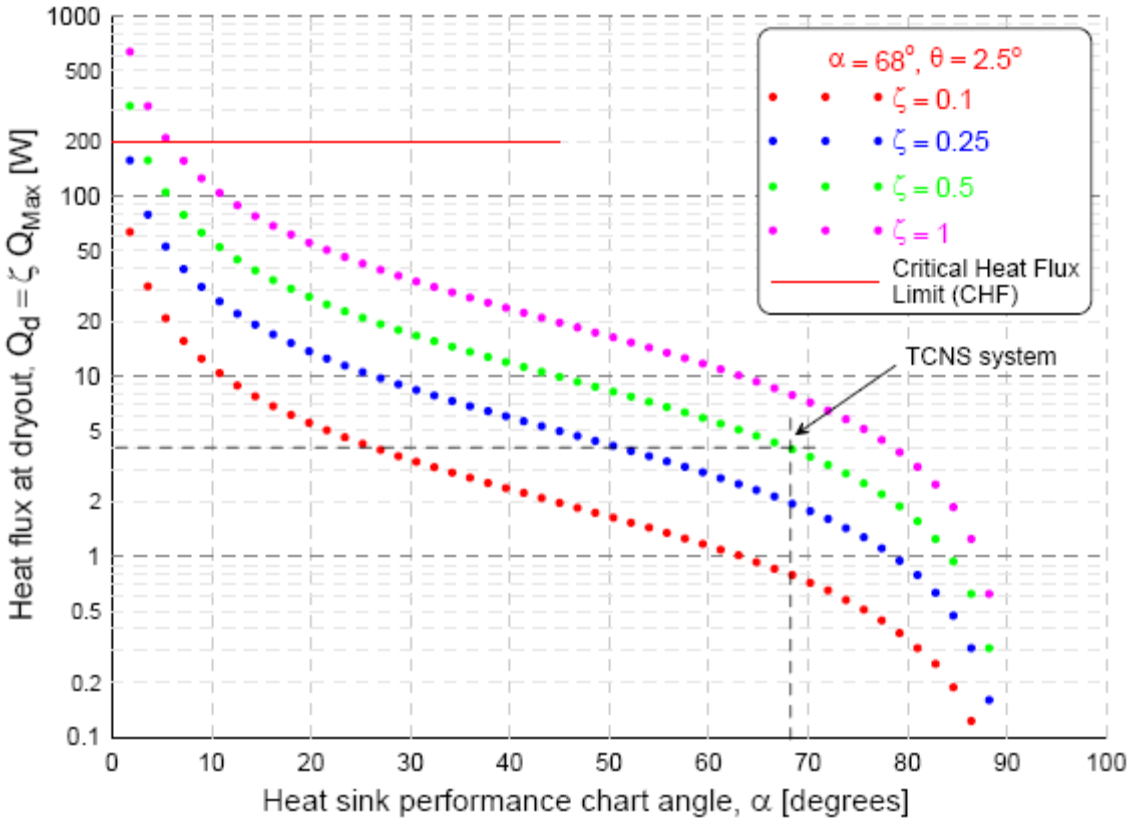

Figure **7-4**: Parametric plot of the heat load at dryout versus the performance characteristic angle α of the cryorefrigeration system (heat sink) at various Capacity Index of two phase closed thermosyphon

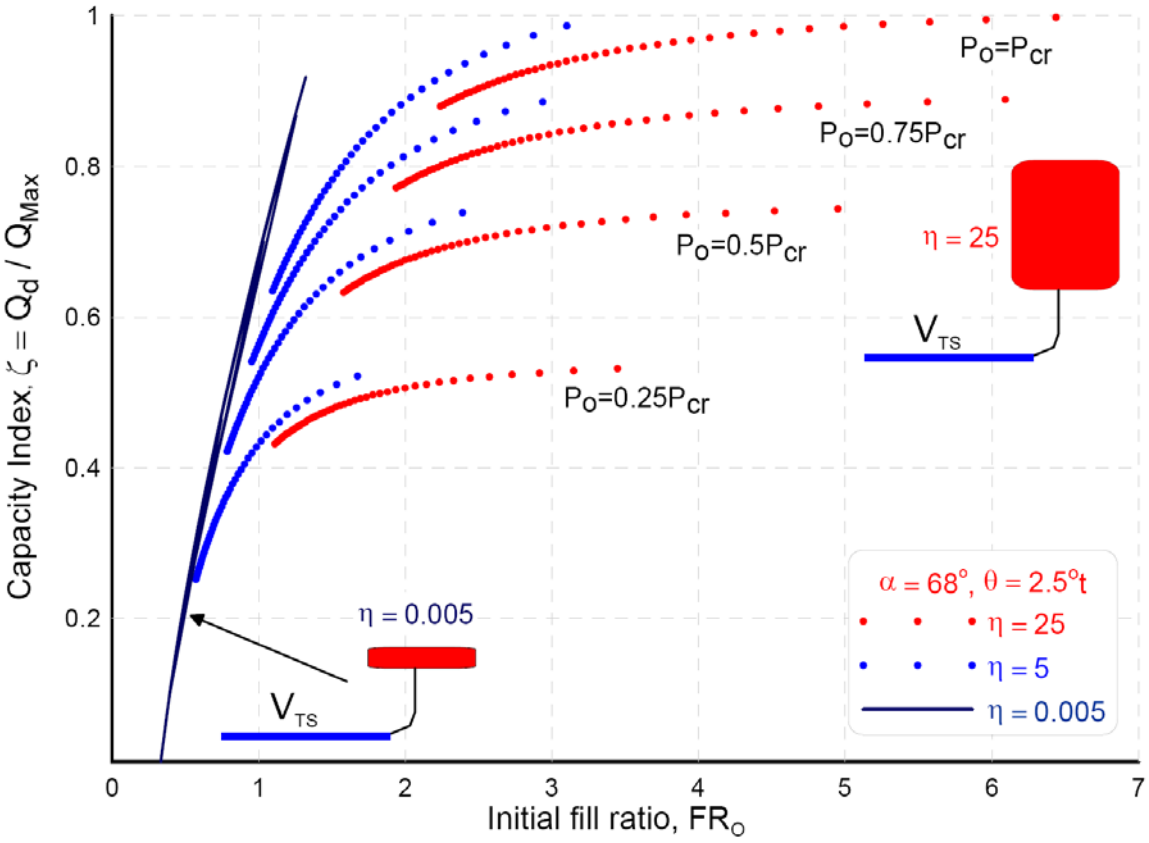

Figure **7-5**: Parametric plot showing Capacity Index versus Initial fill ratio for a two phase closed thermosyphon

Bibliography

Astruc, J.,M., Perroud, P., lacaze, L., 1969, "Comparison of Heat Transfer with Hydrogen, Deuterioum and Neon Boiling with Free Convection at Atmospheric Pressure", Cryogenics, pp 248-250

Carey, V. P., 2008 "Liquid-Vapor Phase Change Phenomena," Taylor and Francis Group, LLC

Clark, D. D., C., G.,Ouellet, Berg, J. S., 1992, "On the Design of a Cold Neutron Source," Nucl. Sci. Engr. Vol. 110, No. 4, 445 (1992)

Cryomech Inc, http://www.cryomech.com

Dobran, F., Casarosa, C., 1988 "Experimental Investigation and Analytical Modeling of a Closed Two-Phase Thermosyphon with Imposed Convection Boundary Conditions," Int. J. Heat Mass Transfer, Vol 31, No 9, pp 1815-1833

El-Genk S. M., Saber H. H., 1998 "Determination of Operation Envelopes for Closed Two Phase Thermosyphons," Int. J. Heat and Mass Transfer 42 889-903

El-Genk S. M., Saber H. H., 1998 "Heat Transfer Correlations for Liquid Film in the Evaporator of Enlosed, Gravity-Assisted Thermosyphons," J. heat Transfer 120 447-484

Fluent 6.3 Documentation, 2007, Fluent Incorporated, Lebanon, NH

Gaugler, R. S., 1944, "Heat Transfer Devices," US Patent 2,350,348

Geisler, K.J.L., 2007, "Bouyancy-Driven Two Phase Flow and Boiling Heat Transfer in Narrow Vertical Channels," PhD Thesis, University of Minnesota, 2007

Ghazouani, J., Chouaieb, O., Bellagi, A., 2005 "Evaluation of the Parameters of Bender Equation of State for Low Acentric Factor Fluids and Carbon dioxide," Thermochimica Acta 430 10-19

Holman, J.P., 1997 "Heat Transfer," McGraw Hill

Jialun H., Tongze Ma., Zhengfang Z., 1992 "Investigation of boiling liquid pool height of a two-phase closed thermosyphon," Proceedings of the Eighth International Heat Pipe Conference, Beijing, China, Inst. Of Eng. Thermophysics, Chines Academy of Sciences, pp 154-159

Jiao, B., Qui, L.M., Zhang, X. B., Zhang, Y., 2007 "Investigation of Effect of Filling Ratio on Steady State heat Transfer Performance of a Vertical Two-Phase Closed Thermosyphon," Applied Thermal Engineering

Khandekar, S., Joshi, Y. M., Mehta, B., 2007 "Thermal Performnace of Closed Two-Phase Thermosyphon Using Nanofluids," International Journal of Thermal Sciences

Kim, M. H., Kim, J., 2006, "On Departure Behaviors of bubble at Nucleate Pool Boiling," Int. J. of Multiphase Flow 32 (2006) 1269-1286

Kusuda, H., and Imura, H., "Boiling Heat Transfer in an Open Thermosyphon," Bull. J.S.M.E. 16, 1734-1740

Lock, G. S. H., Liu, Y., 1989 "The Effect of Geometry on Performance of The Closed Tube Thermosyphon and low Rayleigh Numbers," Int. J. Heat Mass Transfer Vol. 32, No 6, pp. 1175-1182

Lock, G. S. H., Kirchner, J. D. 1992 "Some Characteristics of the Inclined Closed Thermosyphon under Low Rayleigh Number Conditions," Int. J. Heat Mass Transfer, Vol 35, No 1, pp 165-173 Narumanchi, S., Troshko, A., Bharathan, D., Hassani, V., 2008, "Numerical Simulations of Nucleate Boiling in Impinging Jets: Applications in Power Electronics Cooling," Int. J. heat and Mass transfer, 51 (2008) 1-12

Niro A., Beretta G. P, 1990 "Boiling Regimes in a Closed Two-Phase Thermosyphon," Int. J. Heat Mass Transfer, Vol. 33, No. 10, pp 2099-2110

NIST-server http://www.webbook.nist.gov/chemistry

Peterson, G. P. 1994, "An Introduction to Heat Pipes: Modeling, Testing, and Applications" John Wilely & Sons Inc, New York

Shiraishi, M., Kikuchi, K., Yamanishi, T., "Investigation of Heat Transfer Characteristics of a Two-Phase Closed Thermosyphon," heat Recovery Systems Vol. 1 pp 287-297

Spern, S. A., Clark D. D., Atwood, A. G., 1996 "Initial Reactor Performance of the Cornell Cold Neutron Source," Trans. Am. Nucl. Soc., 74, 106 (1996)

Terdtoon, P., Payakaruk, T., Ritthidech, S., 2000 "Correlations to Predict the Heat Transfer Characteristics of Inclined Closed Two-Phase Thermosyphon at Normal Operating Conditions," Applied Thermal Engineering, 20 781-790

Ünlü K., Rios-Martinez C., Wehring B. W., 1994 "The University of Texas Cold Neutron Source," Nucl. Instr. and Meth. in Phys. Res. A 353 (1994) 397

Ünlü, K., Rios-Martinez, C., Wehring, B. W., 1995 "Prompt Gamma Activation Analysis with Texas Cold Neutron Source,"J. of Radioanal. Nucl. Chem., Articles, 193, No.1, (1995) 145

Ünlü, K., Rios-Martinez, C., Wehring, B. W., 1997, "Application of Cold-neutron Prompt Gamma Activation Analysis at the University of Texas," Appl. Radiat. Isot. Vol. 48, No.10-12. pp. 1343-1348, (1997).

Whalley, P.B., 1987 "Boiling, Condensation and Gas-Liquid Flow," Oxford University Press, NY

Young L. J., Ph.D. dissertation, 1982, "The Design and Construction of a Cold Neutron Source for use in the Cornell TRIGA Reactor," Cornell University, (1982)

Appendix A

A.1 Procedure for Calculating Dryout Temperature and Pressures

The following procedures as utilized in calculating the dryout temperature and pressure of a two phase closed thermosyphon that is connected to a reservoir containing working fluid (neon gas) as in the case of TCNS cooling system thermosyphon.

Step 1.**List properties of thermosyphon and gas reservoir**

Calculate the Thermosyphon and gas reservoir geometric and thermo-physical parameters as shown in Table **A-2** , Table **A-3** and Table **A-4**

Step 2.**List properties of working fluid**

Calculate the thermo-physical properties of working fluid (Neon) as shown in Table **A-5** . In this step the physical properties of neon gas can be evaluated at any temperature and pressure using Eq. **4.1**, Eq. **4.2** and using Table **4-1**

Step 3.**Calculate the mass of neon charged into the system**

Once the thermosyphon and gas reservoir are filled to an initial pressure and temperature of T_0 and P_0 respectively then mass of neon in the thermosyphon and reservoir can be calculated using Eq. **A.1** . This would give the total mass of neon gas charged into the system at the given temperature and pressure:

$$M_{Tot}(T,P,V) = \rho(T,P)\big|_{T_0,P_0} \cdot V\big|_{V_{Tot}} \qquad \textbf{A.1}$$

Step 4.Calculate the dryout temperature and pressures

Once the system starts to cooldown, the neon gas temperature inside the thermosyphon continuously drops up until liquid starts to accumulate in the evaporator section, which is marked by the beginning of stage-III in the cooldown process shown in Figure **3-5** . At the dryout condition the effective temperature in the thermosyphon is the saturation temperature at the prevailing pressure. This saturation condition is the dryout point given by T_{dsat} and P_{dsat} . The mass of neon gas inside the thermosyphon at this state is given by (which is a function of the system pressure)

$$m_{TS\_V}(T,P) = M_{Tot}(T,P)\big|_{T_0,P_0} - M_{RS}(T,P)\big|_{T_0} = f(P) \qquad \textbf{A.2}$$

The mass of neon gas in the thermosyphon can also be calculated, using the equation of state, as

$$m_{TS\_V}(T,P) = \left.\frac{P\bar{M}_{Ne}V_{TS}}{R_u T}\right|_{T_{Sat}} = f(T_{Sat}(P),P) = f(P) \qquad \textbf{A.3}$$

Now both Eq. **A.2** and Eq. **A.3** are functions of one variable which is pressure. The two equations can now be solved simultaneously for the unknown pressure. This will be the saturation pressure at the dryout condition P_{dsat} . The dryout temperature T_{dsat} can then be calculated or evaluated using the dryout saturation pressure. For example for the TCNS cooling system, using this method, the dryout condition will be $T_{dsat} = 34.846K$ and the corresponding dryout pressure was $P_{dsat} = 0.631MPa$.

A.2 Derivation of Analytic Equation for Determining Dryout Condition

The method discussed in the previous section can be used to determine the saturation conditions at the dryout point. However a more concise and convenient equation can be derived for determining these state points. Figure **A-1** shows a schematic diagram of a thermosyphon and a vapor reservoir connected by a small diameter pipe. It is shown that the reservoir with a volume V_R kept at a constant temperature of T_∞. As the thermosyphon cools down, the vapor in reservoir starts to flow into the thermosyphon.

Let the initial temperature and pressure of the thermosyphon and reservoir be T_O and P_O respectively. Define volume ratio η, the ratio of volume of reservoir to that of the thermosyphon, as:

$$\eta = \frac{V_R}{V_{TS}} \qquad \textbf{A.4}$$

Assuming Ideal gas behavior of the vapor phase of the working fluid inside (at this point it is also possible to assume real gas model) the mass of the fluid inside the reservoir at any system pressure is given by:

$$m_R = \frac{PV_R}{RT_\infty} \qquad \textbf{A.5}$$

Similarly the total mass inside the thermosyphon is given by

$$m_{TS} = \frac{PV_{TS}}{RT} \qquad \textbf{A.6}$$

Note that the temperature inside the thermosyphon is variable. Applying conservation of mass to the thermosyphon and reservoir, we have

$$\frac{d}{dt}(m_R) = -\frac{d}{dt}(m_{TS}) \qquad \textbf{A.7}$$

Now substituting Eq. **A.5** and Eq. **A.6** into Eq. **A.7** , we have Eq. **A.8**

$$\frac{d}{dt}\left(\frac{PV_R}{RT_\infty}\right) = -\frac{d}{dt}\left(\frac{PV_{TS}}{RT}\right) \qquad \textbf{A.8}$$

Arranging and differentiating Eq. **A.8** we have Eq. **A.9**

$$\begin{aligned}\frac{V_R}{RT_\infty}\frac{d}{dt}(P) &= -\frac{1}{T^2}\left[\frac{V_{TS}}{R}T\frac{d}{dt}(P) + \frac{V_{TS}}{R}P\frac{d}{dt}(T)\right] \\ &= -\frac{V_{TS}}{R}\frac{1}{T}\frac{d}{dt}(P) - \frac{V_{TS}}{R}\frac{P}{T}\frac{d}{dt}(T)\end{aligned} \qquad \textbf{A.9}$$

Simplifying and substituting Eq. **A.4** we have Eq. **A.10**

$$\int_{P_o}^{P}\frac{dP}{P} = \int_{P_o}^{P}\frac{1}{T}\left(1+\eta\frac{T}{T_\infty}\right)^{-1}dT \qquad \textbf{A.10}$$

Integrating, we have the final form as Eq. **A.11**

$$P = P_O\left(\frac{1+\eta}{\frac{T_\infty}{T}+\eta}\right) \qquad \textbf{A.11}$$

This equation relates the pressure in the thermosyphon-reservoir system to the effective temperature inside the thermosyphon, the liquid fraction and reservoir room temperature. To determine the dryout saturation condition, one has to equate the above equation to the saturation curve of the working fluid. Hence the dryout saturation temperature is given by the solution of the following equation:

$$P_O\left(\frac{1+\eta}{\frac{T_\infty}{T_{dSat}}+\eta}\right) - f(T_{dSat}) = 0 \qquad \textbf{A.12}$$

where $f(T_{dSat}) = P_{Sat}$

A.3 Derivation of Equation for Liquid Fraction ξ

In this study the liquid fraction ξ is defined as the ratio of the volume of liquid present in the thermosyphon to the total volume of the thermosyphon. During cooling down process (Stage-II), the liquid condensed will evaporate as it flows down the thermosyphon inside wall. At the end of Stage-II of the cooling process i.e. when the dryout point is reached, there will be a finite amount of liquid film. Let the volume of the liquid film be V_{f0} and the corresponding liquid fraction at this stage ξ_O. Further let's assume that the variation of the volume of liquid film to be proportional to the saturation temperatures corresponding to the initial pressure and the dryout saturation temperature as:

$$\xi = \left(\frac{T - T_{Sat0}}{T_{dSat} - T_{Sat0}} \right)^n ; n = 4 \text{ and } T_{dSat} < T < T_{Sat0} \qquad \textbf{A.13}$$

where $\xi_O = \frac{V_{f0}}{V_{TS}}$ and $T_{Sat0} = T_{Sat} @ P_O$

Now, consider the mass balance for thermosyphon-reservoir system starting at the end of stage-II:

$$M_L = M_T - M_R - M_{TS\_V} + M_f \qquad \textbf{A.14}$$

Where M_T, M_L, M_R, M_{TS_V} and M_f represent the total mass, mass of liquid in the thermosyphon, mass of vapor in the reservoir, mass of vapor in the thermosyphon and mass of liquid film respectively. Substituting equation of state in Eq. **A.14** we have:

$$\rho_L V_L = \frac{P_O \left(V_{TS} + V_R \right)}{RT_O} - \left(\frac{PV_R}{RT_O} + \frac{PV_{TS\_V}}{RT} \right) + \rho_L V_{f0} \qquad \textbf{A.15}$$

Substituting $V_{TS\_V} = V_{TS} - V_f$ and dividing by V_{TS} Eq. **A.15** becomes:

$$\rho_L \xi = \frac{P_O}{RT_O}(1+\eta) - \left(\frac{P}{RT_O}\eta + \frac{P}{RT}(1-\xi) \right) + \rho_L \xi_O \qquad \textbf{A.16}$$

Arranging terms, we have:

$$\left(\rho_L - \frac{P}{RT} \right) \xi = \frac{P_O}{RT_O}(1+\eta) - \frac{P}{RT}\left(\eta \frac{T}{T_O} + 1 \right) + \rho_L \xi_O \qquad \textbf{A.17}$$

Substituting $\rho_O = \frac{P_O}{RT_O}$ and $\rho = \frac{P}{RT}$, the liquid fraction given by:

$$\xi = \frac{\frac{\rho_O}{\rho_L}(1+\eta) - \frac{\rho}{\rho_L}\left(\eta\frac{T}{T_O}+1\right) + \xi_O}{\left(1-\frac{\rho}{\rho_L}\right)}; \quad T_{Min} < T < T_{dSat} \qquad \textbf{A.18}$$

where $\rho = \frac{f(T_{Sat})}{RT_{Sat}}$;

Where: the function $f(T_{Sat})$ is the saturation pressure equation that can be obtained by curve fitting.

A.4 Equation of State Parameters

The parameters used in Eq. **4.2** to evaluate the compressibility factor are listed in Table **A-1** below.

Table **A-1**: Parameters of the Bender equation of state for neon[**Ghazouani et al 2005**]

a1	6.1712000E-03
a2	-2.3860000E-01
a3	-7.5748000E+01
a4	2.2144000E+03
a5	-2.6381000E+04
a6	2.6707000E-06
a7	1.0554000E-03
a8	-7.9161000E-03
a9	2.9108000E-09
a10	-1.4130000E-06
a11	2.2010000E-12
a12	6.2366000E-10
a13	2.8100000E-13
a14	-2.0708000E+01
a15	2.0279000E+03
a16	-5.0109000E+04
a17	5.6119000E-06
a18	-7.6984000E-04
a19	3.0147000E-02
a20	4.8191000E+02

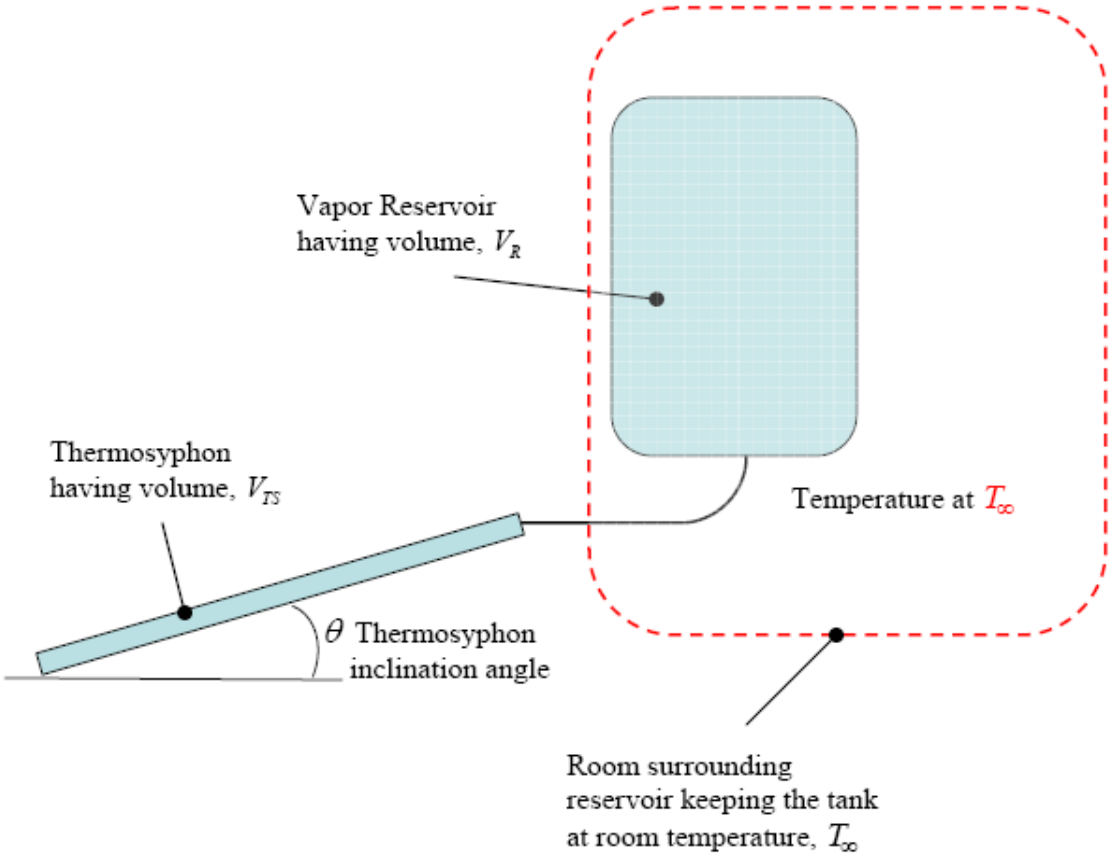

Figure **A-1**: Schematic showing thermosyphon and reservoir setup with the reservoir kept at room temperature

Table **A-2**: Thermosyphon Geometric Parameters

GEOMETRIC PARAMETER	SYMBOL	NUMERICAL VALUE (TCNS)	REMARK
Outer diameter	D	19 mm	
Wall thickness	t_{ts}	1.6 mm	
Inside diameter	$d = D - 2t_{ts}$	15.8 mm	
Length of condenser section	L_C	50 mm	
Length of evaporator section	L_E	19 mm	
Total length	L_{TS}	3350 mm	
Volume of evaporator section	$V_E = \frac{\pi}{4} d^2 L_E$	0.041 Liter	
Volume of condenser section	$V_C = \frac{\pi}{4} d^2 L_C$	0.107 Liter	
Total Volume of thermosyphon	$V_{TS} = \frac{\pi}{4} d^2 L_{TS}$	0.653 Liter	
Volume of gas reservoir	V_R	6.5 Liter	

Table **A-3**: Thermosyphon Thermo-Physical parameters

THERMO-PHYSICAL PARAMETER	SYMBOL	NUMERICAL VALUE (TCNS)	REMARK
Material made of	AL	Aluminum 6090?	
Thermal conductivity	$k_{Al} = k_{Al}(T)$	$156 \frac{W}{m \cdot K}$ at room temp	A function of temperature
Density	ρ_{Al}	$2700 \frac{kg}{m^3}$	constant
Specific heat	$Cp_{Al} = Cp_{Al}(T)$	$956 \frac{J}{kg \cdot K}$	A function of temperature

Table **A-4**: Gas reservoir geometric and thermo-physical properties

THERMO-PHYSICAL PARAMETER	**SYMBOL**	**NUMERICAL VALUE (TCNS)**	**REMARK**
Volume	V_R	6.5 liter	
Material made of	AL	Aluminum 6090?	
Thermal conductivity	$k_{Al} = k_{Al}(T)$	$156\frac{W}{m \cdot K}$ at room temp	Constant since it is placed at room temp
Density	ρ_{Al}	$2700\frac{kg}{m^3}$	constant
Specific heat	$Cp_{Al} = Cp_{Al}(T)$	$956\frac{J}{kg \cdot K}$ at room temp.	Constant since it is placed at room temp
Operating temperature	T_R	300 K	Surrounding is not insulated
Operating pressure	P_R	variable	Pressure varies but is the same as that of thermosyphon
Initial operating pressure	P_0	$10\,atm$	
Initial operating temperature	T_0	300 K	

Table **A-5**: Working fluid (Neon) thermo-physical properties

THERMO-PHYSICAL PARAMETER	**SYMBOL**	**NUMERICAL VALUE (TCNS)**	**REMARK**
Molecular weight	$\bar{M}$	$20.1797\frac{gm}{mole}$	
Critical temperature	T_{Cr}	44.49 K	
Critical temperature	P_{Cr}	$2.678 MPa$	
Thermal conductivity	Neon gas: k_{NeG}	$0.0076\frac{W}{m\cdot K}$	Nearly constant
	Neon liquid: $k_{Ne} = k_{Ne}(T)$	$0.1496\frac{W}{m\cdot K}$ at 28 K	A function of saturation temperature
Density	Neon gas: $\rho_{NeG} = \rho_{NeG}(T,P)$	$8.16\frac{kg}{m^3}$ at 300 K and 10atm	A function of saturation temp. and pressure
	Neon Liquid: $\rho_{NeL} = \rho_{NeL}(T)$	$1.19\frac{kg}{m^3}$ at 28 K	A linear function of sat. temperature
Specific heat	Neon gas: $Cp_{NeG} = Cp_{NeG}(T)$	$1300\frac{J}{kg\cdot K}$ at sat temp of 30 K	A function of saturation temperature
	Neon Liquid: $Cp_{NeL} = Cp_{NeL}(T)$	$2007\frac{J}{kg\cdot K}$ at sat. temp of 30 K	A function of saturation temperature
Latent heat	$h_{Ne} = h_{Ne}(T)$	$82.122\frac{kJ}{kg}$ at sat. temp of 30 K	A function of saturation temperature

VITA

Melaku Habte

EDUCATION

2004 – 2008	THE PENNSYLVANIA STATE UNIVERSITY, University Park, PA **PhD Mechanical Engineering**, Aug 2008 **PhD Computational Science (minor)** Aug 2008
2000 -2003	THE PENNSYLVANIA STATE UNIVERSITY, University Park, PA **M.Sc Mechanical Engineering**, Dec 2003
1992 – 1997	ADDIS ABABA UNIVERSITY, Addis Ababa, Ethiopia **B.Sc. Mechanical Engineering**, June 1997

PROFESSIONAL EXPERIENCE:

Aug 2004 –Aug 2008	Research Assistant in Neutron Beam Group (NBG) of Radiation Science and Engineering Center, The Pennsylvania State University
	Teaching Assistant for Undergraduate Fluid Mechanics, Undergraduate Thermodynamics, Thermal System Design in the Department of Mechanical and Nuclear Engineering, The Pennsylvania State University
	Teaching Undergraduate Fluid Mechanics Laboratory Class and Supervising Laboratory Sessions.
Dec 2003 -Aug2004	Developed Fluid Mechanics case study projects for undergraduate Program, Department of Mechanical and Nuclear Engineering, The Pennsylvania State University
Aug 2000 –Dec2003	Teaching and Research Assistant Department of Mechanical and Nuclear Engineering, The Pennsylvania State University Designed, built and carried out a two-phase flow experiment in studying of flow mal-distribution in brazed aluminum evaporators
Aug 1998 – Aug 2000	Assistant Lecturer in Mechanical Engineering Department, Faculty of Technology, Addis Ababa University, Addis Ababa, Ethiopia
	Research Fellow in Mechanical Engineering Department, University of Cagliari, Italy
Aug 1997 – Aug1998	Graduate Assistant in Mechanical Engineering Department, Faculty of Technology, Addis Ababa University, Addis Ababa, Ethiopia

AWARDS AND HONORS:

1996 ESS Award: The Ethiopian Scientific Society *Academic Excellence* Award for the year 1996 , Addis Ababa University, Faculty of Technology, Addis Ababa, Ethiopia